PERFORMANCE RELATED PARAMETERS OF ELASTOMERIC BEARINGS

by

Alok Kumar, B. Tech., M. S.

DISSERTATION

Presented to the Faculty of the Graduate School of

The University of Texas at Austin

in Partial Fulfillment

of the Requirements

for the Degree of

DOCTOR OF PHILOSOPHY

The University of Texas at Austin

May 2000

PERFORMANCE RELATED PARAMETERS OF ELASTOMERIC BEARINGS

Approved by
Dissertation Committee:

Joseph A. Yura, co-supervisor

Eric B. Becker, co-supervisor

Richard A. Schapery

Michael D. Engelhardt

John L. Tassoulas

Dedication

To my mother Krishna Sharma

Acknowledgements

I would like to express my sincere thanks to Oil States Industries, Arlington, Texas, where part of this research was conducted. Especially, I would like to thank Mike Hogan and David Riggs for all their help. A special note of thanks also goes to Theresa McCullough and Steve Cariker for performing the EDD tests.

At University of Texas, I would like to thank Professor Joseph A. Yura and Professor Eric B. Becker for supervising this dissertation. I would also like to thank the other members of my dissertation committee, Professors Richard A. Schapery, Michael D. Engelhardt and John L. Tassoulas for their invaluable advice. Special thanks must also go to Roy Lou and Blake Stasney for their help during various tests performed at Ferguson Structural Engineering Laboratory.

Finally, I deeply appreciate the encouragement of my family and friends during this important phase of my life.

PERFORMANCE RELATED PARAMETERS OF ELASTOMERIC BEARINGS

Publication No._____

Alok Kumar, Ph.D.

The University of Texas at Austin, 2000

Supervisors: Joseph A. Yura and Eric B. Becker

The effects of laminate misalignment, creep, aging and explosive decompression on the performance of steel laminated elastomeric bearings were investigated. Natural rubber and neoprene at two hardness levels (durometer 50 and 70) were used in the study of laminate misalignment, creep and aging while the effects of explosive decompression were studied on nitrile. Combined limits on vertical misalignment, edge cover misalignment and laminate inclination in the form of an interaction equation were systematically developed by means of computer simulated virtual experiments using the finite element method. The results showed that the tolerances given in AASHTO M241 are well below the laminate misalignments that affect the performance of the bearings. The creep behavior was investigated by means of full-scale tests. The results showed that creep of elastomeric bearings is important and the boundary conditions play an

important role in controlling the long-term deformation. Since full-scale creep tests are time consuming, uneconomical and specific to the bearings tested, a practical method was developed to predict creep of elastomeric bearings using six-hour stress relaxation data obtained from a dual lap shear relaxation test. The effects of aging on shear stiffness were studied by conducting accelerated heat aging tests on four different sizes of shear specimens. As the size increased the percent change in shear stiffness decreased drastically. The results extrapolated to full-size bearings at ambient temperature using Arrenhius relationship predicted that the change in shear stiffness was insignificant. It was concluded that the standardized aging tests performed on thin specimens in tension mode per ASTM D573 assess superficial aging only and does not represent the aging behavior of elastomeric bearings. Therefore ASTM D573 can be eliminated from AASHTO specifications. For elastomeric bearings used as moment-free connections in offshore pipelines transporting high-pressure hydrocarbon fluid/gas mixture, a new test method was developed to study the effects of explosive decompression. Three rubber layer thicknesses tested under extreme exposure conditions showed that under similar environmental and loading conditions, thicker rubber layers were more susceptible to Explosive Decompression Damage (EDD) and with adequate confinement of rubber, the effects of EDD can be reduced to acceptable levels.

Table of Contents

List of Tables

List of Figures

Chapter 1: Introduction

1.1 BACKGROUND

Elastomeric bearings have long been recognized as useful in replacing metal bearings and metal flexible connections (History and Usage, OSI, 1996). The use of rubber as a bearing material dates back to 1889 (Lindley, 1978). The early elastomeric designs were typically flat pads subjected to low bearing stresses on the order of 0.2 to 1.0 MPa. The concept of confined elastomer configurations using metal laminations, as shown in Figure 1-1a, allowed bearing stresses to approach 5 MPa in compression in the early applications (such as common bridge bearing pads for highway constructions). By the early 1960's, serious consideration and application of highly loaded elastomeric bearings to other engineering fields was in its initial stages (Herrick, 1963, Schmidt, 1974). In the 1970's similar development of elastomeric bearings was taking place in the oil industry with applications on floating oilrigs (Vitt, 1974). This field is now mature, and the use of highly loaded elastomeric bearings in offshore platforms, buildings and bridges is widespread.

Bearing designs currently in use are capable of sustaining average bearing stresses on the order of 70 to 100 MPa. The evolution from simple bridge bearings to the complex modern components (used in a multitude of applications and environments) is a result of forty years of development encompassing extensive changes in engineering analytical techniques, manufacturing methodology and quality control.

In spite of continued advances in technology, elastomeric bearing design remains more of an art than a science, primarily due to the peculiarities of rubber behavior. On one hand rubber has a myriad of good qualities. Rubber has a low modulus of elasticity, and is capable of sustaining high shear deformations while maintaining a high compressive stiffness. After such deformations, it quickly and forcibly retracts to essentially its original configuration. It is resilient, and yet exhibits internal damping. It can be processed into a variety of shapes. It forms an excellent bond with metals. It can be compounded to have widely varied properties. It does not corrode and requires no lubrication. It exhibits excellent fatigue resistance and durability. Owing to this versatility of rubber behavior, the designer has unlimited options in selecting the type and configuration of an elastomeric bearing. On the other hand rubber has some undesirable characteristics. The mechanical response of rubber is dependent on time and temperature and it is susceptible to explosive decompression damage. The non-linear stress-strain curves, creep, hysteresis and other properties of rubber are influenced not only by the method of fabrication but also by its previous history (Mullins, 1987). This results not only in less precision in design compared with metals but also in less consistency in properties. Nevertheless, the good qualities of rubber surpass the undesirable characteristics and the elastomeric bearings are widely used in Aerospace, Transportation and Petrochemical Structures.

1.1.1 Structural Configuration

An elastomeric bearing consists of alternate layers of rubber and reinforcements (metal, composite or fabric) integrally bonded together. The basic

characteristic of an elastomeric bearing is its ability to support a high compression load while accommodating high cyclic motions in shear. This is the basis of bearings used in seismic applications, bridge supports and offshore Riser and TLP tendon applications where a high shear flexibility is required to alleviate shear, flexure and torsional stresses while maintaining a high axial stiffness.

There are generally three basic types of steel laminated elastomeric bearings - flat, circular and spherical, that are most commonly used in various civil engineering applications, independently or in combination with each other in series or in parallel. Except for the bearings used in bridge applications, almost all elastomeric bearings are molded to end plates at top and bottom called sole plates. Depending on the system requirements, some bearings have annular holes. The selection of the number and the best combination of these three basic types depends on the application requirements. The three basic types of bearing are schematically shown in Figure 1-1. The simplest form that represents the fundamental behavior of all laminated elastomeric bearings is a flat pad bearing with three rubber layers and two laminates as shown in Figure 1-1 (a).

Natural rubber (NR), neoprene (CR) and nitrile (NBR) are the three most commonly used elastomers in bearings. Table 1-1 shows the general characteristics of NR, CR and NBR. The chemical names for NR, CR and NBR are polyisoprene, polychloroprene and butadiene acrylonitrile respectively.

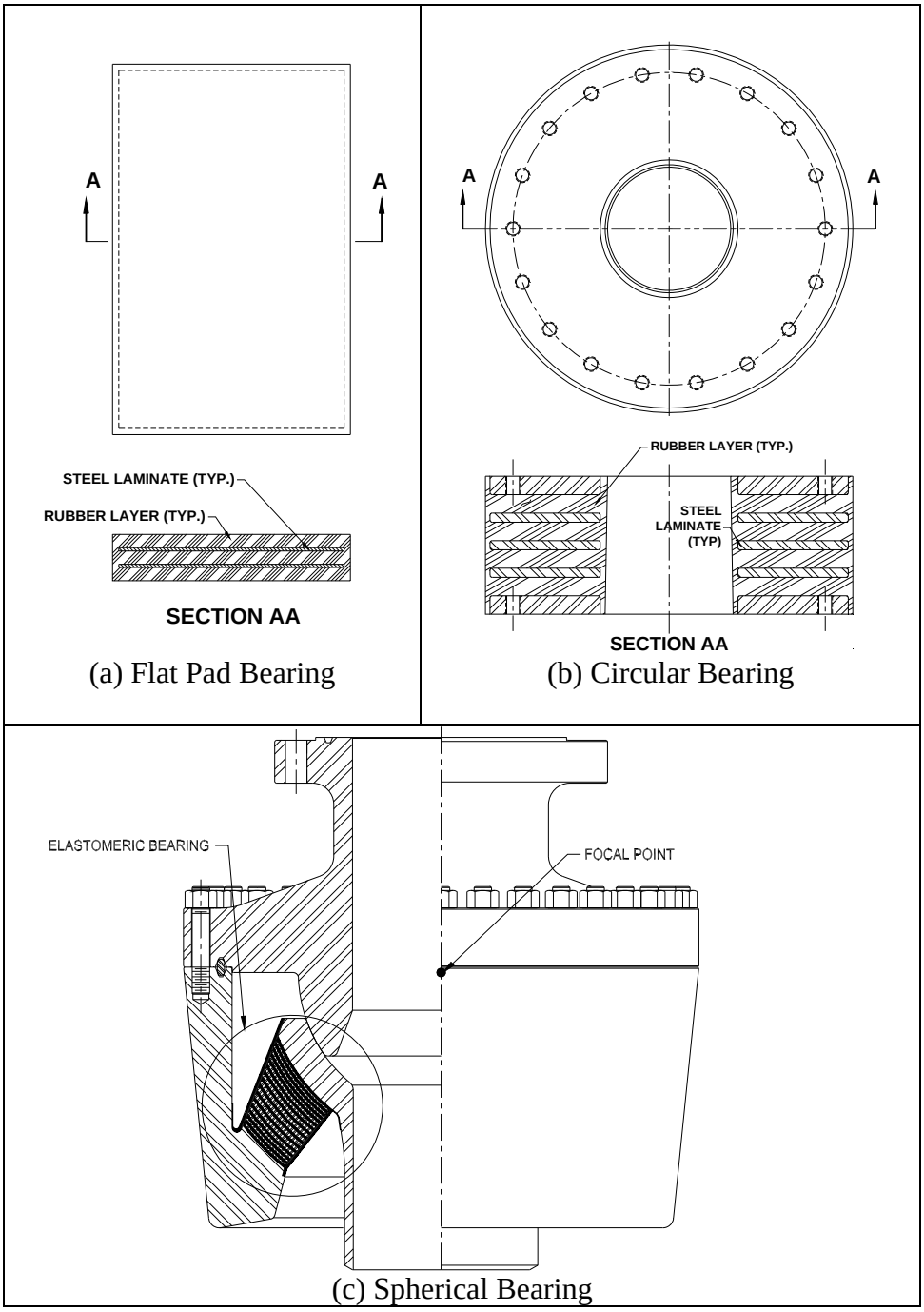

Figure 1-1: Typical Elastomeric Bearings

Each type of rubber has some unique characteristics as shown in Table 1-1. The selection of elastomer compound depends on many variables and is usually made on past experience. Some of the general characteristics of elastomers that are considered in the selection process include: hardness (durometer range as defined in ASTM D2240-86), tensile range, elongation, compression set, resilience, rebound, abrasion resistance, tear resistance, solvent resistance, oil or chemical resistance, low temperature usage, high temperature usage, aging and adhesion to metals.

Table 1-1: General Characteristics of Elastomers used in Bearings (compiled from various sources)

General Characteristics	Natural Rubber	Neoprene	Nitrile
Durometer Range (Shore A)	20 – 100	20 – 95	20-95
Tensile Range (psi)	500-3500	500 – 3000	200-3000
Elongation (max. percent)	700	600	600
Compression Set	Excellent	Good	Good
Resilience – Rebound	Excellent	Excellent	Good
Abrasion Resistance	Excellent	Excellent	Excellent
Tear Resistance	Excellent	Good	Good
Solvent Resistance	Poor	Fair	Good to Excellent
Oil Resistance	Poor	Fair	Good to Excellent
Low Temperature Usage ^{o}C	-30 to -50	-10 to -30	0 to – 40
High Temperature Usage ^{o}C	To 100	To 120	To 120
Aging Weather – Sunlight	Poor	Good	Poor
Adhesion to Metals	Excellent	Good to Excellent	Good to Excellent

1.1.2 Structural Behavior

An elastomeric bearing's structural behavior is governed by its axial and shear stiffness. The nature and properties of rubber greatly influence these stiffnesses. ASTM D 1566-97 defines rubber as:

> "a material that is capable of recovering from large deformations quickly and forcible, and can be, or already is, modified to a state in which it is essentially insoluble (but can swell) in boiling solvent, such as benzene, methyl ethyl ketone, and ethanoltoluene azeotrope. A rubber in this

> modified state, free of diluents, retracts within one minute to less than 1.5 times its original length after being stretched at room temperature (18 to 20^{o} C) to twice its length and held for one minute before release."

From a bearing designer's point of view, the two properties of rubber that give the bearing its unique characteristics are:

- Rubber can be sheared or stretched up to several times its original shape and still return to that shape upon release,
- Rubber is nearly incompressible, i.e., Poisson's ratio is very close to 0.5 and the bulk modulus (or the modulus of volumetric expansion) is many times larger than the shear modulus (except in the vicinity of glass transition temperature).

The rubber elasticity (or hyperelasticity) is very different than the ordinary solids elasticity. As shown in Table 1-2, the typical mechanical properties of rubber are quite different from those of common solids. A Poisson's ratio close to 0.5 means that rubber hardly changes in volume even under high loads so for most types of deformation there must be space into which the rubber can deform. The more restriction that is made on its freedom to deform the stiffer it becomes. When a rubber layer under compression is prevented from slipping at the loaded surfaces (by bonding or friction), its stiffness in compression depends on the shape factor, defined as the ratio of one loaded area to the total force-free area. A higher shape factor means a higher axial stiffness. The shear stiffness of a rubber layer is a function of shear modulus, loaded area and the thickness of the layer. The shear modulus (also referred to as secant shear modulus) is defined as the ratio of shear stress to shear strain at a particular strain as shown in Figure 1-2.

Since the shear modulus is low, as shown in Table 1-2, and is not influenced by the shape factor, the shear stiffness of a layer is much lower than its axial stiffness.

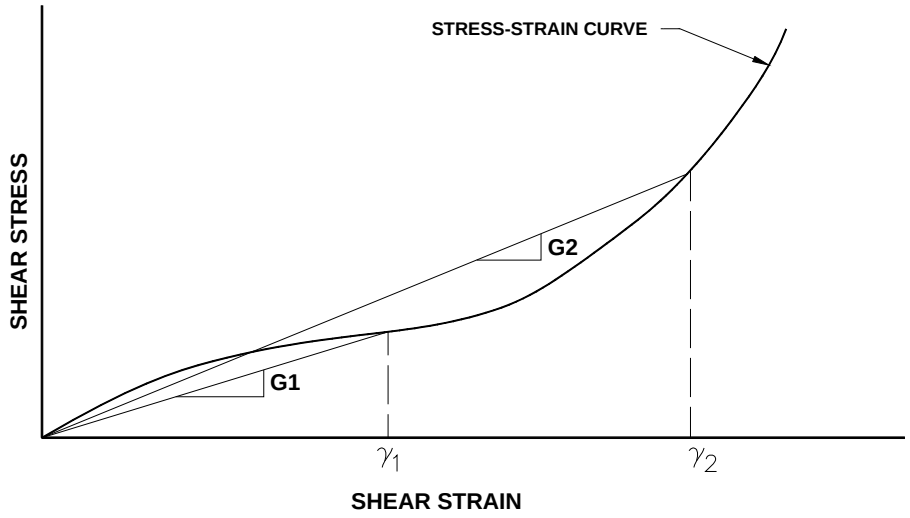

Figure 1-2: Definition of Shear Modulus (G1 and G2 are shear modulii at shear strains γ_1 and γ_2 respectively)

Table 1-2: Comparison of Mechanical Properties (compiled from various sources)

Property	Rubber (Typ.)	Metal (Typ.)	Glass (Typ.)
Density, lb./in^3	0.042	0.289	0.09
Elastic Modulus, psi	~ 500	~ 10^7	7 x 10^6
Breaking Extension, %	500 %	20%-50%	3 %
Elastic Limit, %	500 %	2%	3 %
Tensile Strength, psi	~ 10^3	8 x 10^4	2 x 10^5
Shear Modulus, psi	~150	~ 10^6	3 x 10^6
Bulk Modulus, psi	300000	~ 10^7	7 x 10^6
Poisson's Ratio	0.49	0.3	0.25
Specific Heat Btu/lbm-^{o}F	0.4	0.1	0.2
Thermal Conductivity Btu/hr-ft-^{o}F	0.1	31	0.8
Coefficient of Volume Expansion ^{o}F	4 x 10^{-5}	1.7 x 10^{-5}	1.1 x 10^{-5}

The behavior of a typical elastomeric pad in compression and shear is schematically shown in Figure 1-3. As the rubber layer is compressed, the free edges bulge out to maintain a constant volume. As a result of this bulging, localized shear strains and tensile strains are developed at the extreme fiber of the free edges. When the rubber is sheared a direct shear strain is developed that is inversely proportional to the rubber thickness. Thus, there are two types of shear strains that a rubber layer experiences under combined axial load and shear deformation:

- Direct shear strain due to shearing action,
- Indirect or bulge shear strain due to bulging action.

Since the bulk modulus is more or less constant relative to the shear modulus, the latter is the most important parameter that governs the structural behavior of an elastomeric bearing.

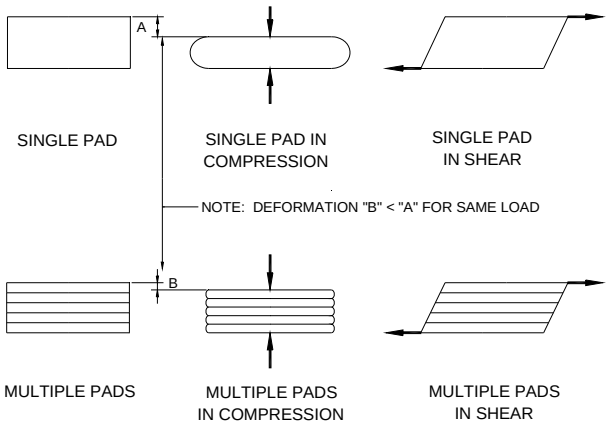

Figure 1-3: Behavior of Elastomeric Pad in Compression and Shear

As shown in Figure 1-3, the shape factor and consequently the vertical stiffness of a rubber block can be increased by inserting metal plates which divide the block into several layers. This provides constraints at the loaded surfaces of each layer and reduces the freedom of rubber to bulge. The shear stiffness is not altered by the presence of these horizontal plates. It is this feature of rubber layer and metal plate interaction that is used in bearing design to provide a high axial stiffness and high shear flexibility.

As mentioned earlier rubber has some undesirable characteristics that can affect the structural performance of an elastomeric bearing if not properly accounted. Some of these are briefly described below.

Non-Linear Stress-Strain Behavior

Rubber is isotropic and linearly elastic only in a very small deformation range. Figure 1-4 shows the shear stress-strain curves at room temperature while Figure 1-5 shows shear modulus versus shear strain curves for five types of rubber studied in this research. In these Figures NR, CR and NBR refer to natural rubber, neoprene and nitrile respectively. The numbers 50, 70 and 80 refer to the Shore A durometer reading which is a measure of hardness. The following points are noteworthy:

- The stress-strains curves are non-linear for all types of rubber, however the synthetic rubbers (neoprene and nitrile) show higher non-linearity as compared to the natural rubber.

- The shear modulus of natural rubber does not change with strain as much as that of neoprene and nitrile. The neoprene's shear modulus is high at large strains while the nitrile's shear modulus is high at low strains.
- A single shear modulus does not represent the entire elastic stress-strain behavior as in the case of metals and therefore most of the evaluation criteria for rubber are based on strains rather than stresses. The effects of non-linearity are more important for fatigue evaluation of laminates in bearings subjected to cyclic loading since the same strain fluctuations at different mean strain levels can result in very different stress ranges in laminates.

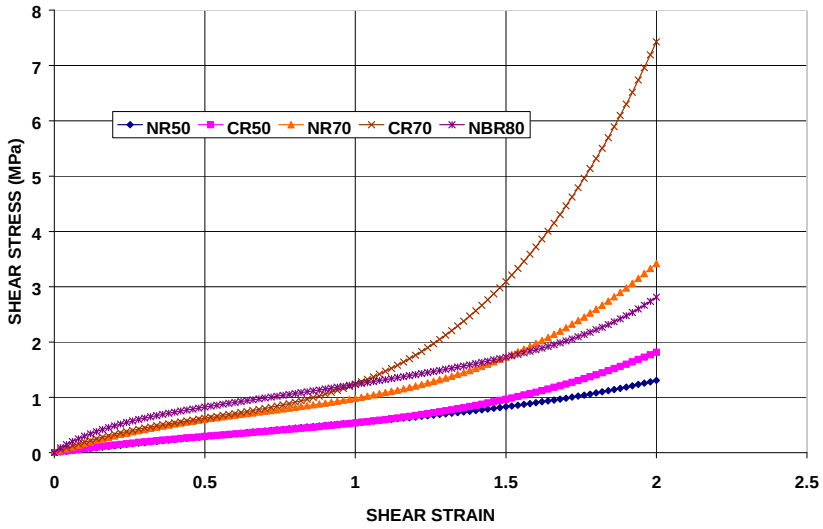

Figure 1-4: Stress-Strain Curve in Simple Shear for NR, CR and NBR (compiled from experiments conducted by author)

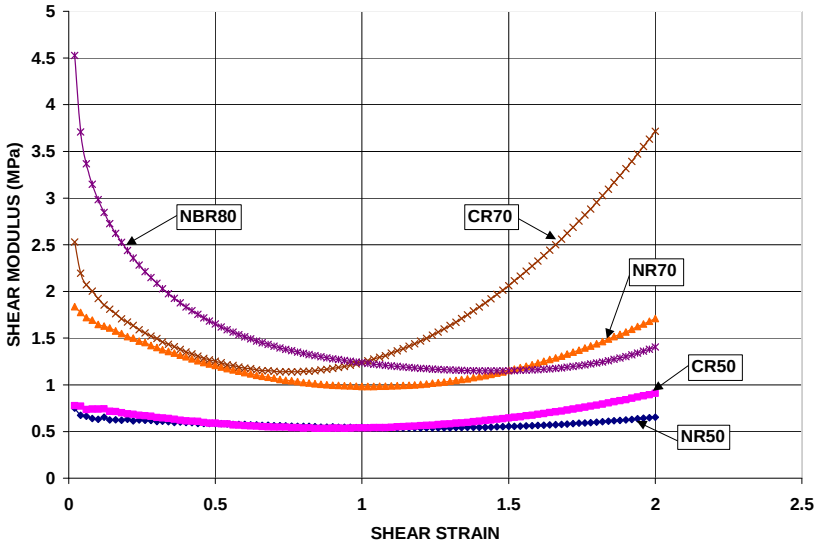

Figure 1-5: Variation of Shear Modulus with Shear Strain for NR, CR and NBR (compiled from experiments conducted by author)

Stress Softening

Rubber, especially when filled with reinforcing carbon black, softens when deformed. This phenomenon is often called the Mullins effect (Mullins and Tobin, 1965). When a filled rubber is extended to a strain ε_1, returned to zero strain and stretched again, the second stress-strain curve lies below the first one, but rejoins it at ε_1. This happens even if the specimen is retested after the first extension for an extended period of time in an attempt to ensure full recovery. Figure 1-6 shows the first six cycles of stress-strain behavior in shear for CR70 rubber.

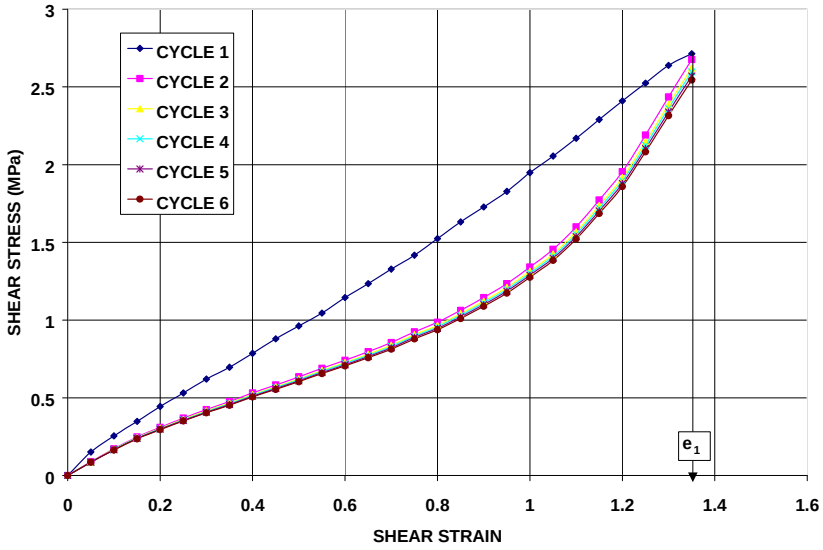

Figure 1-6: Stress Softening of CR70 in Shear (compiled from experiments conducted by author)

Notice that most of the change occurs during the first deformation, but small changes may still be detectable after many cycles. Since the laminate stresses increase as the shear modulus decreases, the effects of stress softening are more important in fatigue evaluation of laminates in bearings subjected to cyclic loading. To incorporate this behavior in the design and analysis of bearings, the shear modulus or material constants are derived using the sixth cycle data. This usually gives a softer material but one on which results are reproducible.

Creep and Stress Relaxation

All rubbers exhibit the characteristics of creep, or continuing time dependent deformation under constant load; and stress relaxation, or time dependent decay in stress at constant deformation. These phenomena occur whenever rubber is subjected to force or deformation of any magnitude, which

differentiates creep and stress relaxation in rubber from that in metal, where they only seem to occur under relatively large stresses and at high temperatures. This time dependent phenomenon makes the shear modulus time dependent. Figure 1-7 shows the relaxation of shear modulus with time at 50 percent strain for CR50 rubber. Notice that most of the relaxation occurs in the first few minutes of loading but small changes in shear modulus continue to occur with time. The consequences of creep and relaxation on the overall bearing performance include: (a) increase in axial displacement, (b) reduction in shear force and (c) increase in indirect shear strains and laminate stresses. From a performance point of view, increase in axial displacement is more important so long as internal stresses and strains are within allowable limits.

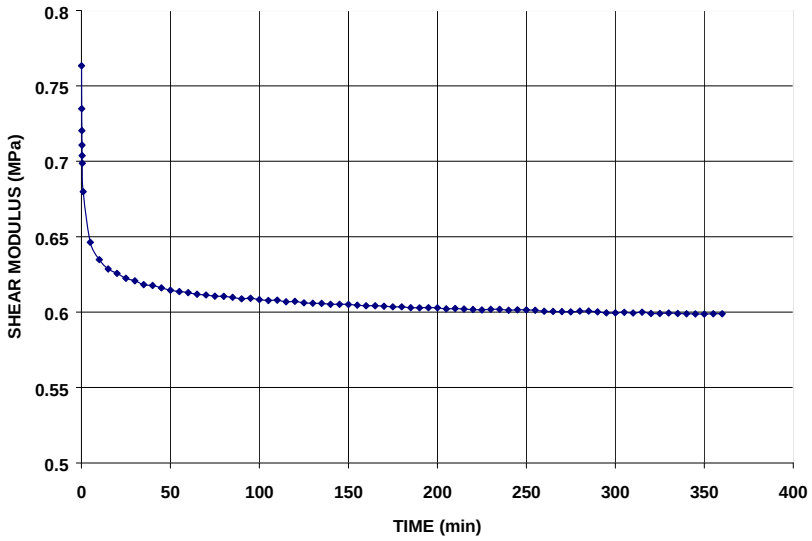

Figure 1-7: Relaxation of Shear Modulus at 50% Shear Strain for CR50 (compiled from experiments conducted by author)

Thermal Effects and Aging

All physical characteristics (elastic modulus, density, coefficient of thermal expansion, thermal conductivity, specific heat, creep etc.) of elastomers change with temperature, some to greater extent than others. However, distinction must be made between short-term and long-term effects of temperature. Short-term effects are generally physical and reversible while long-term effects are chemical and irreversible.

The most important characteristic from the point of view of a structural engineer is the dependence of mechanical response of elastomer layers on temperature changes. According to the kinetic-molecular theory of rubber elasticity, the elastic modulus of rubber increases as its temperature is increased. This is only valid when elastic behavior predominates. The most commonly used elastomers in bearings exhibit viscoelasticity and generally soften with an increase in temperature. Figure 1-8 shows the shear modulus versus shear strain curves for NR50 at various temperatures. Notice that the shear modulus in not as sensitive to temperature changes at higher temperatures as it is at lower temperatures. This phenomenon is more pronounced at low strains. At low temperatures the shear modulus of all types of rubber is very sensitive to temperature changes due to crystallization and vitrification, however, the change in modulus is higher in synthetic rubbers (neoprene and nitrile) as compared to natural rubber.

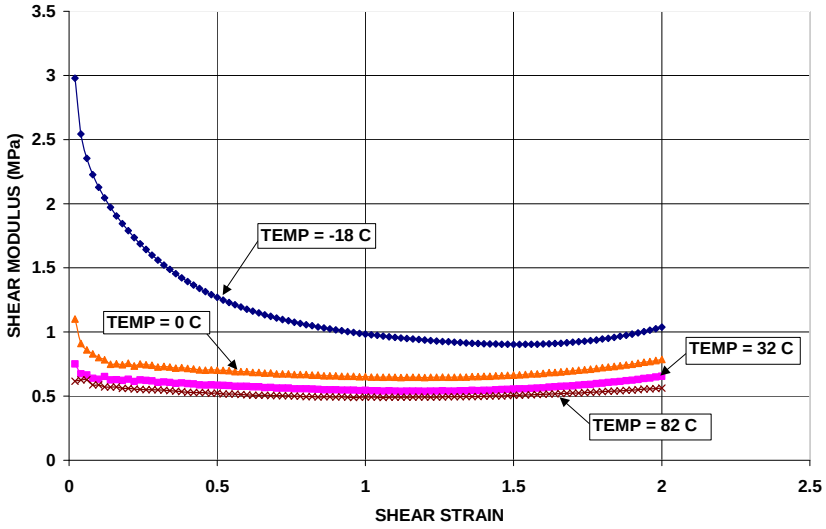

Figure 1-8: Shear Modulus of NR50 at Various Temperatures (compiled from experiments conducted by author)

At sufficiently elevated temperatures all types of rubber undergo degradation reactions leading to a loss of physical properties. Moderately elevated temperatures may cause the exchange of chains and a net formation of additional cross-links leading to some hardening of the rubber. At higher temperatures the scission of cross-links may outweigh cross-link formation with breakdown of the main chain and then charring and embrittlement of rubber. The presence of oxygen is a very important factor in determining the resistance of rubber to elevated temperatures. In the absence of oxygen, most types of rubber (including natural rubber) can survive temperatures up to 175^{o} C (Brown, 1996) when degradation would occur very rapidly in the presence of oxygen at this temperature.

Susceptibility to Chemical Attack and Explosive Decompression

Almost all elastomers are susceptible to chemical and physical effects arising from contact with fluids and gases. For elastomeric bearings used in offshore pipelines that are subjected to high internal pressure fluctuations, absorption of hydrocarbon liquids and gases can deteriorate the bearing performance in two ways:

- Chemical reaction between hydrocarbon and elastomer matrix can reduce the shear stiffness of the rubber.
- When the internal pressure is rapidly decreased, the explosive expansion of the absorbed gases within the elastomer causes internal rupture of the elastomer structure and potential damage known as Explosive Decompression Damage (EDD) to the rubber surfaces that may affect the load carrying capacity of the bearing. The primary damage occurs due to rapid inflation of small spherical voids, initially present at the time of cross-linking either in the form of submicroscopic bubbles of air trapped in rubber processing or in the form of badly wetted particles of dirt or dust.

Deterioration due to chemical reaction can be controlled by using the appropriate rubber that is resistant to thermal and chemical degradation. Explosive decompression on the other hand requires special design considerations.

1.1.3 Advantages of Elastomeric Bearings

In spite of some undesirable characteristics of rubber, a number of unique advantages offered by elastomeric bearings have made them ideally suitable for flexible joint applications. Some of these advantages are briefly described here.

Simple and Efficient Design

A simple one-piece elastomeric bearing can represent a complex universal joint with six degrees of freedom. The bearing performs as a "smart joint" with four independent nonlinear spring stiffnesses (axial, radial, rotation, and torsion). The ability to control the stiffness of this four-in-one spring gives the following unique options to the designers in their development of a structural system with optimum performance. Note that all four stiffnesses may not be important for a given application.

1. The stiffnesses can be designed so that the combined effect produces a restoring force required to return the bearing to a desired position.
2. By merely altering the number and thicknesses of rubber layers and bonded reinforcements, major changes in the spring rates can be achieved without changing the overall geometry.
3. The location of the center of reaction can be easily controlled by altering the cylindrical or spherical radius of the rubber layers and metal laminates.
4. The center of reaction can be located beyond the confines of the bearing to achieve an optimal interaction between various degrees of freedom.
5. The inherent damping characteristics of the rubber layers can be exploited to cushion the shock loads or isolate the vibrations.

6. The viscoelastic behavior of rubber can be exploited to achieve an optimal design for rate and time dependent loading.

No Maintenance

Since the bearing accommodates motion by simple flexing of its elastomer layers, there are no rolling and sliding elements as in more conventional joints. No lubrication or servicing of any kind is required since there is no friction or wear. The result is a connection that provides extremely long life and requires no maintenance of any kind.

High Durability and Reliability

Several case studies have shown that elastomeric bearings have been manufactured with consistent and dependable performance. There has been no evidence of any significant deterioration of these connections over their service lives.

1.1.4 Factors Affecting the Performance

No catastrophic failures of elastomeric bearings have been reported in open literature. Instead bearing failures are often attributed to excessive creep, slip, splitting, debonding, overstressing, and loss of vertical alignment (Stanton and Roeder, 1982). Although the causes of failure have never been precisely identified, the probable factors that affect the structural behavior and/or performance of an elastomeric bearing can be classified in three categories: (a) Structural Design (b) Manufacturing and (c) Environmental.

Several parameters, selected during the structural design phase, affect the performance of an elastomeric bearing. The most important are the material

properties of rubber (short term and long term modulii) and steel laminates (yield strength), shape factors of rubber layers, cover thickness, and boundary conditions. Elastomeric bearings are generally manufactured by fully vulcanized compression molding process. In this process, rubber in a semi-liquid or plastic condition is molded onto cleaned and adhesively-primed steel plates. The spacing between the steel plates is maintained with dowels, pins, or wedges. The assembly is then heated and pressed in a mold, which vulcanizes the rubber and cures the adhesive. The result is an integral rubber bearing. The most important performance related factors associated with the manufacturing of the laminated elastomeric bearings are uneven thickness of cover and rubber layers caused by misalignment of laminates. The most important environmental factors that can affect the performance of elastomeric bearings are: crack formation and growth due to ozone attack, chemical deterioration, aging and fluid/gas ingress. Bearings exposed to high- pressure fluid/gas environment can also be affected by explosive decompression damage.

1.2 OBJECTIVE

The objective of this dissertation is to study the importance of certain material and geometric parameters that potentially affect the short term and long term structural performance of steel laminated elastomeric bearings.

The present research focuses on the following four aspects with regard to the performance of elastomeric bearings:

- Misalignment of Laminates
- Creep

- Aging
- Explosive Decompression in an High Pressure Gaseous Environment

1.2.1 Misalignment of Laminates

Most of the steel laminated elastomeric bearings are manufactured using compression molding wherein the outside dimensions can be precisely controlled by the mold dimensions. However the internal steel laminates (also called shims or reinforcements) if not properly constrained, can shift horizontally, vertically or rotate due to the flow of rubber under pressure inside the mold. The most common external defects such as variation in overall horizontal and vertical dimension, overall horizontal and vertical slopes of surfaces, size and position of holes, slots, or inserts etc. can be easily inspected using the tolerances given in AASHTO M251-97. The effects of marginal laminate movement are more difficult to assess by merely external visual examination. AASHTO M251-97, Table 2 specifies certain tolerances on rubber layer thickness and cover thickness, however there has been no systematic study conducted to substantiate the validity of these tolerances. The dimensional and laminate misalignment tolerances as specified by AASHTO M251-97 are tabulated in Table 1-3. Steel laminated elastomeric bearings are sometimes rejected at the manufacturing stage because of failure to comply with these tolerances. The objective of the present study is to assess the effects of marginal laminate misalignments on the structural behavior of steel-laminated elastomeric bearings by means of computer simulated experiments using the finite element method and systematically develop limits on misalignments of steel laminates.

Table 1-3: Tolerances as per AASHTO M251-97, Table 2

Design Dimensions		Tolerances
Overall vertical dimensions	Design thickness 32 mm or less	-0, +3 mm
	Design thickness over 32 mm	-0, +6 mm
Overall horizontal dimensions	For measurements 914 mm or less	-0, +6 mm
	For measurements over 914 mm	-0, +12 mm
Thickness of individual layers of elastomer (laminated bearing only) at any point within the bearing		±20 percent of design value but no more than ±3 mm
Variation from a plane parallel to the theoretical surface (as determined by measurements at the edge of the bearings)	Top and Bottom	0.005 radians
	Sides	0.02 radians
Position of exposed connection members		±3 mm
Edge cover of embedded laminates or connection members		-0, +3 mm
Size of holes, slots, or inserts		±3 mm
Position of holes, slots, or inserts		±3 mm

1.2.2 Creep

The creep of elastomeric bearings has generally been studied by applying a constant load on full-scale bearing for a long period of time and measuring the deflection at specified intervals. Full-scale creep tests are time consuming, uneconomical and specific to the bearings tested. Detailed procedures on small-scale creep tests were not standardized internationally until ISO 8013, 1988, was published and there is still no general ASTM method. This reflects the relatively small amount of creep testing carried out on elastomers. The standardized creep tests are merely quality control tests and can not be used to predict the behavior of full-scale bearings because the shape factor, boundary conditions, loading conditions and exposure conditions (temperature etc.) of the full-scale bearings can vary considerably as compared to the test specimen. AASHTO 1992 Specifications has set criteria to evaluate creep for elastomeric bearings wherein creep deflection at 25 years expressed as percent of instantaneous deflection is

limited to 25 and 45 percent for 50 and 70 durometer bearings respectively. However, AASHTO has no test to check creep properties. The objective of the present study is to investigate the creep behavior of laminated elastomeric bearings and propose a practical method to predict creep of such bearings based on short-term small-scale testing.

1.2.3 Aging

There are several standardized tests available for quality control and for determining heat resistance or aging. ASTM D573, 1988, describes a test procedure based on accelerated heat aging to determine the influence of elevated temperature on the physical properties (hardness, elongation at break, tensile strength) of vulcanized rubber. The AASHTO elastomeric bearings material specification, M251 (1997) stipulates the use of ASTM D573 to assess the effect of aging on elastomeric bearings. Almost all accelerated aging tests mentioned in various specifications are performed on very thin specimens wherein the oxidation affects the whole specimen and the mode of loading is generally tension. Since aging is related to the oxidation process, the rate and extent of diffusion of oxygen through the elastomer governs the change in properties due to aging. The rate of diffusion is dependent on temperature, pressure, exposed surface area and permeability of elastomer. In the case of elastomeric bearings oxygen ingress is generally limited to a thin layer of exterior surface only because of small exposed surface area (relative to loaded area) and low permeability of elastomer. Moreover, for elastomeric bearings the change in overall shear stiffness due to aging is more relevant than the change in localized tensile

properties represented by the accelerated aging tests. The objective of the present study is to investigate the effect of specimen size on the change in shear characteristics due to accelerated aging and extrapolate the results to ambient temperatures for full size bearings. The terminal objective is to assess the validity of using standardized aging tests for evaluating the effects of aging on elastomeric bearings.

1.2.4 Explosive Decompression in an High Pressure Gaseous Environment

Currently there is no standard test method or analytical technique that can be used to assess the Explosive Decompression Damage (EDD) in elastomeric bearings exposed to sudden fluctuation of pressures commonly encountered in oil field applications. Some information is available on the explosive decompression failure of O-ring seals that behave very differently than elastomeric bearings. The objective of the present study is to develop a test method to assess EDD in elastomeric bearings and identify principal design variables that affect the extent and nature of the damage.

1.3 ORGANIZATION

This report consists of 6 Chapters, three Appendices and a Bibliography. The research on four aspects, listed in Section 1.2, laminate misalignment, creep, aging and explosive decompression damage is presented in Chapters 2, 3, 4 and 5 respectively. The justification for research and the literature review for each aspect are presented in the related chapter. The conclusions and recommendations for further research are presented in Chapter 6. Appendices A, B and C are supplements of Chapters 2, 3 and 5 respectively.

1.4 UNITS

SI units are used throughout this report. Unless otherwise specified the dimensions are given in millimeters (mm), temperature is given in Celsius (^{o}C), stress is given in mega-pascal (MPa), force is given in kilo-newton (KN) and the units of strain are dimensionless (length/length).

Chapter 2: Misalignments of Laminates

2.1 INTRODUCTION

Most of the steel laminated elastomeric bearings are manufactured using compression molding wherein the outside dimensions can be precisely controlled by the mold dimensions. However the internal steel laminates (also called shims or reinforcements) if not properly constrained, can shift horizontally, vertically or rotate due to the flow of rubber under pressure inside the mold. The most common external defects such as variation in overall horizontal and vertical dimension, overall horizontal and vertical slopes of surfaces, position of exposed connection members, size and position of holes, slots, or inserts etc. can be easily inspected. The effects of marginal laminate movement are more difficult to assess by merely external visual examination. The objective of this study is to assess the cumulative effects of most probable internal defects, caused by marginal laminate movements, on the performance of steel laminated elastomeric bearings.

Assuming that the outside dimensions are precisely controlled during molding, the three most probable laminate misalignments are as follows:

1. Vertical shift of laminates causing variations in rubber layer thickness.
2. Horizontal shift of laminates causing variations in external cover.
3. Rotation of laminates resulting in non-uniform rubber layers thickness.

Since the effects of laminate misalignments are difficult to measure directly, finite element computer simulation was used to study the combined effect of the above three probable misalignments on the overall structural

behavior of the bearing. As there can be a myriad of possibilities of the above misalignments, the range of each misalignment was selected based on tolerances of equipment used in molding process. The vertical shift was limited to ± 3 mm, the horizontal shift was limited to ± 6 mm and the angular rotation was limited to $\pm 1.5^{o}$. A two laminate, three rubber layers bearing configuration, shown in Figure 2-1 was used in the study. This configuration was selected because it is the simplest form representative of all laminated elastomeric bearings. Moreover, this configuration is adequate to show the significance of laminate misalignment on the overall structural behavior.

Bearings made from two types of elastomers: neoprene and natural rubber, at two hardness levels: Shore A Durometer 50 and 70 were analyzed. These two hardness levels were chosen since they represent extremes in material stiffness usually found in practice. Hereafter the 50 and 70 durometer neoprene bearings will be referred to as CR50 and CR70 respectively, while the 50 and 70 durometer natural rubber bearings will be referred to as NR50 and NR70 respectively.

Due to many uncertainities involved in modeling the friction between rubber and contacting surface, the top and bottom surfaces were assumed fully bonded for present sensitivity study. For the purpose of comparison with unbonded end conditions, the perfect bearing configuration with a constant coefficient of friction between the rubber surface and contacting surface were also analyzed.

The effects of misalignments were investigated under a combined Axial Load, Shear Deformation and Rotation of the bearing. For NR50 and CR50

bearings an Axial Load corresponding to 3.8 MPa (550 psi) axial stress in conjunction with a shear deformation corresponding to 50 percent direct shear strain and 1^o rotation was used. For NR70 and CR70 bearings an Axial Load corresponding to 7.6 MPa (1100 psi) axial stress in conjunction with a shear deformation corresponding to 50 percent direct shear strain and 1^o rotation was used.

Essentially this study was conducted as a set of computer simulated virtual experiments using the finite element method. The effect of three independent variables (horizontal shift, vertical shift and rotation of laminates) was studied on 8 dependent variables (that govern the structural behavior of the bearings) as follows:

1. Axial Stiffness
2. Shear Stiffness
3. Rotation Stiffness
4. Maximum Shear Strain in Elastomer
5. Maximum Principal Strain in Elastomer
6. Maximum Triaxial Tension in Elastomer
7. Maximum Bond Stress at the Interface of Elastomer and Steel Laminate
8. Maximum von Mises Stress in Steel Laminates

Section 2.2 presents the design of experiments. The evaluation criteria and constraints on the dependent variables are given in Section 2.3. The details of the finite element analysis are described in Section 2.4. The results of the statistical

analysis and development of laminate misalignment limits are given in Section 2.5. Finally the conclusions of this study are presented in Section 2.6.

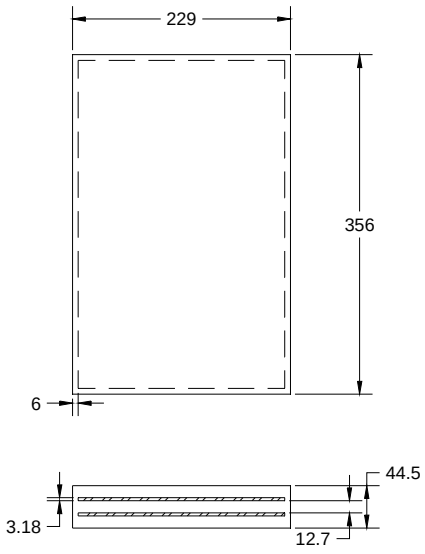

Dimensions shown in mm

Figure 2-1: Structural Configuration of Elastomeric Bearing

2.2 DESIGN OF VIRTUAL EXPERIMENTS

Since there are unlimited combinations of the three misalignments considered, a response surface methodology, generally used in statistical design and analysis of experiments (John, 1971), was used to find an approximating function relating various structural responses (dependent variables) to the combined effect of misalignments (independent variables). A Center Composite Design (CCD) was employed in selecting various runs and values of the three

independent variables. Assuming that the perfect bearing configuration is shown in Figure 2-1, let X1, X2 and X3 be the three independent variables as follows:

X1 = Change in vertical distance between 2 laminates (± 3 mm maximum) with overall vertical height constant. This represents the vertical shift of the laminates.

X2 = Variation in cover on one side (± 6 mm maximum) with overall horizontal dimensions constant. This represents the horizontal shift of the laminates.

X3 = Rotation of each laminate ($\pm 1.5^o$ maximum).

Let x1, x2 and x3 be the transformed values of X1, X2 and X3 respectively mapped to ± 1. CCD for 3 independent variables is a second order design consisting of three sets of points:

1. A 2^3 factorial design with $x_i = \pm 1$. These are called cube points and there are 8 of them.
2. A set of star or axial points. There are 6 such points, two on each axis at a distance α from the origin as shown in Figure 2-2.
3. Two center point representing a perfect bearing configuration.

In the present study $\alpha = \sqrt{3}$ is selected so that all the mapped points lie on the surface of a sphere with a radius equal to $\sqrt{3}$.

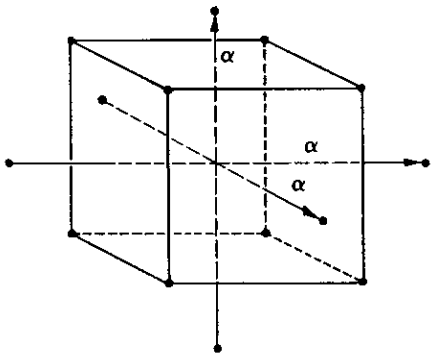

Figure 2-2: Center Composite Design for 3 Independent Variables

Figure 2-2 shows the CCD for three variables. Thus, there are total 16 runs (combinations of X1, X2 and X3). Table 2-1 shows the actual values of X1, X2 ,X3 and the corresponding mapped values x1,x2, x3 respectively for the 16 runs. The second order function relating the response (dependent variable) to the mapped independent variable is given by:

$$Y = a_0 + a_1 x_1 + a_2 x_2 + a_3 x_3 + a_4 x_1^{\,2} + a_5 x_2^{\,2} + a_6 x_3^{\,2} + a_7 x_1 x_2 + a_8 x_1 x_3 + a_9 x_2 x_3$$

(Eq. 2-1)

In the above equation the first term is the intercept, the next three are linear terms, the next three are quadratic terms and the last three are interaction terms. The relationship used for mapping X_i to x_i is given by:

$$x_i = \frac{2\alpha X_i}{\left(X_{\max_i} - X_{\min_i}\right)} - \frac{2\alpha X_{\min_i}}{(X_{\max_i} - X_{\min_i})} - \alpha \qquad \text{(Eq. 2-2)}$$

Here (X_{min} , X_{max}) for (i=1,2 and 3) are (-3,+3), (0,12) and (-1.5, +1.5) respectively.

A multivariate regression analysis was performed to calculate various coefficients in the above equation. The significance of each term was studied by means of ANOVA (analysis of variance). The results are presented in Section 2.5.

Table 2-1: Design Matrix for Independent Variables

RUN	Actual Values			Mapped Values		
	X_1 (mm)	X_2 (mm)	X_3 (Degrees)	x_1	x_2	x_3
1	-1.7321	2.5358	-0.86605	-1	-1	-1
2	1.7321	2.5358	-0.86605	1	-1	-1
3	-1.7321	9.4642	-0.86605	-1	1	-1
4	1.7321	9.4642	-0.86605	1	1	-1
5	-1.7321	2.5358	0.86605	-1	-1	1
6	1.7321	2.5358	0.86605	1	-1	1
7	-1.7321	9.4642	0.86605	-1	1	1
8	1.7321	9.4642	0.86605	1	1	1
9	3	6	0	1.732	0	0
10	-3	6	0	-1.732	0	0
11	0	12	0	0	1.732	0
12	0	0	0	0	-1.732	0
13	0	6	1.5	0	0	1.732
14	0	6	-1.5	0	0	-1.732
15,16	0	6	0	0	0	0

2.3 DEPENDENT VARIABLES AND EVALUATION CRITERIA

The structural behavior of the bearing is dependent on axial, shear and rotation stiffness while the structural integrity is controlled by the limits on internal stresses and strains. From a performance point of view the stiffnesses are more important as long as the internal stresses and strains remain within the allowable limits generally imposed by the strength of materials (elastomer and steel). Therefore to assess both structural behavior and structural integrity of the subject bearing configurations, the effects of three independent variables

described in Section 2-2, were studied on the eight dependent variables. The dependent variables and their evaluation criteria are described below.

2.3.1 Axial Stiffness (AXSTIF)

This represents the ratio of axial load to axial deflection at 3.8 Mpa (550 psi) and 7.6 Mpa (1100 psi) average axial stresses for 50 (NR50, CR50) and 70 (NR70, CR70) durometer bearings respectively. Vertical deflection of the bearing is controlled by axial stiffness, which is important for both single span and multi-span bridges. For single span bridges, excessive axial deflection at supports results in uneven road surface at the supports. Excessive vertical deflection at supports of multi-span bridges can result in excessive stress in girders. Based on past experience the variation of axial stiffness with respect to the axial stiffness of a perfect configuration was limited to ± 10 percent for evaluation purposes.

2.3.2 Shear Stiffness (SHRSTIF)

This represents the ratio of shear load to shear deflection corresponding to 0.5 (50 percent) direct shear strain. Since the shear deflection is caused by the thermal expansion or contraction of the bridge girder, the force transferred from bridge girder to its support is controlled by the shear stiffness of the bearing. Therefore, shear stiffness is also very important. Based on past experience the variation of shear stiffness with respect to the shear stiffness of a perfect configuration was limited to ± 10 percent for evaluation purposes.

2.3.3 Rotation Stiffness (ROTSTIF)

This represents the ratio of cocking moment to cocking rotation corresponding to 1^{o} rotation of the bearing. Since rotation stiffness of flat pads is

not very important no limit on its variation is imposed. For applications where rotational stiffness is important a cylindrical or spherical bearing is usually used.

2.3.4 Maximum Shear Strain in Elastomer (SHSTRN)

This represents the total of direct and indirect shear strain. As mentioned in Chapter 1, there are two types of shear strain that a rubber layer experiences under combined axial load and shear deformation: (a) direct shear strain due to shearing action and (b) indirect or bulge shear strain due to bulging action. As per good engineering practice used in the rubber bearing industry (based on collective experience of several bearing manufacturers), the direct shear strain is limited to 1.75 (175 percent) while the indirect shear strain is limited to 6 (600 percent) for occasional loads. The direct and indirect shear strains are combined to get total shear strain. In the present study since the direct shear strain is just 0.5 (50 percent), the total shear strain is limited to 6 (600 percent).

2.3.5 Maximum Principal Strain in Elastomer (PRNSTN)

This represents the maximum uniaxial strain in elastomer. The maximum allowable uniaxial tensile strain in elastomer layers is limited to 2 (200 percent).

2.3.6 Triaxial Tension in Elastomer (TENS)

The maximum triaxial tension in rubber is limited to 6 times the design shear modulus as per good engineering practice used in rubber industry. Rubber is commonly found to undergo internal cavitation at triaxial tension equivalent to 6G, where G is the linear shear modulus. This phenomenon is a consequence of an elastic instability known as "an unbounded elastic expansion of preexisting cavities, too small to be readily detected" (Gent and Tompkins, 1969). The critical

stress does not depend on the strength of the rubber but only on its elastic modulus.

2.3.7 Maximum Bond Stress (BOND)

This represents the resultant of the tensile stress and shear stress carried at the interface nodes of the elastomer and the steel. This stress is limited to the average shear stress corresponding to a shear strain of 2 (200 percent) as calculated from a simple shear test. The simple shear test results for the subject elastomers are shown in Figures 2-6 through 2-9.

2.3.8 Maximum von Mises Stress in Steel Laminates (MISES)

This represents the stress in laminates corresponding to von Mises failure (yield) theory. In this theory, yielding occurs when, at any point in the laminate, the distortion energy per unit volume in a state of combined stress becomes equal to that associated with yielding in a simple tension test. Mathematically this can be expressed as:

$$(\sigma_1 - \sigma_2)^2 + (\sigma_2 - \sigma_3)^2 + (\sigma_3 - \sigma_1)^2 = 2\sigma_{yp}^2 \qquad \text{(Eq. 2-3)}$$

where $\sigma_1, \sigma_2, \sigma_3$ are the maximum, intermediate and minimum principal stresses respectively and σ_{yp} is the yield strength of the material. The von Mises stress, σ, given by the following expression, calculated from the finite element analyses is limited to the yield strength of the steel laminates.

$$\sigma = \sqrt{\frac{(\sigma_1 - \sigma_2)^2 + (\sigma_2 - \sigma_3)^2 + (\sigma_3 - \sigma_1)^2}{2}} \qquad \text{(Eq. 2-4)}$$

The constraints imposed on dependent variables based on the evaluation criteria for the subject bearings are summarized in Table 2-2.

Table 2-2: Constraints on Dependent Variables

Dependent Variables	Constraints			
	NR50	CR50	NR70	CR70
AXSTIF (kN/mm)	186-227	190-232	342-418	395-483
SHRSTIF (kN/mm)	0.86-1.05	0.86-1.05	1.64-2.0	1.87-2.28
ROTSTIF (kN-m/deg)	No constraint	No constraint	No constraint	No constraint
SHSTRN	< 6	< 6	< 6	< 6
PRNSTN	< 2	< 2	< 2	< 2
TENS (Mpa)	< 3.5	< 3.53	< 7.2	< 7.5
BOND (Mpa)	< 1.31	< 1.81	< 3.4	< 7.4
MISES (Mpa)	< 345	< 345	< 345	< 345

2.4 FINITE ELEMENT ANALYSIS

2.4.1 Finite Element Models

Since rubber is an almost incompressible material, the finite element model of the rubber portion was prepared using three-dimensional 27 node second order solid hybrid finite elements. In this type of elements, pressure degrees of freedom are added to enforce a linear pressure variation inside the finite element such that incompressible material behavior is appropriately incorporated. The hybrid elements are mixed formulation elements, using a mixture of displacement and stress variables with an augmented variational principle to approximate the equilibrium equations and compatibility conditions (ABAQUS, Theory Manual). The steel parts were modeled using three-dimensional 27 node second order solid finite elements. Figure 2-3 shows the general configuration of the finite element used in the analysis. The finite element model for the perfect configuration is shown in Figure 2-4. The finite element models for the 16 configurations

tabulated in Table 2-1 are shown in Figure 2-5. Notice that only half of the bearing was modeled due to the symmetry of geometry and loading. Symmetric boundary conditions were applied at the plane of symmetry.

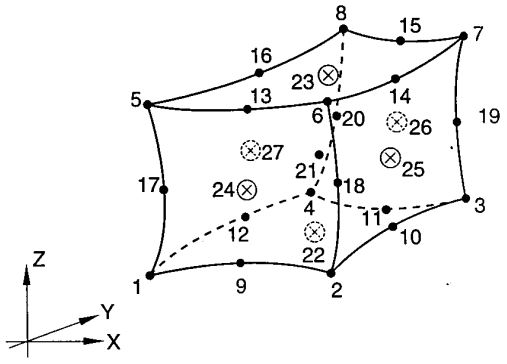

Figure 2-3: 27 node Finite Element

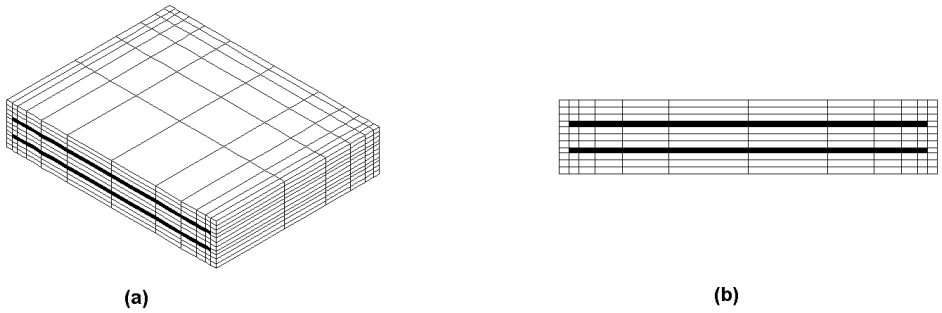

(a) Isometric View, (b) Cross-Section

Figure 2-4: Finite Element Model of Perfect Configuration

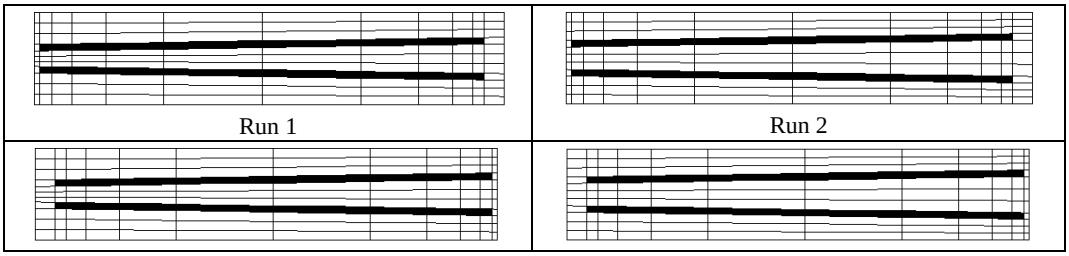

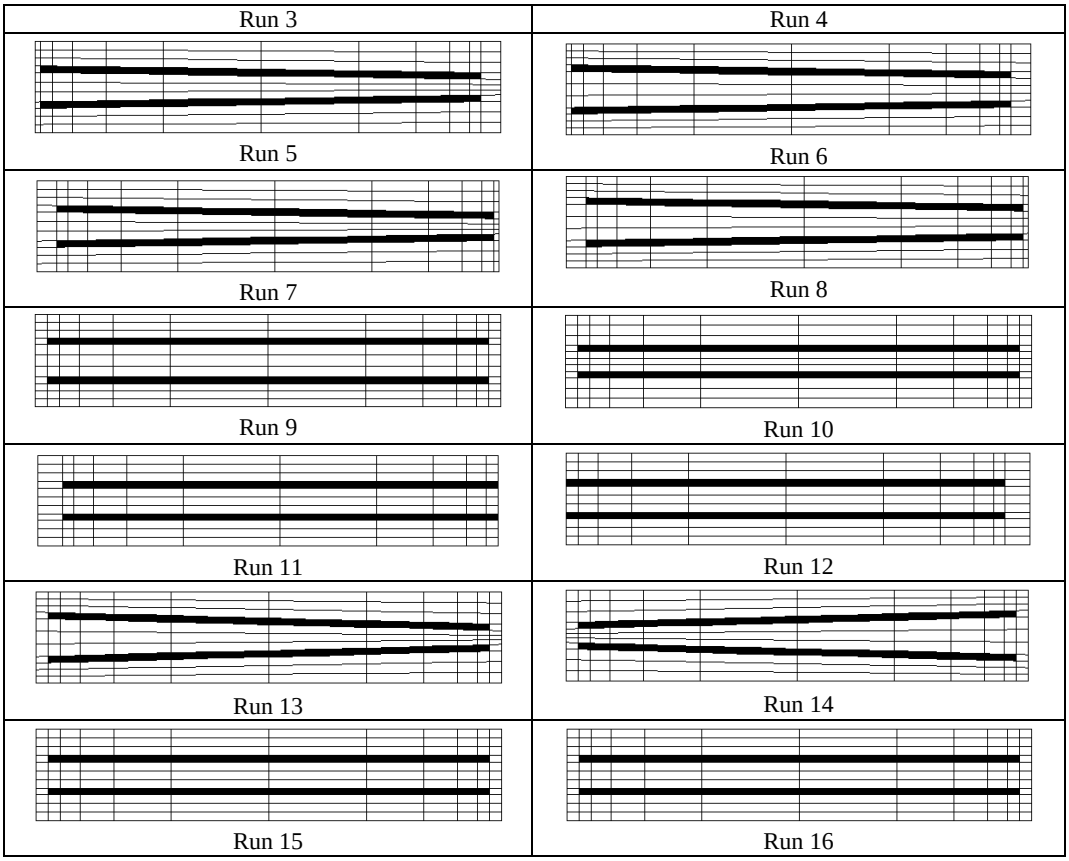

Figure 2-5: Cross-Section of Finite Element Models for Various Runs

2.4.2 Material Models

The hyper-elasticity of the rubber was modeled using Yeoh's approximation (Yeoh, 1993) to Rivilin's formulation (Rivilin, 1956). According to Rivilin's theory, stress-strain behavior depends on the partial derivatives, $\frac{\partial W}{\partial I_1}$ and $\frac{\partial W}{\partial I_2}$, where W is the strain energy density and I_1, I_2 are the strain invariants of the Green deformation tensor. In order to characterize the elastic properties of rubber, $\frac{\partial W}{\partial I_1}$ and $\frac{\partial W}{\partial I_2}$ are determined from experimental measurements.

Generally, it is not possible to determine $\frac{\partial W}{\partial I_1}$ and $\frac{\partial W}{\partial I_2}$ separately from measurements in any one single deformation mode (Kawabata and Kawai, 1977). The required experiments are difficult and the errors are correspondingly large (Rivilin and Saunders, 1951). Since $\frac{\partial W}{\partial I_2}$ is much smaller than $\frac{\partial W}{\partial I_1}$, Yeoh, 1990, assumed $\frac{\partial W}{\partial I_2} = 0$. This simplifies the problem considerably since I_2 is now irrelevant. Substituting $\frac{\partial W}{\partial I_2} = 0$ in Rivilin's formulation and truncating the series after three terms, we get Yeoh's cubic equation (Yeoh, 1990).

$$W = C_{10}(I_1 - 3) + C_{20}(I_1 - 3)^2 + C_{30}(I_1 - 3)^3 \qquad \text{(Eq. 2-5)}$$

Yeoh's approximation is very attractive for practical problems. It describes a material whose secant shear modulus depends on shear strain in a relatively simple form. In simple shear the shear stress, τ, is related to the shear strain, γ, by

$$\frac{\tau}{\gamma} = 2\left[\frac{\partial W}{\partial I_1} + \frac{\partial W}{\partial I_2}\right] \qquad \text{(Eq. 2-6)}$$

So, if $\frac{\partial W}{\partial I_2} = 0$, the secant shear modulus is given by,

$$\frac{\tau}{\gamma} = 2\left[\frac{\partial W}{\partial I_1}\right] = 2C_{10} + 4C_{20}(I_1 - 3) + 6C_{30}(I_1 - 3)^2 \qquad \text{(Eq. 2-7)}$$

The coefficients C_{10}, C_{20} and C_{30}, in Equation 2-7 were obtained by mean of non-linear regression analysis of experimental data in simple shear. It must be

noted here that a constant bulk modulus of 2100 MPa was assumed. One more term was added to Equation 2-5 to account for finite bulk modulus effects. The strain energy density equation used in the finite element analysis is as follows:

$$W = C_{10}(I_1 - 3) + C_{20}(I_1 - 3)^2 + C_{30}(I_1 - 3)^3 + \frac{K}{2}(J - 1)^2 \qquad \text{(Eq. 2-8)}$$

where, K is the bulk modulus and (J-1) is the volume change per unit volume. The stress-strain curves in simple shear were experimentally obtained using a molded shear specimen described in Chapter 3. The stress-strain curves were obtained at nominal exposure temperature (32^o C) using a strain controlled loading system. The test set-up was same as shown in Chapter 3. The test data and non-linear regression analysis results are shown in Figures 2-6 through 2-9 for NR50, CR50, NR70 and CR70 respectively. The material constants C_{10}, C_{20} and C_{30} are tabulated in Table 2-3.

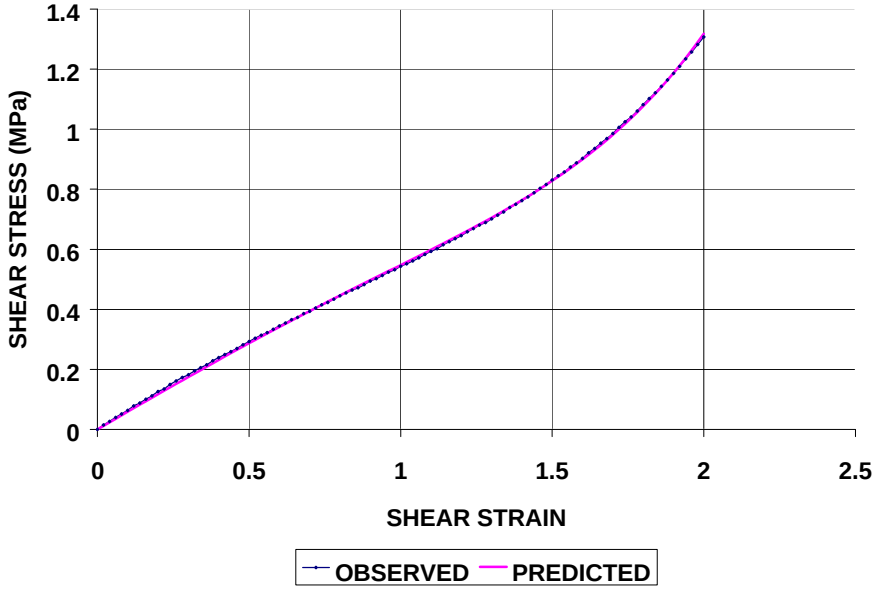

Figure 2-6: Observed Data and Regression Analysis Results for NR50

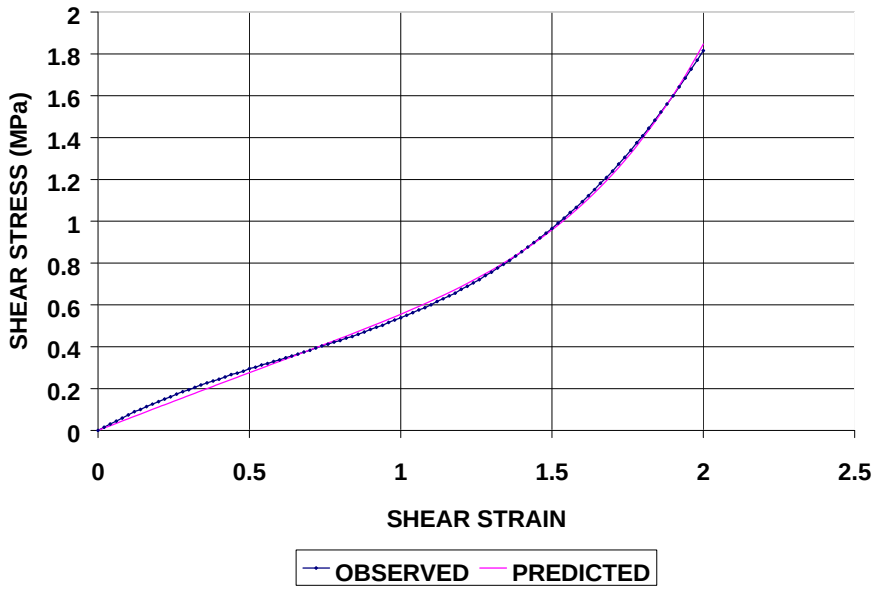

Figure 2-7: Observed Data and Regression Analysis Results for CR50

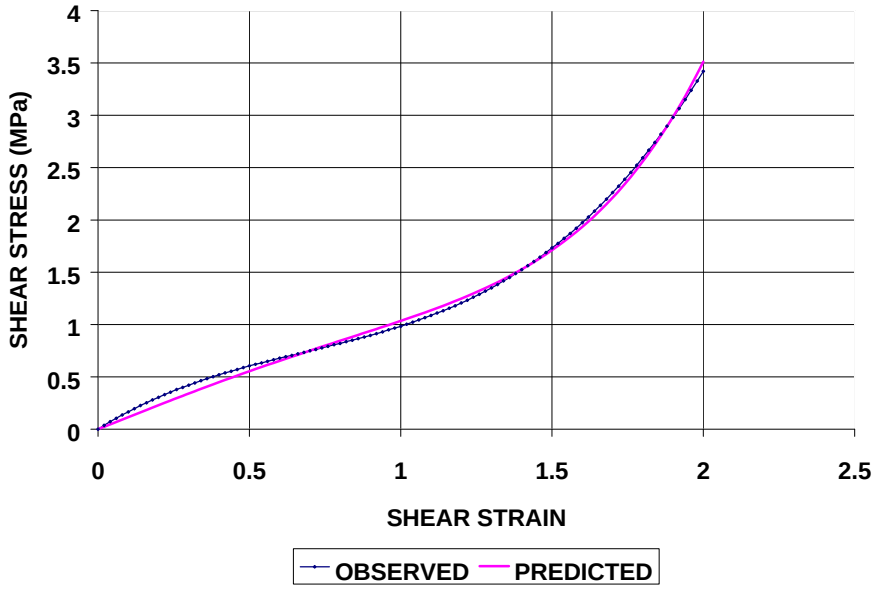

Figure 2-8: Observed Data and Regression Analysis Results for NR70

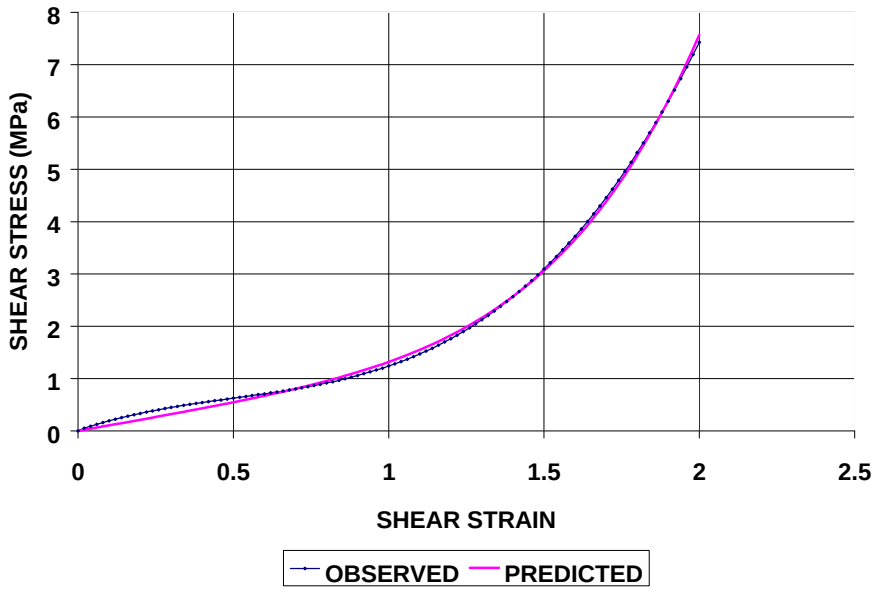

Figure 2-9: Observed Data and Regression Analysis Results for CR70

Table 2-3: Material Coefficients used in Finite Element Analysis

Elastomer	Material Coefficients (MPa)		
	C_{10}	C_{20}	C_{30}
NR50	0.2937	-0.0148	0.003212
CR50	0.2799	-0.009054	0.005299
NR70	0.5763	-0.05169	0.0149
CR70	0.5275	0.03126	0.02323

The steel components were modeled using isotropic material with Young's Modulus equal to 200000 MPa and a Poison's ratio equal to 0.3. A bi-linear, stress-strain curve (first line connecting 0 and yield point (345 MPa) and the second line connecting yield point to ultimate (490 MPa) at 30 percent elongation) was used to define the plastic behavior of steel. Since high

temperature creep effects were not important in this case, classical metal plasticity using standard von Mises yield surface model with associated plastic flow was utilized to include plasticity effects (ABAQUS, Theory Manual). Associated plastic flow means that, as the material is yielding, the inelastic deformation rate is in the direction of the normal to the yield surface. Isotropic strain hardening was used to define the change in yield surface with plastic straining. Isotropic hardening means that the yield surface changes size uniformly in all directions, so that the yield stress increases (or decreases) in all strain directions as plastic straining occurs.

2.4.3 Analysis Procedure

ABAQUS, a general purpose finite element code was used for the finite element analyses. Structural analyses consisted of nonlinear quasi-static analysis with geometric and material nonlinearities to incorporate the effects of large deformation and large strains. Nonlinear static analyses required the solution of nonlinear equilibrium equations, for which Newton-Rapson numerical method was used. The solution was obtained as a series of increments, with iterations within each increment to obtain equilibrium. Since several nonlinearities were acting simultaneously, the loads were applied in small increments to assure correct modeling of history dependent effects and to increase the computational efficiency.

2.4.4 Finite Element Analysis Results

The values of 8 dependent variables, mentioned in Section 2-3, extracted from finite element analyses of bearings with bonded top and bottom surfaces for

the 16 runs are tabulated in Tables 2-4 through 2-7 for NR50, CR50, NR70 and CR70 respectively. The effect of axial load variation on internal stresses and strains in bearings with perfect configuration is shown in Table 2-8. A comparison between perfect bearing configurations with bonded and unbonded top and bottom surfaces in terms of 8 dependent variables is shown in Table 2-9. The displacement plots and key contour plots for perfect configuration with bonded top and bottom surfaces are shown in Figures 2-10 through 2-13 for NR50, CR50, NR70 and CR70 respectively. Similar plots for unbonded end conditions with a constant coefficient of friction equal to 0.3 between rubber and contacting top and bottom surfaces are shown in Figures 2-14 through 2-17 for NR50, CR50, NR70 and CR70 respectively. For all sixteen configurations, the deformed shapes and stress contours for NR50 are given in Appendix A.

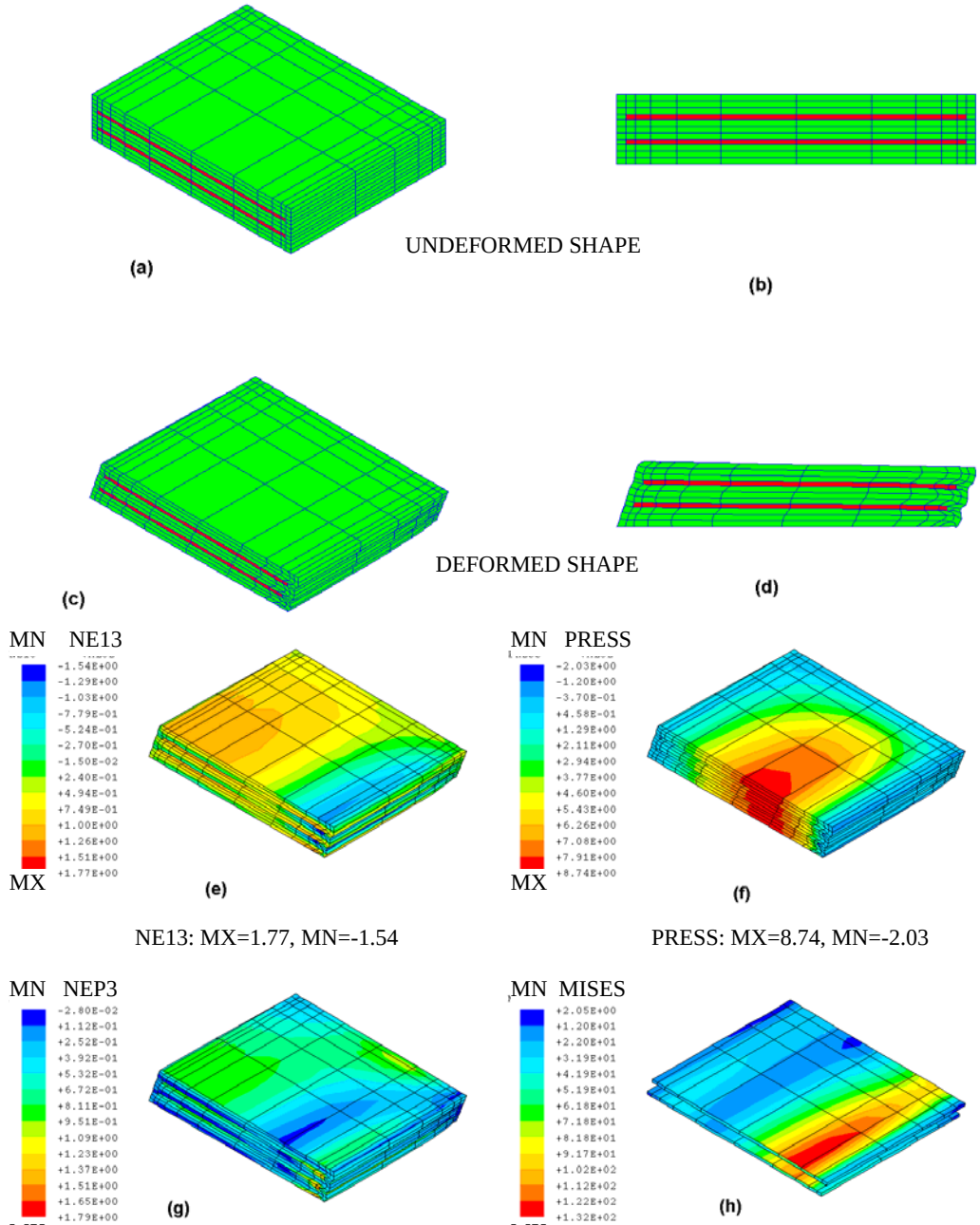

(a), (b) undeformed shape; (c), (d) deformed shape; (e) shear strain in rubber; (f) triaxial stress in rubber (MPa); (g) maximum principal strain in rubber; (h) von Mises Stress in laminates (MPa)

Figure 2-10: NR50 Perfect Configuration - Bonded Top and Bottom Surfaces

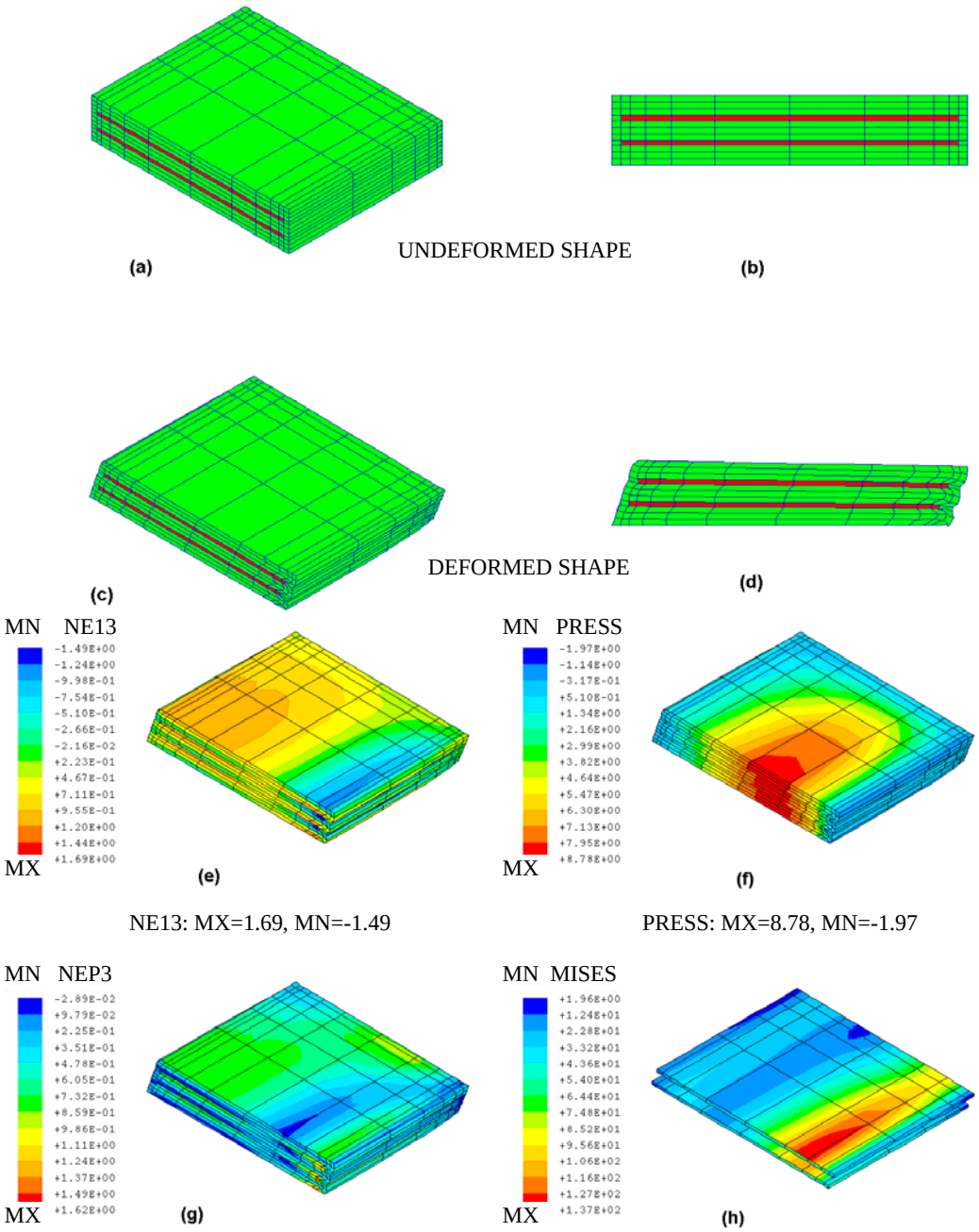

NE13: MX=1.69, MN=-1.49

PRESS: MX=8.78, MN=-1.97

NEP3: MX=1.62, MN=-0.029

MISES: MX=137, MN=1.96

(a), (b) undeformed shape; (c), (d) deformed shape; (e) shear strain in rubber; (f) triaxial stress in rubber (MPa); (g) maximum principal strain in rubber; (h) von Mises Stress in laminates (MPa)

Figure 2-11: CR50 Perfect Configuration - Bonded Top and Bottom Surfaces

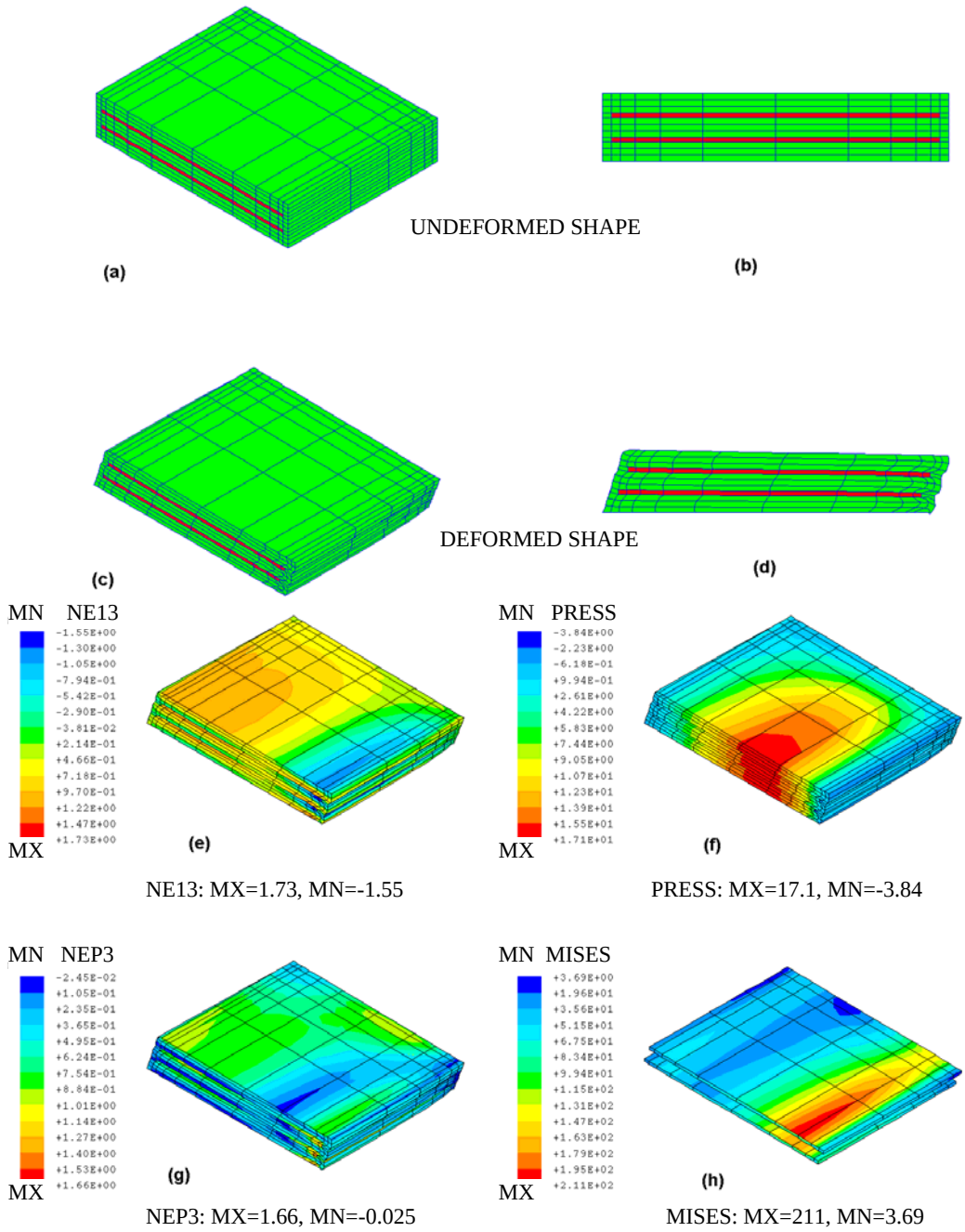

(a), (b) undeformed shape; (c), (d) deformed shape; (e) shear strain in rubber; (f) triaxial stress in rubber (MPa); (g) maximum principal strain in rubber; (h) von Mises Stress in laminates (MPa)

Figure 2-12: NR70 Perfect Configuration - Bonded Top and Bottom Surfaces

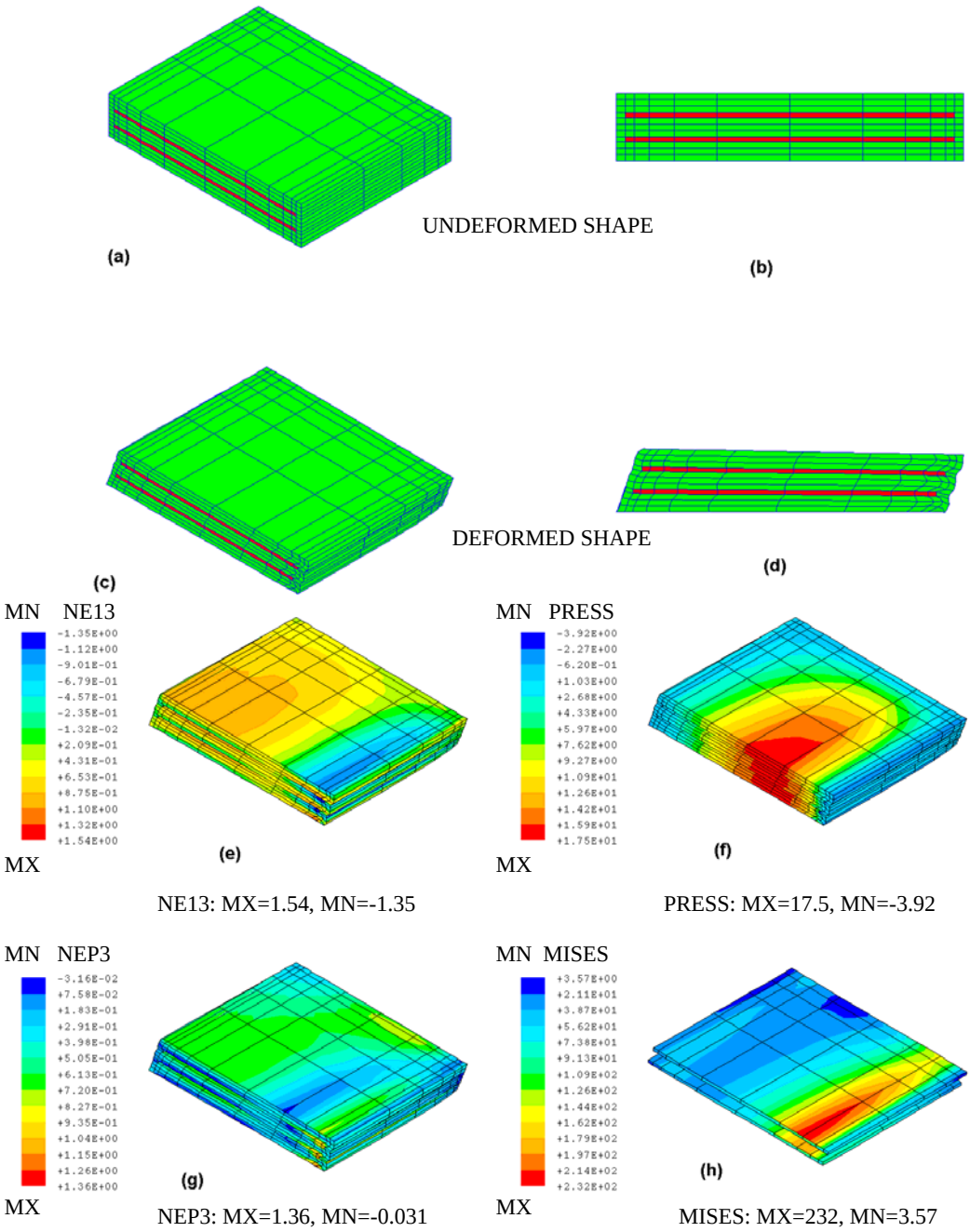

(a), (b) undeformed shape; (c), (d) deformed shape; (e) shear strain in rubber; (f) triaxial stress in rubber (MPa); (g) maximum principal strain in rubber; (h) von Mises Stress in laminates (MPa)

Figure 2-13: CR70 Perfect Configuration - Bonded Top and Bottom Surfaces

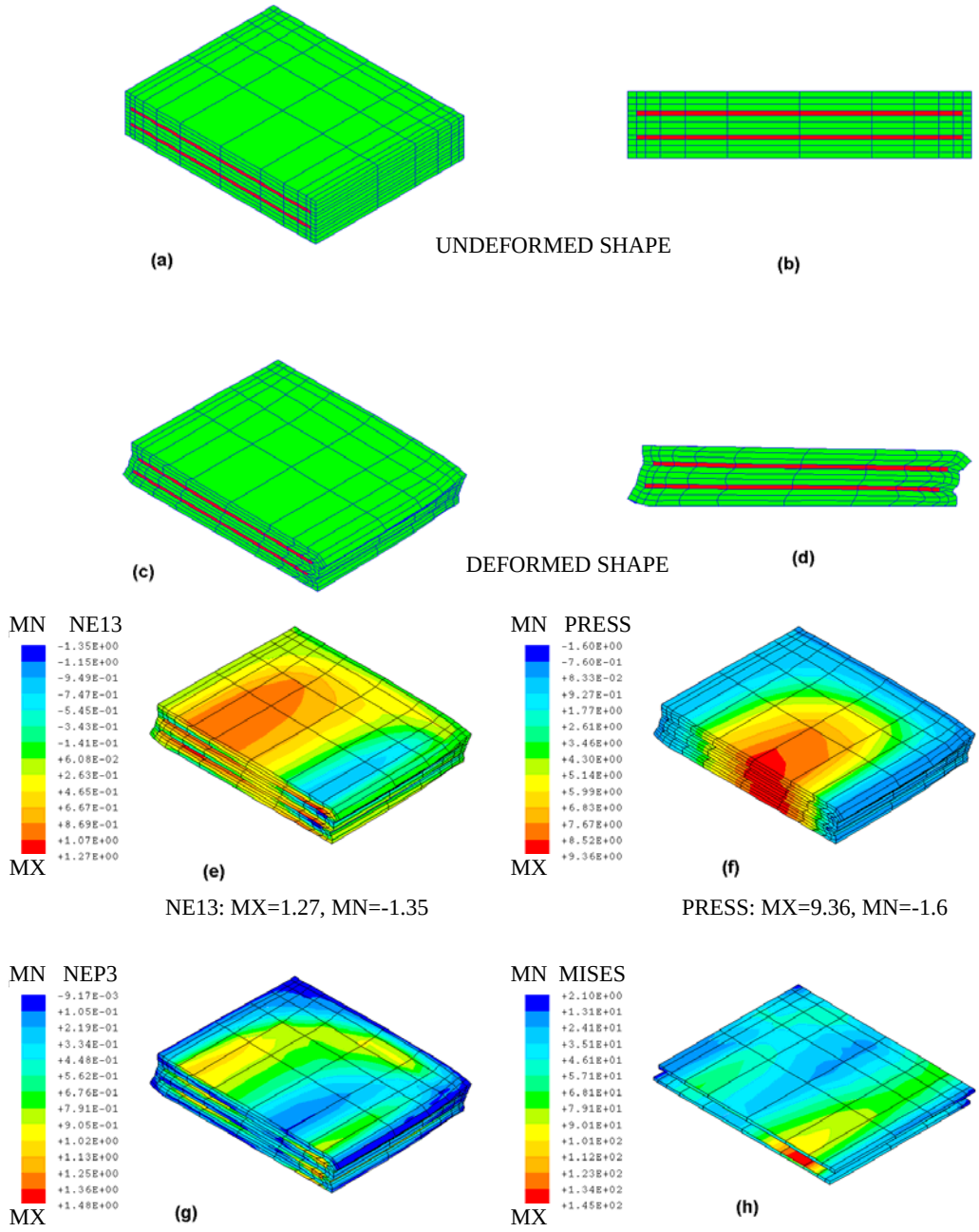

(a), (b) undeformed shape; (c), (d) deformed shape; (e) shear strain in rubber; (f) triaxial stress in rubber (MPa); (g) maximum principal strain in rubber; (h) von Mises Stress in laminates (MPa)

Figure 2-14: NR50 Perfect Configuration - Unbonded Top and Bottom Surfaces

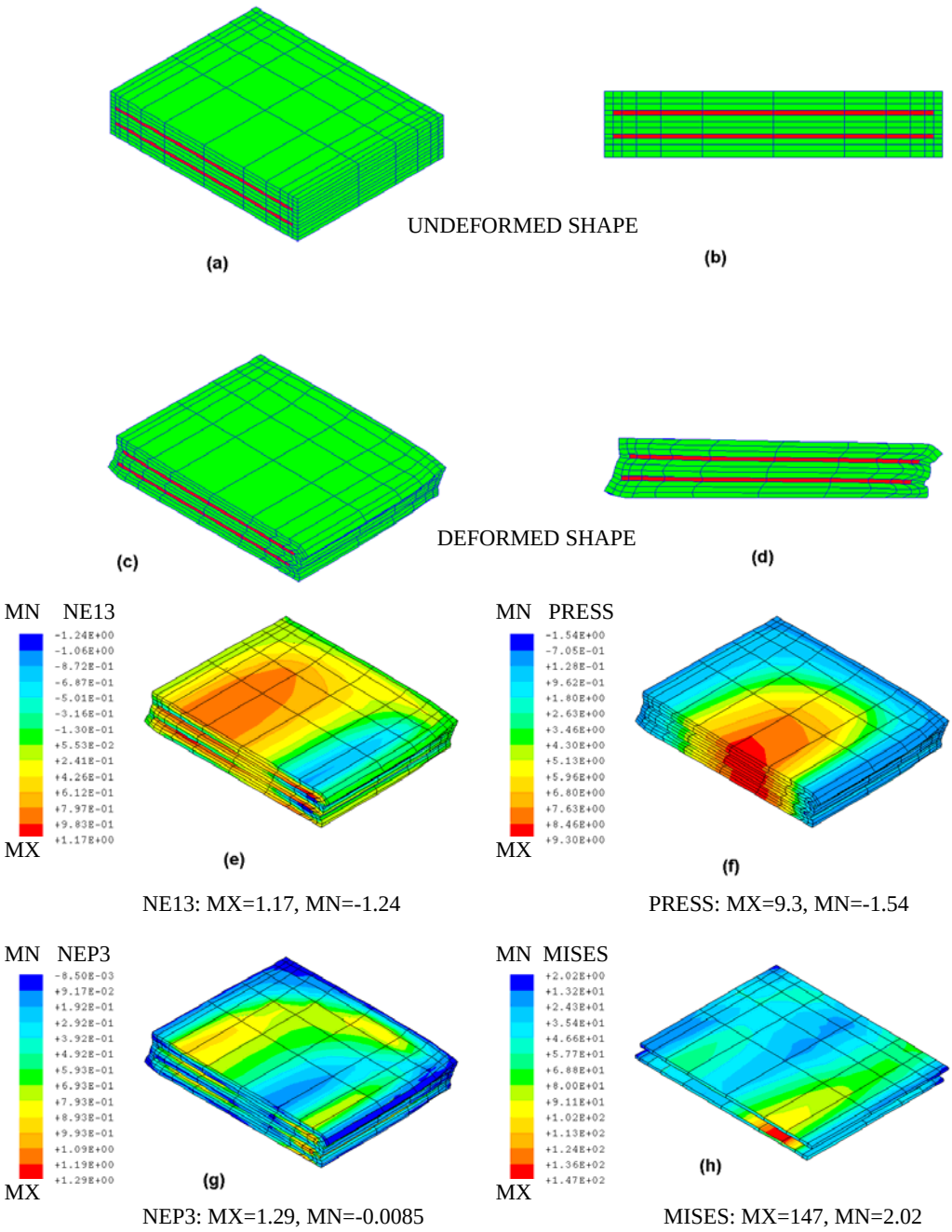

(a), (b) undeformed shape; (c), (d) deformed shape; (e) shear strain in rubber; (f) triaxial stress in rubber (MPa); (g) maximum principal strain in rubber; (h) von Mises Stress in laminates (MPa)

Figure 2-15: CR50 Perfect Configuration - Unbonded Top and Bottom Surfaces

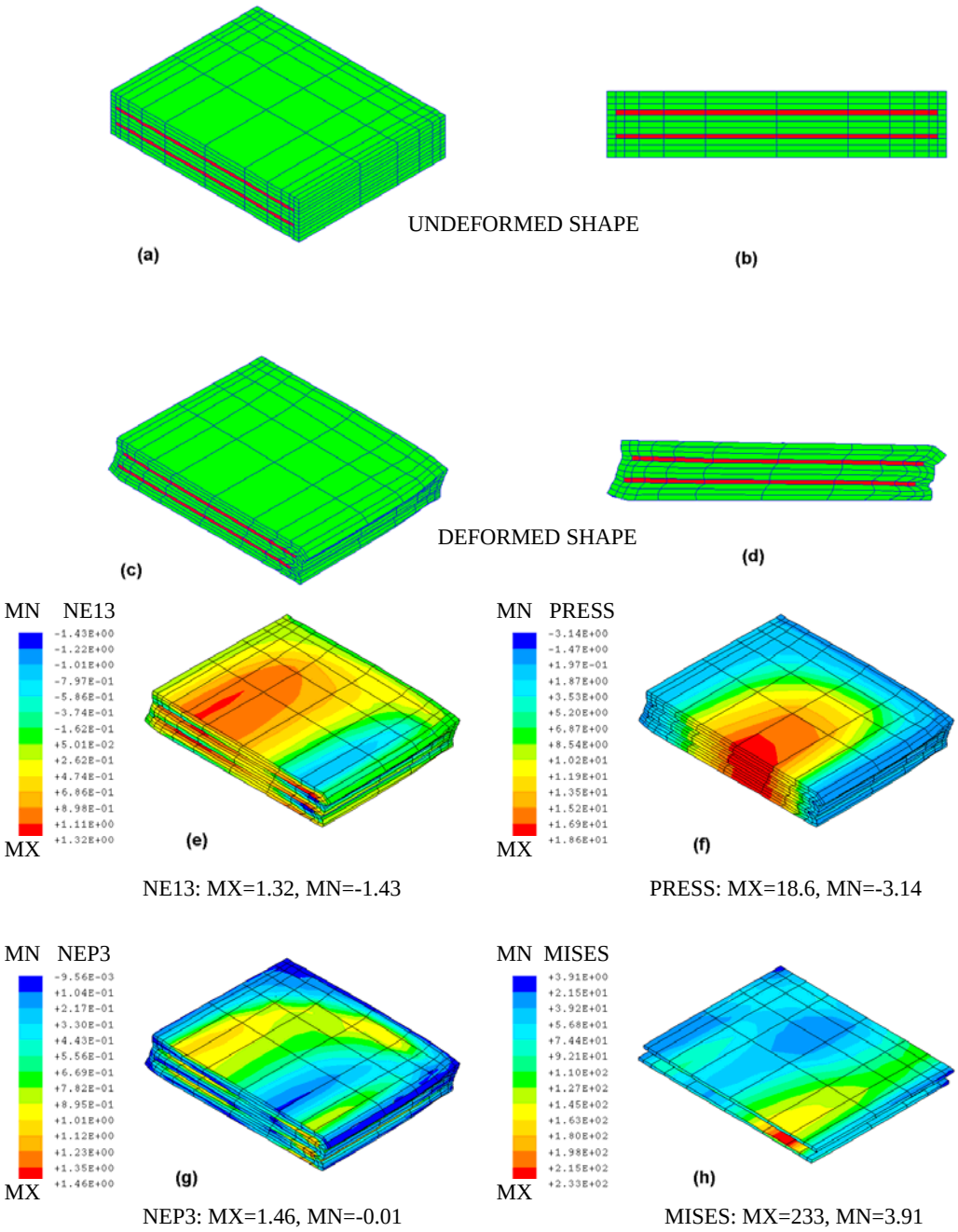

(a), (b) undeformed shape; (c), (d) deformed shapes; (e) shear strain in rubber; (f) triaxial stress in rubber (MPa); (g) maximum principal strain in rubber; (h) von Mises Stress in laminates (MPa)

Figure 2-16: NR70 Perfect Configuration - Unbonded Top and Bottom Surfaces

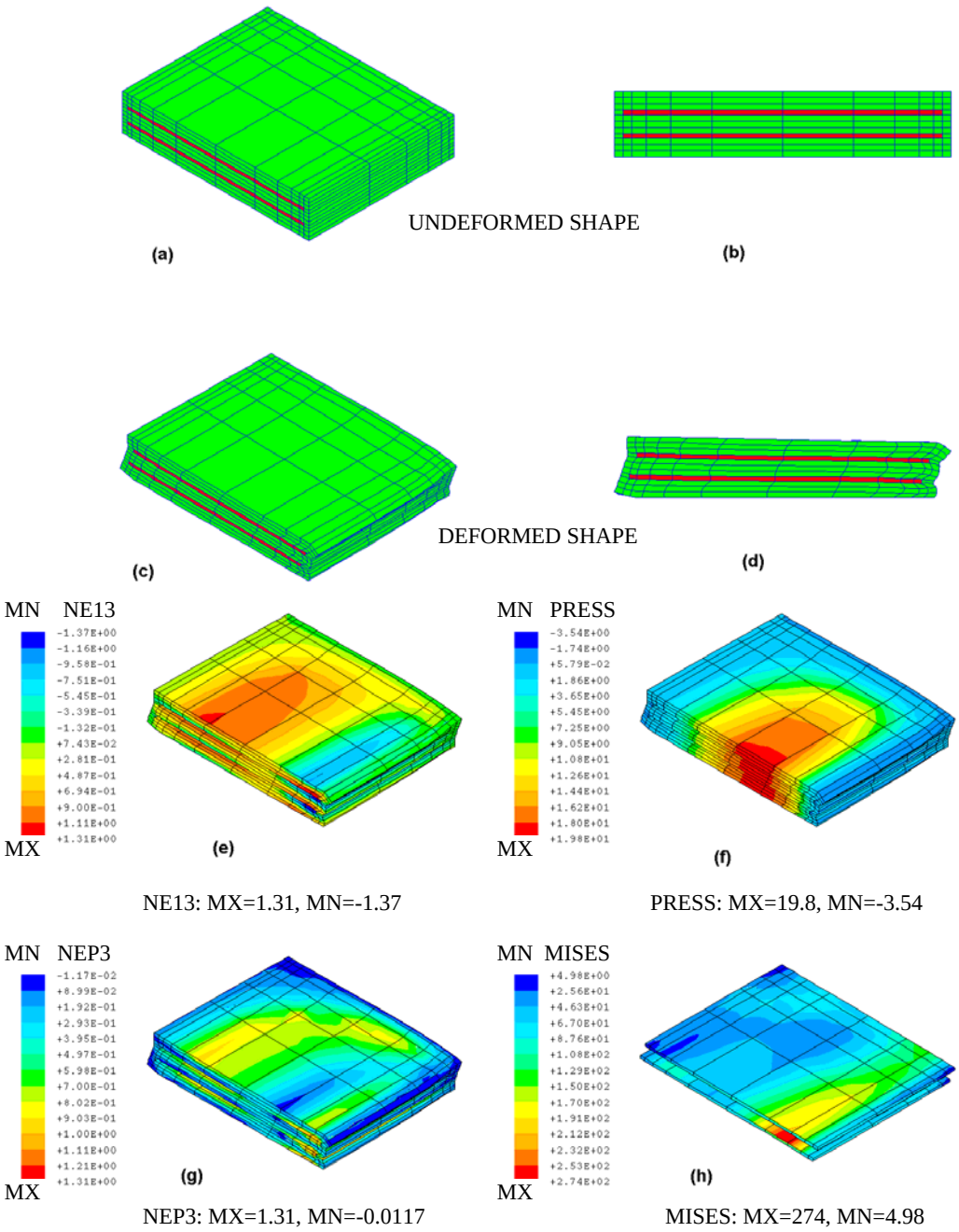

(a), (b) undeformed shape; (c), (d) deformed shape; (e) shear strain in rubber; (f) triaxial stress in rubber (MPa); (g) maximum principal strain in rubber; (h) von Mises Stress in laminates (MPa)

Figure 2-17: CR70 Perfect Configuration - Unbonded Top and Bottom Surfaces

Table 2-4: Values of Dependent Variables for NR50

Run	Axial Stiffness KN/mm	Shear Stiffness kN/mm	Rotation Stiffness kNm/deg	Max. Shear Strain in Rubber	Max. Principal Strain in Rubber	Max. Triaxial Stress in Rubber MPa	Max. Bond Stress (Steel and Rubber) MPa	Max . von Mises Stress in Laminate MPa
1	193.30	0.98761	2.06	1.74	1.81	1.72	1.02328	114
2	187.78	0.98194	1.254	1.72	1.74	1.63	1.005	149
3	203.35	0.97281	3.14	1.72	1.84	1.45	1.005	159
4	196.75	0.97365	2.4	1.68	1.73	1.32	0.96975	206
5	186.64	0.97795	1.146	1.73	1.75	1.76	1.01408	178
6	189.50	0.9726	1.788	1.69	1.73	2.26	0.9784	155
7	194.15	0.9663	2.1	1.6	1.81	1.25	0.90405	188
8	198.77	0.96178	2.88	1.61	1.8	1.31	0.91193	171
9	194.27	0.95612	2.14	1.74	1.73	2.07	0.99603	157
10	196.25	0.96031	2.22	1.8	1.85	1.93	1.08088	162
11	210.99	0.95633	3.22	1.66	1.84	1.33	0.95274	155
12	193.30	0.97249	1.132	1.64	1.71	1.56	0.93613	130
13	183.65	0.99748	1.85	1.73	1.78	2.01	1.01408	187
14	188.81	1.00966	2.28	1.75	1.79	1.62	1.03258	176
15,16	206.07	0.95874	2.42	1.77	1.79	2.03	1.05154	132

Table 2-5: Values of Dependent Variables for CR50

Run	Axial Stiffness kN/mm	Shear Stiffness kN/mm	Rotation Stiffness kNm/deg	Max. Shear Strain in Rubber	Max. Principal Strain in Rubber	Max. Triaxial Stress in Rubber MPa	Max. Bond Stress (Steel and Rubber) MPa	Max . von Mises Stress in Laminate MPa
1	198.26	0.98929	2.345	1.66	1.64	1.61	1.15128	117
2	192.70	0.98205	1.53792	1.64	1.58	1.51	1.06755	150
3	208.85	0.97249	3.4418	1.65	1.66	1.53	1.18072	166
4	202.15	0.97207	2.7024	1.61	1.56	1.41	1.04112	210
5	191.38	0.97974	1.4317	1.64	1.58	1.7	1.06755	182
6	194.52	0.97564	2.0754	1.61	1.56	2.14	1.04112	160
7	199.41	0.96588	2.4192	1.63	1.63	1.33	1.13685	194
8	204.29	0.96294	3.195	1.56	1.63	1.39	1.13685	177
9	199.54	0.95643	2.4338	1.64	1.58	2	1.06755	158
10	201.36	0.96042	2.5128	1.72	1.67	1.88	1.19574	167
11	216.92	0.95475	3.5338	1.61	1.68	1.39	1.21096	162
12	198.01	0.97407	1.41416	1.57	1.55	1.47	1.02818	134
13	188.58	1.00011	2.1578	1.65	1.6	1.97	1.09471	193
14	193.78	1.00945	2.5738	1.68	1.63	1.54	1.13685	180
15,16	211.28	0.9578	2.7042	1.69	1.62	1.97	1.12261	137

Table 2-6: Values of Dependent Variables for NR70

Run	Axial Stiffness kN/mm	Shear Stiffness kN/mm	Rotation Stiffness kNm/deg	Max. Shear Strain in Rubber	Max. Principal Strain in Rubber	Max. Triaxial Stress in Rubber MPa	Max. Bond Stress (Steel and Rubber) MPa	Max . von Mises Stress in Laminate MPa
1	350.62	1.8778	3.952	1.69	1.68	3.21	2.1995	177
2	348.64	1.86509	2.3618	1.68	1.62	3.03	2.0277	232
3	375.33	1.8442	6.119	1.67	1.69	3.16	2.22973	256
4	364.05	1.84577	4.6508	1.64	1.75	2.97	2.42106	316
5	346.49	1.85722	2.0938	1.67	1.62	3.4	2.0277	270
6	351.22	1.84766	3.3722	1.64	1.6	4.27	1.97396	244
7	359.60	1.83097	4.061	1.75	1.66	2.64	2.14044	292
8	367.30	1.8231	5.587	1.61	1.66	2.8	2.14044	272
9	360.23	1.81533	4.1164	1.71	1.62	3.93	2.0277	239
10	363.41	1.82425	4.2718	1.75	1.71	3.69	2.29159	252
11	388.55	1.81144	6.2878	1.64	1.7	2.91	2.26042	249
12	357.73	1.8485	2.0692	1.6	1.58	2.9	1.92192	204
13	341.13	1.89176	3.5174	1.68	1.65	3.9	2.11158	286
14	350.02	1.91412	4.4122	1.72	1.68	3.03	2.1995	279
15,16	380.18	1.81942	4.6082	1.73	1.66	3.84	2.14044	211

Table 2-7: Values of Dependent Variables for CR70

Run	Axial Stiffness kN/mm	Shear Stiffness kN/mm	Rotation Stiffness kNm/deg	Max. Shear Strain in Rubber	Max. Principal Strain in Rubber	Max. Triaxial Stress in Rubber MPa	Max. Bond Stress (Steel and Rubber) MPa	Max . von Mises Stress in Laminate MPa
1	414.07	2.15612	6.1178	1.53	1.39	2.9	2.51714	195
2	402.21	2.13449	4.4912	1.48	1.35	2.63	2.33437	240
3	436.29	2.10824	8.3148	1.51	1.37	3.43	2.42403	280
4	422.57	2.10131	6.8212	1.46	1.31	3.28	2.16508	335
5	399.87	2.13407	4.3176	1.5	1.33	3.29	2.24808	289
6	406.98	2.12997	5.5984	1.47	1.32	3.96	2.20617	261
7	417.43	2.09417	6.2922	1.49	1.68	3.03	4.30409	312
8	428.13	2.09239	7.8462	1.46	1.35	3.12	2.33437	292
9	417.43	2.07643	6.2922	1.51	1.34	3.93	2.29081	253
10	420.84	2.08357	6.4614	1.57	1.39	3.76	2.51714	270
11	452.60	2.06142	8.5102	1.5	1.42	2.93	2.66346	280
12	412.41	2.12105	4.292	1.43	1.31	2.66	2.16508	220
13	395.77	2.18457	5.7798	1.52	1.34	3.95	2.29081	305
14	404.84	2.19643	6.5134	1.56	1.39	2.83	2.51714	295
15,16	439.40	2.07591	6.8844	1.54	1.36	3.92	2.37878	232

Table 2-8: Effect of Axial Load Variation on Internal Stresses and Strains in Perfect Bearing Configuration with Bonded Top and Bottom Surfaces

Dependent Variable	NR50		CR50		NR70		CR70	
	3.8MPa[1] 50% [2] 1 Deg. [3]	7.6MPa[1] 50% [2] 1 Deg. [3]	3.8MPa[1] 50% [2] 1 Deg. [3]	7.6MPa[1] 50% [2] 1 Deg. [3]	3.8MPa[1] 50% [2] 1 Deg. [3]	7.6MPa[1] 50% [2] 1 Deg. [3]	3.8MPa[1] 50% [2] 1 Deg. [3]	7.6MPa[1] 50% [2] 1 Deg. [3]
SHSTRN	1.77	2.03	1.69	1.93	1.51	1.73	1.34	1.54
PRNSTN	1.79	2.26	1.62	2.03	1.36	1.66	1.12	1.36
TENS (Mpa)	2.03	3.76	1.97	3.68	2.51	3.84	2.45	3.92
BOND (Mpa)	1.05	1.36	1.12	1.86	1.45	2.14	1.53	2.38
MISES (Mpa)	132	206	137	213	148	211	166	232

Notes:
(1) Axial Stress
(2) Shear Strain
(3) Rotation

Table 2-9: Comparison between Bonded and Unbonded Perfect Bearing Configuration

Dependent Variable	NR50		CR50		NR70		CR70	
	Bonded	Un-bonded	Bonded	Un-bonded	Bonded	Un-bonded	Bonded	Un-bonded
AXSTIF (kN/mm)	206.1	172.2	211.3	178.6	380.2	313.5	439.4	334.4
SHRSTIF (kN/mm)	0.96	0.78	0.96	0.79	1.82	1.52	2.08	1.72
ROTSTIF (kN-m/deg)	2.42	2.06	2.7	2.37	4.61	4.01	6.88	6.02
SHSTRN	1.77	1.27	1.69	1.17	1.73	1.32	1.54	1.31
PRNSTN	1.79	1.48	1.62	1.29	1.66	1.46	1.36	1.31
TENS (Mpa)	2.03	1.60	1.97	1.54	3.84	3.14	3.92	3.54
BOND (Mpa)	1.05	0.89	1.12	0.87	2.14	2.05	2.38	2.31
MISES (Mpa)	132	145	137	147	211	233	232	274

2.4.5 Interpretation of Finite Element Analysis Results

A summary of the analysis results for bearings with bonded top and bottom surfaces is given in Table 2-10.

Table 2-10: Summary of Finite Element Analysis Results

Bearing Material (G at 50% Strain)	Dependent Variable	Min Value	Max Value	Percent Variation from Perfect Configuration		Maximum Allowable / Limits
NR50 (0.585 MPa)	Axial Stiffness (kN/mm)	183.65	211	-11	+2	186-227
	Shear Stiffness (kN/mm)	0.96	1.01	-0	+5	0.86-1.05
	Rotation Stiffness (kN-m/deg)	1.13	3.22	-53	+33	No constraint
	Shear Strain in Elastomer	1.6	1.8	-9	+2	< 6
	Max. Principal Strain	1.71	1.85	-4	+3	< 2
	Triaxial Tensile Stress (MPa)	1.25	2.26	-38	+11	< 3.5
	Bond Stress (MPa)	0.9	1.08	-14	+3	< 1.31
	Von Mises Stress (MPa)	114	206	-14	+56	< 345
CR50 (0.590 MPa)	Axial Stiffness (kN/mm)	188.58	216.92	-11	+4	190-232
	Shear Stiffness (kN/mm)	0.95	1.01	-1	+5	0.86-1.05
	Rotation Stiffness (kN-m/deg)	1.41	3.53	-52	+31	No constraint
	Shear Strain in Elastomer	1.56	1.72	-8	+2	< 6
	Max. Principal Strain	1.55	1.68	-4	+4	< 2
	Triaxial Tensile Stress (MPa)	1.33	2.14	-32	+9	< 3.53
	Bond Stress (MPa)	1.03	1.21	-8	+8	< 1.81
	Von Mises Stress (MPa)	117	210	-15	+53	< 345
NR70 (1.21 MPa)	Axial Stiffness (kN/mm)	341.14	388.55	-10	+2	342-418
	Shear Stiffness (kN/mm)	1.81	1.91	-0	+5	1.64-2.0
	Rotation Stiffness (kN-m/deg)	2.07	6.29	-55	+36	No constraint
	Shear Strain in Elastomer	1.6	1.75	-8	+1	< 6
	Max. Principal Strain	1.58	1.75	-5	+5	< 2
	Triaxial Tensile Stress (MPa)	2.64	4.27	-31	+11	< 7.2
	Bond Stress (MPa)	1.92	2.42	-10	+13	< 3.4
	Von Mises Stress (MPa)	177	316	-16	+50	< 345
CR70 (1.25 MPa)	Axial Stiffness (kN/mm)	395.77	452.6	-10	+3	395-483
	Shear Stiffness (kN/mm)	2.06	2.2	-1	+6	1.87-2.28
	Rotation Stiffness (kN-m/deg)	4.29	8.51	-38	+24	No constraint
	Shear Strain in Elastomer	1.43	1.57	-7	+2	< 6
	Max. Principal Strain	1.31	1.68	-4	+23	< 2
	Triaxial Tensile Stress (MPa)	2.63	3.96	-33	+1	< 7.5
	Bond Stress (MPa)	2.17	4.3	-9	+81	< 7.4
	Von Mises Stress (MPa)	195	335	-16	+44	< 345

The minimum and maximum values of each performance parameter from all sixteen runs, the percent variation of these extreme limits relative to the case of no laminate misalignment (Run 15, 16), and the recommended performance constraints from Table 2-2 are given. Notice that the axial stiffness and the shear stiffness are proportional to the shear modulus and are not significantly affected by the laminate misalignments. The maximum shear strain and principal strain in the elastomer are not significantly affected by the bearing material specified or the misalignments. The remaining four dependent variables (rotational stiffness, triaxial tensile and bond stresses in the elastomer and the maximum von Mises stress in the steel laminates) are affected by the laminate misalignments, the shear modulus of the elastomer or both. The following observations are based on the results tabulated in Tables 2-4 through 2-10 and the stress and strain data from all the runs.

1. The rotational stiffness varied as much as fifty percent from the perfect case. The maximum and minimum values were always associated with Cases 11 and 12, respectively, for each of the four materials. These two cases only involve edge cover, no other misalignment, so the magnitude of the rotational stiffness is very sensitive to the edge cover. The bearing rotational stiffness is two to three times greater when the edge with no cover is compressed during rotation compared to the case when the edge with large cover is compressed. The rotational stiffness is also directly affected by the shear modulus of the material; the NR70 bearing is about twice as stiff as the NR50 bearing for the perfect configuration. The CR70

bearing is stiffer than the NR70 bearing because of shape of the stress-strain curves shown in Figures 2-8 and 2-9. At 50% strain these two materials have about the same shear modulus, but at 150% strain the CR70 is about twice as stiff as the NR70. The flat pad bearings studied in this research are generally used in bridge applications. Despite the variations noted, the rotational stiffness has little to do with the performance of the bridge because the rotational stiffness of the bearings is so much smaller than the rotational end stiffness of a typical bridge girder. The maximum rotational stiffness determined in the research (Run 11 for CR70) was 8.51 kN-m/deg (6.27 kip-ft/deg), which is about 1/300th of the stiffness of a typical steel girder for a 30 m bridge span and span/depth ratio of 20. No rotational stiffness constraints have been imposed because of the low relative rotational stiffness of an elastomeric bearing and the fact that the maximum end rotation is controlled by the end rotation of the girder, not the characteristics of the bearing. Good design practice, such as avoiding bearing designs with high shape factors (> 12) coupled with a small overall bearing thickness, will provide bearings with low rotation stiffness.

2. The maximum triaxial tensile stress in the elastomer occurs in the bulge region near the edges of the laminates for all four materials and all 16 Runs and its value is proportional to the shear modulus, the 70 durometer material has about twice the stress as the 50 durometer material. Edge cover dominates this performance parameter. The smallest edge cover and largest edge cover on the right edge (Runs 11 and12, respectively as

shown in Figure 2-5) gave about the same level of triaxial tensile stress. For covers between these extremes, the relationship between the stress and the edge cover on the right side is nonlinear. The average of the four cases with a 2.5 mm cover is almost the same as the two extreme covers. Edge covers of 6 and 9.5 mm give triaxial tensile stresses that are about forty percent higher than the minimum values shown in Table 2-10. The highest stress always occurs with Run 6, with a right edge cover of 9.5 mm. This maximum, however, is still only about sixty percent of the allowable stress limit. AASHTO 251-97 requires a minimum cover of 3 mm and a tolerance of -0, +3 mm on the cover specified by the designer. It appears that cover that is smaller or larger than the specified value will not adversely affect the performance.

3. In all cases the maximum bond stress occurs near the edge of the steel laminate and it reasonably follows the principal strain distribution shown in contour (g) of Figures 2-10 through 2-17. The maximum bond stress for the perfect alignment of the laminates is directly proportional to the shear modulus. Bearings with a higher shear modulus have higher bond stresses. Except for CR70, Run 7, the maximum bond stress is insensitive to shim misalignment. For NR50, CR50, NR70 and CR70 (neglecting Run 7), the maximum increase in bond stress compared to the perfect configuration is 3, 8, 13 and 11 percent, respectively. The maximum increase for CR70 is 81 percent for Run 7 because there is a steep increase in the slope of the stress-strain curve at strains greater than 100% as

discussed under Rotational Stiffness. The maximum bond stress is 82, 67, 71, and 58 percent of the allowable limit for NR50, CR50, NR70 and CR70, respectively. This maximum stress is confined to a very small region of the bearing. The bond stress over a more major portion of the bearing is approximately fifty percent of the maximum value.

4. The maximum steel stresses are mainly due to bending of the plate near the edge of the bearing as shown in contour (h) of Figures 2-10 through 2-17. For the perfect configuration the maximum steel stress is somewhat related to the shear modulus; the higher the shear modulus, the higher the steel stress as shown in Table 2-8. Note that in Table 2-10 the laminate stresses in higher modulus bearings are almost double as compared to the lower modulus bearings. This is primarily due to the fact that the compressive force applied on the higher modulus bearings was double that for the lower modulus bearings. The effect of axial load variation on the integrity related variables is shown in Table 2-8 for perfect bearing configuration with bonded top and bottom surfaces. The average maximum stress for NR50 and CR50 is 134 MPa and for NR70 and CR70 is 221 MPa for the perfect configuration – see Run 15,16 of Tables 2-4 through 2-7. The AASHTO-LRFD (1998) formula for minimum thickness of steel reinforcement (Formula 14.7.5.3.7-1) can be rearranged to determine the steel axial (membrane) stress, σ_r, with the factor of safety of 2 removed as follows:

$$\sigma_r = 1.5\sigma_s \frac{h_{r\max}}{h_s} \qquad \text{(Eq. 2-9)}$$

where σ_s = compressive stress, h_{rmax} = thickness of the elastomer layer, and h_s = laminate thickness Based on Equation 2-9, the steel stress should be 23 and 46 MPa for the NR,CR50 and NR,CR70 bearings, respectively. Thus, for the perfect configuration the maximum steel stresses are about five to six times higher than the AASHTO theoretical axial stress but these maximum stresses are confined to small areas less than 1 percent of the plan area near the edge of the bearing. For the CR70 bearing the steel stress for the perfect configuration is at 2/3 of the assumed yield strength, 345 MPa. The analysis implies that for bearings subjected to shear and rotation there should be a minimum steel laminate thickness limit associated with plate bending. If the steel laminate is too thin it will yield in bending and the bearing will have a permanent kink near the edge as observed in some tests (Crozier et al. 1974). The use of a minimum 3-mm (1/8 in. or 12 gauge) plate thickness as used in this research will usually limit the maximum steel bending stresses to prevent permanent plate deformations. The plate bending will have little effect on the function of the bearing but it may be visually objectionable.

5. The laminate misalignments cause significant increases of up to fifty percent of the perfect alignment stresses in laminates. The data indicates that the misalignments associated with Run 4 always give the highest steel stresses for all four materials, and Run 1 always give the lowest steel

stresses. The perfect alignment gives the second lowest stress level. A reduction in the edge cover increases the steel stresses up to twenty percent (compare Runs 11 and 15,16): an increase in edge cover has little effect. The percent change in the elastomer layer thickness at the edge of the bearing due to laminate misalignment from the perfect configuration is directly related to the increase in the maximum steel stresses. For example, the 1.5° rotation of Run 14 changes the edge thickness of the interior layer on the compressed side from 12.7 to 18.7 mm, a 47 percent change in the edge thickness. A similar percent change in edge thickness occurs for Run 13. The change in the steel stress was about 32 percent for Run 14 and 41 percent for Run13. A vertical shift of 3mm in Runs 9 and 10, a 24 percent change in thickness gives a 17 and 22 percent increase in steel stress for NR50 and CR50 bearings, respectively. Other combinations give similar results since the perfect alignment case of three equal elastomer layers is close to ideal, i.e., lowest steel stresses. Any change in thickness generally increases the steel stresses.

6. Because of slip at the contact surface, especially near the edges, an elastomer layer with one of its bearing surfaces unbonded to a steel plate will bulge more than a bearing with sole plates. This additional bulging increases the vertical displacement within the layer by a factor of about 1.4, based on the b = 1.4 factor for cover layers in AASHTO Design (1996). Thus, the axial stiffness of the unbonded bearing should be 3/(1.4+1+1.4) = 0.79 times as stiff as the same bearing with sole plates

(there should be 21 percent more vertical displacement in the unbonded bearing with two steel laminates). The average axial stiffness of the bearings without sole plates to the bearings with sole plates is 0.82 for the four elastomer materials, which is close to the predicted value of 0.79. The average shear stiffness of the unbonded bearings is 0.82 that of the bonded bearings. The stiffness ratio is consistent with the reduction factor of 0.8-0.9 for a bearing with three laminates reported by Hamzeh et al. (1995). The reduced stiffness is caused by the tendency of the elastomer to roll at the edge for unbonded bearings (compare deformed shapes (d) of Figures 2-10 and 2-14). The rotational stiffness and the internal stresses and strains in the rubber (maximum shear strain, maximum principal strain, and bond stress) are all smaller in an unbonded bearing. The stresses in steel laminates are approximately 10 percent higher in the NR50, CR50 and NR70 unbonded bearings and 18 percent higher in the CR70 bearing. Note, however, that the zone of high steel stress is much smaller in the unbonded bearings shown in contour (h) of Figures 2-14 through 2-17 than in the bonded bearings of Figures 2-10-2-13. Overall, if the slip at the contact surface is not critical, an unbonded elastomeric bearing is a better design choice because of its lower stresses and lower shear and rotational stiffnesses.

2.5 DEVELOPMENT OF LAMINATE MISALIGNMENT LIMITS

The regression coefficients in Equation 2-1 for various dependent variables are tabulated in Table 2-11. The results of analysis of variance, sequential statistics and inference on coefficients are included in Appendix-A.

Table 2-12 shows a sample of results for multivariate regression analysis. The most important result is the inference on coefficients that gives a wealth of information on the significance of independent variables. This part of the printout shows the name of the regressor variables, the parameter estimate, its estimated standard deviation and the test that the parameter is zero. The INTCEP is the value of the dependent variable for a perfect bearing configuration. If the data indicates that the variable is significant, then the |t| statistic will be large. This means that if the parameter is really zero, getting so large a |t| statistic is a rare event. Thus we would see a small PROB>|t|, the probability of getting a larger absolute |t| under the hypothesis that the subject parameter is zero. The value $p<0.05$ is often used as cutoff probability or significance level. For example in Table 2-12, the variation in Axial Stiffness of NR50 due to laminate misalignment is significantly affected by X1, X2, X3, $X1^2$, $X2^2$, $X3^2$ and X1X3 (interaction of X1 and X3). Here X1, X2 and X3 are the three independent variables defined in Section 2-2. Note that INTCEP is the value of axial stiffness for a perfect bearing configuration.

Based on the regression Equation 2-1 with appropriate coefficients in Table 2-11 the combined limits on vertical misalignment (X1), edge cover misalignment (X2) and shim inclination (X3) were determined so that the

resulting performance parameter just meets the constraints tabulated in Table 2-2. The minimum value of each misalignment from all eight dependent variables for all four materials were determined and plotted. Usually the axial stiffness constraint ±10 percent, the shear stiffness constraint ±10 percent, or the steel stress limit F_y = 345 MPa controlled the minimum misalignment limit. Figure 2-18 shows the allowable shim misalignments applicable to satisfy all the limits and constraints, tabulated in Table 2-2, for all four types of bearings (NR50, CR50, NR70 and CR70) studied. In this Figure, the equation of the surface is given by:

$$z = a + bx + cx^2 + dx^3 + ey + fy^2 + gy^3 + hy^4 + iy^5 \qquad \text{(Eq. 2-10)}$$

where, $a, b, c, d, e, f, g, h, i$ are regression coefficients given in Figure 2-18 while x, y and z are the absolute values of vertical misalignment (mm), horizontal misalignment (mm) and rotation of the laminate respectively. If two misalignments are known, absolute values can be plugged in this equation to get the maximum ± allowable value of the third misalignment. Note that these misalignments are measured from the perfect configuration. For example if the perfect cover is 6 mm, a horizontal misalignment of 3 mm means that the cover on one side is 3 mm while on the other side is 9 mm. If the perfect layer thickness is 12.7 mm, a vertical misalignment of 3 mm means that the layer thickness can be 9.7 mm or 15.7 mm. Similarly, a rotation misalignment of 1^o means that steel laminates can have an angle of $\pm 1^o$ from the horizontal during the molding process.

Table 2-11: Regression Coefficients in Equation 2-1

Type	Variable	a_o	a_1	a_2	a_3	a_4	a_5	a_6	a_7	a_8	a_9
NR50	AXSTIF	206.0	-.576	4.746	-1.50	-3.75	-1.45	-6.76	0.085	2.452	-.281
	SHRSTIF	0.959	-.001	-.005	-.004	0	0.002	0.015	0.001	0	0
	ROTSTIF	2.42	-.019	0.563	-.12	-.088	-.09	-.127	0.026	0.371	-.023
	SHSTRN	1.77	-.014	-.017	-.019	-.006	-.046	-.016	0.004	0.004	-.019
	PRNSTN	1.79	-.03	0.027	-.003	-.001	-.006	-.003	-.004	0.019	0.014
	TENS	2.03	0.042	-.174	0.081	-.042	-.227	-.103	-.06	0.098	-.11
	BOND	1.052	-.016	-.014	-.016	-.009	-.041	-.014	0.003	0.003	-.015
	MISES	132	2.381	12.24	5.932	9.897	4.23	17.23	2.25	-15.3	-9.5
CR50	AXSTIF	211.2	-.529	5.044	-1.53	-3.75	-1.42	-6.84	0.077	2.534	-.28
	SHRSTIF	0.958	-.001	-.006	-.003	0	0.002	0.015	0.001	0	0
	ROTSTIF	2.704	-.019	0.574	-.116	-.085	-.085	-.121	0.025	0.371	-.019
	SHSTRN	1.69	-.021	-.002	-.012	-.007	-.037	-.012	-.008	-.005	-.003
	PRNSTN	1.62	-.024	0.025	-.007	-.001	-.004	-.004	-.003	0.017	0.015
	TENS	1.97	0.035	-.103	0.089	-.035	-.205	-.097	-.05	0.09	-.118
	BOND	1.123	-.034	0.035	-.009	-.001	-.005	-.006	-.004	0.025	0.02
	MISES	137	1.601	13.32	6.608	9.231	4.397	17.23	2	-14.5	-10
NR70	AXSTIF	380.1	-.453	8.764	-2.10	-6.55	-2.78	-12.0	-.792	3.21	-1.37
	SHRSTIF	1.819	-.003	-.012	-.008	0	0.003	0.028	0.002	-.001	0
	ROTSTIF	4.608	-.037	1.139	-.251	-.155	-.16	-.231	0.046	0.733	-.034
	SHSTRN	1.725	-.02	0.004	-.006	-.001	-.038	-.011	-.016	-.016	0.014
	PRNSTN	1.66	-.013	0.032	-.018	0.002	-.006	0.002	0.017	-.003	-.005
	TENS	3.84	0.077	-.166	0.16	-.05	-.351	-.165	-.09	0.175	-.265
	BOND	2.14	-.035	0.092	-.054	0.008	-.015	0.007	0.052	-.009	-.018
	MISES	211.0	3.32	20.78	7.795	12.62	6.286	24.95	1.375	-20.1	-14.1
CR70	AXSTIF	439.4	-.977	10.78	-2.75	-7.02	-2.56	-13.3	0.216	5.426	-.484
	SHRSTIF	2.076	-.003	-.019	-.005	0.001	0.005	0.038	0.002	0.003	0
	ROTSTIF	6.884	-.041	1.147	-.211	-.185	-.177	-.262	0.051	0.744	-.038
	SHSTRN	1.54	-.019	0.004	-.009	-.005	-.03	-.005	0	0.005	0.003
	PRNSTN	1.36	-.038	0.036	0.012	0.006	0.006	0.006	-.043	-.03	0.055
	TENS	3.92	0.045	0.039	0.221	-.051	-.401	-.203	-.058	0.147	-.285
	BOND	2.379	-.203	0.199	0.09	0.039	0.042	0.039	-.251	-.196	0.306
	MISES	232.0	1.611	24.14	8.666	10.79	6.953	23.62	2.25	-18.5	-15.8

Table 2-12: Regression Analysis Results for NR50 Axial Stiffness

RUN	PREDICTED	OBSERVED	DIFFERENCE
1	193.701	193.304	.397
2	187.477	187.781	-.304
3	203.586	203.357	.229
4	197.700	196.752	.948
5	186.352	186.646	-.294
6	189.934	189.509	.425
7	195.114	194.155	.959
8	199.034	198.777	.257
9	193.831	194.277	-.446
10	195.826	196.252	-.426
11	209.935	210.997	-1.062
12	193.494	193.304	.190
13	183.191	183.650	-.459
14	188.400	188.814	-.414
15	206.071	206.071	.000
16	206.071	206.071	.000

R-squared (percent)	Adjusted R-squared	Est. Std. Dev. of Model Error	Mean	Coefficient of Var. (percent)
99.519	98.797	.8544	195.6	.4368

* * * Analysis of Variance * * *

Source	DF	Sum of Squares	Mean Square	Overall F	Prob. of Larger F
Regression	9	905.6	100.6	137.856	.0000
Residual	6	4.4	.7		
Corrected Total	15	910.0			

* * * Sequential Statistics * * *

Indep. Variable	Degrees of Freedom	Sum of Squares	F-statistic	Prob. of Larger F
X1	1	4.6	6.363	.0451
X2	1	315.4	432.044	.0000
X3	1	31.7	43.366	.0006
X1X1	1	20.1	27.572	.0019
X2X2	1	30.7	42.056	.0006
X3X3	1	454.4	622.489	.0000
X1X2	1	.1	.078	.7888
X1X3	1	48.1	65.874	.0002
X2X3	1	.6	.865	.3883

* * * Inference on Coefficients * * *

Coef.	Estimate	Standard Error	t-statistic	Prob. of Larger |t|	Variance Inflation
INTCEP	206.1	.6041	341.1	.0000	8.000
X1	-.6	.2283	-2.5	.0451	1.000
X2	4.7	.2283	20.8	.0000	1.000
X3	-1.5	.2283	-6.6	.0006	1.000
X1X1	-3.7	.2709	-13.8	.0000	1.382
X2X2	-1.5	.2709	-5.4	.0017	1.382
X3X3	-6.8	.2709	-24.9	.0000	1.382
X1X2	.1	.3021	.3	.7888	1.000
X1X3	2.5	.3021	8.1	.0002	1.000
X2X3	-.3	.3021	-.9	.3883	1.000

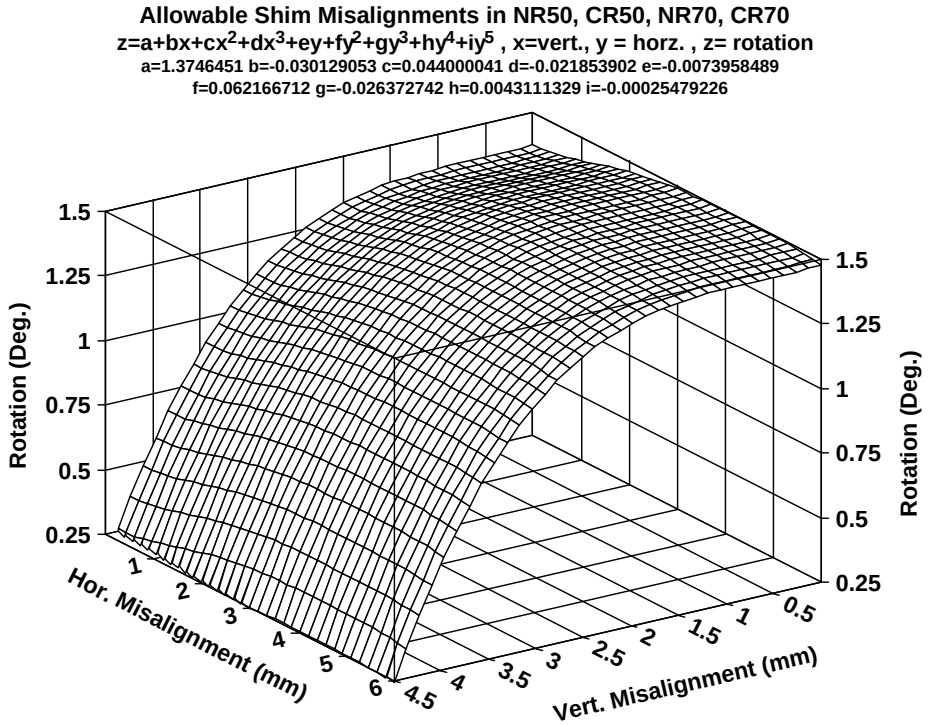

Figure 2-18: Allowable Misalignments of Laminate in NR50, CR50, NR70, CR70

Notice in Figure 2-18 that the effect of horizontal misalignment on the performance is small. By eliminating the horizontal misalignment variable and converting the laminate inclination from degrees to radians, the following conservative equation can be used to define shim-tolerance limits:

$$\theta \le 0.024 - 0.001\left(0.55v - 0.77v^2 + 0.38v^3\right) \qquad \text{(Eq. 2-11)}$$

where θ (radians) and v (mm) are absolute values of laminate rotation and vertical shift respectively. If the specified elastomeric layer thickness is h_r, the bearing length is L, and H_1 and H_2 are the measured maximum and minimum thicknesses

within the layer, then $v = |h_r - 0.5(H_1+H_2)|$ and $\theta = |(H_1-H_2)/2L|$ for interior layers and $\theta = |(H_1-H_2)/ L|$ for top and bottom layers.

During the vulcanization process of bearings a minimum rubber layer thickness is required for the rubber to flow between laminates. For low precision bearings (e.g. bridge bearings) a minimum rubber layer thickness of 5 mm is generally required for this reason. Therefore, Equation 2-11 must be used in conjunction with a 5 mm minimum rubber layer thickness at any location (i.e. $H_2 \geq 5$ mm).

In order to assess the feasibility of using the above procedure for bearing configurations other than shown in Figure 2-1, four test configurations shown in Figures 2-19 through 2-22 respectively were analyzed. Test Configuration 1 consists of five rubber layers as compared to 3 used in sensitivity study. In Test Configuration 2, the width is twice and the rubber layer thickness is 1.5 times as compared to the configuration shown in Figure 2-1. Test Configuration 3 is twice as wide as the configuration shown in Figure 2-1 with same rubber layer thickness. The plan dimensions of Test Configuration 4 are same as shown in Figure 2-1, while the thickness of rubber layers is half. The allowable vertical and rotation misalignments were calculated using Equation 2-11 in conjunction with 5 mm minimum rubber layer thickness requirement. NR50 material model was used for all cases. A shear deflection corresponding to 50 percent shear strain was applied on all models. The compressive stress and rotation were adjusted so that the resulting maximum shear strain in rubber and maximum von

Mises stress in laminates of the perfect configuration were almost same as that of perfect configuration shown in Figure 2-1.

The results are tabulated in Table 2-13. Note that for all four configurations, the change in axial stiffness and shear stiffness due to laminate misalignment is less than 10 percent and various stresses and strains meet the criteria set in Section 2.3. Based on these results, it can be concluded that Equation 2-11 can be conservatively used for any bearing configuration so long as the resulting minimum thickness of a rubber layer at any location is greater than 5 mm. As noted earlier, the variation of cover thickness is less important, however a minimum cover is needed to control shrinkage that is determined by mold design.

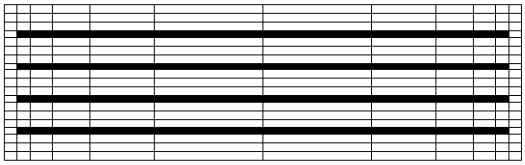

(a) Perfect Configuration – Plan Dimensions = 255 x 356 mm, Rubber Layer Thickness = 12.7 mm, Laminate Thickness = 3.18 mm, Cover = 6 mm

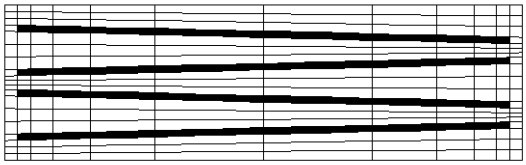

(b) Maximum Rotation Misalignment based on Equation 2-11 in conjunction with 5 mm minimum thickness limit; Rotation = 1.375^o, Vertical Shift = 0 mm; Note that the 5 mm minimum thickness requirement does not control the maximum rotation allowed and this configuration represents an extreme point on the interaction surface shown in Figure 2-18

(c) Maximum Vertical Misalignment based on Equation 2-11 in conjunction with 5 mm minimum thickness limit; Vertical Shift = 4.625 mm, Rotation = 0^o ; Note that the 5 mm minimum thickness requirement does not control the maximum vertical shift allowed and this configuration represents an extreme point on the interaction surface shown in Figure 2-18

(d) Combined Vertical Shift and Rotation Misalignments based on Equation 2-11 in conjunction with 5 mm minimum thickness limit; Vertical Shift = 3 mm, Rotation =1.087 ^{o}; Note that this configuration represents an intermediate point on the interaction surface shown in Figure 2-18

Figure 2-19: Test Configuration 1: Bearing with 5 Rubber Layers where Misalignments are not Governed by Minimum Thickness Requirement

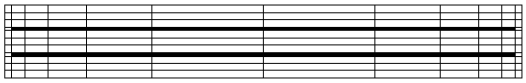

(a) Perfect Configuration – Plan Dimensions = 458 x 356 mm, Rubber Layer Thickness = 19.05 mm, Laminate Thickness = 3.18 mm, Cover = 6 mm

(b) Maximum Rotation Misalignment based on Equation 2-11 in conjunction with 5 mm minimum thickness limit; Rotation = 1.375^o, Vertical Shift = 0 mm; Note that the 5 mm minimum thickness requirement does not control the maximum rotation allowed and this configuration represents an extreme point on the interaction surface shown in Figure 2-18

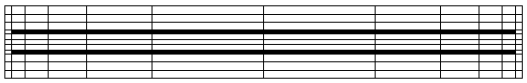

(c) Maximum Vertical Misalignment based on Equation 2-11 in conjunction with 5 mm minimum thickness limit; Vertical Shift = 4.625 mm, Rotation = 0^o ; Note that the 5 mm minimum thickness requirement does not control the maximum vertical shift allowed and this configuration represents an extreme point on the interaction surface shown in Figure 2-18

(d) Combined Vertical and Rotation Misalignments based on Equation 2-11 in conjunction with 5 mm minimum thickness limit; Vertical Shift = 3 mm, Rotation =1.087 ^{o}; Note that this configuration represents an intermediate point on the interaction surface shown in Figure 2-18

Figure 2-20: Test Configuration 2: Bearing Width = 2xOriginal Bearing Width and Rubber Thickness = 1.5 x Original Bearing Rubber Thickness and Misalignments are not Governed by Minimum Thickness Requirement

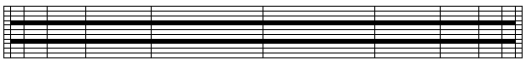

(a) Perfect Configuration – Plan Dimensions = 458 x 356 mm, Rubber Layer Thickness = 12.7 mm, Laminate Thickness = 3.18 mm, Cover = 6 mm

(b) Maximum Rotation Misalignment based on Equation 2-11 in conjunction with 5 mm minimum thickness limit; Rotation = 1.0^o, Vertical Shift = 0 mm; Note that the 5 mm minimum thickness requirement controls the maximum rotation allowed

(c) Maximum Vertical Misalignment based on Equation 2-11 in conjunction with 5 mm minimum thickness limit; Vertical Shift = 4.625, Rotation = 0^o; Note that the 5 mm minimum thickness requirement does not control the maximum vertical shift allowed and this configuration represents an extreme point on the interaction surface shown in Figure 2-18

Figure 2-21: Test Configuration 3: Bearing Width = 2xOriginal Bearing Width and Rubber Thickness = Original Bearing Rubber Thickness

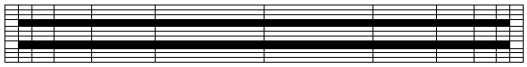

(a) Perfect Configuration – Plan Dimensions = 229 x 356 mm, Rubber Layer Thickness = 6.35 mm, Laminate Thickness = 3.18 mm, Cover = 6 mm

(b) Maximum Rotation Misalignment based on Equation 2-11 in conjunction with 5 mm minimum thickness limit; Rotation = 0.36^o, Vertical Shift = 0 mm; Note that the 5 mm minimum thickness requirement controls the maximum rotation allowed

(c) Maximum Vertical Misalignment based on Equation 2-11 in conjunction with 5 mm minimum thickness limit; Vertical Shift = 1.35, Rotation = 0^o; ; Note that the 5 mm minimum thickness requirement controls the maximum vertical shift allowed

Figure 2-22: Test Configuration 4: Bearing Width = Original Bearing Width and Rubber Thickness = 0.5 x Original Bearing Rubber Thickness

Table 2-13: Summary of Results for Test Configurations Based on Equation 2-11 and 5 mm Minimum Rubber Layer Thickness Requirement

Test Configuration and Loading	Dependent Variable	Perfect Configuration	Allowable Variation/ Limit per Section 2.3	Configuration with Maximum Allowable Rotation Misalignment	Configuration with Maximum Allowable Vertical Shift	Combined Rotation and Vertical Shift at an Intermediate Location on Interaction Surface (Figure 2-18)
Configuration 1 (Figure 2-19) 3.8 MPa Compressive Stress, 50 % Shear Deflection, 1° Rotation	Axial Stiffness (kN/mm)	145.8	131-160	136.15	133.35	131.67
	Shear Stiffness (kN/mm)	0.61	0.55-.67	0.65	0.60	0.64
	Rotation Stiffness (kN-m/deg)	1.1	-	1.92	1.67	3.44
	Shear Strain	1.71	< 6	1.68	1.77	1.68
	Maximum Principal Strain	1.74	< 2	1.71	1.81	1.7
	Triaxial Tensile Stress (MPa)	2.07	< 3.5	1.96	1.86	1.51
	Bond Stress (MPa)	1.03	< 1.31	0.99	1.09	0.98
	Von Mises Stress (MPa)	181	< 345	220	224	200
Configuration 2 (Figure 2-20) 3.8 MPa Compressive Stress, 50 % Shear Deflection, 0.5° Rotation	Axial Stiffness (kN/mm)	276.8	249-305	256.7	264.8	251.4
	Shear Stiffness (kN/mm)	1.34	1.21-1.47	1.41	1.33	1.37
	Rotation Stiffness (kN-m/deg)	31.4	-	26.11	30.04	24.22
	Shear Strain	1.82	< 6	1.71	1.74	1.67
	Maximum Principal Strain	1.93	< 2	2.0	1.84	1.79
	Triaxial Tensile Stress (MPa)	2.75	< 3.5	2.98	2.36	2.78
	Bond Stress (MPa)	1.22	< 1.31	1.31	1.12	1.07
	Von Mises Stress (MPa)	173	< 345	258	227	254
Configuration 3 (Figure 2-21) 3.8 MPa Compressive Stress, 50 % Shear Deflection, 0.5° Rotation	Axial Stiffness (kN/mm)	831.8	749-915	757.3	788	Combined Misalignments are controlled by 5 mm minimum rubber layer thickness requirement
	Shear Stiffness (kN/mm)	2.18	1.96-2.4	2.35	2.19	
	Rotation Stiffness (kN-m/deg)	104	-	84.2	90.5	
	Shear Strain	1.56	< 6	1.54	1.58	
	Maximum Principal Strain	1.88	< 2	1.72	1.83	
	Triaxial Tensile Stress (MPa)	2.17	< 3.5	1.8	1.83	
	Bond Stress (MPa)	1.16	< 1.31	1.0	1.11	
	Von Mises Stress (MPa)	134	< 345	168	163	
Configuration 4 (Figure 2-22) 5.7 MPa Compressive Stress, 50 % Shear Deflection, 0.5° Rotation	Axial Stiffness (kN/mm)	1344.3	1210-1479	1308	1299	Combined Misalignments are controlled by 5 mm minimum rubber layer thickness requirement
	Shear Stiffness (kN/mm)	2.11	0.86-1.05	2.13	2.12	
	Rotation Stiffness (kN-m/deg)	30.73	-	30	29.5	
	Shear Strain	1.78	< 6	1.73	1.71	
	Maximum Principal Strain	1.89	< 2	1.84	1.87	
	Triaxial Tensile Stress (MPa)	1.37	< 3.5	1.34	1.24	
	Bond Stress (MPa)	1.17	< 1.31	1.12	1.15	
	Von Mises Stress (MPa)	98	< 345	123	118	

2.6 CONCLUSIONS

Based on the results of the present finite element analysis and sensitivity study, the following conclusions can be derived:

1. The stiffnesses (Axial, Shear and Rotation) of bearings with unbonded top and bottom surfaces are generally lower as compared to the bonded bearings. This is due to the loss in contact at the edges as the bearing is loaded. The internal stresses and strains in rubber are also lower for unbonded bearings as compared to the bonded bearings. However, the stresses in steel laminates are higher. If the slip at the contact surface is not critical, an unbonded elastomeric bearing appears to be a better design choice because of its lower stresses and lower shear and rotational stiffnesses.
2. The stresses and strains in rubber and steel laminates of a perfect configuration are well below allowable limit set in Section 2-3. The peak von Mises stress is generally limited to 1 percent region of the bearing. The peak von Mises stress is highly localized and is located at the extreme fibers of the laminate mainly due to local bending of the laminate. The average membrane stress is much less. The peak von Mises stress is critical only when the bearing undergoes cyclic loading. For bridge bearings this is not very important.
3. The axial stiffness and the shear stiffness are proportional to the shear modulus and are not significantly affected by the laminate misalignments. The maximum shear strain and principal strain in the elastomer are not

significantly affected by the bearing material specified or the misalignments. The remaining four performance parameters (rotational stiffness, triaxial tensile and bond stresses in the elastomer and the maximum von Mises stress in the steel reinforcements) are affected by the steel laminate misalignments, the shear modulus of the elastomer or both.

4. As shown in Figure 2-18, the subject bearings can tolerate considerable misalignments of laminates without deterioration in performance. The horizontal misalignment (cover) is less influential on the performance of the bearing as compared to the variation of rubber layer thickness and the rotation misalignment. Equation 2-11 can be conservatively used for any bearing configuration so long as the resulting minimum thickness of a rubber layer at any location is greater than 5 mm.
5. The allowable vertical shift and rotation of the laminates is controlled by three design variables: axial stiffness, shear stiffness and von Mises stresses in laminates. Note that rotation stiffness controls the allowable horizontal shift, however, it was not included in the present sensitivity study since rotation stiffness in not important for flat bearings as mentioned earlier. The von Mises stress dominates the allowable misalignments only in bearings with stiffer elastomers as in the case of CR70.
6. In general, the tolerances given in Table 2 of AASHTO M251-97 are well below the laminate misalignments that affect the performance of the bearings. Equation 2-11 indicates that greater tolerances can be permitted

without affecting performance. The existing AASHTO layer thickness tolerance, ±20 percent of the design value but no more than ±3 mm should be replaced by Equation 2-11 or conservatively by ±4.5 mm its minimum value corresponding to $\theta = 0$. The minimum measured layer thickness dimension should be greater than 5 mm. The current 20 percent of design limit controls the tolerance for specified layer thicknesses of 15 mm or less. Since elastomeric layer thicknesses less than 6 mm are not very practical the 20 percent limit varies the tolerance between 1 and 3 mm. Because of the cover it is difficult to precisely measure and locate the edge of each laminate so it is doubtful that any measurement of layer thickness could be accurate to better than ±1.5 mm. Therefore it is recommended that the same tolerances be applied to all bearings. The minimum layer dimension of 5 mm will control the permitted laminate misalignment for bearings with small specified layer thicknesses. It is recommended that the current tolerance for edge cover be maintained at –0,+3 mm.

7. As shown in Figure 2-23, the bond integrity at the interface of rubber layer and steel laminate is governed by a tangential stress “t” and a normal stress “n”. A tensile normal stress is detrimental to the metal to rubber bond while a compressive normal stress strengthens it. For the elastomeric bearings analyzed in the present study, the normal stresses at all locations at the bond line were always compressive. The maximum tangential stresses, tabulated in Table 2-10 as BOND, were well below the failure limit for the respective bearing.

8. AASHTO Specifications requires a peel test, shown in Figure 2-24(a), to assess the integrity of the metal to rubber bonds. Note that this test is a measure of bond failure in tension and therefore is not representative of the loading mode experienced by elastomeric bearings as shown in Figure 2-23. The shear test shown in Figure 2-24(b) is more applicable for the elastomeric bearings. The experimental data shown in Figure 2-6 through 2-9 was obtained using a similar test shown in Figure 2-24(b). In these figures average shear stress, which can also be interpreted as average bond stress, is plotted against average shear strain. Note that the experimental data extend above the maximum allowable bond stress tabulated in Table 2-10. No bond failure was observed during these tests implying that the allowable bond stresses tabulated in Table 2-10 are adequate to address the failure due to delamination at bond line. Based on these analytical and experimental results, a shear test shown in Figure 2-24 (b) is more appropriate than the peel test currently stipulated by AASHTO specifications.

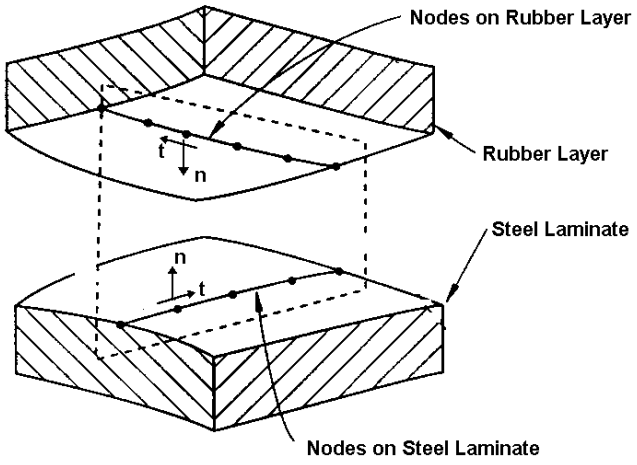

Figure 2-23: Bond Stress at the Interface of Rubber Layer and Steel Laminate

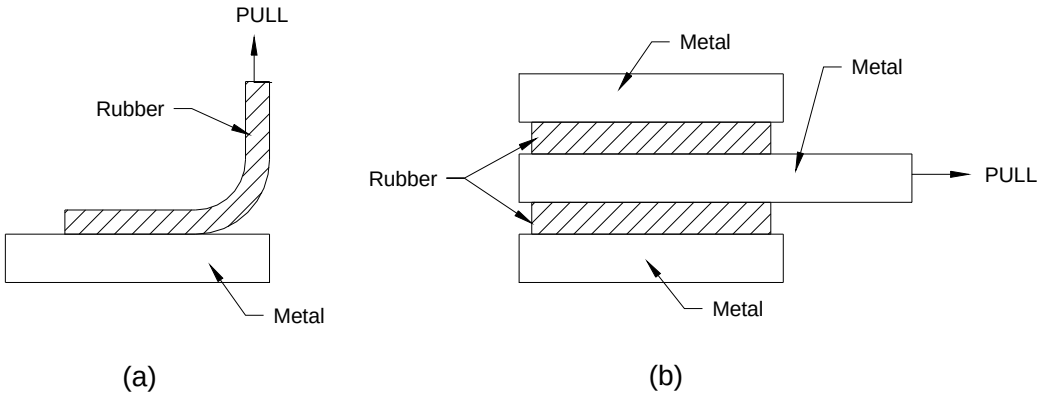

Figure 2-24: Peel Test and Shear Test to Measure Bond Strength

Chapter 3: Creep

3.1 INTRODUCTION

All elastomers exhibit the undesirable behavior of creep, or continuing time dependent deformation under constant load; and stress relaxation, or time dependent decay in stress at constant deformation. The processes contributing to creep and relaxation behavior of rubber are both physical and chemical in nature (Derham, 1973, Curro and Salazar, 1977). Under ambient temperature, physical processes dominate the relaxation of rubber, while at elevated temperatures, chemical processes dominate the relaxation of rubber. Stress relaxation is an important research technique, as the decay in stress can be correlated with changes in chemical network, providing an insight into the processes involved in network breakdown (Clark and Manley, 1986, Gillen, 1988). Some noteworthy features of creep and relaxation of rubber are as follows (Derham, 1973, Freakley and Payne, 1978):

- Physical relaxation usually decreases linearly with the logarithm of time while chemical relaxation is approximately linear with time.
- The physical relaxation rates are dependent upon the difference between the service temperature and the glass transition temperature under static conditions. The glass transition temperature is a reference temperature at which molecular segments move so slowly, about once in 10 seconds, that for all practical purposes they do not move at all and the material becomes a rigid glass. Typical glass transition temperatures for elastomers used in

elastomeric bearings are –45^{o} C to –65^{o} C. The creep and relaxation rates are high near the glass transition temperature and decrease as the temperature rises and molecules become more mobile.

- The rate of creep and relaxation depends on the mode of deformation. For the same stress, creep is highest in tension and lowest in compression.
- Relaxation rate decreases with increasing crosslink density.
- Reinforcing fillers, e.g. carbon black, in rubber increases the relaxation rate.
- Relaxation rate of rubber swollen with appropriate solvent is higher as compared to dry rubber.
- Oxidative chemical relaxation decreases as the rubber layer thickness increases.

The creep of elastomers has generally been studied by applying a constant load for a long period of time and measuring the deflection at specified intervals. Detailed procedures on creep were not standardized internationally until ISO 8013, 1988, was published and there is still no general ASTM method. This reflects the relatively small amount of creep testing carried out on rubbers, although for particular applications of rubber where creep is important (e.g. elastomeric bearings), some data has been generated. Recently, based on the results of a two-year on-going creep study, conducted on full-scale laminated elastomeric bearings, Takayama and Morita, 1998, reported that under axial stresses of 110 Kg/cm^2, 150 Kg/cm^2 and 200 Kg/cm^2 the maximum creep deformation was about 0.15% to 0.6% of the total rubber thickness.

There is some ambiguity on the definition of creep. In the rubber industry, creep is defined as the increase in deformation after a specified time interval expressed as a percentage of test piece deformation at the start of that time interval. In other industries creep is defined as the increase in deformation expressed as a percentage of original unstressed thickness of the test piece. ISO 8013 has both definitions called creep increment and creep index respectively. AASHTO, 1992, uses the first definition and estimates the creep to 45% and 25% of instantaneous deformation for 70 and 50 durometer hardness respectively. AASHTO has no test to check creep properties.

Creep can be measured under compression load or shear load. In the international standard, the test pieces for measurements in compression are discs either 29 mm in diameter and 12.5 mm thick or 13 mm in diameter and 6.3 mm thick, i.e. the same as used for compression set. It is optional whether the test pieces are bonded to end plates; i.e. the measurements can be made with no slippage at the compressed surfaces or with some slip, lubrication being recommended. The essential requirements for the apparatus in compression tests are that one compression plate is fixed and the other is free to move without friction. The force must be applied smoothly and without overshoot and the mechanism must be such that the line of action of the applied force remains coincident with the axis of the test piece as it creeps. The compression of the test piece should be measured to ±0.1% of the test piece thickness. For measurements in shear, a double sandwich test piece is used, preferred dimensions being 25mm diameter and 5mm thick. Apparatus for measurements in shear is essentially the

same as for compression except for the differences in geometry of the test piece and its mounting. The international standard recommends that the test piece be mechanically conditioned by straining five times to a higher strain than used in the test between 16 and 48 hours before the test that will remove any irreversible behavior. A force is applied within 6 seconds such that an initial strain of 20 ± 2% is realized. The deformation of the test piece is measured after 10 min with further measurements after 10, 100, 1000 min, etc. There are no particular load fixtures and there is no method suggested for estimating the long-term deflection.

The standard creep test is basically a quality control test and can not be used to predict the behavior of full-scale bearings because the shape factor, boundary conditions, loading conditions and exposure conditions (temperature etc.) of the full-scale bearings can vary considerably as compared to the test specimen. The objective of the present study is to investigate the creep behavior of laminated elastomeric bearings and propose a method to predict creep of such bearings based on small-scale testing. To understand the long-term behavior of elastomeric bearings under sustained axial loads, full-scale testing of selected bearings was performed. The methodology, results and findings of this study are presented in Section 3.2. Full-scale creep tests are time consuming, uneconomical and specific to the bearings tested. Since creep of elastomers is a material property, it must be controlled by imposing limitations on the time dependent shear modulus. To study the time dependent shear modulus, stress relaxation tests on small-scale specimens were performed in controlled environment. The effects of strain level and the size of the specimen on the relaxation shear modulus were

investigated. The methodology, results and findings of this study are presented in Section 3.3. A short-term method to predict long-term creep of elastomeric bearings based on the time dependent shear modulus is suggested in Section 3.4. Finally the conclusions are presented in Section 3.5.

3.2 FULL SCALE CREEP TESTS

3.2.1 Test Setup and Procedure

The full-scale creep tests were performed on bearings with smooth unbonded top and bottom surfaces and fully bonded top and bottom surfaces. Thus the two extreme boundary conditions were considered. Bearings molded from two types of elastomer: neoprene and natural rubber, at two hardness levels: Shore A Durometer 50 and 70 were tested. Hereafter the 50 and 70 durometer neoprene bearings will be referred to as CR50 and CR70 respectively, while the 50 and 70 durometer natural rubber bearings will be referred to as NR50 and NR70 respectively. Figure 3-1 shows the structural configuration of the bearings. Note that the cover at the edges was trimmed so that the laminates were clearly visible at all four sides. Figures 3-2, 3-3 and 3-4 show the test setup. The following are salient features of the setup:

1. Bearings were stacked on top of a heavy-duty hydraulically controlled ram (447 mm ram diameter and 8900 kN capacity) and reacted by means of a portal frame in tension. The ram was pressurized by means of a hydraulic system controlled by a constant weight hanging as shown in Figure 3-2 schematically.

2. The bearings were separated by means of smooth 12.7 mm aluminum plates. The axial deflection of each bearing was recorded with respect to time. The deflection at the center of the bearing was calculated from the relative displacement between the top and bottom plate surfaces by four calibrated linear pots. The load was measured by means of a load cell (890 kN capacity).
3. The data was acquired by means of an Analog-to-Digital data acquisition system connected to a PC. The 25 channels (24 connected to linear pots – 4 for each bearing and one connected to the load cell) were automatically scanned simultaneously at predetermined time intervals.

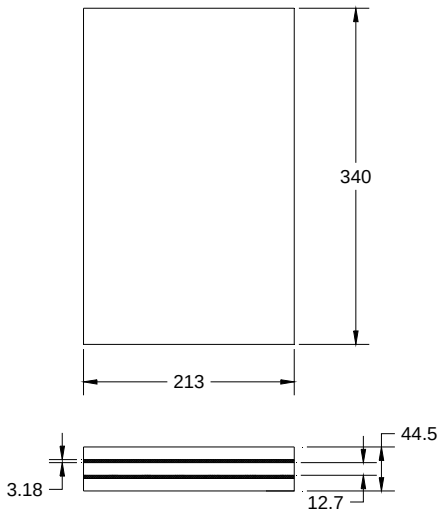

Dimensions shown in mm

Figure 3-1: Structural Configuration of Bearings used in Creep Tests

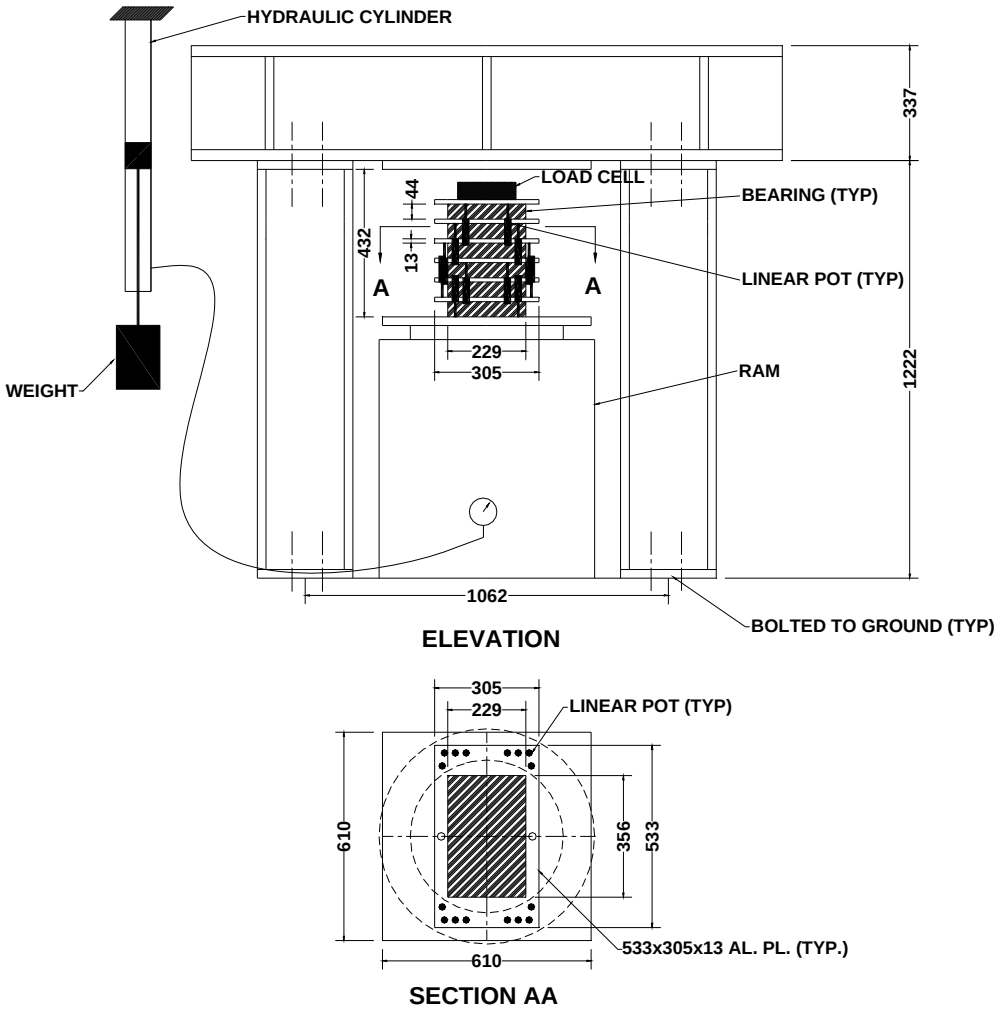

Dimensions shown in mm

Figure 3-2: Schematic of Test Setup for Creep Tests of Full-Scale Bearings

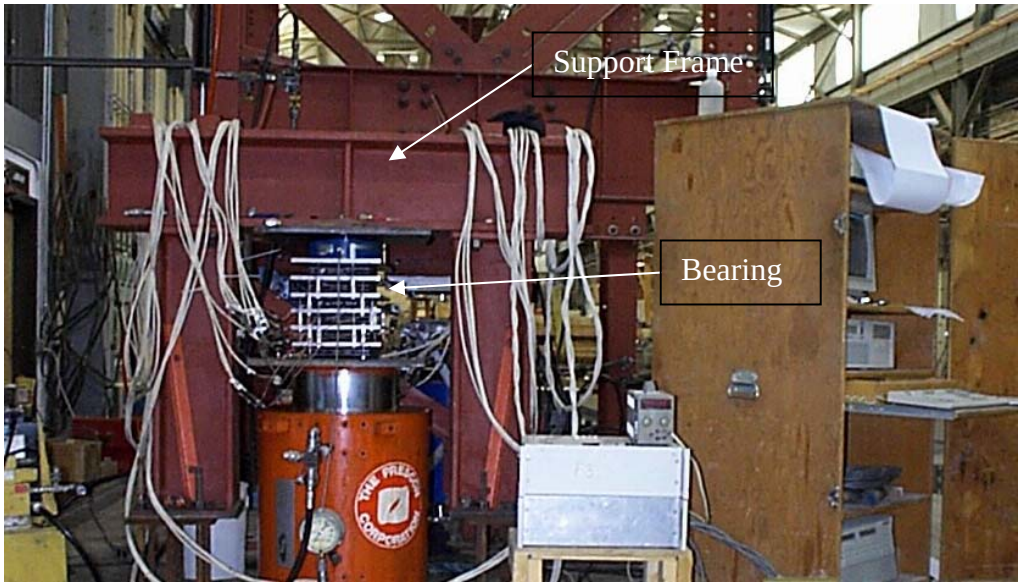

Figure 3-3: Test Setup for Creep Tests of Full-Scale Bearings

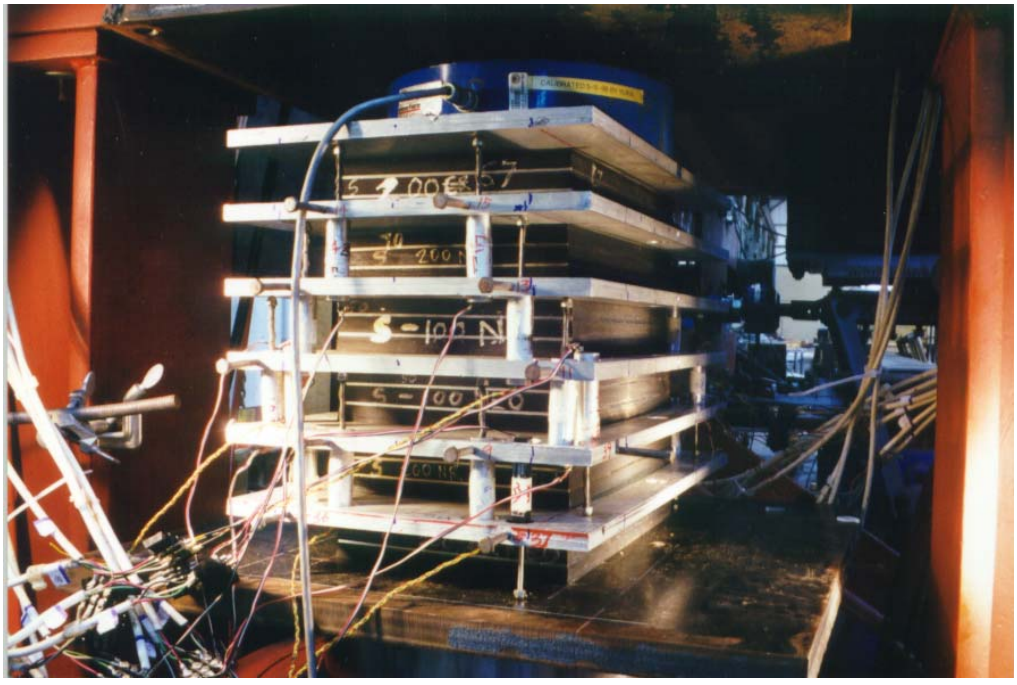

Figure 3-4: Test Setup for Creep Tests of Full-Scale Bearings (Close-up)

A buckling analysis was performed using the finite element method to estimate the maximum number of bearings that could be tested at a time. This calculation predicted a maximum number of six bearings in a stack. To account for test setup limitations a considerable amount of pilot testing was performed (about six months of testing) wherein six bearings, with and without top and bottom surfaces bonded, were tested at a time. The results of pilot testing indicated that there was a significant amount of friction in the loading system and the load increased with time (10-15 percent in one month of testing period). Also there were some minor undetectable leaks in the hanging weight system that caused the weight to gradually slide down with time eventually hitting the bottom of the cylinder. The total time for the weight to translate its full stroke was about one month. Also bearings at the top and bottom of the stack showed considerable end effects. The initial intent of placing six bearings was to have two replicates. To account for these deficiencies in the test setup, the following measures were taken in the final testing:

1. Load was recorded by means of a load cell and the variation of load was included in the creep calculations.
2. In order to ensure monotonically increasing load and eliminate cyclic effects, the duration of testing was limited to one month each for bonded and unbonded bearings tests.
3. The bearings were arranged from top to bottom in the following order: CR70A, NR70, CR50, NR50, CR70, NR70A so that the subject bearings NR70, CR50, NR50 and CR70 are free from end effects. The stiffer

bearings were placed at the ends of the stack for stability reasons. Note that the initial intent of placing six bearings was to have two replicates; however, due to test setup limitations, this idea was dropped and the two stiffer bearings were placed at the ends to mitigate the end effects.

4. A weight of 413 Kg was hung and sustained for 30 days to produce an intended maximum axial load equal to 418 kN. The actual load varied from 310-370 kN as shown in Figure 3-6 for NR50, due to the friction in the loading system. The corresponding average bearing stresses were 4.29-5.12 MPa, which is roughly the maximum design compressive stress (shape factor = 5.15) for CR50 or NR50 unbonded bearings.

3.2.2 Results of Full-Scale Creep Tests

The results of the creep tests for NR50 with bonded top and bottom surfaces are shown in Figures 3-5 through 3-7. Figure 3-5 shows a plot of axial deflection versus time while Figure 3-6 shows a plot of axial load versus time. Figure 3-5 and 3-6 are combined in Figure 3-7 that also shows the results of a regression analysis and the regression equation that relate the total deflection to time and load variation in the region of the measurements. Other plots, similar to Figure 3-7, for NR50, CR50, NR70 and CR70 are included in Appendix B.

Notice that the form of regression equation is same for all bearings as follows:

$$\ln(z) = a + b\ln(x) + c\ln(y) \qquad \text{(Eq. 3-1)}$$

where z, x and y are total axial deflection (mm), time (min) and axial load (kN) respectively and a, b and c are the regression coefficients tabulated in Table 3-1.

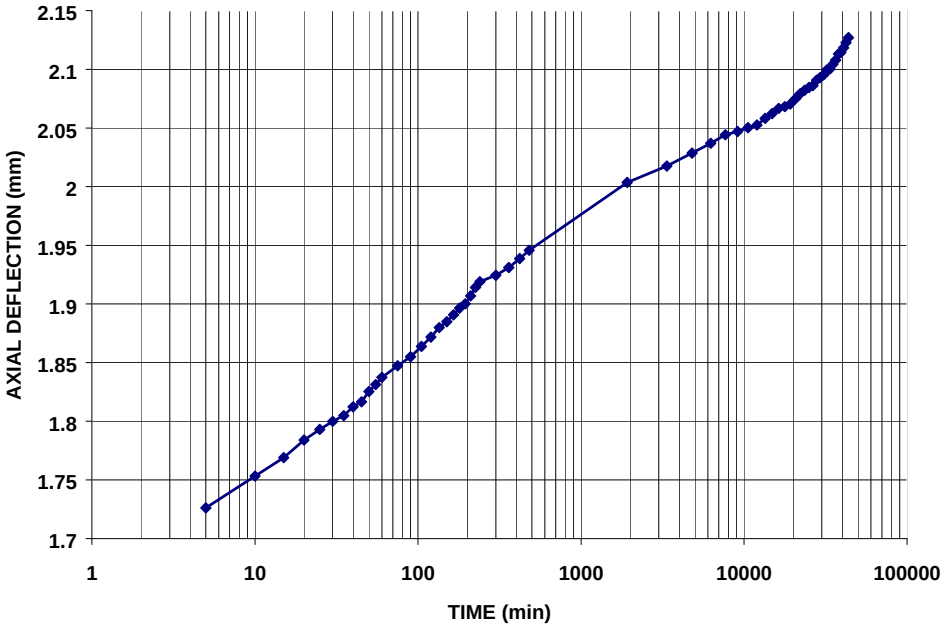

Figure 3-5: NR50-Bonded End Plates-Axial Deflection Versus Time

The instantaneous deflections and creep deflections after 1 hour, 30 days and 25 years predicted using the regression equations for the subject bearings under 350 kN axial load are tabulated in Table 3-2. Deflections at other times and loads can be calculated using Equation 3-1 with appropriate coefficients from Table 3-1. A comparison of axial deflections of bearings with bonded and unbonded top and bottom surfaces are shown in Figure 3-8.

Creep deflection expressed as percent of instantaneous deflection (deflection at 1 min) for various bearings and end conditions are tabulated in Table 3-3. Creep deflection expressed as percent of total deflection after one hour for various bearings and end conditions are tabulated in Table 3-4. Creep deflection expressed as percentage of original unstressed rubber thickness for various bearings and end conditions are tabulated in Table 3-5.

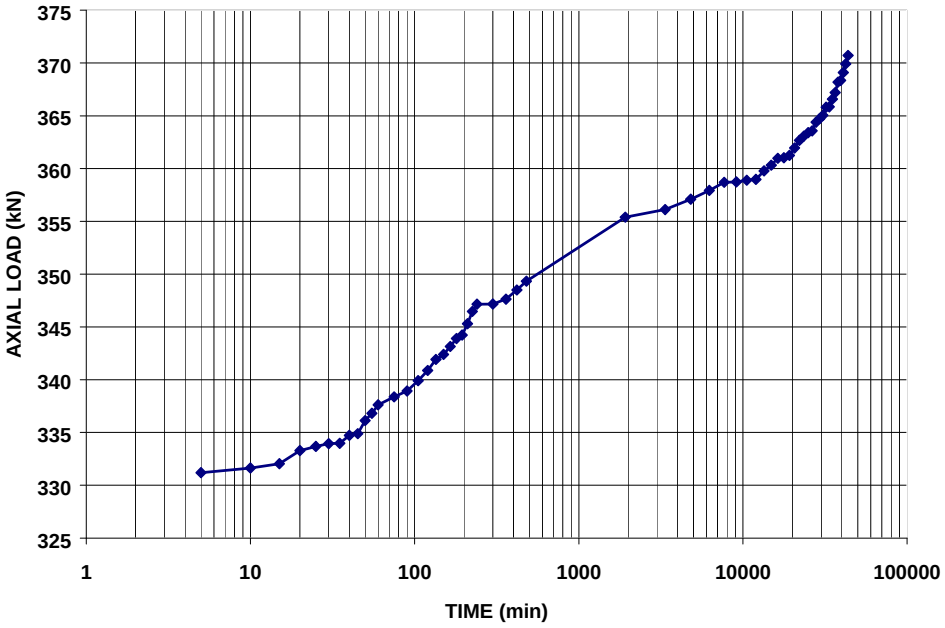

Figure 3-6: NR50-Bonded End Plates-Axial Load Versus Time

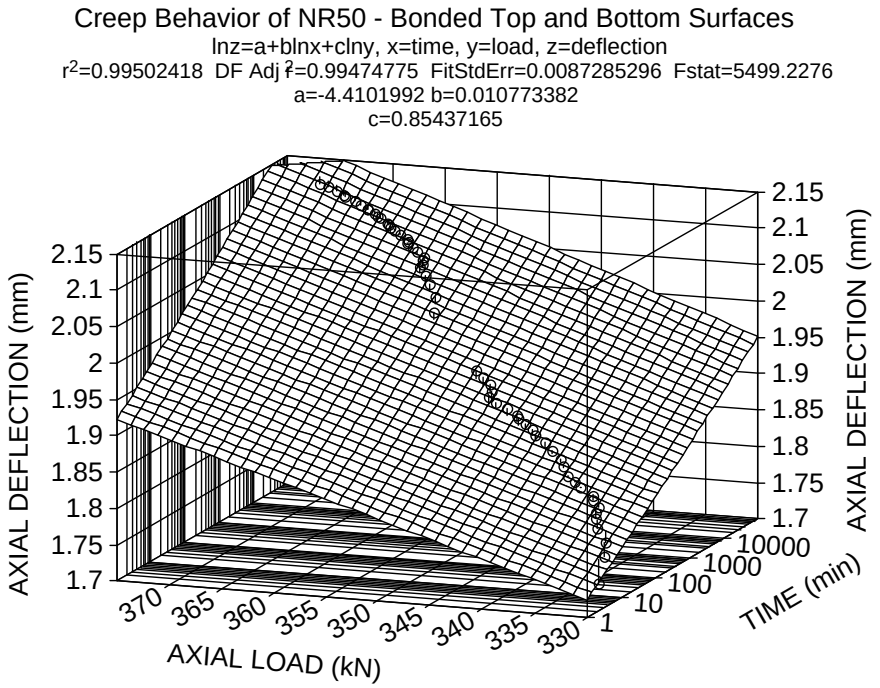

Figure 3-7: NR50-Combined Axial Load and Axial Deflection Versus Time

Table 3-1: Regression Coefficients in Equation 3-1

Bearing Type	Regression Coefficients							
	Bonded Top and Bottom Surfaces				Smooth Unbonded Top and Bottom Surfaces			
	a	b	c	R^2	A	b	c	R^2
NR50	-4.4102	0.010773	0.854372	0.995	-2.63104	0.018138	0.634728	0.996
CR50	-4.0886	0.009053	0.802724	0.987	-2.0482	0.016151	0.537228	0.986
NR70	-5.49775	0.012885	0.955414	0.99	-3.65523	0.023189	0.727482	0.993
CR70	-5.05718	0.01178	0.874482	0.991	-3.05407	0.02152	0.618314	0.993

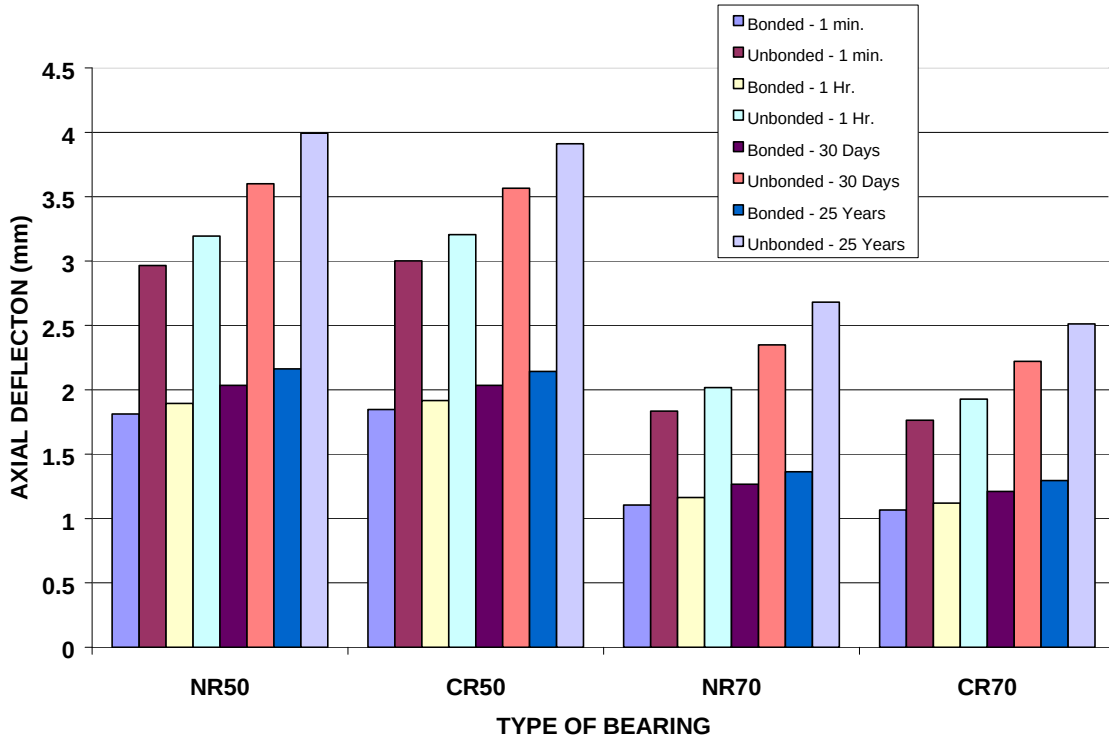

Figure 3-8: A Comparison of Axial Deflections at Various Times

Table 3-2: Deflections Based on Equation 3-1 under 350 kN Load

Bearing Type	Axial Deflection (mm) at Various Times for 350 kN Axial Load							
	Bonded Top and Bottom Surfaces				Smooth Unbonded Top and Bottom Surfaces			
	1 min	1 hour	30 days	25 years	1 min	1 hour	30 days	25 years
NR50	1.812	1.894	2.033	2.162	2.966	3.194	3.599	3.993
CR50	1.847	1.917	2.035	2.143	3.001	3.206	3.565	3.910
NR70	1.104	1.164	1.267	1.364	1.834	2.016	2.349	2.682
CR70	1.068	1.120	1.211	1.295	1.765	1.927	2.220	2.511

Table 3-3: Creep Deflection Expressed as Percent of Instantaneous Deflection

Bearing Type	Percent Creep Deflection at 350 kN Axial Load					
	Bonded Top and Bottom Surfaces			Unbonded Top and Bottom Surfaces		
	1 hour	30 days	25 years	1 hour	30 days	25 years
NR50	4.51	12.19	19.31	7.71	21.36	34.62
CR50	3.78	10.15	16.00	6.84	18.81	30.31
NR70	5.42	14.74	23.52	9.96	28.08	46.24
CR70	4.94	13.40	21.30	9.21	25.82	42.30

Table 3-4: Creep Deflection Expressed as Percent of One Hour Deflection

Bearing Type	Percent Creep Deflection at 350 kN Axial Load			
	Bonded Top and Bottom Surfaces		Unbonded Top and Bottom Surfaces	
	30 days	25 years	30 days	25 years
NR50	7.35	14.17	12.67	24.99
CR50	6.14	11.78	11.21	21.97
NR70	8.85	17.17	16.48	33.00
CR70	8.06	15.59	15.21	30.29

Table 3-5: Creep Deflection Expressed as Percent of Original Unstressed Rubber Thickness

Bearing Type	Percent Creep Deflection at 350 kN Axial Load					
	Bonded Top and Bottom Surfaces			Unbonded Top and Bottom Surfaces		
	1 hour	30 days	25 years	1 hour	30 days	25 years
NR50	0.21	0.58	0.92	0.60	1.66	2.70
CR50	0.18	0.49	0.78	0.54	1.48	2.39
NR70	0.16	0.43	0.68	0.48	1.35	2.23
CR70	0.14	0.38	0.60	0.43	1.20	1.96

3.2.3 Findings of Full Scale Creep Tests

Based on the results of full-scale creep tests, the following inferences can be drawn:

1. As shown in Figure 3-8 and Table 3-3, time dependent deformation of elatomeric bearings is significant and must be considered in design of such bearings.
2. Both natural rubber and neoprene bearings fabricated from low or high durometer rubber deform significantly due to elastomer creep.
3. Bearings with bonded top and bottom surfaces exhibit considerably less creep deformation as compared to bearings placed on smooth unbonded top and bottom surfaces (refer to Figure 3-8 and Table 3-3). The axial deflection of unbonded bearings was about twice as much as the axial deflection of bearings with bonded sole plates. Without creep the unbonded bearings would be expected to have about 30 percent more axial displacement than the same bearings with bonded sole plates. In bonded bearings the time dependent deformation is mainly due to material creep whereas not only material creep but also gradual slip of top and bottom surfaces with time significantly contributes to the time dependent deformation of unbonded bearings. The rubber is almost incompressible so the axial deformation of bearings is due to bulging of the rubber that is controlled by the constraints imposed by top and bottom contacting surfaces. The slip of top and bottom bearing surfaces with respect to contacting surfaces give rise to additional bulge as shown in Figure 3-9.

In the unbonded specimens the bearings have two layers with unbonded surfaces (exterior layers) and one interior layer. The external metal contact surfaces are very smooth. All rubber layers have the same thickness so the two external layers would be expected to contribute at least 75 percent of the initial deflection. As the number of internal rubber layers increase, the influence of the creep in the external layers on the overall creep deflection will diminish.

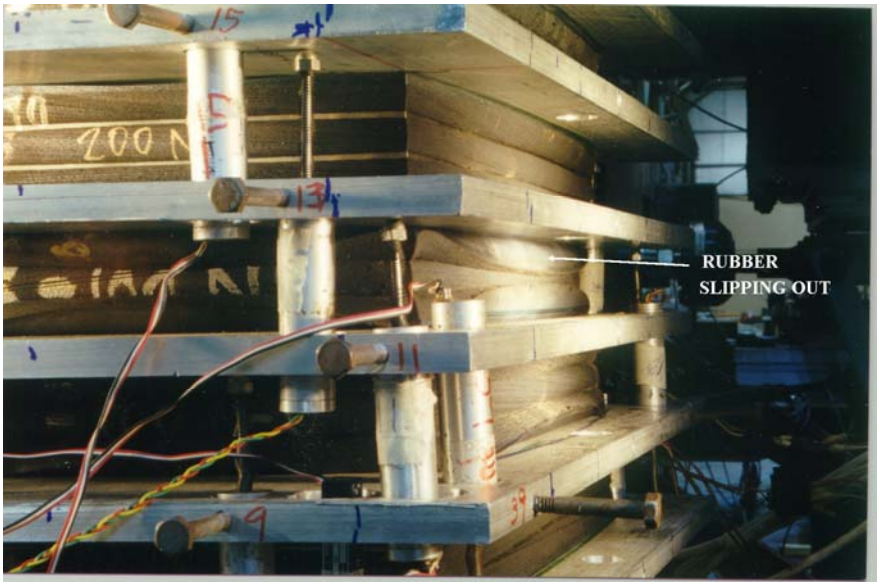

Figure 3-9: Condition of Loaded Bearings with Unbonded Top and Bottom Surfaces after One Month of Sustained Loading

4. As expected, high durometer bearings show higher percent creep as compared to low durometer bearings due to a higher carbon black (filler) content (refer to Tables 3-3 and 3-4). For example the 30 day creep of NR70 is 15 percent as compared to 12 percent for NR50 while 30 day

creep of CR70 is 13 percent as compared to 10 percent for CR50. Note that these numbers refer to bearings with bonded top and bottom surfaces based on instantaneous deflection. Refer to Tables 3-3 and 3-4 for other results. Also note that the absolute creep deformation of high durometer bearings is lower than those of the low durometer bearings as shown in Figure 3-8 and Table 3-2. So, if the designer is interested in absolute creep deformation, high durometer bearings can be used.

5. Neoprene bearings show slightly less percent creep as compared to natural rubber bearings, however the difference is not significant (refer to Tables 3-3 and 3-4).
6. The percent creep deflection is insensitive to small fluctuations of loads, however for large load variations the creep deformation at higher loads will be higher as compared to the lower loads as implied in Figure 3-18 in Section 3.3 that shows that percent change in shear modulus with time is higher at higher strains. For example with reference to AASHTO Specification M251, bearings subjected to a compressive stress of 7600 kPa will exhibit slightly more creep deformation (1-3 percent higher) as compared to bearings subjected to a compressive stress of 6900 kPa.
7. AASHTO Specifications has set criteria to evaluate creep for elastomeric bearings wherein creep deflection at 25 years expressed as percent of instantaneous deflection is limited to 25 and 45 percent for 50 and 70 durometer bearings respectively. Bearings with bonded top and bottom surfaces meet these criteria, while bearing placed on smooth top and

bottom surfaces marginally fail to meet these criteria (except CR70). Note that the smooth surface as in the case of smooth Aluminum plates is an extreme situation. In real life the surfaces may not be that smooth and the bearings will probably meet the creep criteria. However, it must be emphasized that the unbonded end surfaces result in highly uncertain boundary conditions.

8. The consequences of creep and relaxation on the overall bearing performance include: (a) increase in axial displacement, (b) reduction in shear force and (c) increase in indirect shear strains and reinforcement stresses. From a performance point of view, increase in axial displacement is more important so long as internal stresses and strains are within allowable limits. For single span simply supported girders, excessive creep can cause misalignment in adjacent spans while for multi-span continuous girders excessive creep affects the moment distribution in the girder. Reduction in shear force is generally beneficial, however it can affect the performance of a bearing seated on a sloping abutment.
9. The true instantaneous deformation of an elastomeric bearing is very difficult to measure because a considerable amount of creep occurs within first few minutes of loading. AASHTO specifications compare the creep deformation to the instantaneous total deformation of the bearing. A better criterion for creep is to compare the creep deformation to the total deformation after one hour of loading as shown in Table 3-4. This is more

representative of a real situation where the full load is realized after several hours of bearing placement.

3.3 RELAXATION SHEAR MODULUS

As mentioned earlier creep is a material property, so it must be considered during the design phase of the bearings. Since time dependent behavior of an elastomeric bearing, including creep is governed by time dependent shear modulus, limitations must be imposed on the variation of shear modulus over time rather than on axial deflection. This way not only will the axial deflection be controlled but the shear stiffness will also be controlled. This Section summarizes the methodology, results and findings of stress relaxation tests performed on small scale specimens in controlled environment to study the time dependent shear modulus of the elastomers (NR50, CR50, NR70 and CR70) used in the bearings tested in Section 3.2.

3.3.1 Test Specimens

The stress relaxation tests were performed on three sizes of specimens: (a) 1x1 shear specimen (25x25 mm), (b) 2x2 shear specimens (51x51 mm) and (c) 3x3 shear specimens (76x76 mm).

1x1 Shear Specimens

Figure 3-10 shows the structural configuration of 1x1 shear specimen used in the stress relaxation studies. The specimens using NR50, CR50, NR70 and CR70 unvulcanized rubbers were molded and cured at 127^{o} C for 3 hours. Lords Corporation's Chemlok 205/220 rubber-to-metal bonding agents were used to bond the rubber to the metal plates during the vulcanization process. A

compression molding process was used to mold the specimens. Prior to molding the three metal bars were sand blasted and thoroughly cleaned using vapor degreasing and a chemical rinsing system. The primer 205 and adhesive 220 were applied per Chemlok specifications. These surface preparation and bonding agents were the same as those used in the fabrication of the full size bearings.

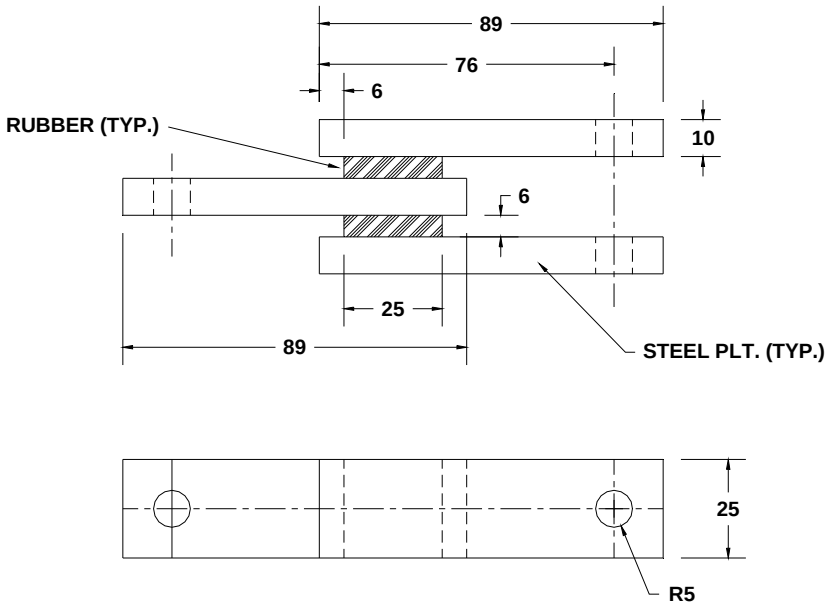

Dimensions shown in mm

Figure 3-10: Structural Configuration of 1x1 Shear Specimens

2x2 and 3x3 Shear Specimens

Figure 3-11 shows the structural configuration of 2x2 (51x51 mm) and 3x3 (76x76 mm) shear specimens used in the stress relaxation tests. The specimens were cut from the actual bearings of all four materials CR50, CR70,

NR50 and NR70 and cold bonded to metal plates. Industrial grade Crazy-Glue™ (manufactured by Alpha Industries) was used for rubber-to-metal cold bonding. Prior to adhesive application and assembly the three metal plates were sand blasted and thoroughly cleaned using vapor degreasing and chemical rinsing system. The rubber surfaces were thoroughly cleaned and the primer and adhesive was applied per manufacturers specifications.

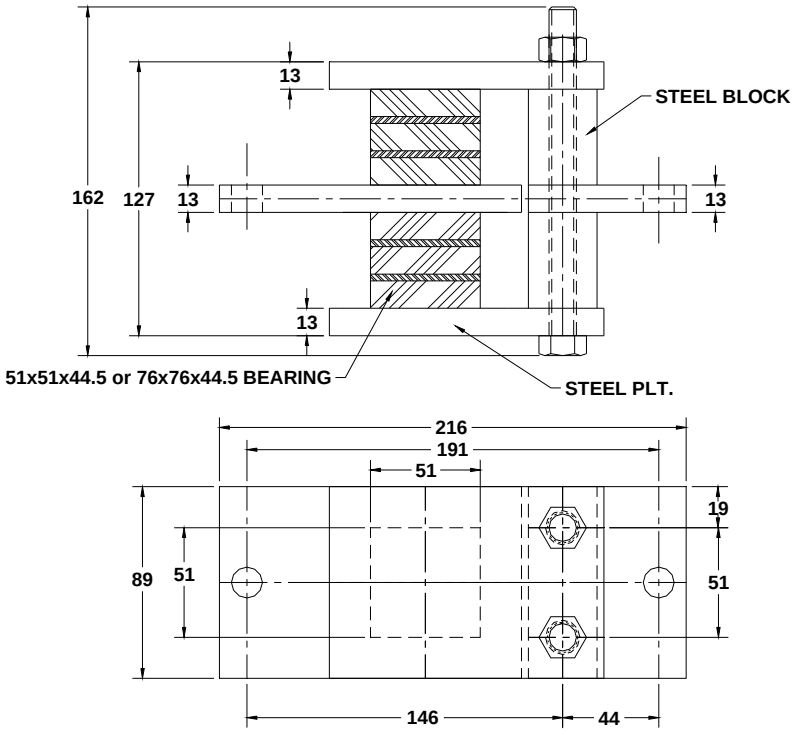

Dimensions shown in mm

Figure 3-11: Structural Configuration of 2x2 and 3x3 Shear Specimens

3.3.2 Test Setup and Procedure

The specimens were tested using a MTS system. An environmental chamber was used to precisely control the testing temperature as shown in Figure 3-12. The test setup and fixtures for 1x1 specimens are shown in Figure 3-13 while the test setup and fixtures for 2x2 and 3x3 specimens are shown in Figure 3-14. The fixtures and test setup were exactly same for both 2x2 and 3x3 specimens. In order to find the strain dependence of the relaxation modulus, the relaxation shear modulus of 1x1 specimens was measured at three shear strain levels 50%, 100% and 150% respectively. Since 2x2 and 3x3 specimens were cold bonded, the relaxation shear modulus for these specimens was measured only at 50% strain to avoid debonding during the test. The test procedure is summarized as follows. The test procedure was used for all three sizes and four type of rubbers.

1. The test specimen was mounted on the displacement controlled MTS system in an environmental chamber and a steady state test temperature of 32^{o} C was maintained during the test. This temperature was chosen because the full-scale testing was performed around 32^{o} C.
2. The 1x1 specimen was loaded to 150 percent shear strain while 2x2 and 3x3 specimens were loaded to 50% shear strain 10 times at 10% strain/sec to eliminate the Mullins effect. This was done only once for each specimen tested.
3. The specimen was loaded to 50% strain level in 1 second and the stress relaxation test was started. The strain level was maintained at 50 percent

while the stress and elapsed time was recorded for six hours using an automated National Instrument's Data Acquisition System. The relaxation modulus was calculated as the ratio of stress to strain at pre-determined times. Note that strain was constant while the stress was varying with time.

4. For 1x1 specimen, Step 3 was repeated at 100 percent and 150 percent strain levels.

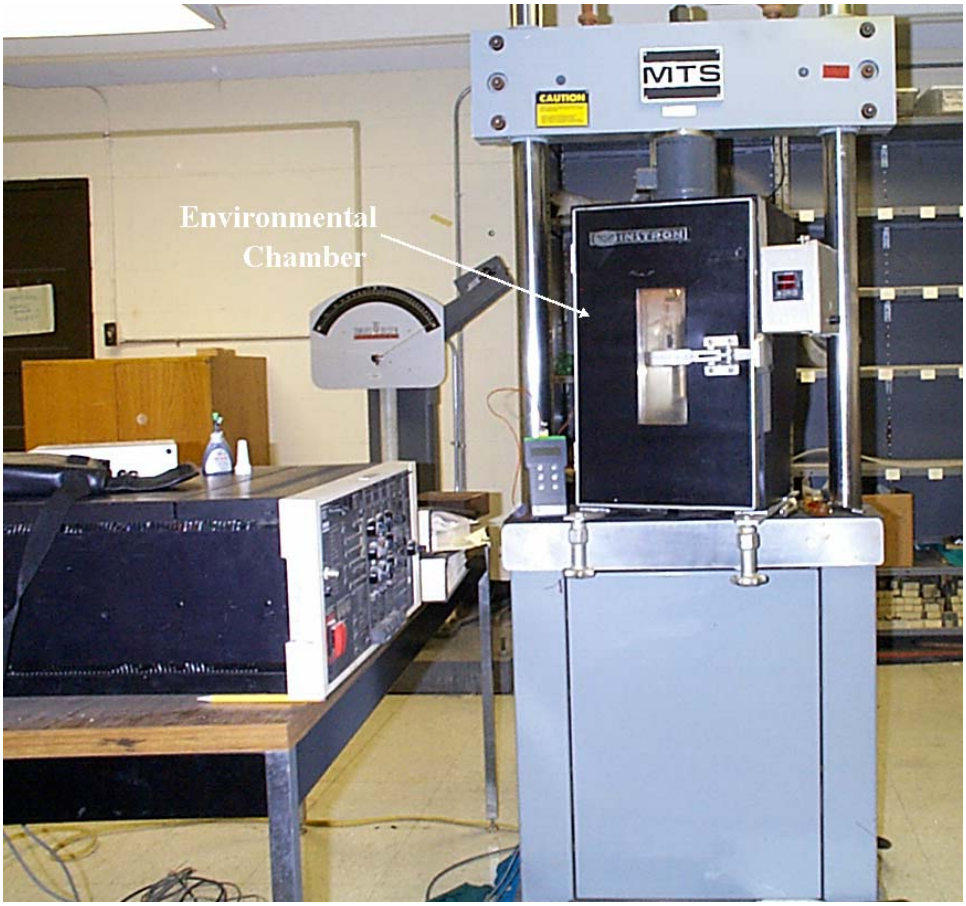

Figure 3-12: MTS System with Environmental Chamber used for Small-Scale Tests

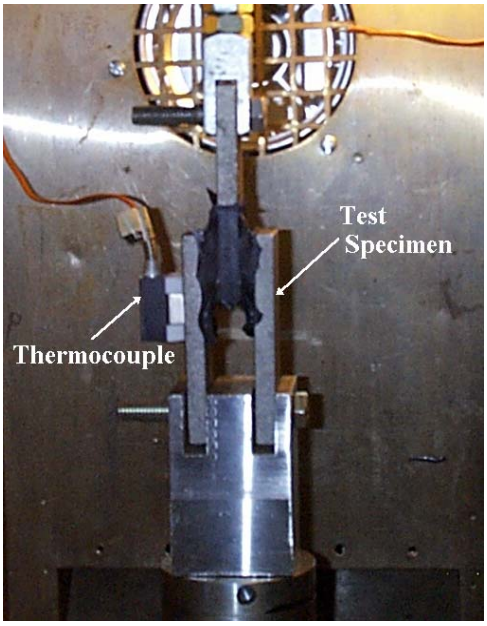

Figure 3-13: Test Setup and Fixtures for 1x1 Specimens

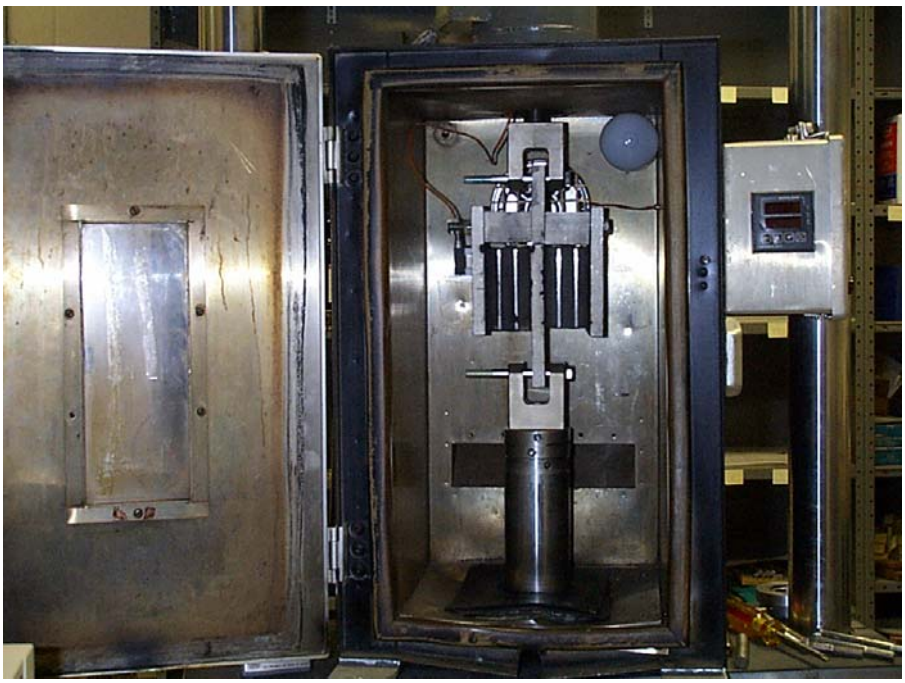

Figure 3-14: Test Setup and Fixtures for 2x2 and 3x3 Specimens

3.3.3 Reduction of Data and Results

The experimentally determined values of relaxation modulii at 1, 60 and 360 minutes at various shear strain levels for 1x1 specimen and at 50% shear strain for 2x2 and 3x3 specimens are tabulated in Table 3-6 for NR50, CR50, NR70 and CR70 rubbers.

Plots of shear modulus versus time at the three different strain levels were prepared and a regression analysis was performed to estimate a function relating shear modulus to time. The following modified power law gave a good correlation with all types of rubbers (NR50, CR50, NR70 and CR70) and at all strains levels (50%, 100% and 150%).

$$G(t) = a + \frac{b-a}{\left(1+\frac{t}{c}\right)^{d}} \qquad \text{(Eq. 3-2)}$$

where G(t) is the shear modulus at time t and a, b, c and d are regression coefficients. Note that coefficients “a” and “b” can be interpreted as shear modulii at times infinity and zero respectively. The regression coefficients for Equation 3-2 for various rubbers and strains levels are tabulated in Table 3-7.

Appendix B contains the plots of test data and modulus predicted by Equation 3-2 for NR50, CR50, NR70, and CR70 at 50%, 100% and 150% shear strain levels for 1x1 specimens. An example is shown in Figure 3-15 wherein the test data and the regression analysis results for NR50 at 50% strain are shown.

Table 3-6: Experimentally Determined Relaxation Shear Modulus

Rubber Type	Time (min)	Shear Modulus (MPa)				
		1x1 Shear Specimen			2x2 Shear Specimen (50 % Strain)	3x3 Shear Specimen (50 % Strain)
		50 % Strain	100 % Strain	150 % Strain		
NR50	1	0.5768	0.5583	0.5464	0.6164	0.6338
	60	0.5284	0.5077	0.4915	0.5654	0.5793
	360	0.5144	0.4932	0.4760	0.5532	0.5656
CR50	1	0.6799	0.6717	0.7322	0.6911	0.7086
	60	0.6129	0.6019	0.6531	0.6516	0.6593
	360	0.5989	0.5860	0.6330	0.6385	0.6447
NR70	1	1.1415	1.0371	1.2189	1.2500	1.1717
	60	1.0069	0.9088	1.0695	1.1012	1.0328
	360	0.9753	0.8776	1.0305	1.0691	1.0023
CR70	1	1.1173	1.1383	1.8304	1.3222	1.2836
	60	0.9998	1.0057	1.6145	1.1720	1.1451
	360	0.9712	0.9739	1.5584	1.1378	1.1163

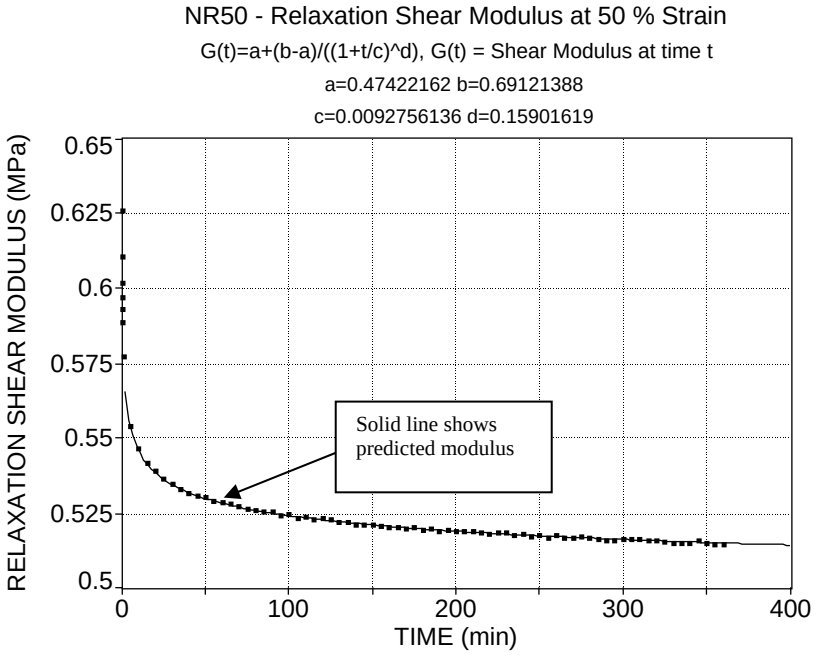

Figure 3-15: Test Data and Regression Analysis Results using Equation 3-2

Table 3-7: Regression Coefficients in Equation 3-2

Rubber Type	Regression Coefficients (refer to Appendix B for higher significant digits)											
	50% Shear Strain				100% Shear Strain				150% Shear Strain			
	a MPa	b MPa	c	d	a MPa	b MPa	c	d	a MPa	b MPa	c	d
NR50	0.4742	0.6912	0.0093	0.1590	0.4430	0.6725	0.0072	0.1396	0.4226	0.6756	0.0070	0.1440
CR50	0.5719	0.8997	0.0093	0.2372	0.5529	0.8764	0.0104	0.2186	0.5830	0.9764	0.0054	0.1854
NR70	0.9032	1.6060	0.0051	0.2043	0.8018	1.5708	0.0021	0.1919	0.9242	1.6637	0.0051	0.1738
CR70	0.9009	1.5736	0.0026	0.1908	0.9022	1.6885	0.0027	0.2027	1.4096	2.3750	0.0093	0.1767

If the first thirty minutes of relaxation modulus versus time data is excluded, a simplified power law of the following form can be conservatively used to predict the relaxation modulus at times greater than thirty minutes.

$$G(t) = at^b \qquad \text{(Eq. 3-3)}$$

The regression coefficients in Equation 3-3 for various rubbers and strain levels are tabulated in Table 3-8 for 1x1 specimen. In order to compare the results of Equation 3-2 to 3-3, the regression analysis was performed so that the shear modulii predicted by Equations 3-2 and 3-3 at 1 hour was identical. Figure 3-16 shows the curve fitting of Equation 3-3 for NR50 at 50% strain. Note that Equation 3-3 is very attractive for practical purposes because it represents a straight line on a log paper as follow:

$$\log(G(t)) = \log(a) + b\log(t) \qquad \text{(Eq. 3-4)}$$

Figure 3-17 shows a plot of log(G(t)) versus log(t) using the test data for 1x1 NR50 at 50% strain level and a straight line fit using the method of least squares.

Table 3-8: Regression Coefficients in Equation 3-3 for 1x1 Specimen

Rubber Type	Regression Coefficients					
	50% Shear Strain		100% Shear Strain		150% Shear Strain	
	a	b	a	b	a	b
NR50	0.561126	-0.01481	0.543704	-0.01652	0.530035	-0.01848
CR50	0.648426	-0.01374	0.641033	-0.0155	0.70225	-0.01774
NR70	1.086329	-0.01856	0.987704	-0.02019	1.166732	-0.02129
CR70	1.070865	-0.01673	1.083917	-0.01836	1.755371	-0.02036

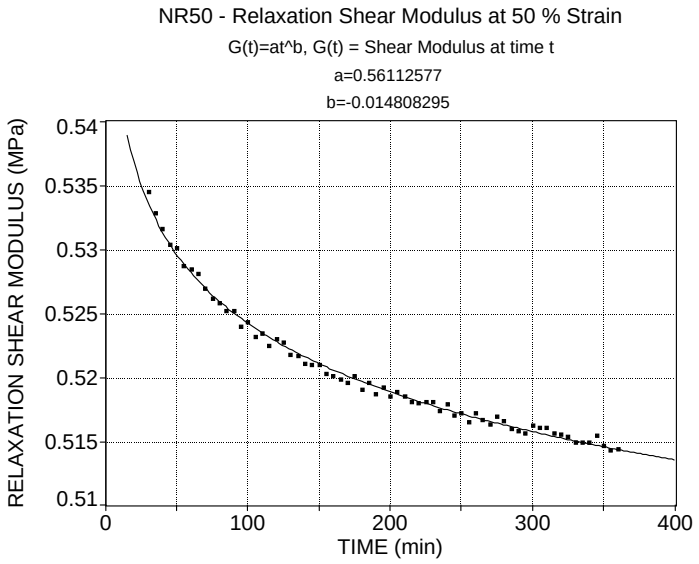

Figure 3-16: Test Data Excluding First 30 Minutes and Regression Analysis Results using Equation 3-3

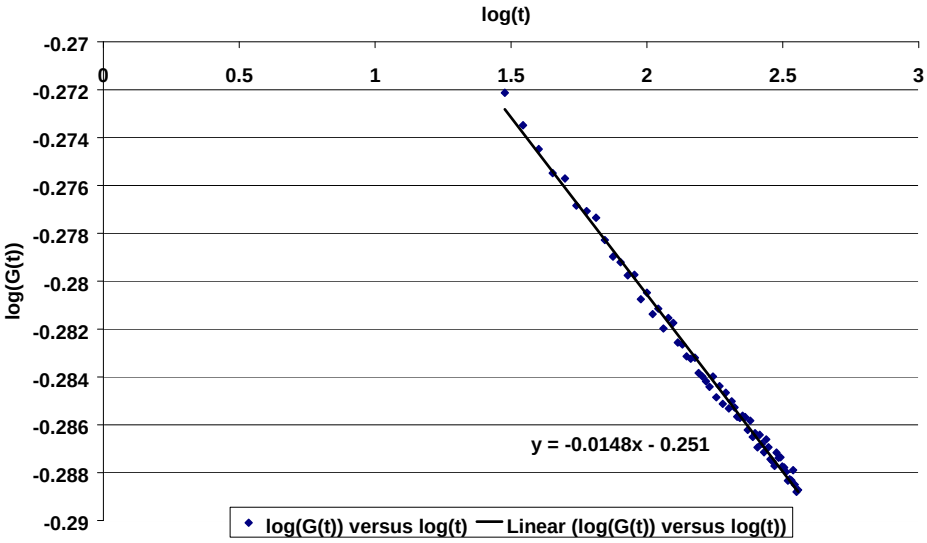

Figure 3-17: Least Square Fit of Equation 3-4 for NR50 at 50% Strain using 1x1 Test Data

3.3.4 Findings of Shear Relaxation Tests

Figure 3-18 shows the percent change in shear modulus after six hours of relaxation at various strains based on 1x1 test specimen results. Figure 3-19 shows the percent change in shear modulus after six hours of relaxation at 50% strain for the three sizes tested (1x1, 2x2 and 3x3). Table 3-9 shows the shear modulii after 1 min, 1 hour, 30 days and 25 years for NR50, CR50, NR70 and CR70 rubbers at 50%, 100% and 150% shear strain levels as predicted using Equation 3-2. Table 3-10 shows the shear modulii after 1 hour, 30 days and 25 years for NR50, CR50, NR70 and CR70 rubbers at 50%, 100% and 150% shear strain levels as predicted using Equation 3-3. Table 3-11 shows the predicted

shear modulii using Equation 3-3 for (1x1), (2x2) and (3x3) specimens at 50% shear strain. Table 3-12 shows the shear modulii after 1 hour, 30 days and 25 years for NR50, CR50, NR70 and CR70 rubbers at 50% shear strain levels as predicted using Equation 3-3 expressed as ratios for easy comparison.

Based on the results of stress relaxation tests, the following inference can be drawn:

1. At a constant temperature the shear modulus varies with both time and strain. As shown in Table 3-9, the modulus decreases with time and increases or decreases with strain depending on the strain level. As shown in Figure 3-15, a considerable amount of relaxation occurs within first few minutes of loading.
2. The reduction in shear modulus with time is higher at higher strains, however the difference is not very significant as shown in Figure 3-18.
3. The percent change in shear modulus with time is insensitive to the size of the specimen except for CR50 as shown in Figure 3-19.
4. Higher modulus rubbers show higher percent change in shear modulus with time as compared to lower modulus rubbers at all strain levels (refer to Figures 3-18 and 3-19).
5. As shown in Table 3-12, the shear modulii determined for the 2x2 and 3x3 specimens cut from the full size bearing are very similar. The 1x1 specimens show modulii that are about 10 percent lower than the larger specimens for NR50, CR50 and NR70 and 15 percent lower for the CR70 specimens. The difference between the 1x1 and the larger specimen can

be attributed to the fact that 1x1 specimens were vulcanized as part of this research and the 2x2 and 3x3 specimens were cut from manufactured bearings. All specimens within each rubber type presumably came from the same rubber batch.

Table 3-9: Predicted Shear Modulus for 1x1 Specimens using Equation 3-2

Rubber Type	Shear Modulus (MPa) at Various Times											
	50% Shear Strain				100% Shear Strain				150% Shear Strain			
	1 min	1 hour	30 days	25 years	1 min	1 hour	30 days	25 years	1 min	1 hour	30 days	25 years
NR50	0.577	0.528	0.493	0.482	0.558	0.508	0.469	0.455	0.546	0.491	0.449	0.434
CR50	0.680	0.613	0.581	0.574	0.672	0.602	0.564	0.556	0.732	0.653	0.604	0.590
NR70	1.142	1.007	0.930	0.912	1.037	0.909	0.832	0.812	1.219	1.069	0.970	0.941
CR70	1.117	1.000	0.929	0.910	1.139	1.005	0.929	0.911	1.831	1.614	1.474	1.433

Table 3-10: Predicted Shear Modulus for 1x1 Specimens using Equation 3-3

Rubber Type	Shear Modulus (MPa) at Various Times											
	50% Shear Strain				100% Shear Strain				150% Shear Strain			
	1 min	1 hour	30 days	25 years	1 min	1 hour	30 days	25 years	1 min	1 hour	30 days	25 years
NR50	-	0.528	0.479	0.440	-	0.508	0.456	0.415	-	0.491	0.435	0.391
CR50	-	0.613	0.560	0.518	-	0.602	0.543	0.497	-	0.653	0.581	0.525
NR70	-	1.007	0.891	0.801	-	0.909	0.796	0.709	-	1.069	0.930	0.823
CR70	-	1.000	0.896	0.814	-	1.005	0.891	0.802	-	1.615	1.413	1.257

Table 3-11: Predicted Shear Modulus for 1x1, 2x2 and 3x3 Specimens using Equation 3-3

Rubber Type	Shear Modulus (MPa) at 50% Strain for Various Times											
	1x1 Specimen				2x2 Specimen				3x3 Specimen			
	1 min	1 hour	30 days	25 years	1 min	1 hour	30 days	25 years	1 min	1 hour	30 days	25 years
NR50	-	0.528	0.479	0.440	-	0.565	0.522	0.487	-	0.579	0.528	0.488
CR50	-	0.613	0.560	0.518	-	0.652	0.604	0.566	-	0.659	0.605	0.561
NR70	-	1.007	0.891	0.801	-	1.101	0.987	0.898	-	1.032	0.925	0.842
CR70	-	1.000	0.896	0.814	-	1.172	1.052	0.958	-	1.145	1.042	0.960

Table 3-12: Predicted Shear Modulus for 1x1, 2x2 and 3x3 Specimens using Equation 3-3 Expressed as Ratios.

Rubber Type	Shear Modulus (MPa) at Various Times											
	1x1 Specimen				Ratio of 1x1 to 2x2				Ratio of 2x2 to 3x3			
	1 min	1 hour	30 days	25 years	1 min	1 hour	30 days	25 years	1 min	1 hour	30 days	25 years
NR50	-	0.528	0.479	0.440	-	0.934	0.917	0.903	-	0.975	0.988	0.998
CR50	-	0.613	0.560	0.518	-	0.940	0.927	0.915	-	0.989	0.998	1.009
NR70	-	1.007	0.891	0.801	-	0.914	0.902	0.891	-	0.970	1.067	1.067
CR70	-	1.000	0.896	0.814	-	0.853	0.851	0.850	-	1.02	1.010	0.998

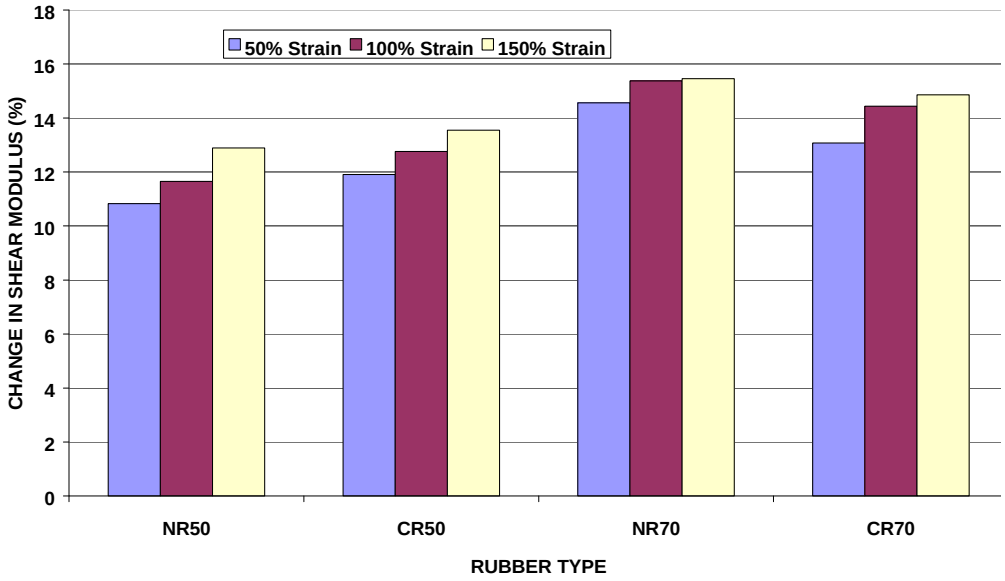

Figure 3-18: Percent Change in Shear Modulus After Six Hours of Relaxation of 1x1 Specimen at Various Strain Levels

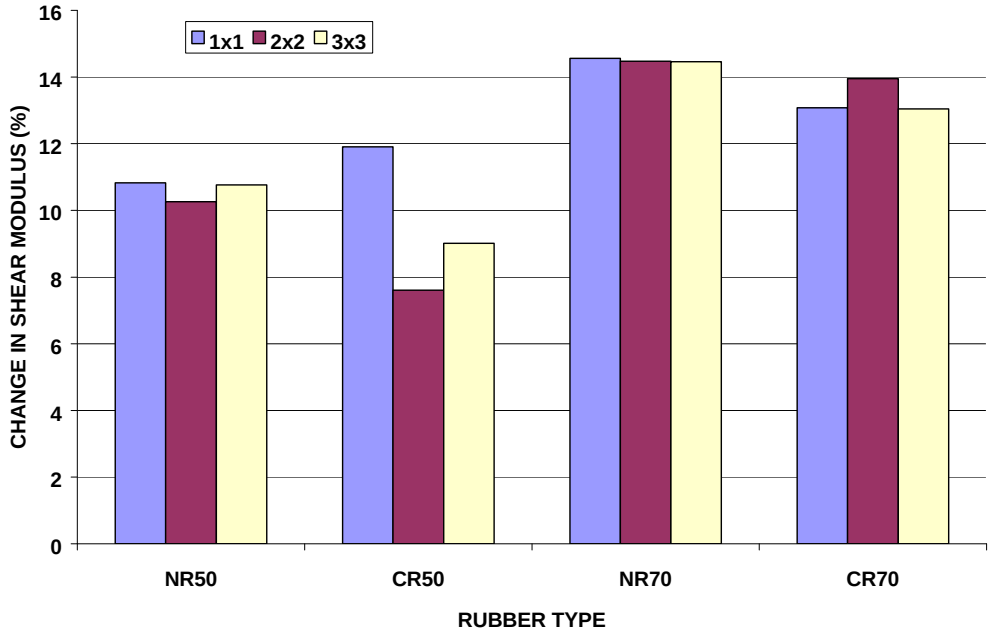

Figure 3-19: Percent Change in Shear Modulus After Six Hours of Relaxation of 1x1, 2x2 and 3x3 Specimens at 50% strain.

3.4 PREDICTION OF CREEP DEFORMATION

The instantaneous axial deformation (i.e., deformation after 1 min or 1 hour depending on the criteria) of an elastomeric bearing is generally known either by a physical test or design calculations. The average shear strain level is also known at the time of initial design. If the deformation at time t1 (1 min or 1 hour) is known, an estimate of long term axial deformation at time 't' can be approximately calculated as follows:

$$d_t = d_{t1} \frac{G_{t1}}{G_t} \qquad \text{(Eq. 3-5)}$$

where d_{t1} and d_t are the axial deformation at time t1 and t respectively while G_{t1} and G_t are the shear modulus at times t1 and t respectively calculated using Equation 3-2 or 3-3 at a strain level close to the average strain.

The above concept was used to predict the creep of full size bearings tested (refer to Section 3.2). The long-term axial deflection of the bearings with bonded top and bottom surfaces were predicted using Equation 3-5 in conjunction with Equations 3-2 and 3-3 based on 6 hour relaxation test data of 1x1, 2x2 and 3x3 specimens given in Section 3.3. The predicted values were compared to the full-scale test results given in Section 3.2. The results are summarized as follows:

Assuming that the instantaneous axial deflection is the 1 hour value given in Table 3-2 for the full-size bearings, Figure 3-20 shows the predicted axial deformation after 30 days for NR50, CR50, NR70 and CR70 bearings at three strain levels (50%, 100% and 150%) using Equations 3-2 and 3-3 based on 1x1 specimen's relaxation data. Figure 3-21 shows the effect of specimen size on the

predicted axial deflections based on simplified power law (Equation 3-3). Table 3-13 shows the predicted axial deformation expressed as percent of 1-hour deflection for various bearings using approximate procedure based on 1x1, 2x2 and 3x3 specimen's six hour relaxation data. A comparison of predicted axial deflection over 25 year period based on small-scale tests (simplified power law) and full-scale tests for NR50, CR50, NR70 and CR70 is shown in Figures 3-22, 3-23, 3-24 and 3-25 respectively.

Table 3-13: Predicted Axial Deformation Expressed as Percent of One Hour Deflection using Approximate Procedure

Rubber Type	Creep Deflection Expressed as Percent of Instantaneous Deflection (1 hour)							
	Full Size Bearing (refer to Table 3-4)		1x1 Specimen at 50% Shear Strain using Equation 3-3		2x2 Specimen at 50% Shear Strain using Equation 3-3		3x3 Specimen at 50% Shear Strain using Equation 3-3	
	30 Days	25 Year	30 Days	25 Year	30 Days	25 Year	30 Days	25 Year
NR50	7.35	14.17	10.23	19.97	8.28	16.03	9.68	18.84
CR50	6.14	11.78	9.46	18.41	7.87	15.21	8.97	17.41
NR70	8.85	17.17	12.99	25.64	11.48	22.53	11.55	22.66
CR70	8.06	15.59	11.64	22.84	11.35	22.26	9.88	19.25

From Figures 3-20, 3-21 and Table 3-13, the following inferences can be drawn:

1. The predicted deflections using Equation 3-5 in conjunction with Equation 3-2 or 3-3 compare fairly well with the full scale bearing deflections.

2. Relaxation shear modulus obtained at higher strains predicts higher axial deflections, however, the difference is not very significant.
3. The size of the specimen used for stress relaxation test has insignificant effect on the predicted deflection.
4. Axial deflections predicted based on simplified power law (Equation 3-3) gives a conservative estimate of axial creep deformation for bearing with bonded top and bottom surfaces. The 30 day deflection can be predicted conservatively within 3-4 percent based on Equation 3-3 and the 6 hour relaxation test while the 25 year estimate is 5-7 percent conservative.

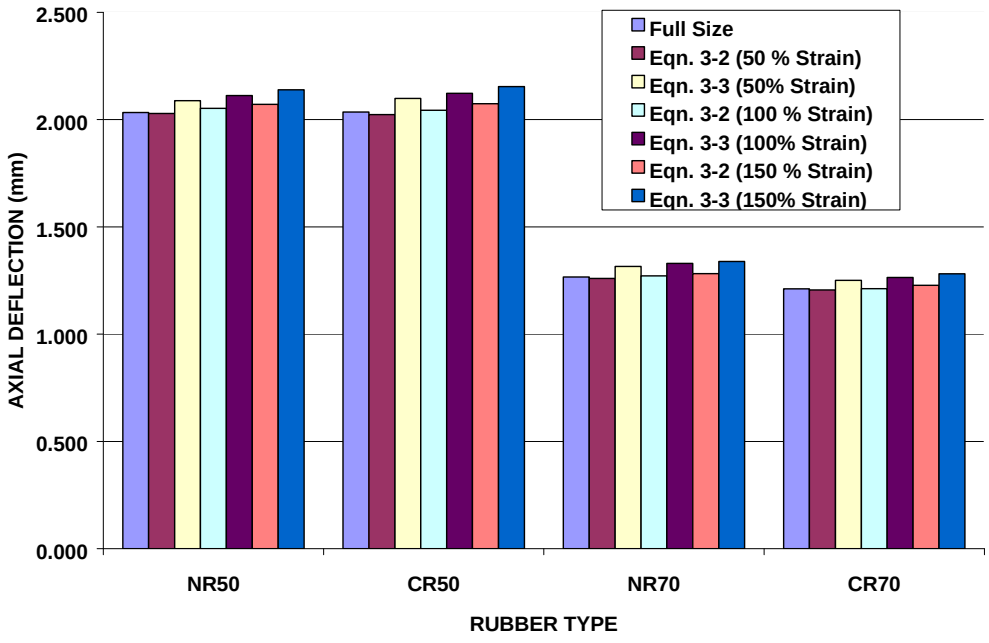

Figure 3-20: Axial Deflection of Various Bearings after 30 Days of Loading Predicted using Stress Relaxation Modulus at Various Strains.

It must be noted here that the simplified procedure presented in this section is applicable for bearings where the creep deformation is mainly due to material creep as in the case of bearings with bonded top and bottom surfaces. For bearings with unbonded top and bottom surfaces, the friction at the contact surface plays an important role and the long-term axial deformation is highly unpredictable. More research is needed to predict the long-term behavior of such bearings.

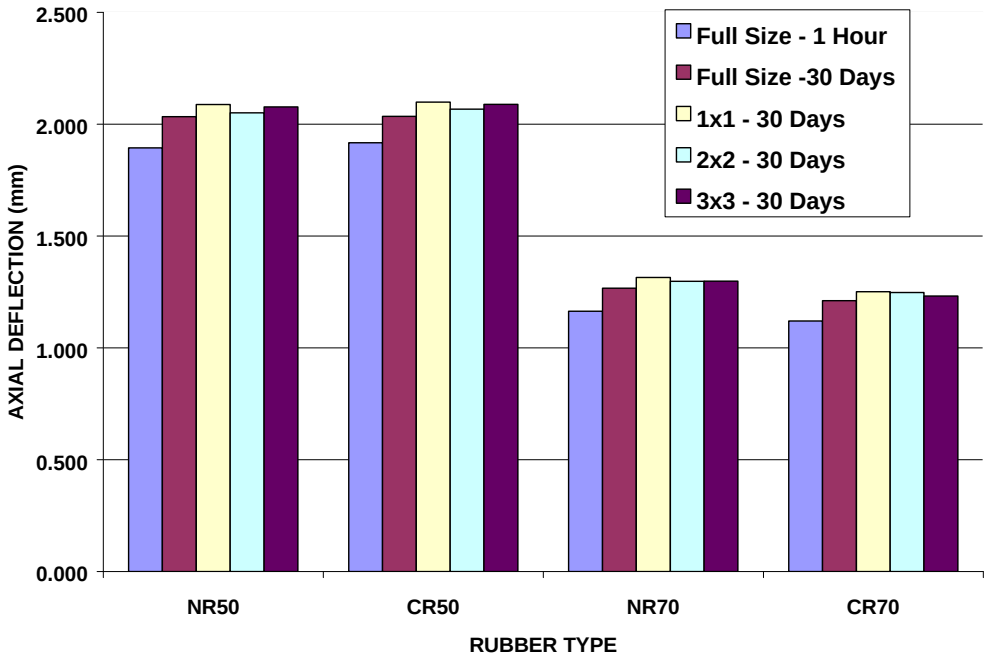

Figure 3-21: Axial Deflection of Various Bearings after 30 Days of Loading Predicted using Stress Relaxation Modulus Obtained from Different Sizes of Specimens

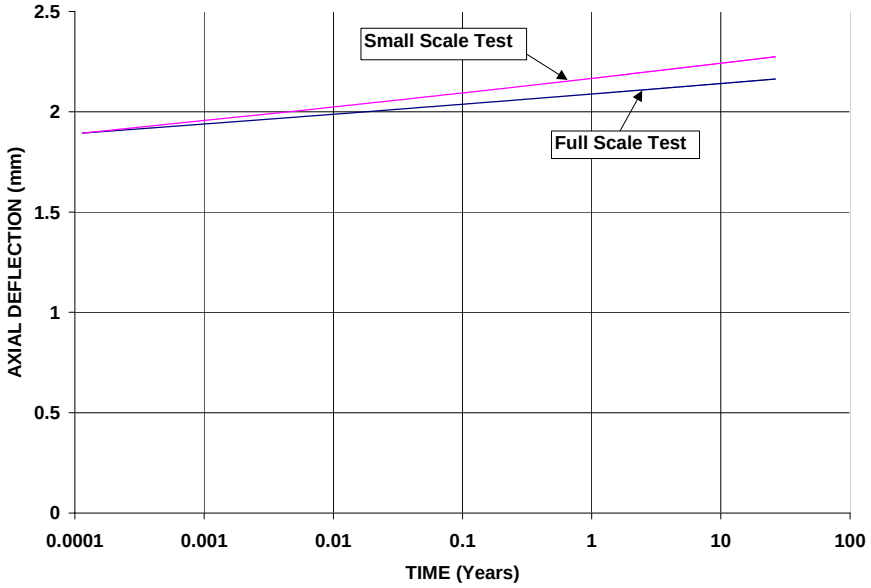

Figure 3-22: NR50-Axial Deflection Predicted Over 25 Years Based on Small Scale Test (Simplified Power Law) and Full Scale Test

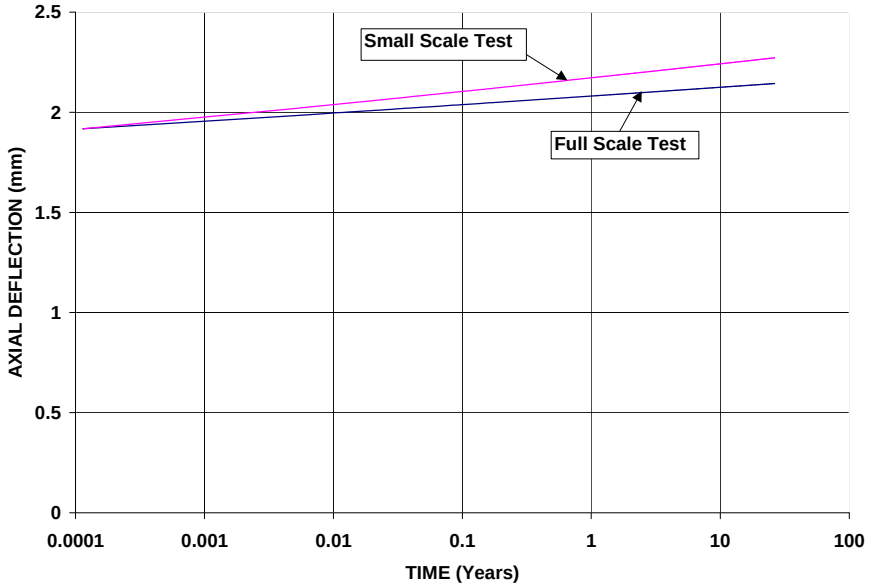

Figure 3-23: CR50-Axial Deflection Predicted Over 25 Years Based on Small Scale Test (Simplified Power Law) and Full Scale Test

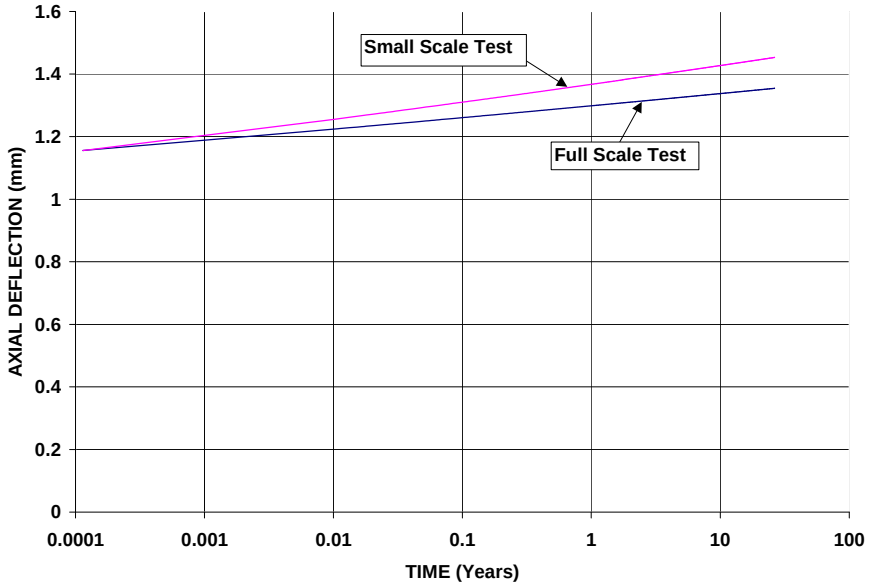

Figure 3-24: NR70-Axial Deflection Predicted Over 25 Years Based on Small Scale Test (Simplified Power Law) and Full Scale Test

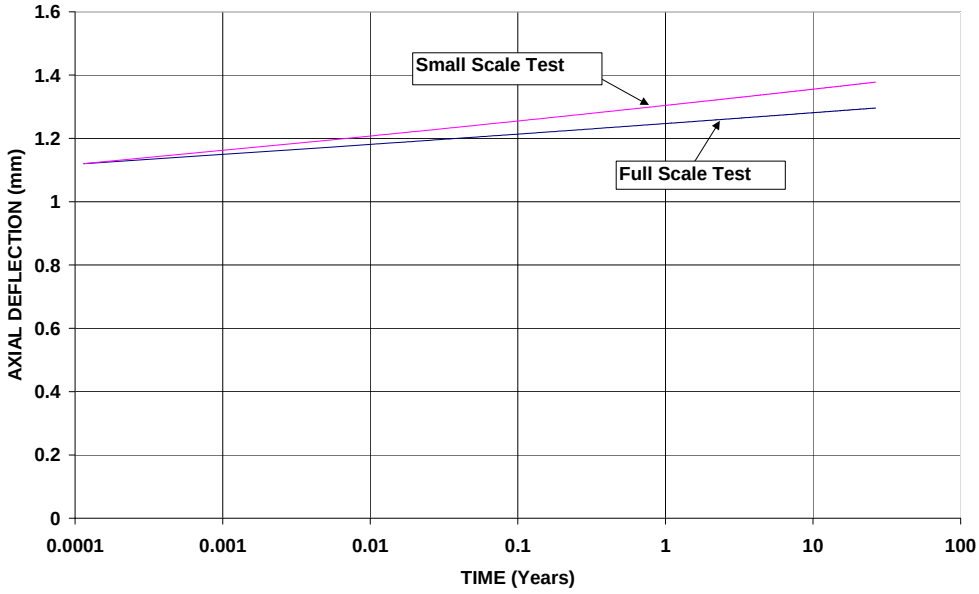

Figure 3-25: CR70-Axial Deflection Predicted Over 25 Years Based on Small Scale Test (Simplified Power Law) and Full Scale Test

Also note that the temperature (32^o C) at which the shear relaxation tests were performed was almost same as the temperature at which the full-scale bearings were tested. The temperature dependence of creep and stress relaxation of rubber is well known (Ferry, 1980), however, a pilot study on temperature dependence of shear modulus, conducted during this research indicated that the relaxation modulus is insensitive to small fluctuations of temperature ($\pm 10^o C$) in the proximity of room temperature and thermorheologically simple assumption (e.g. WLF relation) can not be used directly at higher temperatures due to chemical aging effects. The small-scale tests can be performed at room temperature, however, if the full size bearing temperature is outside the above range, it is advisable to perform the small-scale tests at the full size bearing temperature.

In order to meet the AASHTO creep criteria the limitations on time dependent shear modulus can be calculated. Table 3-14 shows the limitation on time dependent shear modulus corresponding to AASHTO criteria.

Table 3-14: Percent Change in Time Dependent Shear Modulus Corresponding to AASHTO Creep Criteria

Type of Rubber	Percent Change in 25 years	
	Creep Deformation	Shear Modulus
50 Durometer	25	20
60 Durometer	35	26
70 Durometer	45	31

3.5 CONCLUSIONS

1. Creep deformation can significantly affect the performance of an elastomeric bearing and must be considered during the design phase of such bearings.
2. The boundary condition at the top and bottom surfaces of an elastomeric bearing plays an important role in controlling the long-term deformation. The creep of bearings with unbonded top and bottom surfaces is highly unpredictable due to a gradual decay in friction forces at the interface of the bearing and the contacting surfaces.
3. For bearings with top and bottom surfaces bonded to metal plates, the axial deflection is mainly due to the bulging of rubber that is governed by the shear modulus. For such bearings a time dependent shear modulus obtained from short-term stress relaxation tests can be conservatively used to predict the long-term axial deflection (refer to Figures 3-22 through 3-25).
4. The true instantaneous deformation of an elastomeric bearing is very difficult to measure because a considerable amount of creep occurs within first few minutes of loading. AASHTO specifications compare the creep deformation to the instantaneous total deformation of the bearing. A better criterion for creep is to compare the creep deformation to the total deformation after one hour of loading.
5. Current AASHTO specifications also require a compression set test (ASTM D395 Method B). The compression set is essentially a

measurement of recovery after the removal of an applied stress or strain so it cannot be used to address creep or relaxation. If the purpose of specifying the compression set test is for the evaluation of creep of elastomeric bearings, then it can be eliminated from the AASHTO specifications because it does not serve this purpose.

6. Since the time dependent behavior of an elastomeric bearing, including creep is governed by time dependent shear modulus, limitations must be imposed on the variation of shear modulus over time rather than on axial deflection. This way not only will the axial deflection be controlled but the shear stiffness will also be controlled.

7.

Chapter 4: Aging

4.1 INTRODUCTION

All elastomers are attacked by oxygen even at room temperature and the reaction is accelerated by heat, light and presence of certain metallic impurities that catalyze the decomposition of peroxides to form free radicals (Shelton, 1972). This process is called aging. Degradation of physical properties is observed in elastomers even at quite low levels of oxidation. The nature of the changes observed vary considerably depending upon the specified elastomer, and the aging conditions to which it is subjected. The net effect on the properties is the resultant of two competing processes of chain scission and crosslinking. A review of these basic oxidation processes in elastomers is well documented by Shelton, 1972. If chain scission dominates, the elastomer softens and eventually become sticky with aging. Most elastomers, however, harden and eventually embrittle as a result of aging – a consequence of cross-linking dominance (Hamed, 1992).

There are several standardized tests available for quality control and for determining heat resistance or aging. ASTM D573, 1988, describes a test procedure to determine the influence of elevated temperature on the physical properties (hardness, elongation at break, tensile strength) of vulcanized rubber. Specimens of vulcanized rubber are exposed to deteriorating influence of air at specified temperatures for known periods of time, after which their physical properties are determined. These are compared with the properties measured on

unaged specimens and changes are noted. The changes should be below the specified requirements. ASTM D573 does not specify the value of exposure temperature and time for the test. The AASHTO elastomeric bearings material specification, M251 (1997) require different periods of exposure time and temperature as well as different tolerances for the changes in the physical properties for neoprene and natural rubber. The specimens are tested to determine hardness, tensile strength and elongation at break before and after the aging procedure. Although the specified aging time is the same for both elastomers, the exposure temperatures are 70^{o}C(158^{o} F) and 100^{o}C (212^{o} F) for natural rubber and neoprene, respectively. The tolerances specified for the physical properties are different for each elastomer. The AASHTO requirements from M251-97 are summarized in Table 4-1. The international standard for heat aging is ISO 188, 1982, which specifies an air oven and an oxygen bomb method.

Table 4-1: AASHTO M251-97 Heat Resistance Requirements per ASTM D573

Test Requirements	Polyisoprene (Natural Rubber)			Polychloroprene (Neoprene)			Units
	50 Duro	60 Duro	70 Duro	50 Duro	60 Duro	70 Duro	
Specified Temperature of the test	70	70	70	100	100	100	^{o}C
Aging Time	168	168	168	70	70	70	Hours
Max Change in Durometer Hardness	+10	+10	+10	+15	+15	+15	Shore A
Max Change in Tensile Strength	-25	-25	-25	-15	-15	-15	Percent
Max Change in Ultimate Elongation	-25	-25	-25	-40	-40	-40	Percent

Since aging is related to the oxidation process, the rate and extent of diffusion of oxygen through the elastomer governs the change in properties due to

aging. The rate of diffusion is dependent on temperature, pressure, exposed surface area and permeability of elastomer. In the case of elastomeric bearings oxygen ingress is generally limited to a thin layer of exterior surface only because of small exposed surface area (relative to loaded area) and low permeability of elastomer. Several case studies have shown that there has been no evidence of any significant deterioration of elastomeric bearng over the period that the bearing had been in service. Nakauchi et al (1992) analyzed and characterized small samples of a 100 year old bridge bearing from a viaduct in Australia by means of microanalytical methods. The results obtained with the microanalytical methods illustrated a convincing view on longevity of rubber pads for civil engineering applications. Aging of natural rubber is only limited to the surface and further ingress of oxygen to rubber deep inside is inhibited by the oxidized rubber formed.

Doody and Noonan, 1998, compared the results of accelerated aged tests, per AASHTO specifications, versus as-received recovered conditions of steel laminated elastomeric bearings placed on twin structures carrying the NY 400 Aurora Expressway over Conrail and NY 16 in Erie County. They found insignificant differences in mean tensile strength and elongation between the accelerated tests and bearings in service after 22 years. The mean hardness, however, differed significantly. They concluded that bearings performed very well in service and were relatively insensitive to deficiencies in design, construction and material properties.

Since heat accelerates the oxidation process, heat aging (also known as accelerated aging) has been used to predict the long-term elastomer properties at ambient temperatures. Moakes, 1975, reported changes in tensile modulus, observed over a 15 year period, of small specimens of different elastomers in temperate, tropical and desert conditions. He reported that aged tensile modulus increased between 60% and 100% as compared to unaged values for nitrile and between 20% and 110% as compared to unaged values for natural rubber. Accelerated aging tests were performed on each elastomer at 70^{o} C and 82^{o} C. Moakes stated that, for nitrile, 14 days at 82^{o} C appeared to be equivalent to 10 years of aging in tropical temperatures, and that use of aging temperatures above 100^{o} C would give misleading results.

In another study performed by Barker, 1988, four natural rubber compounds were aged at 23^{o} C over 5 years. Increases in tensile modulus were observed in the range of 10% to 75% over 5 years at 23^{o} C. The results were compared with Arrenhius based predictions (as discussed in Section 4.4) from measurements taken at an accelerated aging temperature of 40^{o} C. He observed that the lower aging temperature of 40^{o} C provided a better basis for predictions of changes in modulus, and concluded that at high aging temperatures reactions that break down an elastomer's component network have dominant influence whereas at lower aging temperatures crosslinking is dominant.

A more direct study on the effects of aging on elastomeric bearings used in oil field applications was recently performed by Hogan et. al., 1997. They predicted changes in shear modulus of nitrile and natural rubber elastomer

compounds over thirty years using the time-temperature reaction rate transformation applied to controlled aging experiments. Several different experimental techniques for obtaining the necessary measurements of accelerated material behavior were employed and compared. Various analytical techniques for characterizing rates change over time and across temperatures were applied to the measured data. Significantly different results were obtained depending upon the choice of assumptions. Variation in results depended upon accelerated aging temperatures, the relative availability of oxygen to the test specimen during aging, and the size of the test specimen. More research is needed to resolve some of these issues.

Almost all accelerated aging tests mentioned in various specifications are performed on very thin specimens wherein the oxidation affects the whole specimen and the mode of loading is generally tension. For elastomeric bearings, the change in overall shear stiffness due to aging is more relevant than the change in localized tensile properties represented by the accelerated aging tests. The objective of the present study is to investigate the effect of specimen size on the change in shear characteristics due to accelerated aging and extrapolate the results to ambient temperatures for full size bearings. Four different sizes of specimens were studied under the shear mode of deformation. Specimens molded from two types of elastomers: neoprene and natural rubber, at two hardness levels: Shore A durometer 50 and 70 were tested. Hereafter the 50 and 70 durometer neoprene bearings will be referred to as CR50 and CR70 respectively, while the 50 and 70 durometer natural rubber bearings will be referred to as NR50 and NR70

respectively. The specimen geometries, test methodology and results of accelerated aging tests are summarized in Section 4.2 while the interpretations and predictions at ambient temperature are presented in Section 4.3 and 4.4 respectively. The conclusions are presented in Section 4.5.

4.2 TEST SPECIMENS, METHODOLOGY AND RESULTS

The effect of accelerated aging on the shear characteristics of four sizes of specimens was studied (a) Rheometer specimens, (b) 1x1 shear specimen (25x25 mm), (c) 2x2 shear specimens (51x51 mm) and (d) 3x3 shear specimens (76x76 mm). In order to use Arrenhius relation (refer to Section 4.4), the accelerated aging was done at two temperatures 82^{o} C and 100^{o} C. The sizes and aging temperatures were selected based on the results of a pilot study so that significant spread of post-aging shear characteristics could be observed without damaging the specimens due to overheat.

4.2.1 Moving Die Rheometer (MDR) Specimens

The rheometer (also known as curemeter) shown in Figure 4-1 is generally used by rubber manufactures to study the vulcanization characteristics of elastomers. In vulcanization process there are two things that are most important (a) vulcanization temperature, and (b) thermal stability of the rubber compound. The vulcanization temperature is chosen to produce a properly cured product having uniform physical properties in the shortest possible molding time. The molding time varies inversely with temperature. Each type of rubber has a definite range of temperatures that may be used for vulcanization. In order to reduce the molding time and thereby the cost, the vulcanization is usually

performed at the highest allowable temperatures. The allowable temperatures are based on “degree of cure” or “optimum cure” tests performed in a Rheometer.

As schematically shown in Figure 4-2, a 5 gram sample of raw elastomer is placed in a die cavity that is sealed and maintained at a constant temperature and pressure. The cavity is formed by two dies one of which is oscillated through a rotary amplitude of $\pm 0.5^{o}$ at 1.66 Hz while the other is kept stationary. This produces a sinusoidal alternating torsional strain equivalent to a shear strain of 14 percent in the test piece and a sinusoidal reaction torque, measured at the stationary die, that is directly proportional to the shear modulus of the rubber compound. The lower die is shown in Figure 4-3 while a schematic of the lower die and specimen cross-section is shown in Figure 4-4. The appearance of upper die is very similar to lower die. The reaction torque is continuously recorded during the vulcanization process. Various terms associated with the reaction torque-time curve are shown in Figure 4-5. As the rubber vulcanizes cross-linking is dominant and the torque increases during this process until it reaches a maximum value M_H after which reversion is dominant. The time to reach 90 percent of M_H is call t_{90} and is generally used as a measure of cure rate. Figure 4-6 shows a typical MDR specimen after it is fully cured. The average thickness is 2 mm while the outer diameter is 40 mm. Note that the size is small enough for the oxygen to affect the whole specimen.

In order to estimate the optimum cure characteristics, rheometer torque-time curves were obtained at various temperatures. Figures 4-7 through 4-10 show the reaction torque versus time curves at two temperatures 127^{o}C and 182^{o}

C for NR50, CR50, NR70 and CR70 respectively. The following points are noteworthy:

1. As the vulcanization temperature is reduced, the curing time increases drastically for all compounds.
2. At lower vulcanization temperatures, the resulting stiffness of the cured compounds is higher. This can be attributed to two reason: (a) since rubber is a visco-elastic material, at lower temperature the viscosity is higher and therefore the shear stiffness is higher and (b) at lower temperature the cross-linking is more dominant than reversion.
3. Neoprene is thermally more stable than natural rubber at higher vulcanization temperatures.
4. At 127 ^{o}C vulcanization temperature, both natural rubber and neoprene compounds show insignificant reversion and a steady-state condition is reached in approximately one hour. Consequently, all rheometer and 1x1 specimens were vulcanized at 127 ^{o}C. As mentioned earlier, 2x2 and 3x3 specimens were cut from full size bearings that were vulcanized around same temperature.

As demonstrated in the present study, a rheometer can be effectively used to study the aging response in shear, since the weight, geometry and testing environment (temperature and pressure) of the specimen can be precisely controlled and the torque, that is directly proportional to the shear stiffness, can be precisely measured. As shown in Figure 4-11 a rheometer can also be effectively used to estimate the shear modulus at small strains. Based on 1x1 specimen shear

modulus data, Figure 4-11 shows an empirical relationship between rheometer reaction torque and shear modulus at 14 percent shear strain.

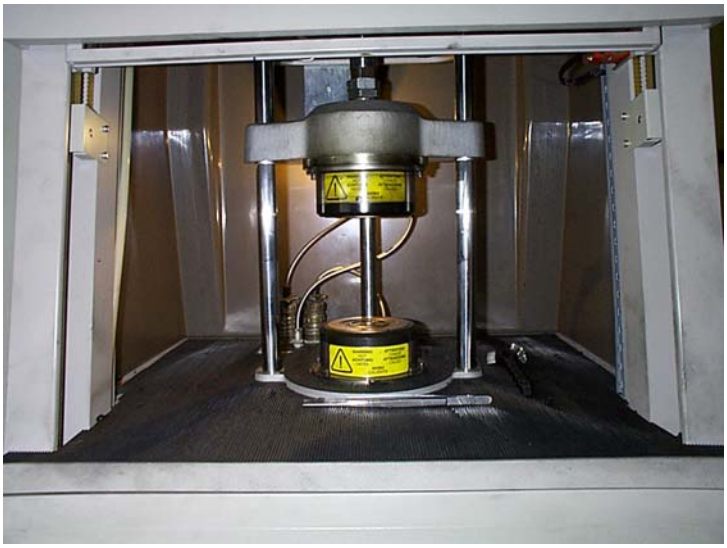

Figure 4-1: Moving Die Rheometer

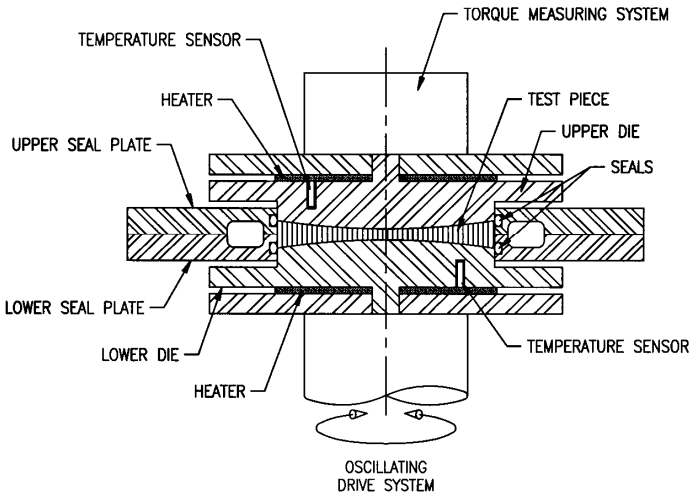

Figure 4-2: Schematic of Moving Die Rheometer Operation

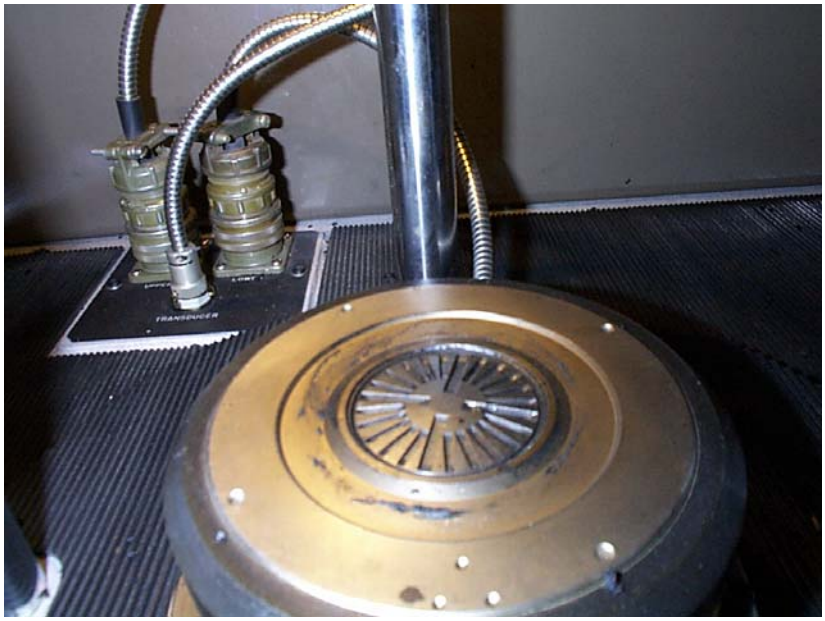

Figure 4-3: Close-up of Lower Die

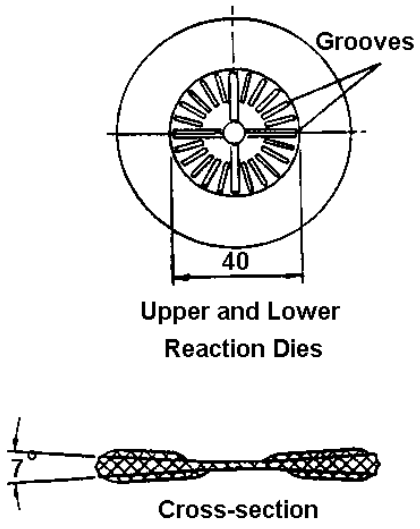

Figure 4-4: Schematic of Rheometer Dies and Specimen Cross-Section

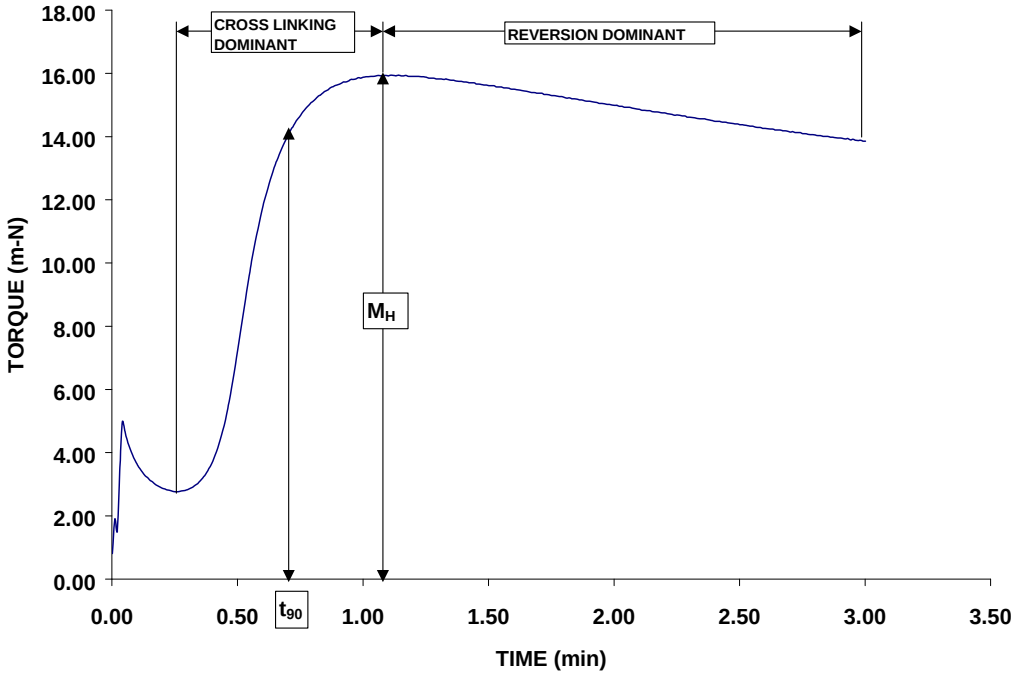

Figure 4-5: Terminology used in Vulcanization Curves

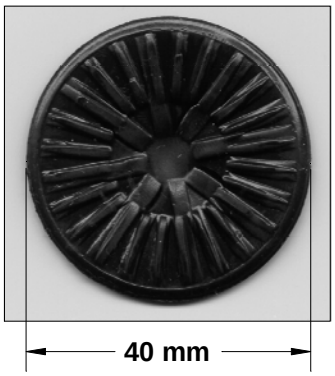

Figure 4-6: Moving Die Rheometer Specimen after Curing

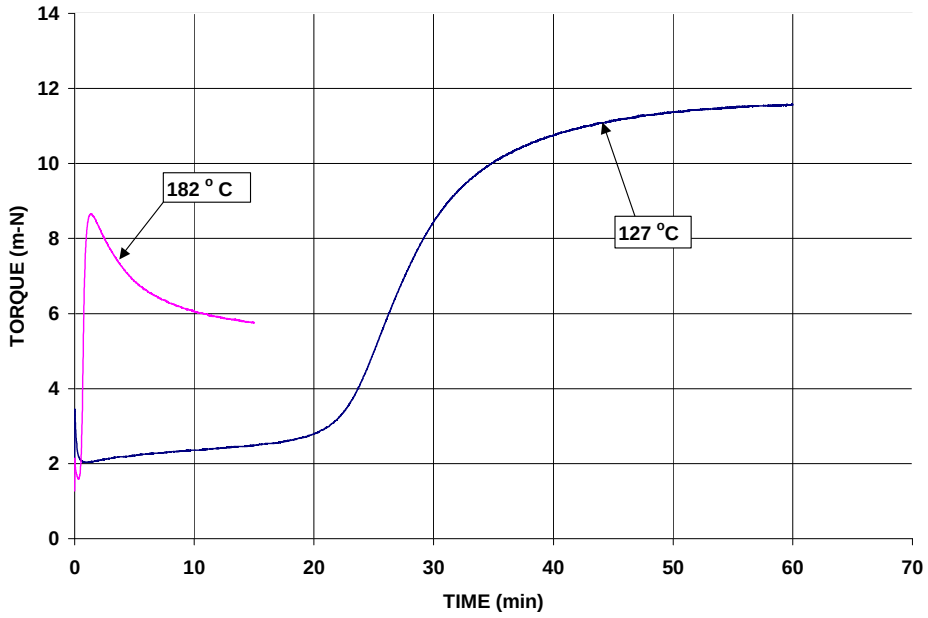

Figure 4-7: Vulcanization Curves for NR50

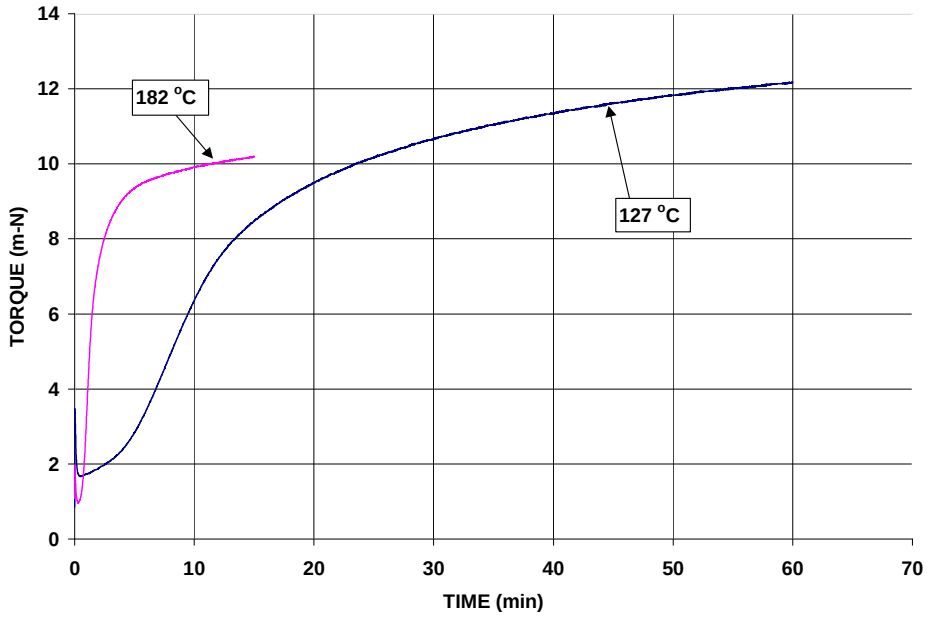

Figure 4-8: Vulcanization Curves for CR50

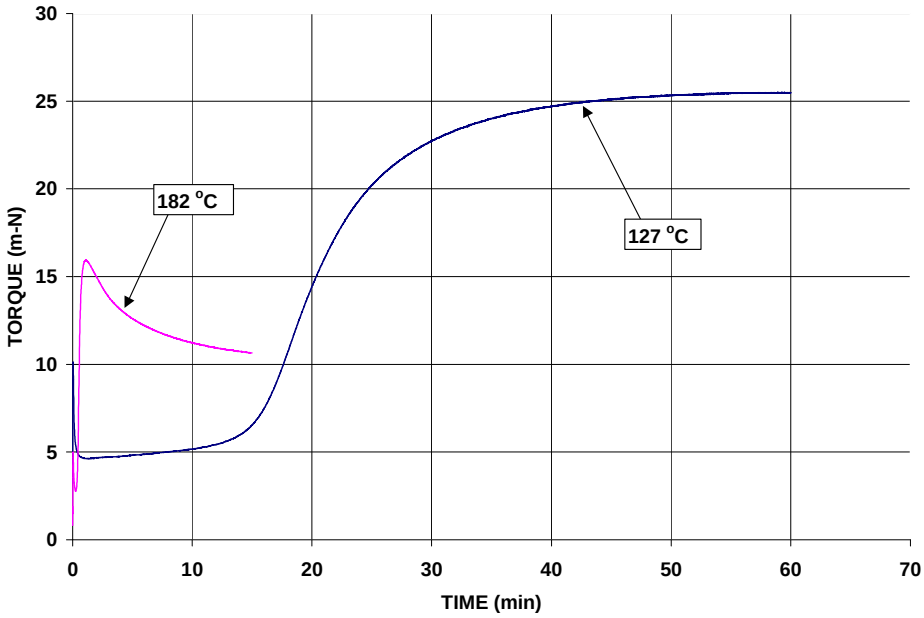

Figure 4-9: Vulcanization Curves for NR70

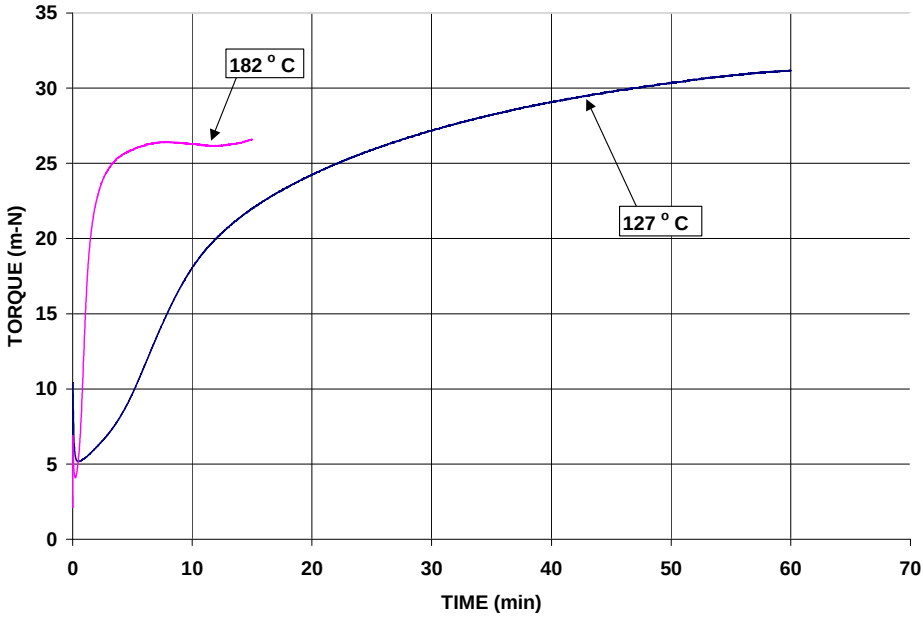

Figure 4-10: Vulcanization Curves for CR70

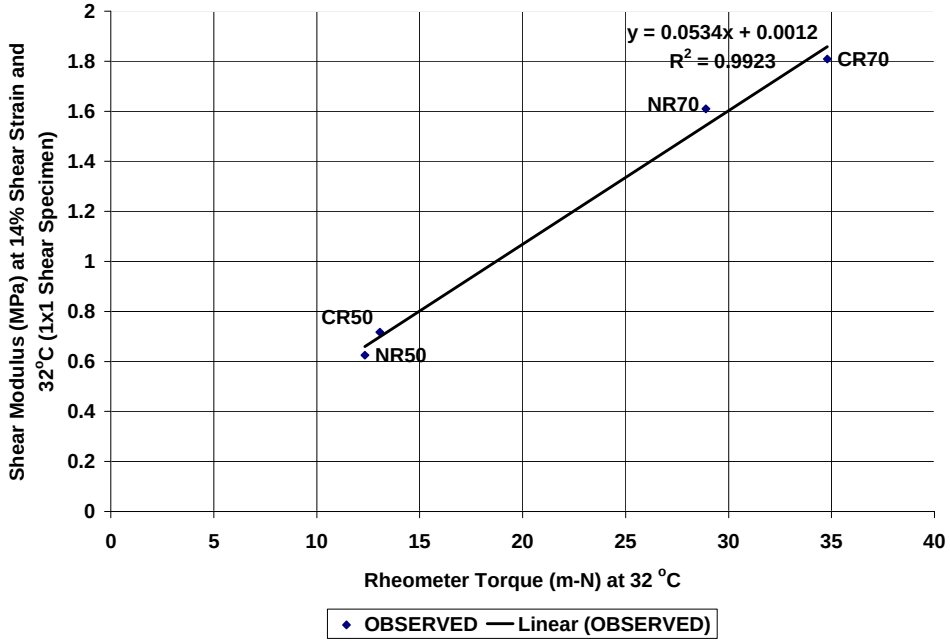

Figure 4-11: Relationship between Shear Modulus and Rheometer Torque

The MDR specimens were prepared by placing a 5 gram sample of raw elastomer into the die of the rheometer and cured at a temperature of 127^{o} C until the reaction torque was almost constant (steady state condition). Specimens from all four rubbers (NR50, CR50, NR70 and CR70) were prepared. The specimens were removed from the rheometer and stored at room temperature for 3 days. The post-vulcanization torque was measured in the rheometer and the aging was done in an air oven, wherein the airflow and temperature were precisely controlled. In order to determine the activation energy in the Arrenhius equation (refer to Section 4.3), Aging was performed at two temperatures 82^{o} C and 100^{o} C respectively, so that Arrenhius based aging prediction methods described in

Section 4.3 could be used. The specimens were removed from the oven after 3, 10, 17, 24, 31, 38, 45, 52 days and the reaction torque was measured in the rheometer. All the post-vulcanization and post-aging tests were performed at 32^{o} C. In these tests, since the specimens were already cured, a steady state torque was achieved only a few seconds after the start of the test. The torque was recorded after 2 minutes to ensure a steady state condition.

The results from rheometer specimen aging are shown in Figure 4-12 on a log-log scale. Note that the temperatures shown in the legend (82^{o} C and 100^{o} C) are the aging temperatures. The percent change in shear stiffness is relative to the torque or shear stiffness at 0 days of aging, i.e. before the specimens were placed in the air ovens.

4.2.2 1x1, 2x2 and 3x3 Shear Specimens

The structural configuration, fabrication method, test setup and fixtures for 1x1, 2x2 and 3x3 shear specimens was same as those used in the shear relaxation tests described in Chapter 3. The aging was done in an air oven, wherein the airflow and temperature were precisely controlled. Aging was performed at the same two temperatures 82^{o} C and 100^{o} C used in the rheometer test phase. The shear stiffness was measured at 0, 1, 2, 3, 4, 5, 6 and 7 weeks of aging

The specimens were tested using a MTS system with an attached environmental chamber to precisely control the testing temperature at 32^{o} C as described in Chapter 3. In order to find the strain dependence of the aging effects, the shear stiffness was measured at three shear strain levels 50%, 100%

and 150% respectively. The test procedure used for all four rubbers types is summarized as follows.

1. The test specimen was mounted on the displacement controlled MTS fixtures in an environmental chamber and a steady state test temperature of 32 ^{o}C was maintained during the test.
2. The 1x1 specimen was loaded to 150 percent shear strain while 2x2 and 3x3 specimens were loaded to 50 percent shear strain 5 times at 1 percent strain/sec to eliminate the Mullins effect. This was done every time after the specimens were removed from air oven.
3. The specimen was loaded to the 50% strain @ 1% per second and the load was recorded.
4. Step 3 was repeated at 100 percent and 150 percent strains for 1x1 specimens only.
5. The secant shear modulus was calculated at each strain level.

The results of accelerated aging of 1x1 specimens are shown in Figures 4-13 through 4-16 for NR50, CR50, NR70 and CR70 elastomers respectively. In the legends of these plots, the strain level refers to the shear strain at which shear stiffness (or shear modulus) was calculated and the temperature refers to the temperature of air oven at which the specimens were aged. The percent change in stiffness is relative to stiffness or secant shear modulus at 0 time of aging, i.e. before the specimens were placed in the air oven.

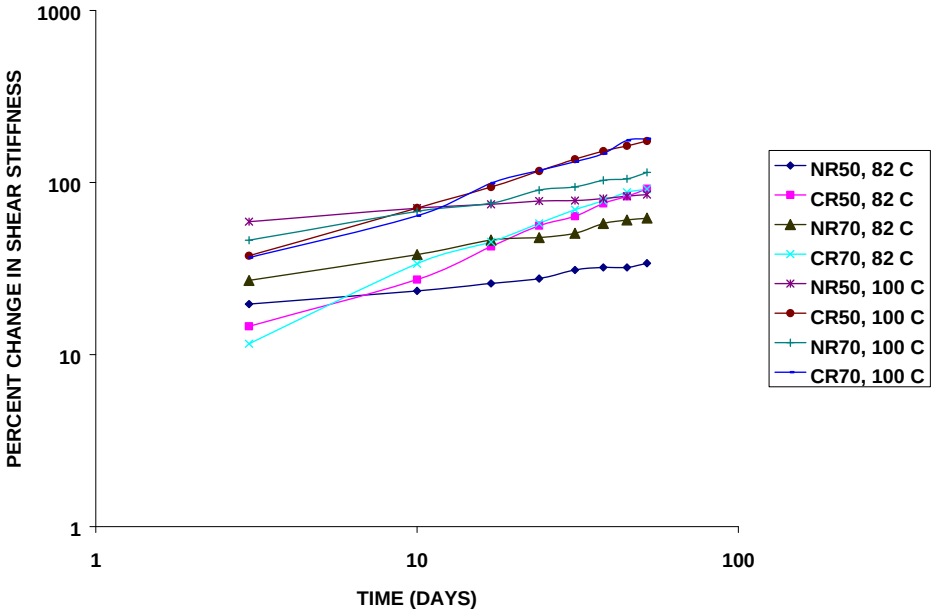

Figure 4-12: Results of Accelerated Aging Tests on Rheometer Specimens

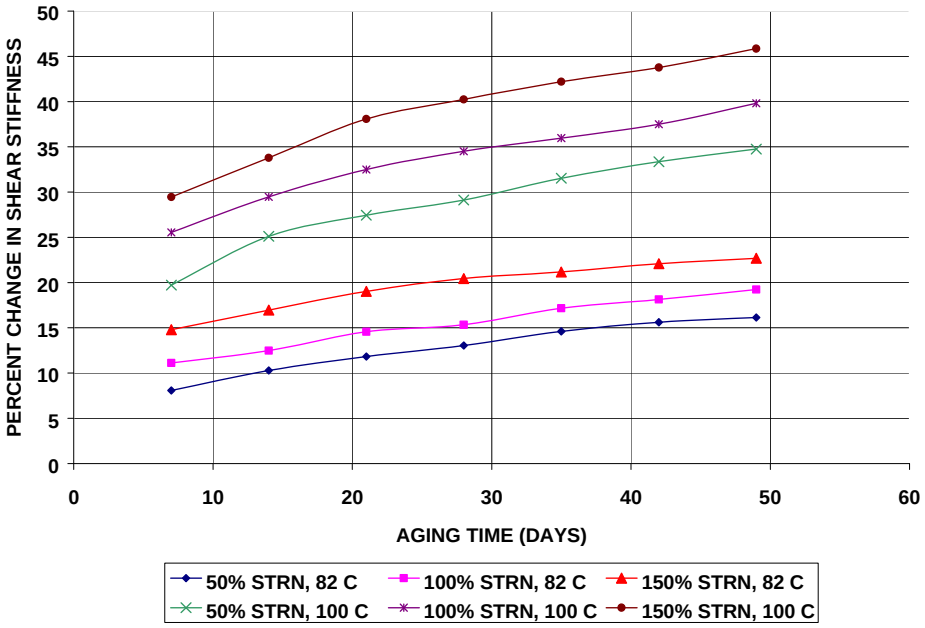

Figure 4-13: Results of Accelerated Aging of 1x1 NR50 Specimens

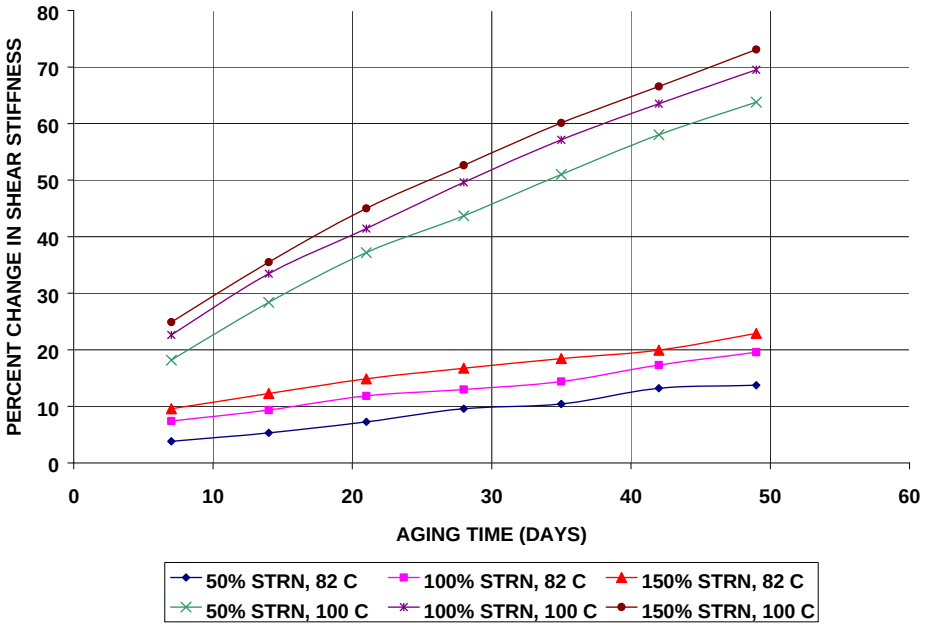

Figure 4-14: Results of Accelerated Aging of 1x1 CR50 Specimens

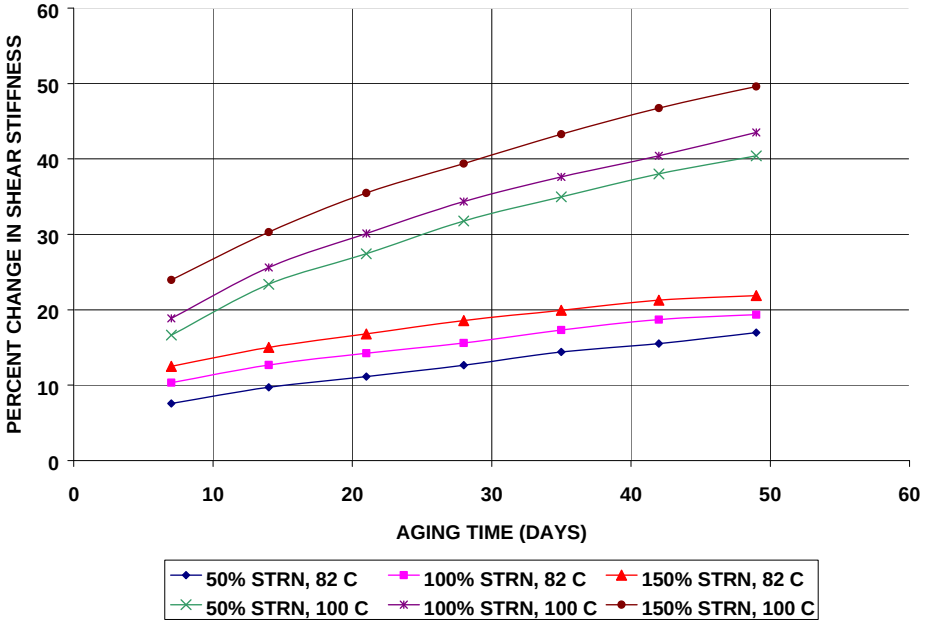

Figure 4-15: Results of Accelerated Aging of 1x1 NR70 Specimens

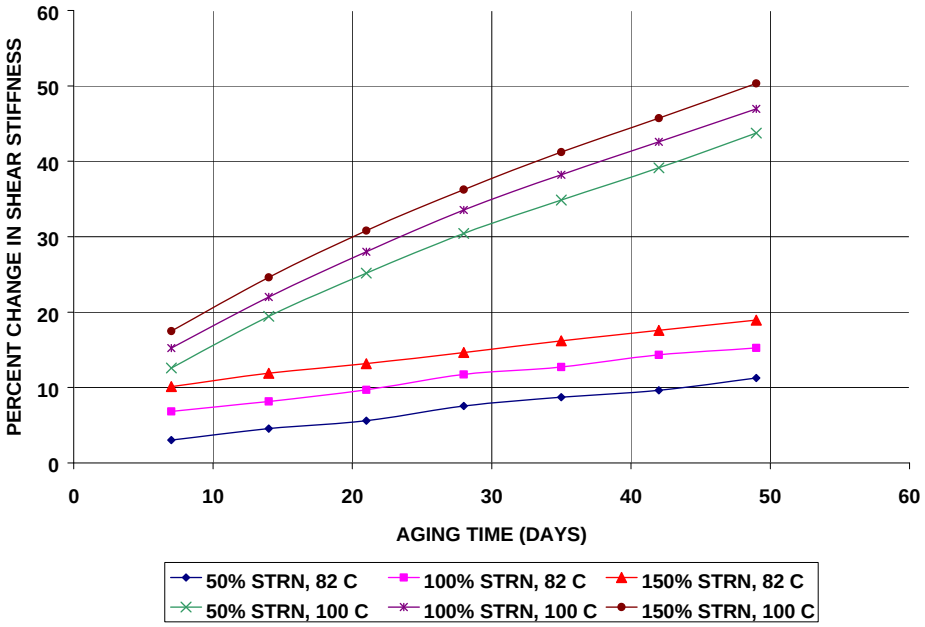

Figure 4-16: Results of Accelerated Aging of 1x1 CR70 Specimens

The results of accelerated aging of 2x2 and 3x3 specimens are shown in Figures 4-17 through 4-20 for NR50, CR50, NR70 and CR70 elastomers respectively. The results of 1x1 specimen aging tests at 50 percent shear strain are also included for comparison purposes. The legends of these plots, refer to the sizes of the specimens and the temperature of the air oven at which the specimens were aged. The percent change in stiffness is relative to stiffness or secant shear modulus at 0 time of aging , i.e. before the specimens were placed in the air oven.

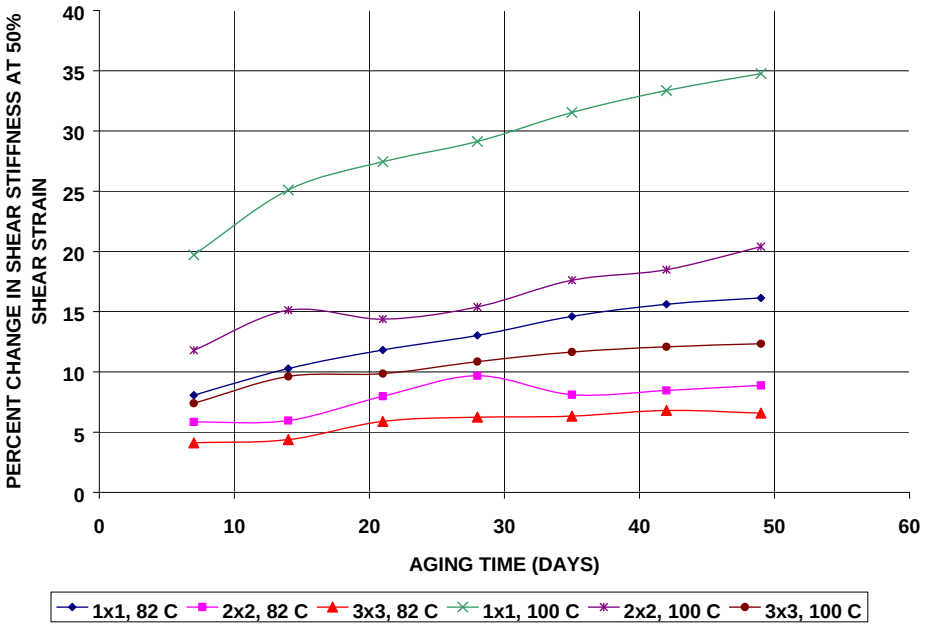

Figure 4-17: Results of Aging Tests for 1x1, 2x2 and 3x3 NR50 Shear Specimens

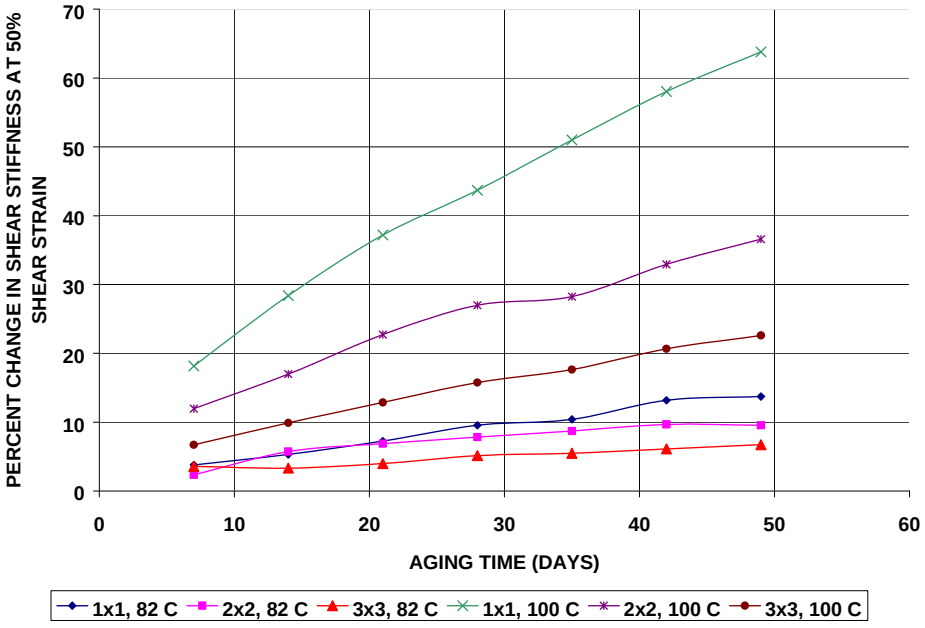

Figure 4-18: Results of Aging Tests for 1x1, 2x2 and 3x3 CR50 Shear Specimens

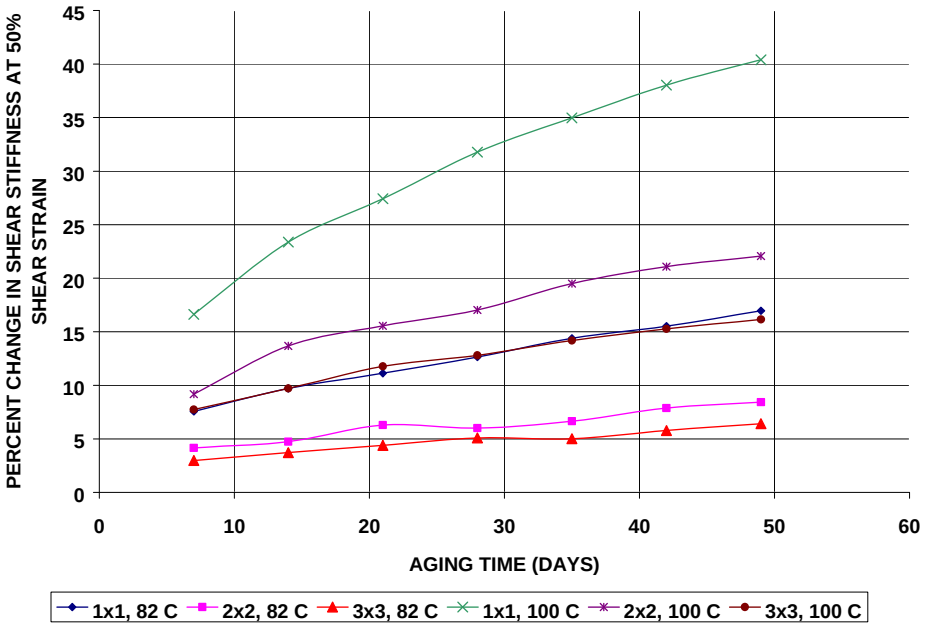

Figure 4-19: Results of Aging Tests for 1x1, 2x2 and 3x3 NR70 Shear Specimens

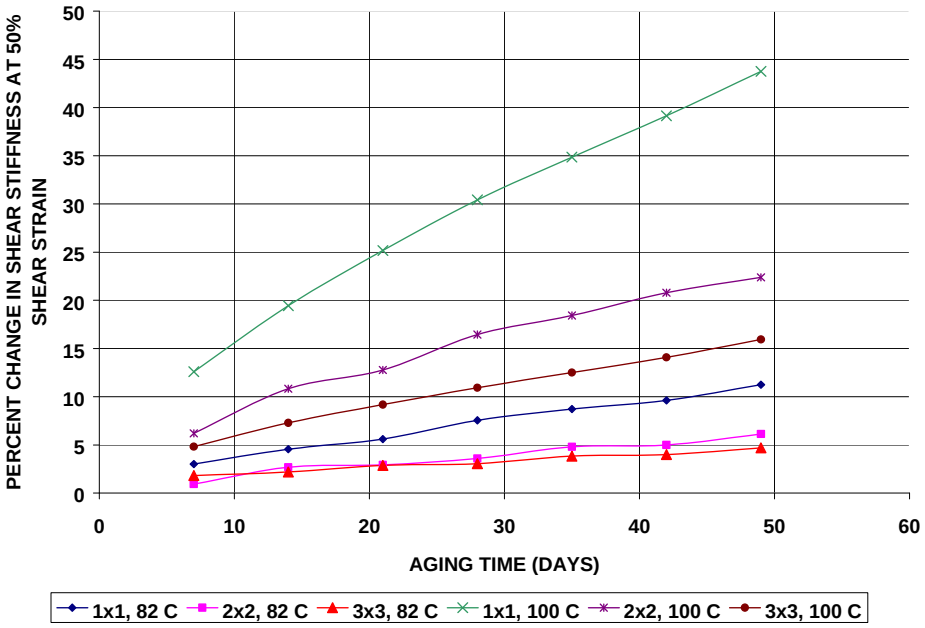

Figure 4-20: Results of Aging Tests for 1x1, 2x2 and 3x3 CR70 Shear Specimens

4.3 INTERPRETATION OF RESULTS

The results of aging tests are summarized in Figures 4-21 and 4-22. These figures show the change in shear stiffness for the four sizes of specimens after 7 weeks of accelerated aging at 82^{o} C and 100^{o} C respectively for the four rubber compounds tested.

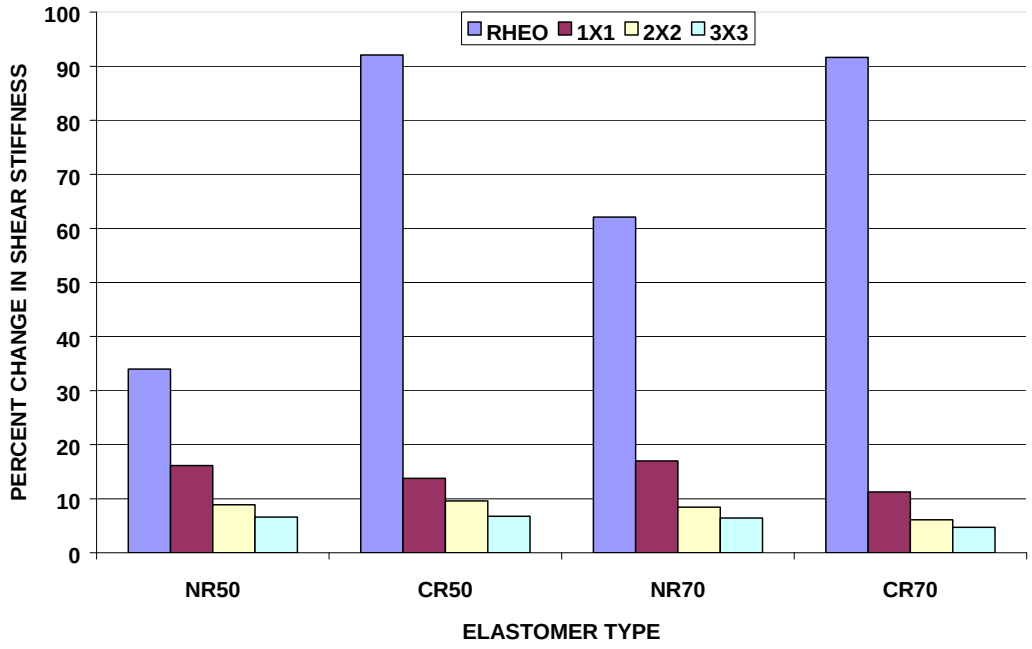

Figure 4-21: Summary of Aging Results after 7 Weeks of Aging at 82^{o} C

The following observations are valid for all the four types of rubber compounds tested:

1. The change in shear stiffness due to aging is definitely dependent on the size of the specimen. As the size increases the percent change in shear stiffness decreases drastically. This can be attributed to the amount of

rubber affected by oxidation process. For the rheometer specimens, since the whole specimen is affected by aging process, the stiffness change is quite significant. As the size increases the ratio of the affected zone to the total rubber volume decreases and therefore the effect of aging on the overall shear stiffness decreases.

2. At higher aging temperatures the stiffness change is higher. This is due to a higher oxygen diffusion rate at higher temperatures. The ingress of oxygen is faster and deeper at higher temperatures and therefore the percentage of affected zone to unaffected zone is higher.

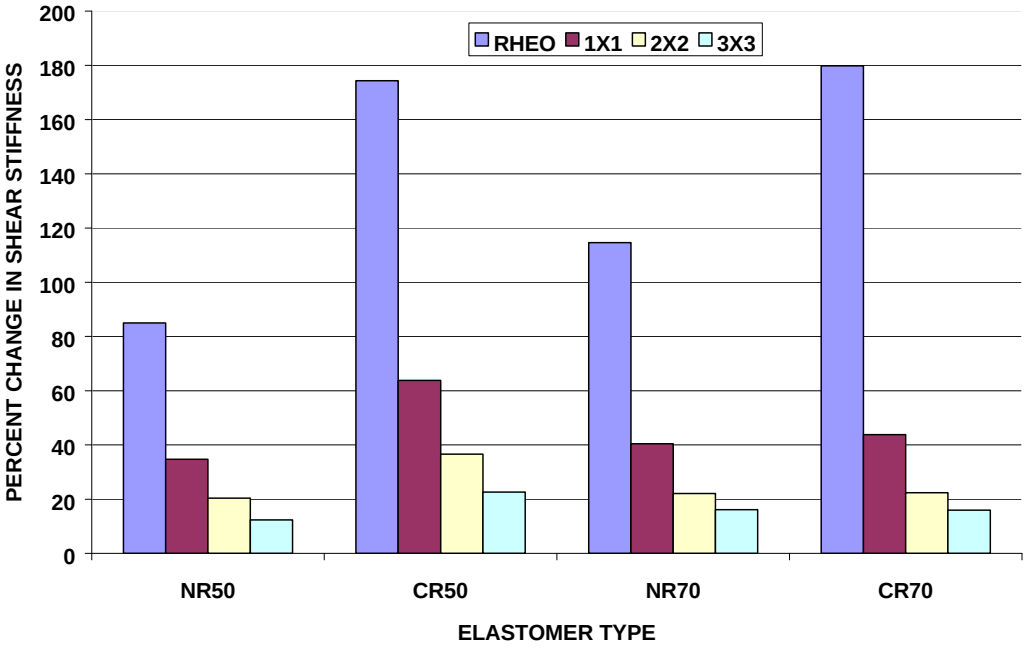

Figure 4-22: Summary of Aging Results after 7 Weeks of Aging at 100^{o} C

3. In general the effects of aging is higher in neoprene as compared to natural rubber.
4. For the rheometer specimens, the stiffer rubber compounds age faster.
5. Figures 4-13 through 4-16 show that the effects of aging are more dominant at higher shear strains.

4.4 PREDICTION AT AMBIENT TEMPERATURE

From the results of the present study it is apparent that the change in shear stiffness due to aging is the consequence of chemical reactions and the diffusion rate of oxygen. Since both chemical reaction and diffusion rate are dependent on temperature, the Arrenhius relation that gives the chemical reaction rate as a function of absolute temperature can be used to predict the effect of aging at various temperatures. The Arrenhius relation is given by:

$$k = Ae^{-\frac{Ea}{RT}} \qquad \text{(Eq. 4-1)}$$

where k is the general rate of reaction (changes/unit time), A is the rate of reaction constant (changes/unit time), Ea is the activation energy (J/mol), R is the molar gas constant (J/mol-K^o) and T is absolute (Kelvin) temperature ($K^o = C^o + 273^o$).

Equation 4-1 can be rearranged to obtain an expression for equivalent times for the same property change with exposures at different temperatures as follows:

$$\Delta t_2 = \Delta t_1 e^{\left(\frac{Ea}{R}\right)\left(\frac{1}{T_2}-\frac{1}{T_1}\right)} \qquad \text{(Eq. 4-2)}$$

where Δt_1 is the aging time at test temperature T_1 while Δt_2 is the aging time at test temperature T_2.

Since the 3x3 specimen was the largest tested, it was used to predict the percent change in stiffness at ambient temperature (32^o C or 305 K) using the Arrenhius relationship. The procedure is summarized as follows.

From the results of the aging studies a relationship between time and percent change in shear stiffness was developed using regression analysis. A power law of the following form seemed to work fairly well.

$$Y = aX^b \qquad \text{(Eq. 4-3)}$$

where Y is the time in days , X is the percent change in shear stiffness, a and b are regression coefficients. As an example the results of regression analysis for aging of NR50 at 100^o C are shown in Figure 4-23. The results for other conditions are tabulated in Table 4-2. Since testing was performed at two temperatures the value of $\frac{Ea}{R}$ for various compounds corresponding to a particular change in shear stiffness were calculated using the test results in Equation 4-2. Once $\frac{Ea}{R}$ is known, Equation 4-2 in conjunction with one of the test temperatures is used to predict the percent change in shear stiffness at ambient temperature. Based on this method, the time required to change the shear stiffness by 5% and 10% at ambient temperature (32^o C) are tabulated in Table 4-2 for the four rubber compounds tested.

Note that these times are for 76x76 mm (3x3) specimens cut from an actual bearing. The size of the actual bearing is 356mm x 229 mm that is much larger than the test specimen. The results of this study show (see Figures 4-21 and 4-22) that the aging effects reduce exponentially as the specimen size increases so the effect of aging on the full size bearing will be insignificant.

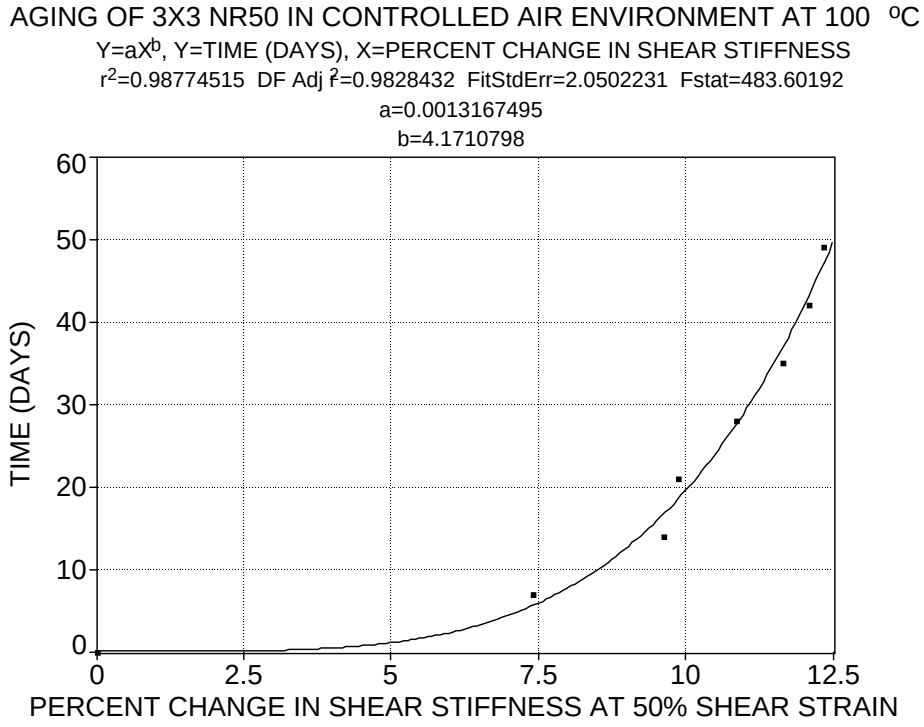

Figure 4-23: Regression Analysis to Determine Relationship Between Aging Time and Percent Change in Stiffness

Table 4-2: Prediction of Time Required to Age 3x3 Specimen at Ambient Temperature

Rubber Compound	NR50		CR50		NR70		CR70		Test Temperature 355 K			Test Temperature 373 K			Ea/R	Time Required at Ambient Temperature (32^{o} C) YEARS
% Change in Shear Stiffness	5	10	5	10	5	10	5	10	Regression Coeff. a	Regression Coeff b	Time Required DAYS	Regression Coeff. a	Regression Coeff b	Time Required DAYS		
	5	10	5	10	5	10	5	10								
3.7223282	0.0356815	0.0356815	1.0288355	1.0288355	0.7820815	0.7820815	3.7223282	3.7223282	0.0356815	3.7235387	14.29	0.0013168	4.1710798	1.08	18973	250.00
1.6933165	3.7235387	3.7235387	2.0368511	2.0368511	2.2493142	2.2493142	1.6933165	1.6933165	0.0356815	3.7235387	188.79	0.0013168	4.1710798	19.52	16691	1151.25
183.71	14.29	188.79	27.29	111.99	29.20	138.86	56.81	183.71	1.0288355	2.0368511	27.29	0.4280422	1.5201955	4.94	12568	24.79
0.6480163	0.0013168	0.0013168	0.4280422	0.4280422	0.0417034	0.0417034	0.6480163	0.6480163	1.0288355	2.0368511	111.99	0.4280422	1.5201955	14.18	15203	343.43
1.570216	4.1710798	4.1710798	1.5201955	1.5201955	2.5393504	2.5393504	1.570216	1.570216	0.7820815	2.2493142	29.20	0.0417034	2.5393504	2.48	18130	346.14
24.09	1.08	19.52	4.94	14.18	2.48	14.44	8.11	24.09	0.7820815	2.2493142	138.86	0.0417034	2.5393504	14.44	16652	831.30
14946	18973	16691	12568	15203	18130	16652	14318	14946	3.7223282	1.6933165	56.81	0.6480163	1.570216	8.11	14318	115.76
500.25	250.00	1151.25	24.79	343.43	346.14	831.30	115.76	500.25	3.7223282	1.6933165	183.71	0.6480163	1.570216	24.09	14946	500.25

4.5 CONCLUSIONS

Aging does not affect the performance of an elastomeric bearing at ambient temperatures. As shown in Table 4-2, it will take hundreds of years to change the shear stiffness of 3x3 specimen by 10 percent. For full size bearings it will take several hundred years to change the shear stiffness by 10 percent. As mentioned in Section 4-1, other researchers have drawn this conclusion based on microanalytical methods.

Based on the results of this study it can be concluded that full size bearings at ambient temperatures will experience insignificant change in stiffness due to aging over their lifetime and therefore the aging tests given in the various specifications are irrelevant for the elastomeric bearings of the moderate to high shape factor rubber layers used in bridges. Therefore, ASTM D573 can be eliminated from the AASHTO specification M251-97.

Aging can have significant effect on the stiffness characteristics of elastomeric bearings exposed to high temperatures generally encountered in oil field applications. For such bearings the effects of aging must be considered during the design phase.

Chapter 5: Explosive Decompression Damage

5.1 INTRODUCTION

Elastomeric bearings are commonly used as moment-free connections in offshore pipelines transporting high-pressure hydrocarbon fluid/gas mixture. Figure 5-1 shows an inside view of a typical elastomeric bearing used in offshore pipelines and risers. The bearing consists of spherical laminates and elastomer layers integrally bonded together so that the axial tension and internal pressure in connecting pipes are transformed to axial compression in elastomer layers that can freely flex conically. Thus, the high internal pressure, axial tension and shear are properly transferred between two connecting pipes, without introducing high flexure stresses. Under sustained internal pressure, rubber layers absorb hydrocarbon gases. As explained in Chapter 1, when the internal pressure is rapidly decreased, the explosive expansion of the absorbed gases within the elastomer causes internal rupture of the elastomer structure and potential damage known as Explosive Decompression Damage (EDD) to the rubber surfaces that may affect the load carrying capacity of the bearing.

The factors that potentially affect the explosive decompression failure of rubber are schematically shown in Figure 5-2 (Briscoe et. al., 1994). Currently there is no standard test method or analytical technique that can be used to assess the EDD in elastomeric bearings exposed to sudden fluctuation of pressures commonly encountered in oil field applications. Some information is available on the explosive decompression failure of O-ring seals (Griffiths, 1985, Potts, 1985,

Shade and Legg, 1988, Peters et. al., 1988), which behave very differently than elastomeric bearings. Briscoe and Zakaria, 1990, studied some general aspects of gas-induced damage in elastomeric composites. A more comprehensive review of the origins of pneumatic stress induced rupture in elastomers was presented by Briscoe et. al., 1994. The review describes the general features of gas-induced rupture in elastomers and introduces the main variables such as the gas-polymer transport and equilibrium properties. The phenomenological nature of the failure processes are also described and the characteristics of the failures encountered are summarized. It is proposed that the failure processes, which involve bubble expansion and subsequent tearing of the interior and exterior of the elastomer, arise from the action of at least two stress fields; one is provided by a simple triaxial tension and the other by an evolving gas concentration gradient. Cain et. al., 1990, explored the use of finite element analysis to design the oil field seals. Ho et. al., 1993, developed a software to predict elastomer/fluid interaction in elastomer seals.

The objective of the present study is to identify principal design variables that affect the extent and nature of damage in elastomeric bearings susceptible to explosive decompression damage. In order to accomplish this objective a new test method using a small-scale test specimen was developed. The premise behind the new method is described in Section 5.2. Since all the parameters that govern the EDD in elastomers were difficult to incorporate in the small-scale testing, only those parameters that potentially influence the elastomeric bearings were considered as described in Section 5.3. The structural configuration and

fabrication of the small-scale specimen is described in Section 5.4 while the test procedure is described in Section 5.5. The results and findings of the explosive decompression testing are presented in Section 5.6 and finally the conclusions are presented in Section 5.7.

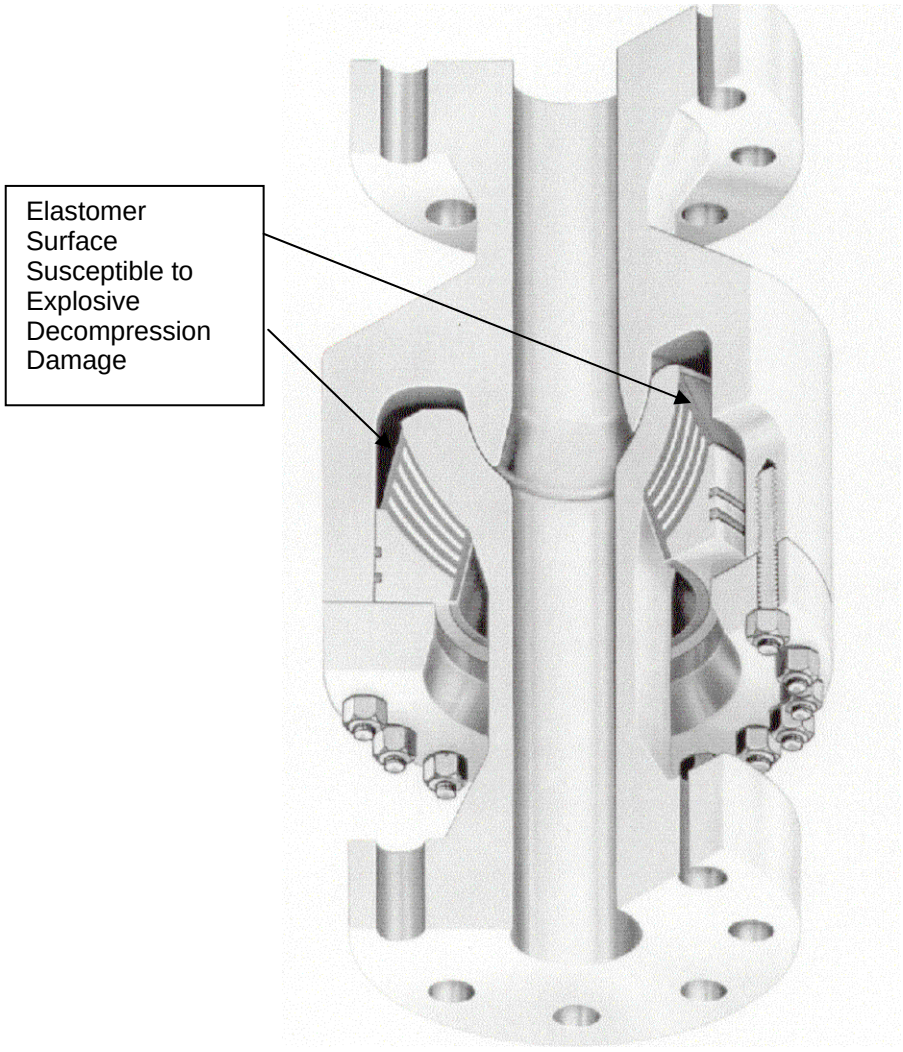

Figure 5-1: Inside View of a Typical Spherical Elastomeric Bearing used in Offshore Oil Field Applications

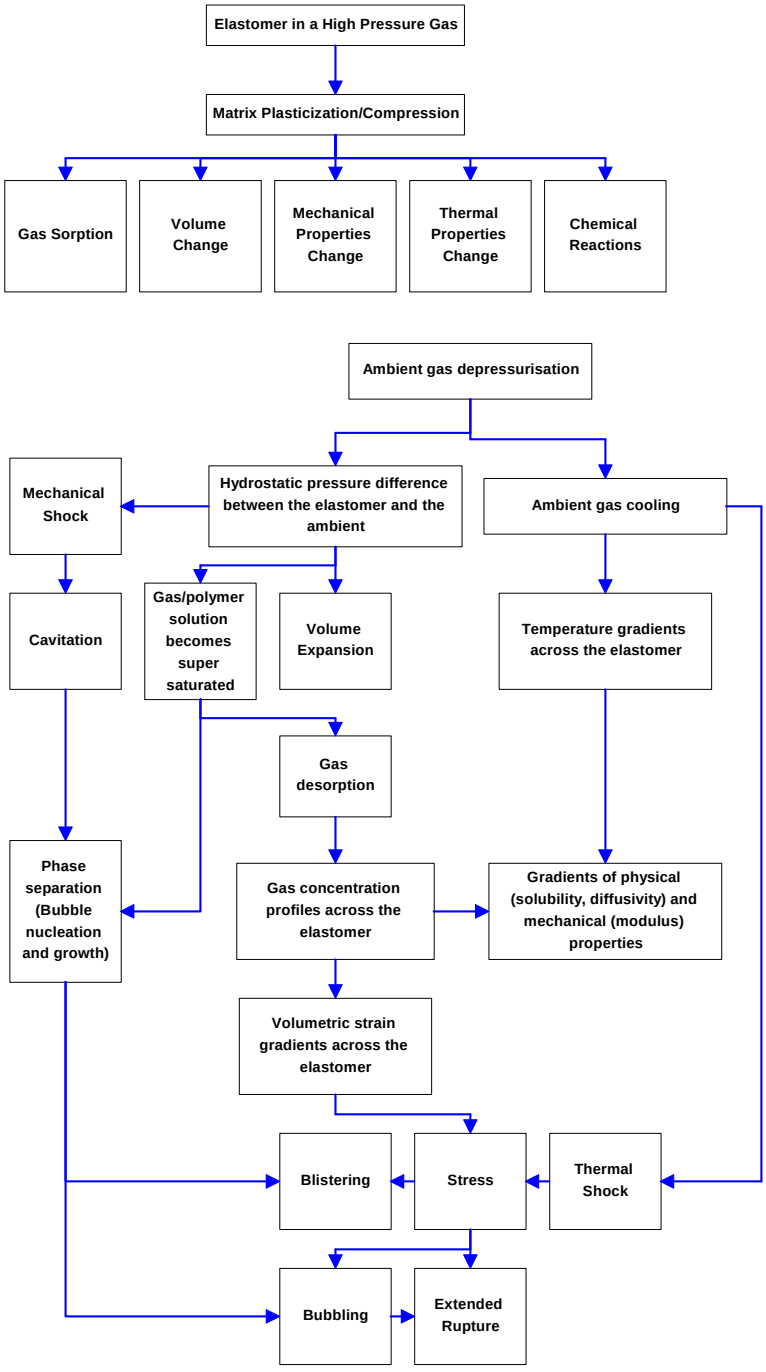

Figure 5-2: Factors Affecting the Explosive Decompression Failure

5.2 PREMISE

As shown in Figure 5-2, the explosive decompression failure of rubber is an extremely complex problem and depends on several factors. All the factors shown in Figure 5-2 may not be critical for an elastomeric bearing. Since the present objective is to simulate the effects of explosive decompression in an elastomeric bearing, the design of the new test method is based on the following premise.

The primary damage occurs due to rapid inflation of small spherical voids, initially present at the time of cross-linking either in the form of submicroscopic bubbles of air trapped in rubber processing or in the form of badly wetted particles of dirt or dust. Gent and Tompkins, 1969, estimated the size of these voids on the order of 10^{-5} cm or larger in radius. When a rubber layer is subjected to a sustained high-pressure in a gas environment, gas permeates inside these small spherical voids. The permeation of gas through an elastomer takes place in two steps, the gas dissolves in the elastomer and the dissolved gas diffuses through the elastomer. When the elastomer is fully saturated with gas, a steady state condition is reached. After a certain duration of sustained pressure in steady state condition, an equilibrium is reached between the internal pore pressures and the external compressive pressure. When the external pressure is suddenly released, the initially compressed spherical voids experience a mechanical shock caused by a disruption in the above mentioned equilibrium. Due to the low permeability of the rubber, the compressed gas inside the voids cannot escape instantaneously. Consequently, the voids are subjected to a high-pressure

differential and sudden volume expansion. The voids will not expand indefinitely because the supply of gas is limited due to the limited solubility. Depending on the magnitude of the pressure differential, the inside spherical surface of the void stretches until one of the following takes place. (a) the pressure inside the void drops in accordance with the increased volume and equilibrium is reached between the tri-axial internal and external stresses without fracture, or (b) energy is dissipated due to rupture of the interior surface of the void, and the system attains its original energy state.

By the virtue of high shape factors of the rubber layers (necessary to support high axial load caused by high-pressure) the explosive decompression damage is generally restricted to the cover rubber or generally noticed in areas where the confinement of rubber is minimum. In a typical rubber layer of a high-pressure elastomeric bearing, the top and bottom surfaces are bonded to steel reinforcements and it is assumed that the bond provides adequate confinement of these surfaces. The side surfaces, however, are free to bulge and therefore most susceptible to explosive decompression damage. In order to predict the extent of damage that will not adversely affect the overall performance of the bearing, only the damage in the bulge region need to be studied. If the damage is noticed beyond the bulge region, the elastomeric bearing will definitely fail to perform adequately.

Therefore, a small-scale specimen that replicates the structural behavior of bulge region of most critical rubber layer of the full-scale elastomeric bearing can be used to assess the effects of EDD. In other words, a small-scale test specimen

of same material and same thickness as an actual rubber layer, that experiences same pressure distribution (before and after decompression) in the vicinity of the bulge region as an actual rubber layer will exhibit the same decompression damage as an actual rubber layer. The foregoing concept is used in the design of the small-scale test specimen.

5.3 VARIABLES

The variables that potentially influence the EDD in an elastomeric bearing include: (a) type of rubber (b) thickness of the rubber layer, (c) thickness of cover, (d) axial compression of rubber layer, (e) decompression pressure, (f) type of gas, (g) exposure temperature, (h) exposure time (i) rate of decompression and (j) number of compression-decompression cycles.

From a structural designer's point of view, most of these variables are constant, except the type of rubber, thickness of rubber layers and cover rubber. Since high-acrylonitrile compounds have performed well in O-Ring seals in high-pressure natural gas applications (Griffiths, 1985, Potts, 1985), a high-acrylonirile elastomer was used in the present study and the thickness of rubber layer and cover rubber were varied. The values of constant and variable parameters and the reasons behind selecting these values are described as follows:

Thickness of Rubber Layer

Based on a survey of high-pressure and high shape factor bearings used in offshore environment, the thickness of rubber layers varies from 2 mm to 8 mm. To cover this range of thickness, three representative thicknesses, 8 mm, 5 mm,

and 2.5 mm, were selected for investigation. All these thicknesses have been used in existing bearings.

Thickness of Cover Rubber

In most elastomeric bearings cover rubber is provided to shield the steel reinforcements and rubber-to-metal bonds from corrosive environments. Since cover rubber is not constrained in any way, it is highly susceptible to explosive decompression damage. Damage in cover rubber is structurally not important, however, excessive damage in the form of cracks can propagate to the load-bearing region of the layers and can influence the structural performance. The most commonly used cover-thickness in offshore elastomeric bearings is 6 mm. In order to study the effect of explosive decompression on cover rubber, two extreme cases were selected for investigation – (a) no cover, i.e., cover-thickness equal to 0.0 mm and (b) maximum cover, i.e., cover thickness equal to 6 mm.

Axial Compression of Rubber Layer

The axial compression of the small-scale specimen with 8 mm thick rubber layer was derived by means of finite element computer simulation. The axial deflection that produced nearly the same pressure distribution and strains in the bulge region of the small-scale specimen as the pressure distribution and strains in the bulge region of a typical well designed full-scale bearing was used. The same axial load was applied on specimens with 5 mm and 2.5 mm rubber thickness so that the loading conditions were identical. The results of finite element analysis of small-scale specimen are given in Appendix C.

Decompression Pressure

The selection of decompression pressure (ΔP or pressure drop) was based on two criteria:

- The decompression pressure must be greater than the pressure that causes damage in unconstrained elastomer blocks, and
- The decompression pressure must represent extreme conditions that might be encountered in offshore oil production due to shutdown or other emergencies.

Gent and Tompkins, 1969, suggested that the minimum super-saturation pressure for a dissolved gas to form a visible bubble is 2.5 times the shear modulus. They assumed rubber to be a Neo-Hookean material with a constant shear modulus. The elastomer used in the present study exhibits a highly non-linear stress-strain behavior as shown in Figure 5-3. To account for the non-linear rubber behavior, finite element analysis was performed to study the behavior of a small spherical void (10^{-5} cm in radius as suggested by Gent and Tompkins, 1969) in an unconstrained block of rubber. The finite element analysis approach and material modeling was the same as described in Chapter 2. The material constants for the acrylonitrile rubber, hereafter referred to as NBR80, were derived from the actual test data. Figure 5-3 shows the observed data, predicted values and the corresponding material constants for NBR80 used in the present study.

The maximum principal strains in the vicinity of the spherical void due to an internal pressure of 11 MPa are shown in Figure 5-4 while a plot of maximum principal strain versus radius is shown in Figure 5-5. Notice that there is a very

high strain gradient near the inside surface of the void and the maximum principal strain varies from 150 to 615 percent in this region.

Based on a tensile experiment performed on a 6 mm sheet of the subject elastomer, the tensile strain at break was 475 percent. The internal pressure in the pore corresponding to 475 percent maximum principal strain is 9.1 MPa. This is about 7.5G and not 2.5G as suggested by Gent and Tompkins, 1969. Therefore, the decompression pressure must be greater than 9.1 Mpa for EDD to occur in an unconstrained elastomer block. Based on consultation with several oil companies involved in offshore exploration a pressure of 21 MPa was selected because it met the two criteria stated above.

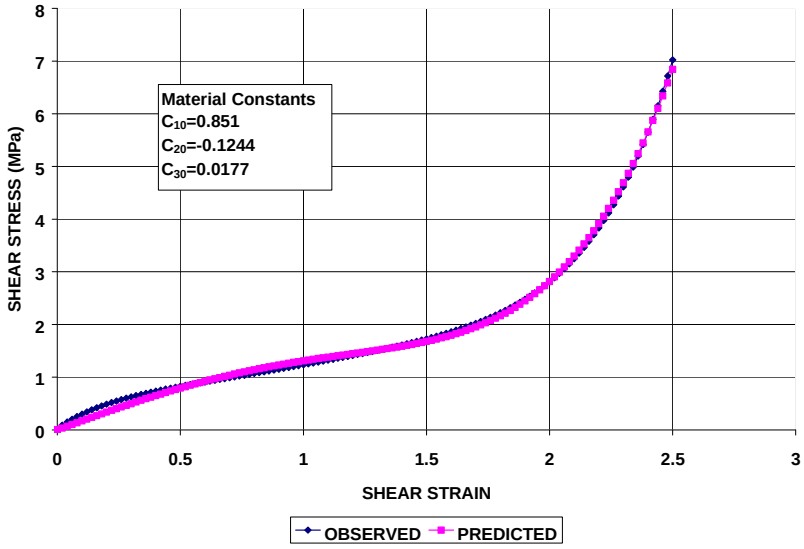

Figure 5-3: Observed Data and Regression Analysis Results for NBR80 Rubber used in Explosive Decompression Specimens.

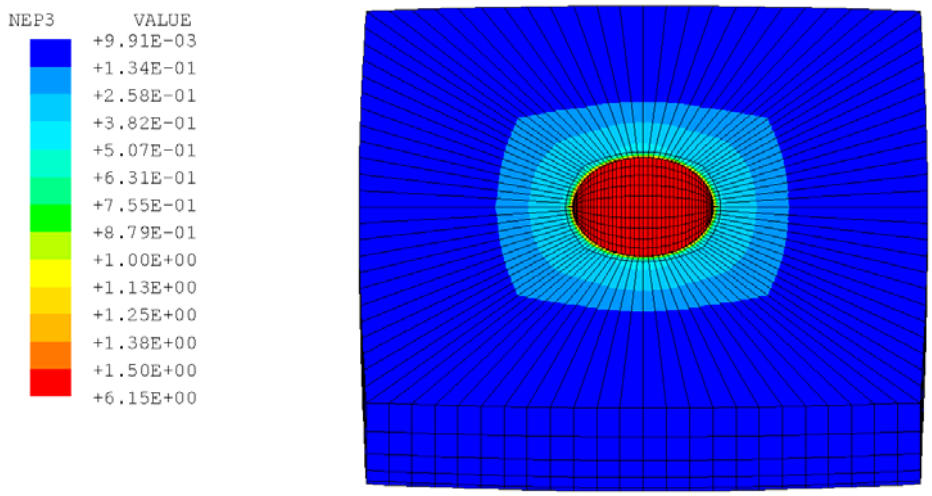

Figure 5-4: Maximum Principal Strain Distribution in the Vicinity of a 10^{-5} cm Radius Void in an Unconfined Elastomer Block due to an Internal Pressure of 11 Mpa

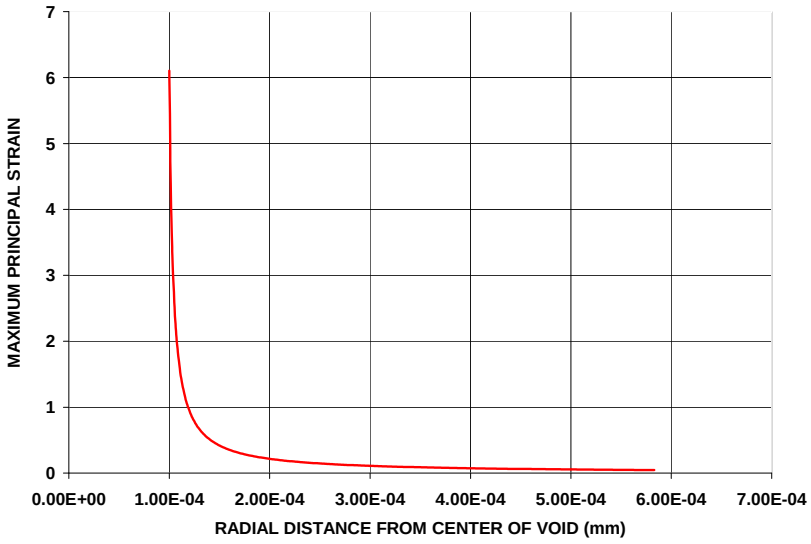

Figure 5-5: Plot of Maximum Principal Strain Versus Radius in the Vicinity of a 10^{-5} cm Radius Void in an Unconfined Elastomer Block due to an Internal Pressure of 11 Mpa

Type of Gas

Since the diffusion rate depends on the type of gas, it was very important to use a gas that replicated the exposure environment found in a real situation. A typical crude oil consists of a mixture of hydrocarbon gases and fluids. Since methane is the most commonly found gas in the crude mixture, commercially available 98 percent pure methane was used in the present study.

Exposure Temperature

The selection of the exposure temperature was based on three criteria:

- It must be well below the elastomer degradation temperature.
- It must represent extreme temperature that might be encountered in an offshore oil production pipeline, and
- It must be conducive to a high diffusion rate.

Based on the curing time-temperature curve of NBR80, no degradation occurs below 180^{o}C. The extreme temperature of crude can be as high as 80^{o}C. As shown in Figure 5-6, the diffusion rate increases exponentially with temperature. For the present study, a high diffusion rate was necessary to reduce the time to saturate the elastomer with gas. An exposure temperature of 100^{o}C (boiling point of water) was selected for the present study since it met all the above criteria and was easy to maintain for long period of time.

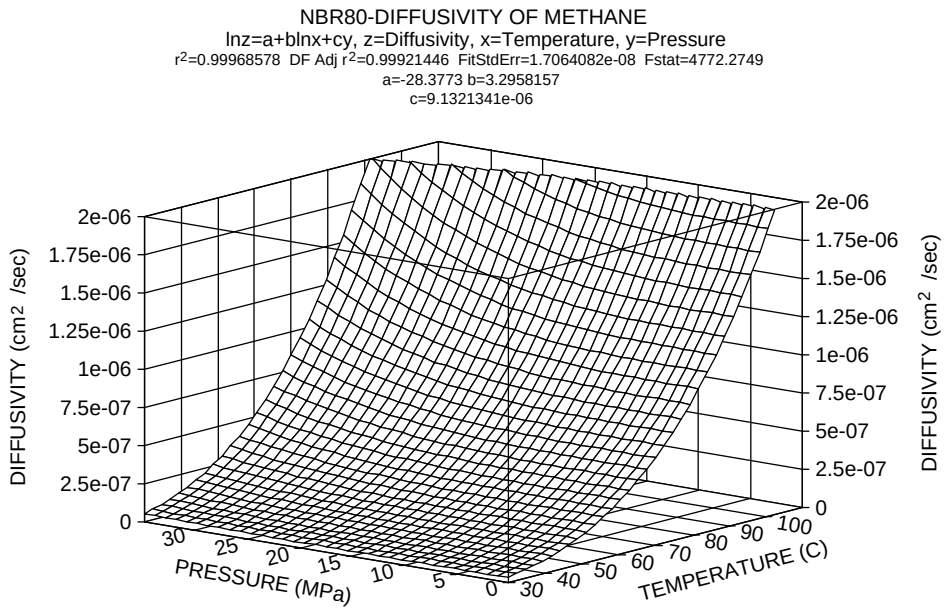

Figure 5-6: Diffusivity of Methane Based on Experimental Data Obtained at Various Temperatures and Pressures (compiled from experiments conducted at OSI and SHELL)

Exposure Time

Exposure time was estimated as the time required to fill all the voids in the vicinity of the bulge region with methane. A simple diffusion analysis was performed using the diffusivity values shown in Figure 5-6. This analysis indicated that 29 days were required to diffuse the gas from the outside surface to the inside surface of the elastomer layer if the pressure was maintained at 21 MPa and the temperature was maintained at 100^{o}C. The test specimens were exposed to methane for 45 days at 100^{o}C temperature and 21 MPa pressure to ensure adequate saturation of the bulge region with methane.

Rate of Decompression

The extent of damage depends on the rate at which pressure is reduced. In a typical oil field application it takes about one hour to drop the pressure from 21 to 1.5 MPa. In the present study, the pressure was dropped from 21 to 0.3 MPa in 30 minutes to ensure a conservative decompression rate.

Number of Compression-Decompression Cycles

As assumed in the premise and later shown by analysis, there is a threshold pressure drop below which permanent damage of elastomer matrix is highly improbable. If the decompression pressure is greater than the threshold pressure drop, required for EDD, most of the damage should occur during the first few compression-decompression cycles. Once a permanent damage in the form of rupture occurs, it is assumed that the damage will propagate as the subsequent pressure cycles are applied. In the present study 10 compression-decompression cycles were applied to ensure that the number of cycles were adequate to produce the damage if it occurs.

5.4 SMALL-SCALE TEST SPECIMEN

The exploded view of the small-scale test specimen is shown in Figure 5-7 while the assembly is shown in Figure 5-8. This configuration was obtained with the aid of finite element analysis after seven design iterations. It closely represents the bulge region behavior of a typical bearing used in offshore applications. The finite element analysis results for the final iteration are given in Appendix C. The noteworthy features of the test specimen are summarized as follows:

1. The test specimen consisted of a 102 mm Inner Diameter (ID) and 178 mm Outer Diameter (OD) rubber disk (item 1) bonded to two steel blocks (items 7 and 8). Thus the net width of the rubber layer was 38 mm.
2. The spacing of the steel blocks in the compressed state was controlled by means of a center insert (item 6). Depending on the as-built thickness of the rubber layer, the spacing was determined by actual load-deflection tests of each test specimen such that the initial axial load was approximately 180 kN in all the test specimens (all thickness). Under this load, the stress/strain distribution in the vicinity of the bulge region of the 8 mm test specimen closely resembles the stress/strain distribution in the bulge region of a full size bearing. The same axial load was used for 5 and 2.5 mm specimens to ensure identical initial loading conditions.
3. The specimen was mounted on a 32 mm diameter threaded rod (item 4) and the initial bulge of the rubber layer was accomplished by turning the two nuts (item 5) at either end of the test specimen until the lower metal and the center insert (items 8 and 6 respectively) were fully seated. The nuts were further twisted to apply a pre-tension in the rod that exerted a sealing pressure on the two metallic seals (items 2 and 3) to shield the inside free surface of the rubber layer from external pressure. This was necessary to control the bulge response due to external pressure only.
4. The tapered regions of the upper and lower heads (items 7 and 8 respectively) were designed to provide the variable stiffness required to

control the pressure distribution and bulge pattern of the outside free surface of the rubber layer under external pressure.

5. As shown in Figure 5-8, cover rubber was used in the two alternate quadrants. The other two 90^{o} sectors were without cover rubber.
6. Compression molding was used to mold the specimens. The mold design is shown in Figure 5-9. The same mold was used for all three thicknesses with appropriate inserts. Usual practice was followed to assemble the mold and bond the elastomer to upper and lower heads. The bonding surfaces were blasted with clean sharp 36-mesh aluminum oxide grit, steam cleaned and dried with dry nitrogen. Chemlok 205/220 adhesive system was applied to the abraded surfaces. The specimens were cured at 143^{o}C for 90 minutes under the pressure necessary to flow the elastomer and provide adequate wetting of the adhesive-elastomer interface. Three specimen of each thickness (total nine specimen) were molded.
7. A typical molded element is shown in Figure 5-10 while the assembled test specimen is shown in Figure 5-11. The as-built heights of the nine small-scale specimens are tabulated in Table 5-1.

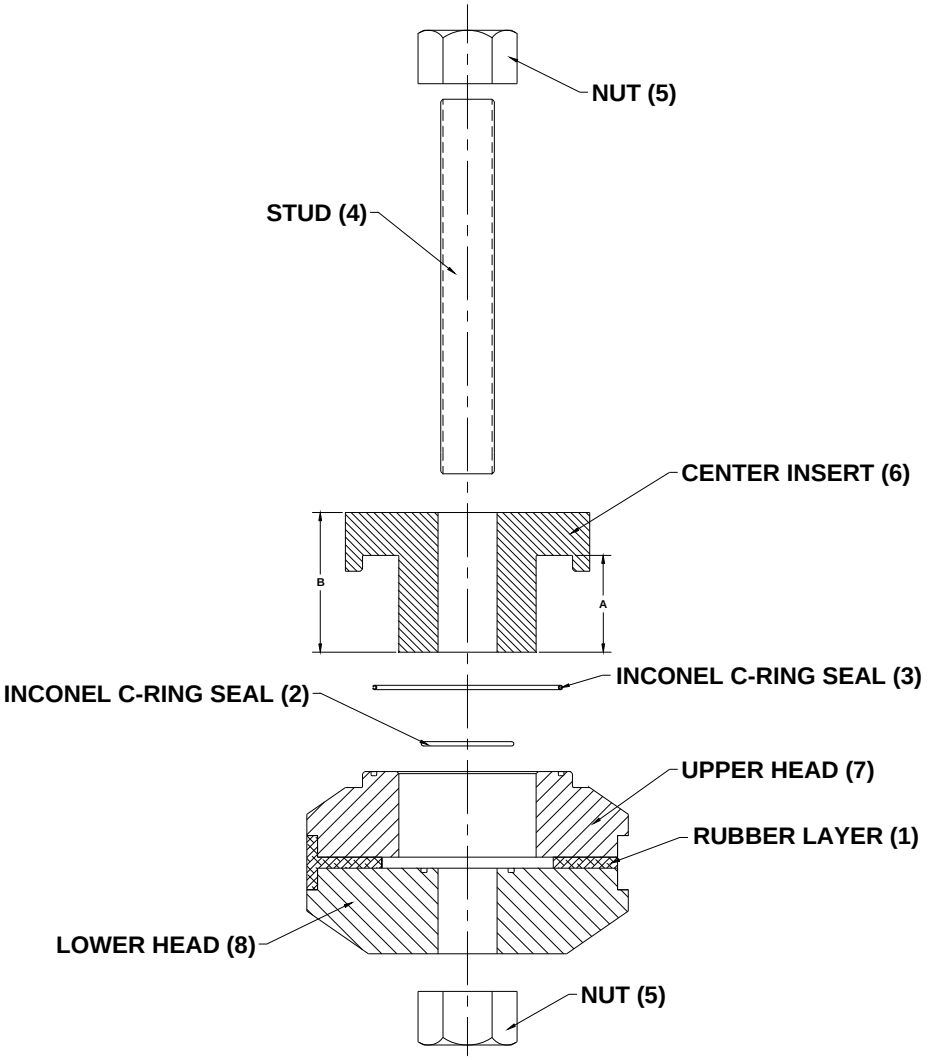

Figure 5-7: Exploded View of the Small-Scale Test Specimen

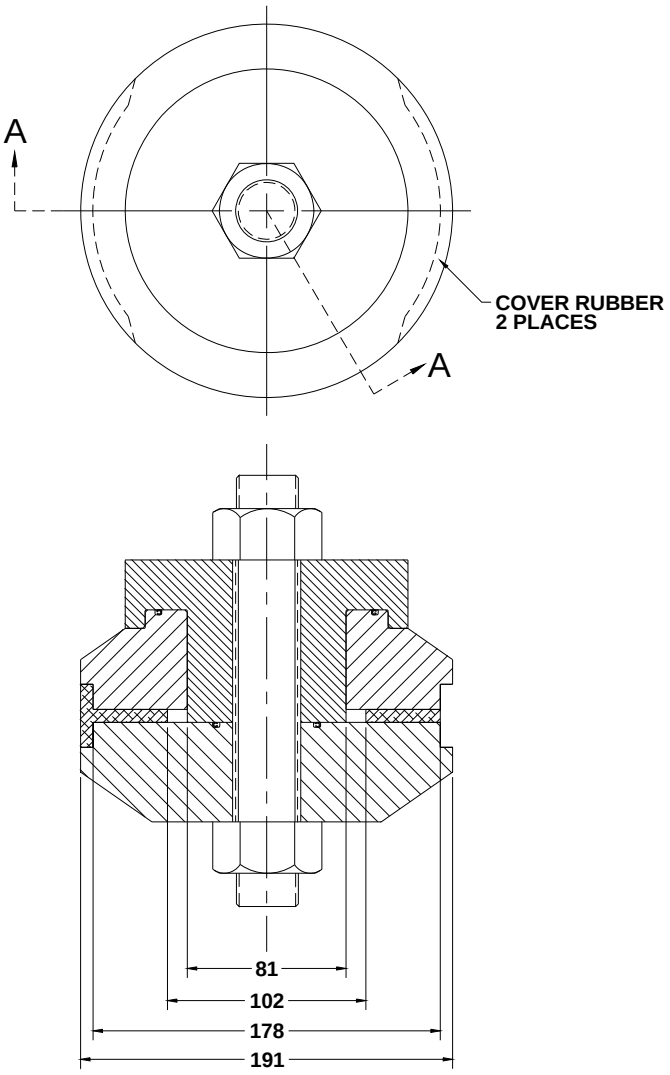

Figure 5-8: Small-Scale Test Specimen Assembly (mm)

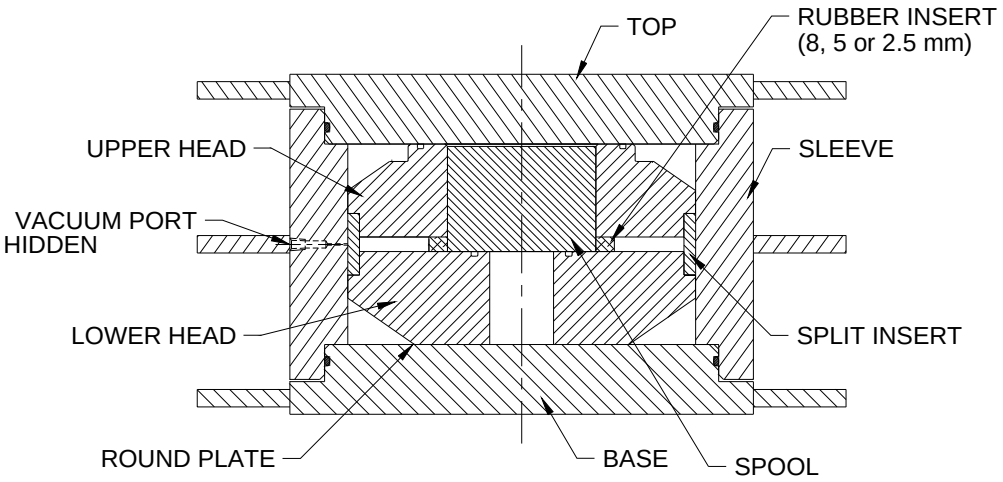

Figure 5-9: Schematic of Small-Scale Test Specimen Mold Design

Figure 5-10: 8 mm Molded Element

Figure 5-11: Assembled Small-Scale Test Specimen (8 mm Rubber Layer)

Table 5-1: As-Built Heights of Small Scale Specimens and Axial Deflection of Rubber Layer

Serial Number (Specimen)	Upper Head Height (mm)	Lower Head Height (mm)	Total Molded Height (mm)	Rubber Thickness (mm)	Center Insert Height (Dim A) (mm)	Complete Assembly Height (mm)	Axial Deflection of Rubber Layer (180 kN Axial Load) (mm)
011 (A)	50.83	50.77	109.35	7.75	57.48	133.78	1.1
015 (B)	50.80	50.80	109.27	7.67	57.45	133.76	1.02
016 (C)	50.80	50.75	109.32	7.77	57.48	133.86	1.09
012 (A)	50.80	50.83	106.68	5.05	55.14	131.57	0.71
013 (B)	50.80	50.80	106.68	5.08	55.17	131.55	0.71
014 (C)	50.77	50.83	106.68	5.08	55.14	131.57	0.71
006 (A)	50.80	50.83	104.17	2.54	52.88	129.46	0.46
007 (B)	50.80	50.83	104.27	2.64	52.88	129.64	0.56
010 (C)	50.83	50.80	104.19	2.57	52.91	129.44	0.49

5.5 TEST PROCEDURE

A schematic of the test setup is shown in Figure 5-12. The test procedure is summarized as follows:

1. Three test specimens (referred to as A, B and C as shown in Table 5-1) of each rubber layer thickness (8, 5 and 2.5 mm) were placed in a specially designed pressure vessel shown in Figure 5-13. The pressure vessel was designed to handle up 90 MPa of internal pressure. Note that two replicates of each rubber layer thickness were tested to verify the repeatability of EDD. Inside the pressure vessel the specimens were positioned by means of alignment plates with holes such that the gas could flow easily all around the specimens as shown in Figure 5-12(b).
2. Prior to placing in the pressure vessel, axial load-deflection behavior of each specimen was measured on a MTS machine as shown in Figure 5-14. The specimens were loaded 5 times to eliminate the Mullins effect and the sixth cycle data was recorded.
3. The pressure vessel was placed in an insulated tank filled with anti-freeze fluid that was used to heat the specimens. The tank was equipped with a heating coil and a pump to circulate the fluid. Since methane is highly inflammable gas, the insulated tank was located in a pit under ground to control any explosions or accidents. Figure 5-15 shows the sealed pressure vessel prior to placing in the insulated tank. Figure 5-16 shows the instrumentation and the control system.

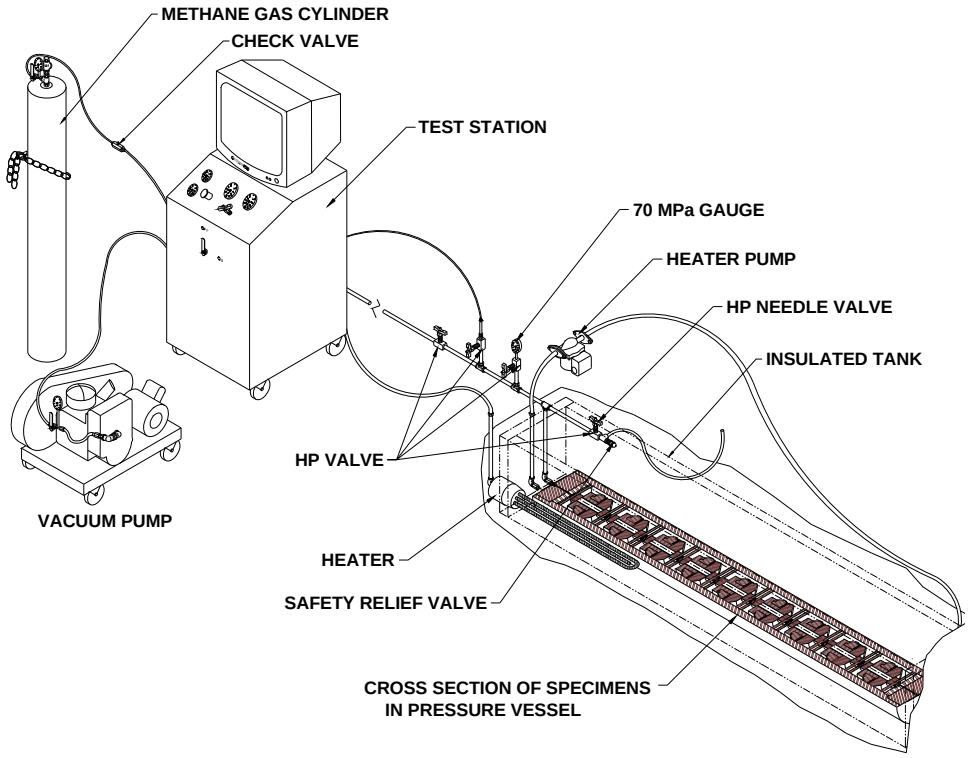

(a) Test Setup

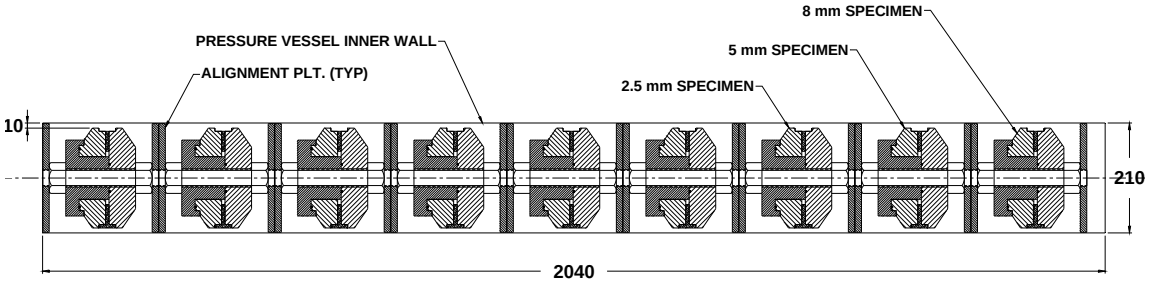

(b) Arrangement of Specimens Inside Pressure Vessel (dimensions shown in mm)

Figure 5-12: Schematic of Explosive Decompression Test Setup

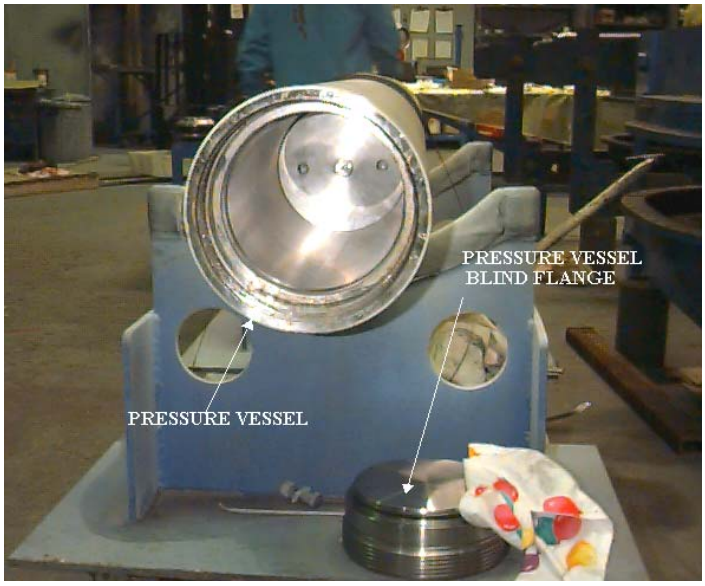

Figure 5-13: Specially Designed 90 MPa Pressure Vessel used in Explosive Decompression Testing

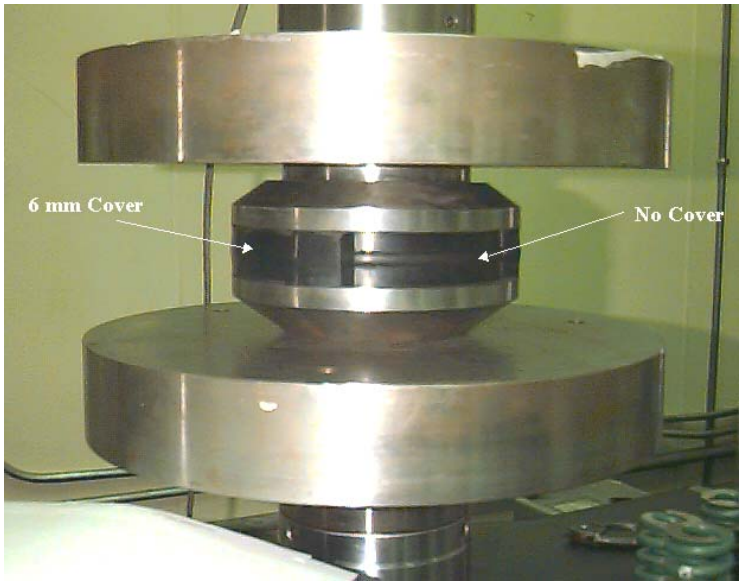

Figure 5-14: Test Setup for Load-Deflection Tests of Small Scale Specimens

Figure 5-15: Sealed Pressure Vessel being Placed in Insulated Tank

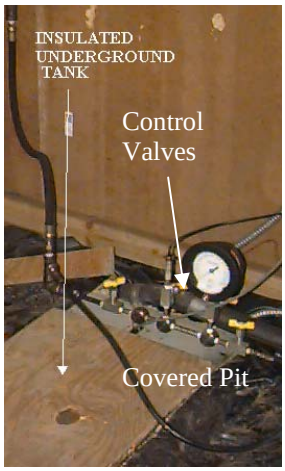

Instrumentation at Insulated Tank

Control System

Figure 5-16: Instrumentation and Control System

4. The air was evacuated from the system and the pressure vessel was heated until a steady state temperature of 100 ^{o}C was reached. Methane was then pumped into the vessel and the pressure was increased to 21 MPa. The specimens were exposed to methane for 45 days under 21 MPa pressure and 100^{o}C temperature. Three thermocouples along the pressure vessel length were used to measure the temperature. The temperature and pressure were recorded and maintained by means of automatic data acquisition and relay system.
5. After 45 days, the pressure was lowered to 0.3 MPa in 30 minutes to simulate the first decompression cycle. The specimens were left in the methane environment at 0.3 MPa pressure and 100^{o}C temperature for two days to simulated actual field conditions and then the pressure was increased back to 21 MPa. The 21 MPa pressure was held constant for three days at 100^{o}C to replenish the loss of methane during two days of 0.3 MPa exposure. The pressure was dropped again to 0.3 MPa and left for two days. This 0.3-21-0.3 MPa cycle was repeated five times.
6. At the end of fifth pressurization-depressurization cycle, specimens were taken out of the pressure vessel for a general visual inspection of the system to ensure that it was working as designed. The condition of the specimens, pressure vessel and the sealing system was quickly observed and the specimens were placed back in the pressure vessel and subjected to five more 0.3-21-0.3 MPa pressurization-depressurization cycles.

7. After a total of ten cycles, the specimens were taken out and subjected to a rigorous visual inspection, wherein the four quadrants of all the nine specimens were photographed from outside as shown in Figures 5-21 through 5-29. After visual inspection the specimens were stored at ambient temperature and pressure for one month to degas the dissolved methane.
8. After degassing, the axial load-deflection characteristics of each specimen was measured again. The specimens were loaded 5 times to eliminate the Mullins effect and the sixth cycle data was recorded.
9. The most damaged specimens were then dissected to determine the extent of damage caused by explosive decompression.

5.6 RESULTS AND FINDINGS

A comparison of axial stiffnesses before and after ten 0.3-21-0.3 MPa pressurization-depressurization cycles at 100^{o}C are shown in Figures 5-17, 5-18 and 5-19 for 8, 5 and 2.5 mm test specimens respectively. Figure 5-20 shows a plot of percent change in axial stiffness versus rubber layer thickness. The condition of the three specimens A, B and C are shown in Figures 5-21, 5-22 and 5-23 respectively for the 8 mm, Figures 5-24, 5-25 and 5-26 respectively for the 5 mm specimens and Figures 5-27, 5-28 and 5-29 respectively for the 2.5 mm specimens. In Figures 5-21 through 5-29, “Side 1” and “Side 3” show the covered quadrants while “Side 2” and “Side 4” shown the quadrants with no cover. The extent of damage along the width of the layer for most severely damaged 8, 5 and 2.5 mm specimens is shown in Figures 5-30, 5-31 and 5-32

respectively. The following observations are based on the results shown in Figures 5-17 through 5-32 and the general visual inspection performed after the 5^{th} compression-decompression cycle.

1. All specimens show blisters in the covered regions (refer to side 1 and side 3 in Figures 5-21 through 5-29) and extrusion of rubber in uncovered regions (refer to side 2 and side 4 in Figures 5-21 through 5-29). Note that the extrusion is the phenomenon where the rubber layer is permanently damaged in the bulge region by sharp edges of the top and bottom surfaces, to which it is bonded, while it bulges out due to compression. The size of blisters and extent of extrusion increases with thickness of rubber layer. Note that the pictures shown in Figures 5-21 through 5-29 were taken right after the specimens were taken out of the pressure vessel. As the gas permeates out, the blisters decrease in size and eventually vanish. After a month of degassing, very few blisters were visually noticeable, however the structural damage was still there as observed in the load-deflection tests.
2. Specimens of the same rubber thickness (replicates) show similar damage both in the covered and uncovered regions confirming the repeatability of the results.
3. The 8 mm specimens show extensive explosive decompression damage. The 5 mm specimens show some damage, while the 2.5 mm specimens show almost negligible damage.

4. The external damage after 5th cycle, visible by naked eye, was about same as the damage observed after 10th cycle in all the specimens except the 8 mm specimens where the damage in the cover region after 10th cycle was much more severe as compared to the 5th cycle damage. This implies that the damage occurs in first few cycles and once occurred it propagates as more cycles are applied. It also implies that the cover region is more susceptible to damage as compared to the region with no cover. These observations substantiates the finite element analysis results shown in Appendix C and the premise which stated that most of the damage will occur in first cycle and the unconstrained elastomer (cover region) will experience more damage as compared to the constrained elastomer.
5. There is a significant reduction in the axial stiffness of 8 and 5 mm specimens (approximately 90% and 45% respectively) after pressurization-depressurization cycles as shown in Figures 5-17 and 5-18 respectively whereas the axial stiffness of 2.5 mm specimens has slightly increased (5 %) as shown in Figure 5-19. Since there is negligible damage in 2.5 mm specimens, this increase in stiffness can be attributed to the aging effects.
6. As shown in Figure 5-20, the reduction in axial stiffness due to explosive decompression damage is directly proportional to the thickness of the rubber layer.
7. The damage across the width of the 8 mm specimen is quite severe as shown in Figure 5-30. The metal to rubber bond is severely damaged. The

5 and 2.5 mm specimens do not show any macroscopic damage across the width of the rubber layer as shown in Figure 5-31 and 5-32 respectively, however, there is definitely some microscopic damage in the 5 mm specimens because the axial stiffness after the decompression cycles is considerably lower. Therefore, the explosive decompression is damaging the rubber at microscopic level as assumed in the premise.

8. In spite of a decompression pressure much greater than 7.5G (refer to Section 5.3), no structural damage in the 2.5 mm specimens substantiates the assumption that with adequate confinement of rubber the effects of explosive decompression can be diminished to acceptable levels.
9. A comparison of 5^{th} cycle and 10^{th} cycle observations indicate that the specimens susceptible to EDD will be damaged in first few compression-decompression cycles and there is no need of applying more cycles. However, more research is needed to determine the exact number of cycles that must be applied to check the integrity of rubber layer under explosive decompression cycles.

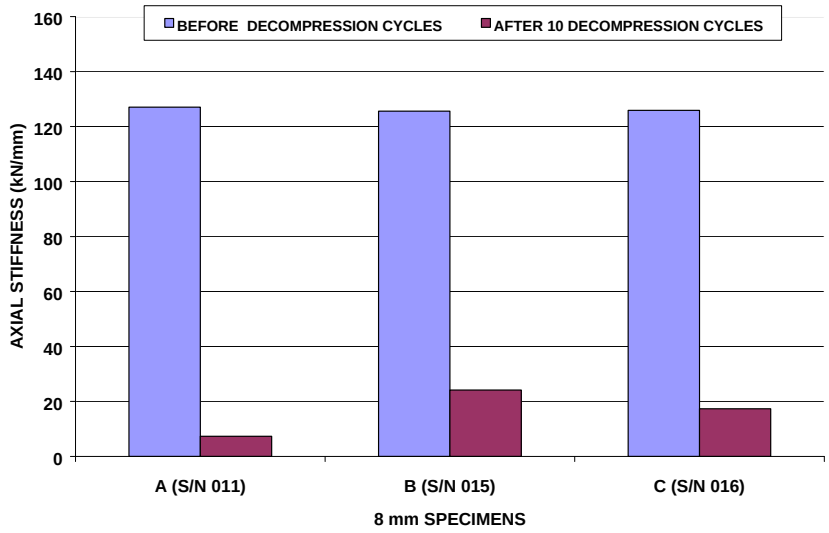

Figure 5-17: Axial Stiffness of 8 mm Specimens Before and After Ten 0.3-21-0.3 MPa Pressurization-Depressurization Cycles

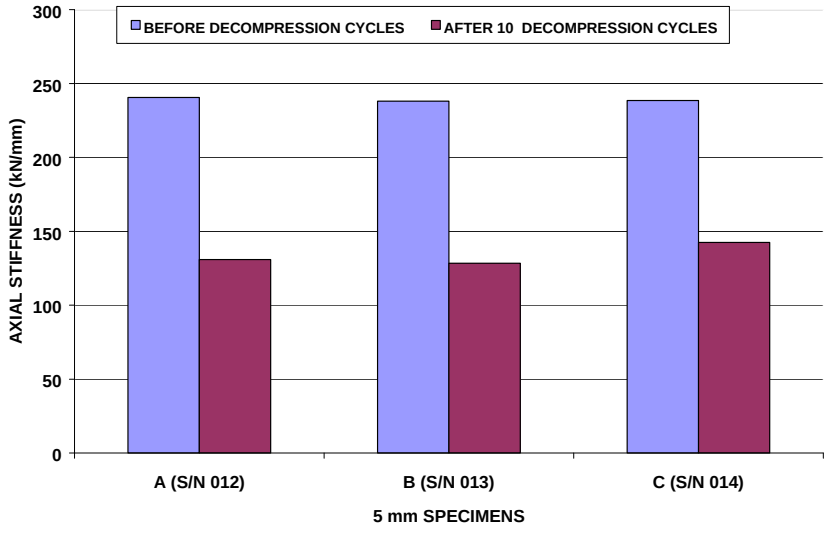

Figure 5-18: Axial Stiffness of 5 mm Specimens Before and After Ten 0.3-21-0.3 MPa Pressurization-Depressurization Cycles

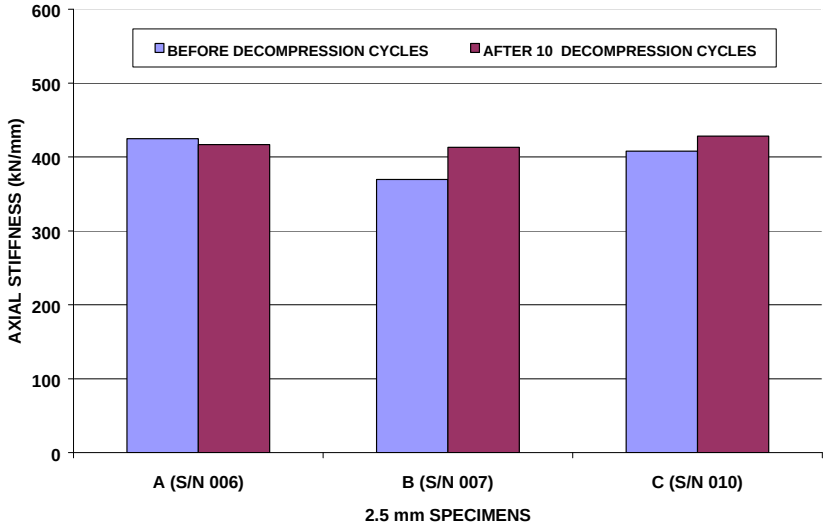

Figure 5-19: Axial Stiffness of 2.5 mm Specimens Before and After Ten 0.3-21-0.3 MPa Pressurization-Depressurization Cycles

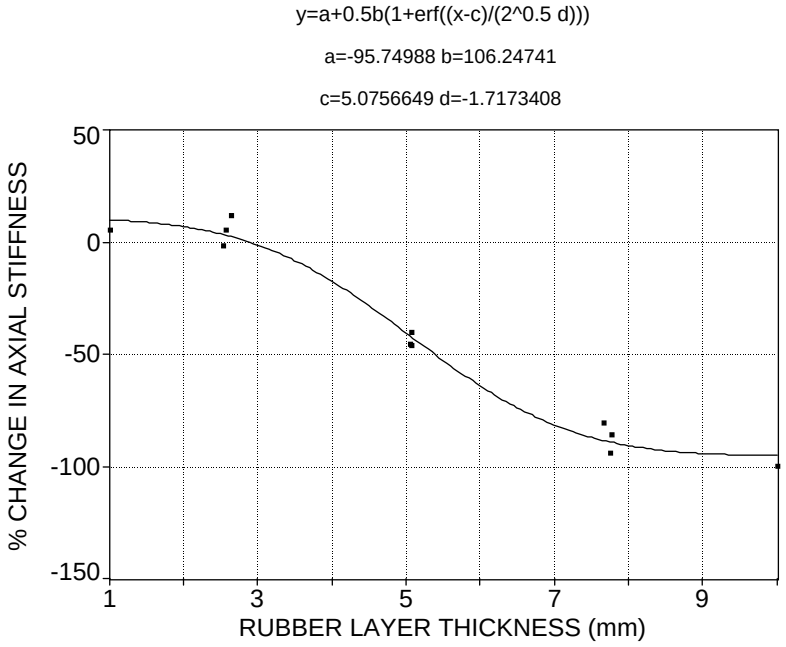

Figure 5-20: Percent Change in Axial Stiffness due to Explosive Decompression Damage Versus Rubber Layer Thickness

Side 1 (Cover)

Side 2 (No Cover)

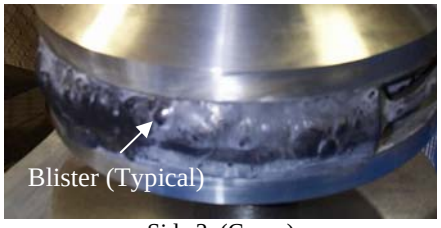

Side 3 (Cover)

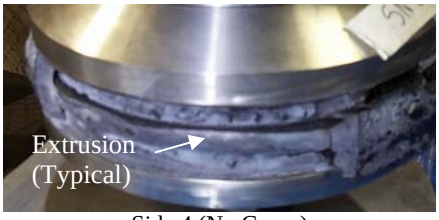

Side 4 (No Cover)

Figure 5-21: Explosive Decompression Damage in 8 mm Specimen (A)

Side 1 (Cover)

Side 2 (No Cover)

Side 3 (Cover)

Side 4 (No Cover)

Figure 5-22: Explosive Decompression Damage in 8 mm Specimen (B)

Side 1 (No Cover)

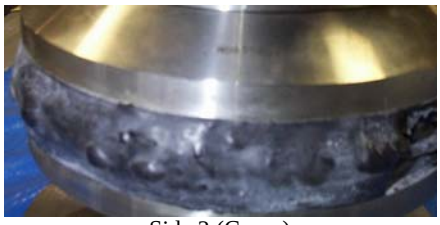

Side 2 (Cover)

Side 3 (No Cover)

Side 4 (Cover)

Figure 5-23: Explosive Decompression Damage in 8 mm Specimen (C)

Side 1 (No Cover)

Side 2 (Cover)

Side 3 (No Cover)

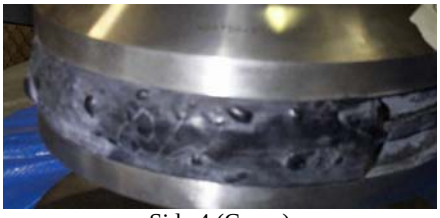

Side 4 (Cover)

Figure 5-24: Explosive Decompression Damage in 5 mm Specimen (A)

Side 1 (No Cover)

Side 2 (Cover)

Side 3 (No Cover)

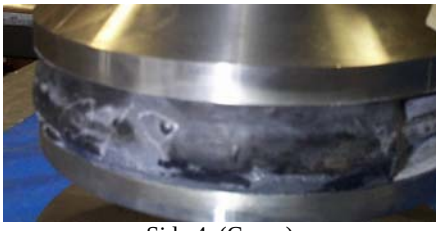

Side 4 (Cover)

Figure 5-25: Explosive Decompression Damage in 5 mm Specimen (B)

Side 1 (Cover)

Side 2 (No Cover)

Side 3 (Cover)

Side 4 (No Cover)

Figure 5-26: Explosive Decompression Damage in 5 mm Specimen (C)

Side 1 (No Cover)

Side 2 (Cover)

Side 3 (No Cover)

Side 4 (Cover)

Figure 5-27: Explosive Decompression Damage in 2.5 mm Specimen (A)

Side 1 (No Cover)

Side 2 (Cover)

Side 3 (No Cover)

Side 4 (Cover)

Figure 5-28: Explosive Decompression Damage in 2.5 mm Specimen (B)

Side 1 (Cover)


Side 2 (No Cover)


Side 3 (Cover)

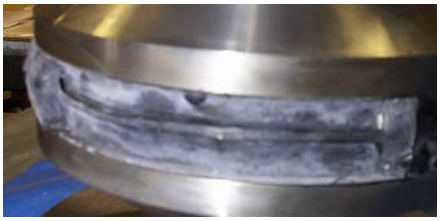
Side 4 (No Cover)

Figure 5-29: Explosive Decompression Damage in 2.5 mm Specimen (C)

5.7 CONCLUSIONS

1. The explosive decompression damage can severely affect the performance of an elastomeric bearing and must be considered in the design of bearings that are exposed to fluid/gas environment in conjunction with precipitous changes in pressure.
2. Under similar environmental and loading conditions, thicker rubber layers are more susceptible to explosive decompression damage (EDD).
3. For thick rubber layers that experience EDD, the damage is not limited to the bulge region only. It propagates inside as more pressurization-depressurization cycles are applied.
4. For thick rubber layers that are prone to EDD, a thick cover layer makes things worse.

5. Reduction in axial stiffness correlates very well with the extent of explosive decompression damage, therefore comparison of axial stiffness before and after pressurization-depressurization cycles can be used as a measure of explosive decompression damage.
6. The extrusion of rubber can be attributed to the localized tearing at sharp uncovered edges exasperated by high temperature to which the specimens were exposed In the present study, high temperature was needed to accelerate the diffusion rate, however in real life the highest temperature seen is about half of what was used in this study.
7. The presence of cover increased blisters, however, it helped to restrict extrusion at high temperatures. Therefore, cover is definitely needed, however more research is needed to determine the thickness of cover that will provide a compromise between the damage due to blisters and damage due to extrusion.
8. Finally, the present test method can be effectively used to design a rubber layer thickness that will perform well under the subject explosive decompression environment.

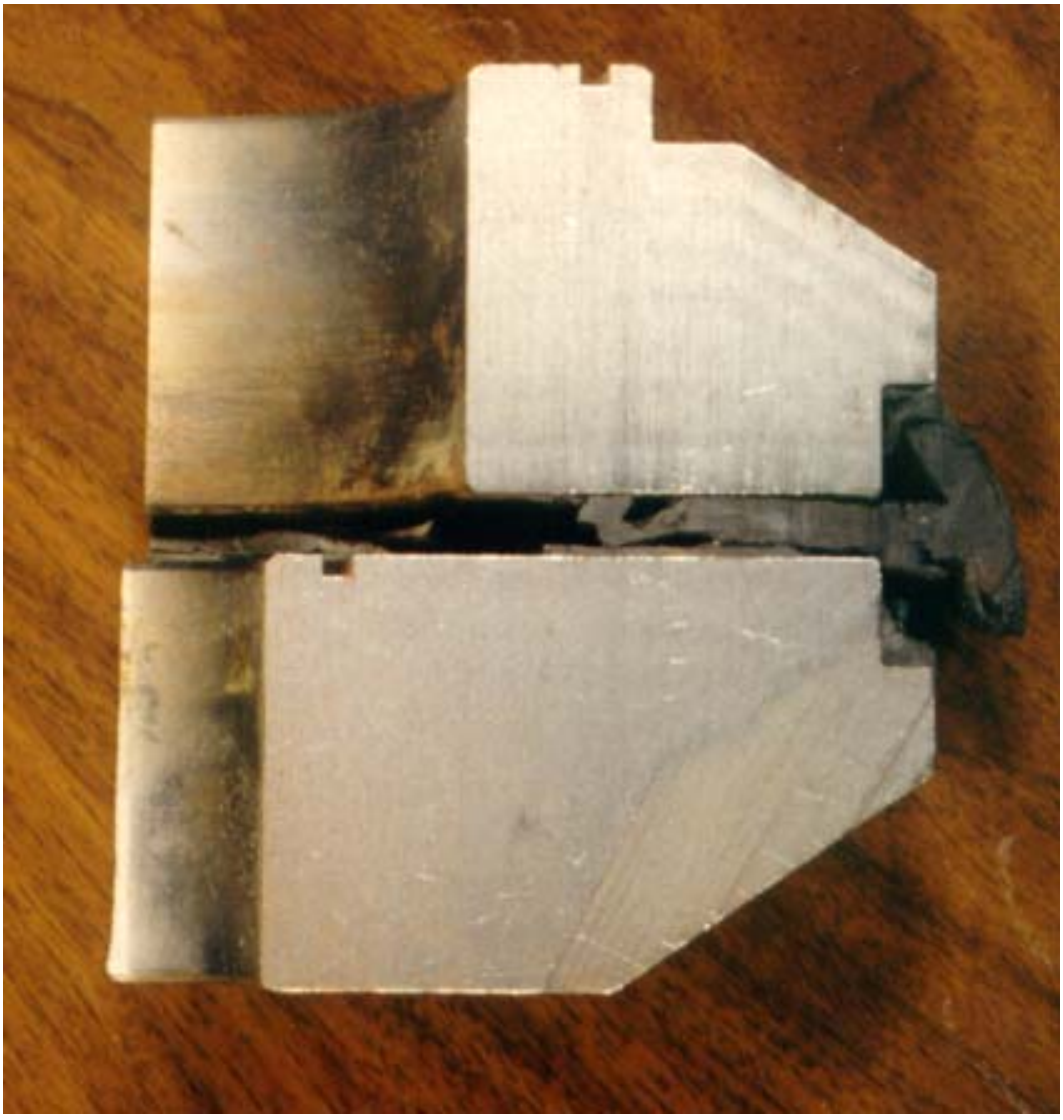

Figure 5-30: Cross-Section of an 8 mm Specimen

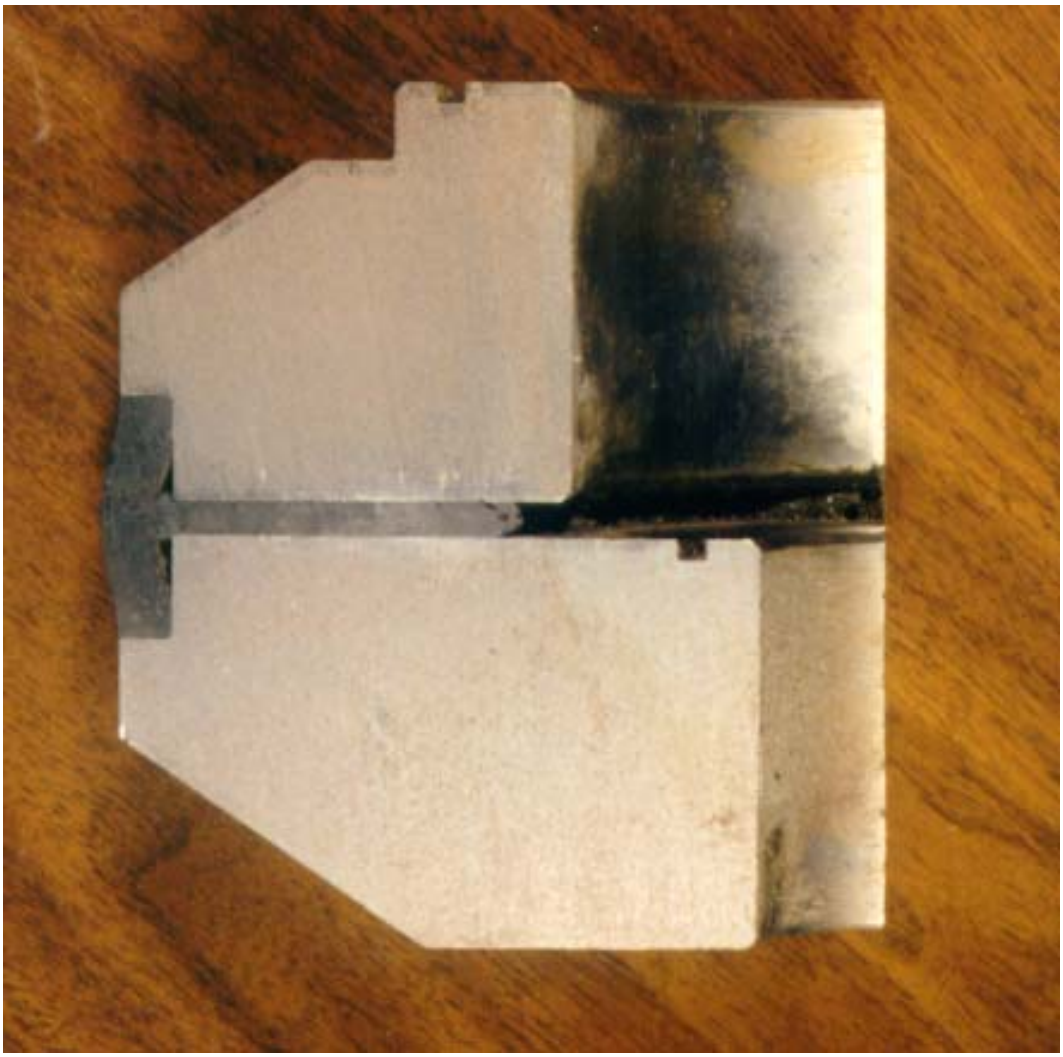

Figure 5-31: Cross-Section of a 5 mm Specimen

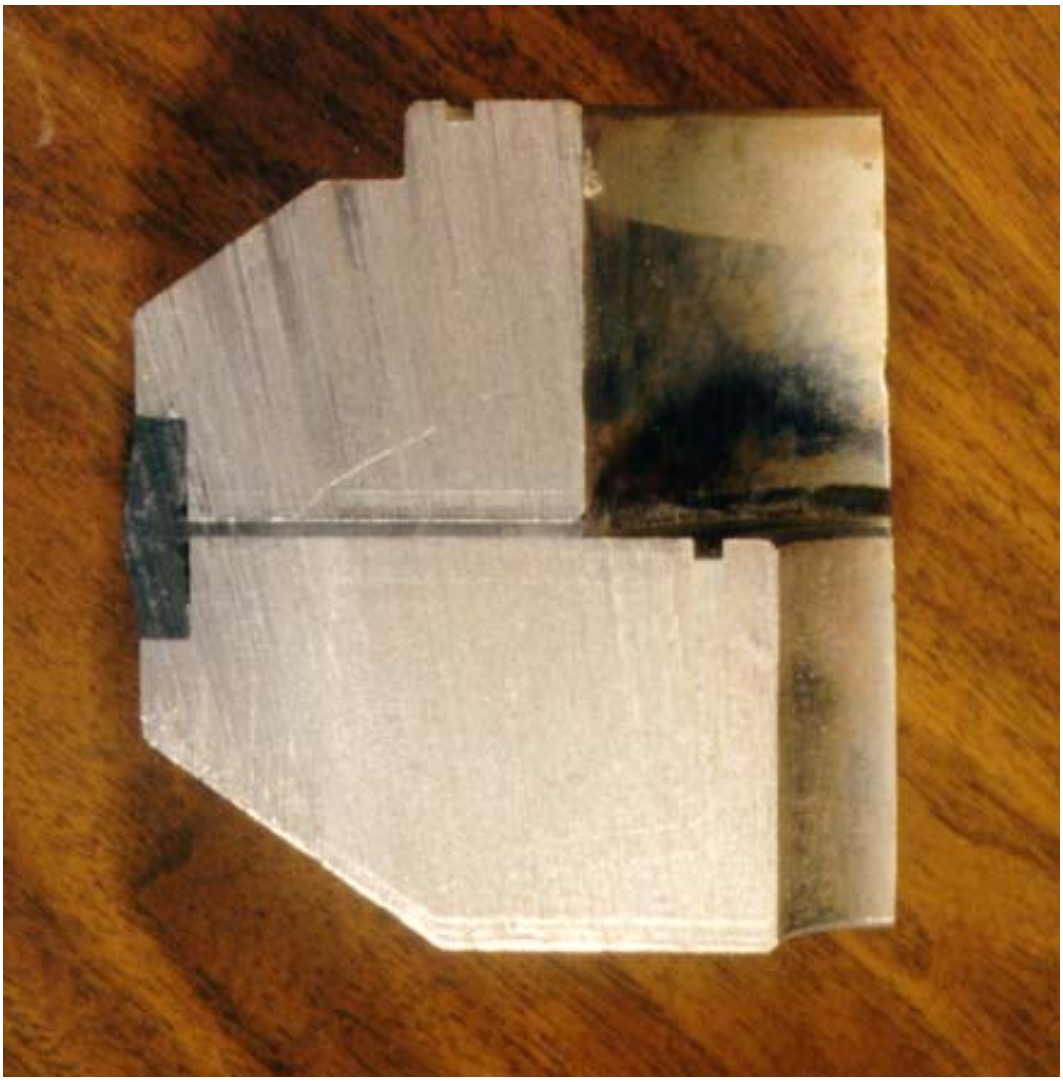

Figure 5-32: Cross-Section of a 2.5 mm Specimen

9.

Chapter 6: Summary and Recommendations

6.1 SUMMARY

The effects of laminate misalignment, creep, aging and explosive decompression on the performance of steel laminated elastomeric bearings were studied. To represent the extreme range of the material behavior found in elastomeric bearings, natural rubber (NR) and neoprene (CR) at two hardness levels (durometer 50 and 70) were used in the study of laminate misalignment, creep and aging. The effects of explosive decompression were studied on nitrile due to its superior performance in oil/gas environment. The following is a summary and conclusions of the work performed in the present study.

6.1.1 Misalignment of Laminates

Steel laminated elastomeric bearings are generally manufactured using compression molding wherein the outside dimensions can be precisely controlled by the mold dimensions. However the internal steel laminates if not properly constrained, can shift horizontally, vertically or rotate due to the flow of rubber under pressure inside the mold. AASHTO M251-97, Table 2 specifies certain tolerances on rubber layer thickness and cover thickness, however there has been no systematic study conducted to substantiate the validity of these tolerances. Steel laminated elastomeric bearings are sometimes rejected at the manufacturing stage because of failure to comply with these tolerances.

In the present work, limits on laminate misalignments were developed by systematically studying their effects on the structural behavior of steel-laminated

elastomeric bearings. The cumulative effect of three most probable laminate misalignments (vertical shift of laminates causing variations in rubber layer thickness, horizontal shift of laminates causing variations in external cover and rotation of laminates resulting in non-uniform rubber layers thickness) were studied on eight performance variables (axial, shear and rotation stiffnesses, maximum shear strain, principal strain and triaxial stress in the elastomer, bond stress at the interface of the steel laminates and rubber, and maximum von Mises stress in steel laminates) by means of computer simulated experiments using the finite element method. Since rubber is an almost incompressible material, the finite element model of the rubber portion was prepared using three dimensional 27- node second order solid hybrid finite elements. The steel parts were modeled using three-dimensional 27 node second order solid finite elements. The general purpose finite element code ABAQUS was used to perform the analysis. The hyper-elasticity of the rubber was modeled using Yeoh's approximation to Rivilin's formulation. The material constants were obtained by mean of non-linear regression analysis of experimental data in simple shear. Structural analyses consisted of nonlinear quasi-static analysis with geometric and material nonlinearities to incorporate the effects of large deformation and large strains. Since there are unlimited combinations of the three misalignments considered, a response surface methodology, generally used in statistical design and analysis of experiments, was used to develop approximating functions relating the performance variables (dependent variables) to the combined effect of misalignments (independent variables). These approximating functions were used

in conjunction with comprehensive evaluation criteria to develop combined limits on vertical misalignment, edge cover misalignment and laminate inclination in the form of an interaction equation. The comprehensive evaluation criteria limited the variation of axial and shear stiffness to $\pm 10\,\%$ while shear strain, maximum principal strain, triaxial tensile stress and von Mises stress were limited to 6, 2.0, 6G and F_y respectively, where G is the shear modulus of elastomer and F_y is the yield strength of steel laminates. The bond stress was limited to the average shear stress corresponding to a shear strain of 2. No constraints were imposed on rotation stiffness since it is not important for flat pad bearings. A Center Composite Design (CCD) was employed in selecting various runs and values of the three independent variables. For the number of variables considered, sixteen computer runs were needed for each of the four materials (NR50, CR50, NR70 and CR70) in order to establish a statistically reliable evaluation of the misalignments. The effects of misalignments were investigated under a combined axial stress (3.8 MPa and 7.6 MPa for 50 and 70 durometer bearings respectively), shear deformation (corresponding to 50 percent direct shear strain) and 1^o rotation.

The results of this investigation showed that an elastomeric bearing can tolerate considerable amount of vertical, horizontal and rotation misalignments of laminates without deterioration in performance. The horizontal misalignment (cover) is less influential on the performance of the bearing than the variation of rubber layer thickness and the rotation misalignment. There is a significant interaction between the vertical and rotation misalignments. If one is less, then a

higher value of the other can be tolerated without affecting the performance of the bearing. The interaction equation can be effectively used to calculate the allowable value of the vertical or rotation misalignment if the value of the other is known. In general, the tolerances given in Table 2 of AASHTO specification M241 are well below the laminate misalignments that affect the performance of the bearings.

6.1.2 Creep

All elastomers exhibit the characteristics of creep, or continuing time dependent deformation under constant load; and stress relaxation, or time dependent decay in stress at constant deformation. The creep of elastomeric bearings has generally been studied by applying a constant load on full-scale bearing for a long period of time and measuring the deflection at specified intervals. There are some standardized tests (ISO 8013, 1988) that are generally used to assess creep characteristics of elastomers. The standardized creep tests are merely quality control tests and can not be used to predict the behavior of full-scale bearings because the shape factor, boundary conditions, loading conditions and exposure conditions (temperature etc.) of the full-scale bearings can vary considerably as compared to the test specimen. AASHTO 1992 Specifications has set criteria to evaluate creep for elastomeric bearings, however, AASHTO has no test to check creep properties.

In the present study the creep behavior of laminated elastomeric bearings was investigated by means of full-scale tests. Since full-scale creep tests are time consuming, uneconomical and specific to the bearings tested, a practical method

was developed to predict creep of elastomeric bearings using six-hour stress relaxation data obtained from dual lap shear relaxation tests. The method is based on the concept that axial deformation d_t at time 't' can be approximately calculated from the axial deformation d_{t1} at time t_1 as $d_t = d_{t1}\frac{G_{t1}}{G_t}$, where G_{t1} and G_t are the shear modulus at times t1 and t respectively determined from stress relaxation data at a strain close to the average strain in the bearing. A simple power law can be conservatively used to predict the long-term shear modulus from six-hour stress relaxation data. Axial deflections predicted using this method gave a conservative estimate of axial creep deformation for bearings with bonded top and bottom surfaces. The 30 day deflection was predicted conservatively within 3-4 percent while the 25 year estimate was 5-7 percent conservative.

The stress relaxation tests were performed on three sizes of specimens: (a) 1x1 shear specimen (25x25 mm), (b) 2x2 shear specimens (51x51 mm) and (c) 3x3 shear specimens (76x76 mm). The shear relaxation modulii determined for the 2x2 and 3x3 specimens cut from the full size bearing were very similar. The 1x1 specimens showed modulii that was about 10 percent lower than the larger specimens for NR50, CR50 and NR70 and 15 percent lower for the CR70 specimens. The difference between the 1x1 and the larger specimen can be attributed to the fact that 1x1 specimens were vulcanized as part of this research and the 2x2 and 3x3 specimens were cut from manufactured bearings. All specimens within each rubber type presumably came from the same rubber batch.

The full-scale creep tests were performed on bearings with smooth unbonded top and bottom surfaces and fully bonded top and bottom surfaces. Thus the two extreme boundary conditions were considered. Full-scale creep tests showed that time dependent deformation of elatomeric bearings is significant and must be considered in design of such bearings. The boundary condition at the top and bottom surfaces plays an important role in controlling the long-term deformation. The creep of bearings with unbonded top and bottom surfaces is highly unpredictable due to a gradual decay in friction forces at the interface of the bearing and the contacting surfaces. High durometer bearings show higher percent creep as compared to low durometer bearings due to a higher carbon black (filler) content, however the absolute creep deformation of high durometer bearings is lower than those of the low durometer bearings, so, if the designer is interested in absolute creep deformation, high durometer bearings can be used. neoprene bearings show slightly less percent creep as compared to natural rubber bearings, however the difference is not significant. The percent creep deflection is insensitive to small fluctuations of loads, however for large load variations the creep deformation at higher loads will be higher as compared to the lower loads. The true instantaneous deformation of an elastomeric bearing is very difficult to measure because a considerable amount of creep occurs within first few minutes of loading. AASHTO specifications compare the creep deformation to the instantaneous total deformation of the bearing. A better criterion for creep evaluation is to compare the creep deformation to the total deformation after one hour of loading. Assuming 1-hour deflection as instantaneous deflection, the

current AASHTO creep criteria, given in Table 14.7.5.2-1 (AASHTO 1998), is adequate to address the creep of elastomeric bearings.

Since the time dependent behavior of an elastomeric bearing, including creep is governed by time dependent shear modulus, limitations must be imposed on the variation of shear modulus over time rather than on axial deflection. This way not only will the axial deflection be controlled but the shear stiffness will also be controlled.

6.1.3 Aging

All elastomers are attacked by oxygen even at room temperature and the reaction is accelerated by heat, light and presence of certain metallic impurities that catalyze the decomposition of peroxides to form free radicals. This process is called aging. Degradation of physical properties is observed in elastomers even at quite low levels of oxidation. The nature of the changes observed vary considerably depending upon the specified elastomer, and the aging conditions to which it is subjected. There are several standardized tests available for quality control and for determining heat resistance or aging. ASTM D573, 1988, describes a test procedure based on accelerated heat aging to determine the influence of elevated temperature on the physical properties (hardness, elongation at break, tensile strength) of vulcanized rubber. The AASHTO elastomeric bearings material specification, M251 (1997) stipulates the use of ASTM D573 to assess the effect of aging on elastomeric bearings. Almost all accelerated aging tests mentioned in various specifications are performed on very thin specimens wherein the oxidation affects the whole specimen and the mode of loading is

generally tension. Since aging is related to the oxidation process, the rate and extent of diffusion of oxygen through the elastomer governs the change in properties due to aging. The rate of diffusion is dependent on temperature, pressure, exposed surface area and permeability of elastomer. In the case of elastomeric bearings oxygen ingress is generally limited to a thin layer of exterior surface only because of small exposed surface area (relative to loaded area) and low permeability of elastomer. Moreover, for elastomeric bearings the change in overall shear stiffness due to aging is more relevant than the change in localized tensile properties represented by the accelerated aging tests.

In the present study the effects of aging on shear stiffness were investigated by conducting accelerated heat aging tests on four different sizes of shear specimens: (a) Rheometer specimens, (b) 1x1 shear specimen (25x25 mm), (c) 2x2 shear specimens (51x51 mm) and (d) 3x3 shear specimens (76x76 mm). In order to use Arrenhius relation the accelerated aging was done at two temperatures 82^{o} C and 100^{o} C. The sizes and aging temperatures were selected based on the results of a pilot study so that significant spread of post-aging shear characteristics could be observed without damaging the specimens due to overheat. The aging was done in an air oven, wherein the airflow and temperature were precisely controlled. The shear stiffness was measured at 0, 1, 2, 3, 4, 5, 6 and 7 weeks of aging. Based on the results of this study the following conclusions can be made.

The change in shear stiffness due to aging is dependent on the size of the specimen. As the size increases the percent change in shear stiffness decreases

drastically. This can be attributed to the amount of rubber affected by oxidation process. At higher aging temperatures the stiffness change is higher. This is due to a higher oxygen diffusion rate at higher temperatures. The ingress of oxygen is faster and deeper at higher temperatures and therefore the percentage of affected zone to unaffected zone is higher. In general the effects of aging is higher in neoprene as compared to natural rubber. The compounds with higher carbon black content age faster and the effects of aging are more dominant at higher strains. Arrenhius based predictions show that the full size bearings at ambient temperatures will experience insignificant change in stiffness due to aging over their lifetime and therefore the aging tests given in various specifications are irrelevant for the elastomeric bearings of moderate to high shape factor rubber layers used in civil engineering applications. Therefore, ASTM D573 can be eliminated from the AASHTO specification M251-97. However, aging can have significant effect on the stiffness characteristics of elastomeric bearings exposed to high temperatures generally encountered in oil field applications. For such bearings the effects of aging must be considered during the design phase. Currently there are no test methods that directly address the heat aging of elastomeric bearings. The small-scale tests developed in this research can be effectively used to study the aging of elastomeric bearings at high temperatures.

6.1.4 Explosive Decompression Damage

Elastomeric bearings are commonly used as moment-free connections in offshore pipelines transporting high-pressure hydrocarbon flud/gas mixture. Under sustained internal pressure, rubber layers absorb hydrocarbon gases. When

the internal pressure is rapidly decreased, the explosive expansion of the absorbed gases within the elastomer causes internal rupture of the elastomer structure and potential damage known as Explosive Decompression Damage (EDD) to the rubber surfaces that may gradually affect the load carrying capacity of the bearing. The primary damage occurs due to instantaneous inflation of small spherical voids, initially present at the time of cross-linking either in the form of submicroscopic bubbles of air trapped in rubber processing or in the form of badly wetted particles of dirt or dust.

In the present study a test method was developed to identify the principal design variables that affect the extent and nature of the explosive decompression damage in elastomeric bearings. Prior to this research no test method was available that could be used to assess the EDD in elastomeric bearings exposed to sudden fluctuation of pressures commonly encountered in oil field applications. Some information was available on the explosive decompression failure of O-ring seals that behave very differently than elastomeric bearings. The new test method is based on the concept that the explosive decompression damage is generally restricted to the cover rubber or generally noticed in areas where the confinement of rubber is minimum. In a typical rubber layer of a high-pressure elastomeric bearing, the top and bottom surfaces are bonded to steel reinforcements and it is assumed that the bond provides adequate confinement of these surfaces. The side surfaces, however, are free to bulge and therefore most susceptible to explosive decompression damage. In order to predict the extent of damage that will not adversely affect the overall performance of the bearing, only the damage in the

bulge region needs to be studied. If the damage is noticed beyond the bulge region, the elastomeric bearing will definitely fail to perform adequately. A small-scale specimen that replicates the structural behavior of bulge region of most critical rubber layer of the full-scale elastomeric bearing can be used to assess the effects of EDD. In other words, a small-scale test specimen of same material and same thickness as an actual rubber layer, that experiences same pressure distribution (before and after decompression) in the vicinity of the bulge region as an actual rubber layer will exhibit the same decompression damage as an actual rubber layer.

Small-scale specimens with three different rubber layer thicknesses 8, 5 and 2.5 mm representing the range of thicknesses used in high shape factor elastomeric bearings were designed with the aid of finite element analysis. The specimens consisted of a 102 mm Inner Diameter (ID) and 178 mm Outer Diameter (OD) rubber disk bonded to two metal heads. A 6 mm cover rubber was used in the two alternate quadrants. The other two 90^{o} sectors were without cover rubber. An axial displacement was applied by means of a self-reacting system consisting of a stud and two nuts reacting against the top and bottom metal heads to which the rubber layer was bonded. Depending on the as-built thickness of the rubber layer, the axial displacements for various specimens were determined by actual load-deflection tests of each test specimen such that the initial axial load was approximately 180 kN in all the test specimens (all thicknesses). Under this load, the stress/strain distribution in the vicinity of the bulge region of the 8 mm test specimen closely resembled the stress/strain distribution in the bulge region

of a full size bearing. The same axial load was used for 5 and 2.5 mm specimens to ensure identical initial loading conditions. The specimens with two replicates were tested in a specially designed pressure vessel. Exposure and environment were chosen to represent extreme conditions that are encountered offshore oil production due to shutdown or other emergencies. Methane gas at a temperature of 100 ^{o}C and a pressure of 21 MPa was used as the energizing source. After 10 pressurization-depressurization cycles the specimens were subjected to a rigorous visual examination and a load-deflection test. The results showed that the explosive decompression damage can adversely affect the performance of an elastomeric bearing. All specimens showed blisters in the covered regions and extrusion of rubber in uncovered regions. The 8 mm specimens showed extensive explosive decompression damage. The 5 mm specimens showed some damage, while the 2.5 mm specimens showed almost negligible damage. There was a significant reduction in the axial stiffness of 8 and 5 mm specimens (approximately 90% and 45% respectively) after pressurization-depressurization cycles whereas the axial stiffness of 2.5 mm specimens has slightly increased (5 %). Since there was negligible damage in 2.5 mm specimens, this increase in stiffness can be attributed to the aging effects.

Based on the results of EDD testing it can be concluded that under similar environmental and loading conditions, thicker rubber layers are more susceptible to explosive decompression damage and with adequate confinement of rubber, the effects of EDD can be reduced to acceptable levels. The small-scale test developed here can be effectively used to select the type of elastomers for

explosive decompression applications or design a rubber layer thickness that will perform well in an environment subjected to explosive decompression. The results of this research are currently being used in the development of new elastomeric bearing designs for explosive decompression applications.

6.2 RECOMMENDATIONS FOR FURTHER RESEARCH

Based on the results of the present study, the following areas were identified that needs further research:

1. The creep of elastomeric bearings with unbonded top and bottom surfaces is a complex problem due to the uncertainities involved at the interface of rubber and the contacting surface. More research is needed to address the long-term axial deformation of such bearings.
2. Relaxation shear modulus can be effectively used to predict the creep of full size bearings at moderate to higher temperatures but more research is needed for its use to predict creep at low temperatures. As mentioned in Chapter 1, at low temperatures (in the vicinity of glass transition temperature) there is an abrupt change in the mechanical properties of elastomers.
3. The results of aging studies given in this report are generally applicable for bearings subjected to monotonic loads. To extend these results to bearings subjected to cyclic loads under adverse environmental conditions, more research is needed to address the effects of aging on stress-softening under different exposure conditions.

4. Only one set of environmental conditions was tested to study the explosive decompression effects. More research is needed to study the explosive decompression effects on different types of rubbers at different pressures. The effect of number of compression-decompression cycles on the explosive decompression damage also needs further study. There are some analytical models that predict EDD of elastomeric O-ring seals. More research is needed to extend their use to predict EDD of elastomeric bearings.

5.

Appendix A

This Appendix is a supplement of Chapter 2. The results of regression analysis and finite element analysis performed to study the effects of misalignment of laminates in elastomeric bearing NR50 are included in this Appendix. Results for other Bearings CR50, NR70 and CR70 can be obtained from the author.

Tables A1 through A8 show the results of regression analysis while Figures A1 through A15 show the results of finite element analysis of various misalignment configurations. These figures show the undeformed and deformed shapes; the shear strain (NE13) the triaxial stress (PRESS) and the maximum principal strain (NEP3) in the rubber; and the von Mises stress (MISES) in the steel laminates. The units of stress are MPa.

Refer to Chapter 2 for definition of various independent and dependent variables shown in Tables A1 through A8. In these tables the most important result is the inference on coefficients that gives a wealth of information on the significance of independent variables. This part of the printout shows the name of the regressor variables, the parameter estimate, its estimated standard deviation and the test that the parameter is zero. The INTCEP is the value of the dependent variable for a perfect bearing configuration. If the data indicates that the variable is significant, then the |t| statistic will be large. This means that if the parameter is really zero, getting so large a |t| statistic is a rare event. Thus we would see a small PROB>|t|, the probability of getting a larger absolute |t| under the

hypothesis that the subject parameter is zero. The value $p<0.05$ is often used as cutoff probability or significance level. For example in Table F1, the variation in Axial Stiffness of NR50 due to laminate misalignment is significantly affected by X1, X2, X3, $X1^2$, $X2^2$, $X3^2$ and X1X3 (interaction of X1 and X3). Here X1, X2 and X3 are the three independent variables defined in Section 2-2. Note that INTCEP is the value of axial stiffness for a perfect bearing configuration.

TABLE A1-NR50 AXIAL STIFFNESS

RUN	PREDICTED	OBSERVED	DIFFERENCE
1	193.701	193.304	.397
2	187.477	187.781	-.304
3	203.586	203.357	.229
4	197.700	196.752	.948
5	186.352	186.646	-.294
6	189.934	189.509	.425
7	195.114	194.155	.959
8	199.034	198.777	.257
9	193.831	194.277	-.446
10	195.826	196.252	-.426
11	209.935	210.997	-1.062
12	193.494	193.304	.190
13	183.191	183.650	-.459
14	188.400	188.814	-.414
15	206.071	206.071	.000
16	206.071	206.071	.000

R-squared (percent)	Adjusted R-squared	Est. Std. Dev. of Model Error	Mean	Coefficient of Var. (percent)
99.519	98.797	.8544	195.6	.4368

* * * Analysis of Variance * * *

Source	DF	Sum of Squares	Mean Square	Overall F	Prob. of Larger F
Regression	9	905.6	100.6	137.856	.0000
Residual	6	4.4	.7		
Corrected Total	15	910.0			

* * * Sequential Statistics * * *

Indep. Variable	Degrees of Freedom	Sum of Squares	F-statistic	Prob. of Larger F
X1	1	4.6	6.363	.0451
X2	1	315.4	432.044	.0000
X3	1	31.7	43.366	.0006
X1X1	1	20.1	27.572	.0019
X2X2	1	30.7	42.056	.0006
X3X3	1	454.4	622.489	.0000
X1X2	1	.1	.078	.7888
X1X3	1	48.1	65.874	.0002
X2X3	1	.6	.865	.3883

* * * Inference on Coefficients * * *

Coef.	Estimate	Standard Error	t-statistic	Prob. of Larger |t|	Variance Inflation
INTCEP	206.1	.6041	341.1	.0000	8.000
X1	-.6	.2283	-2.5	.0451	1.000
X2	4.7	.2283	20.8	.0000	1.000
X3	-1.5	.2283	-6.6	.0006	1.000
X1X1	-3.7	.2709	-13.8	.0000	1.382
X2X2	-1.5	.2709	-5.4	.0017	1.382
X3X3	-6.8	.2709	-24.9	.0000	1.382
X1X2	.1	.3021	.3	.7888	1.000
X1X3	2.5	.3021	8.1	.0002	1.000
X2X3	-.3	.3021	-.9	.3883	1.000

TABLE A2-NR50 SHEAR STIFFNESS

RUN	PREDICTED	OBSERVED	DIFFERENCE
1	.986	.988	-.002
2	.982	.982	.000
3	.974	.973	.001
4	.974	.974	.000
5	.979	.978	.001
6	.973	.973	.000
7	.966	.966	.000
8	.964	.962	.002
9	.955	.956	-.001
10	.960	.960	.000
11	.954	.956	-.002
12	.973	.972	.001
13	.996	.997	-.001
14	1.011	1.010	.001
15	.959	.959	.000
16	.959	.959	.000

R-squared (percent)	Adjusted R-squared	Est. Std. Dev. of Model Error	Mean	Coefficient of Var. (percent)
99.581	98.952	.001583	.9728	.1627

* * * Analysis of Variance * * *

Source	DF	Sum of Squares	Mean Square	Overall F	Prob. of Larger F
Regression	9	.003571	3.968E-04	158.331	.0000
Residual	6	.000015	2.506E-06		
Corrected Total	15	.003586			

* * * Sequential Statistics * * *

Indep. Variable	Degrees of Freedom	Sum of Squares	F-statistic	Prob. of Larger F
X1	1	.000031	12.483	.0123
X2	1	.000388	154.857	.0000
X3	1	.000262	104.375	.0001
X1X1	1	.000413	164.857	.0000
X2X2	1	.000316	126.008	.0000
X3X3	1	.002151	858.408	.0000
X1X2	1	.000008	3.192	.1242
X1X3	1	.000002	.798	.4061
X2X3	1	.000000	.000	1.0000

* * * Inference on Coefficients * * *

Coef.	Estimate	Standard Error	t-statistic	Prob. of Larger |t|	Variance Inflation
INTCEP	.9590	.001119	856.7	.0000	8.000
X1	-.0015	.000423	-3.5	.0123	1.000
X2	-.0053	.000423	-12.4	.0000	1.000
X3	-.0043	.000423	-10.2	.0001	1.000
X1X1	-.0005	.000502	-.9	.3943	1.382
X2X2	.0015	.000502	3.1	.0220	1.382
X3X3	.0147	.000502	29.3	.0000	1.382
X1X2	.0010	.000560	1.8	.1242	1.000
X1X3	-.0005	.000560	-.9	.4061	1.000
X2X3	.0000	.000560	.0	1.0000	1.000

TABLE A3-NR50 ROTATION STIFFNESS

RUN	PREDICTED	OBSERVED	DIFFERENCE
1	2.065	2.060	.005
2	1.234	1.254	-.020
3	3.186	3.140	.046
4	2.457	2.400	.057
5	1.127	1.146	-.019
6	1.780	1.788	-.008
7	2.158	2.100	.058
8	2.913	2.880	.033
9	2.122	2.140	-.018
10	2.187	2.220	-.033
11	3.127	3.220	-.093
12	1.175	1.132	.043
13	1.831	1.850	-.019
14	2.248	2.280	-.032
15	2.420	2.420	.000
16	2.420	2.420	.000

R-squared (percent)	Adjusted R-squared	Est. Std. Dev. of Model Error	Mean	Coefficient of Var. (percent)
99.599	98.997	.06317	2.153	2.934

* * * Analysis of Variance * * *

Source	DF	Sum of Squares	Mean Square	Overall F	Prob. of Larger F
Regression	9	5.943	.6603	165.460	.0000
Residual	6	.024	.0040		
Corrected Total	15	5.967			

* * * Sequential Statistics * * *

Indep. Variable	Degrees of Freedom	Sum of Squares	F-statistic	Prob. of Larger F
X1	1	.005	1.234	.3092
X2	1	4.445	1113.802	.0000
X3	1	.203	50.805	.0004
X1X1	1	.006	1.594	.2536
X2X2	1	.014	3.407	.1145
X3X3	1	.160	40.063	.0007
X1X2	1	.005	1.304	.2971
X1X3	1	1.101	275.920	.0000
X2X3	1	.004	1.015	.3526

* * * Inference on Coefficients * * *

Coef.	Estimate	Standard Error	t-statistic	Prob. of Larger |t|	Variance Inflation
INTCEP	2.420	.04467	54.18	.0000	8.000
X1	-.019	.01688	-1.11	.3092	1.000
X2	.563	.01688	33.37	.0000	1.000
X3	-.120	.01688	-7.13	.0004	1.000
X1X1	-.088	.02003	-4.42	.0045	1.382
X2X2	-.090	.02003	-4.48	.0042	1.382
X3X3	-.127	.02003	-6.33	.0007	1.382
X1X2	.026	.02233	1.14	.2971	1.000
X1X3	.371	.02233	16.61	.0000	1.000
X2X3	-.023	.02233	-1.01	.3526	1.000

TABLE A4- NR50 SHEAR STRAIN IN ELASTOMER

RUN	PREDICTED	OBSERVED	DIFFERENCE
1	1.739	1.740	-.001
2	1.696	1.720	-.024
3	1.735	1.720	.015
4	1.708	1.680	.028
5	1.731	1.730	.001
6	1.704	1.690	.014
7	1.653	1.600	.053
8	1.640	1.610	.030
9	1.727	1.740	-.013
10	1.775	1.800	-.025
11	1.602	1.660	-.058
12	1.660	1.640	.020
13	1.688	1.730	-.042
14	1.753	1.750	.003
15	1.770	1.770	.000
16	1.770	1.770	.000

R-squared (percent)	Adjusted R-squared	Est. Std. Dev. of Model Error	Mean	Coefficient of Var. (percent)
76.613	41.533	.04436	1.709	2.595

* * * Analysis of Variance * * *

Source	DF	Sum of Squares	Mean Square	Overall F	Prob. of Larger F
Regression	9	.03868	.004298	2.184	.1770
Residual	6	.01181	.001968		
Corrected Total	15	.05049			

* * * Sequential Statistics * * *

Indep. Variable	Degrees of Freedom	Sum of Squares	F-statistic	Prob. of Larger F
X1	1	.00269	1.365	.2870
X2	1	.00396	2.010	.2060
X3	1	.00500	2.542	.1620
X1X1	1	.00232	1.181	.3190
X2X2	1	.01899	9.650	.0209
X3X3	1	.00269	1.364	.2871
X1X2	1	.00011	.057	.8190
X1X3	1	.00011	.057	.8190
X2X3	1	.00281	1.429	.2770

* * * Inference on Coefficients * * *

Coef.	Estimate	Standard Error	t-statistic	Prob. of Larger |t|	Variance Inflation
INTCEP	1.770	.03137	56.42	.0000	8.000
X1	-.014	.01186	-1.17	.2870	1.000
X2	-.017	.01186	-1.42	.2060	1.000
X3	-.019	.01186	-1.59	.1620	1.000
X1X1	-.006	.01407	-.46	.6637	1.382
X2X2	-.046	.01407	-3.30	.0164	1.382
X3X3	-.016	.01407	-1.17	.2871	1.382
X1X2	.004	.01568	.24	.8190	1.000
X1X3	.004	.01568	.24	.8190	1.000
X2X3	-.019	.01568	-1.20	.2770	1.000

TABLE A5 - NR50 MAXIMUM PRINCIPAL STRAIN IN ELASTOMER

RUN	PREDICTED	OBSERVED	DIFFERENCE
1	1.814	1.810	.004
2	1.725	1.740	-.015
3	1.848	1.840	.008
4	1.743	1.730	.013
5	1.743	1.750	-.007
6	1.728	1.730	-.002
7	1.831	1.810	.021
8	1.802	1.800	.002
9	1.734	1.730	.004
10	1.838	1.850	-.012
11	1.817	1.840	-.023
12	1.725	1.710	.015
13	1.775	1.780	-.005
14	1.787	1.790	-.003
15	1.790	1.790	.000
16	1.790	1.790	.000

R-squared (percent)	Adjusted R-squared	Est. Std. Dev. of Model Error	Mean	Coefficient of Var. (percent)
93.431	83.577	.01797	1.781	1.009

* * * Analysis of Variance * * *

Source	DF	Sum of Squares	Mean Square	Overall F	Prob. of Larger F
Regression	9	.02756	.003062	9.482	.0064
Residual	6	.00194	.000323		
Corrected Total	15	.02949			

* * * Sequential Statistics * * *

Indep. Variable	Degrees of Freedom	Sum of Squares	F-statistic	Prob. of Larger F
X1	1	.01247	38.619	.0008
X2	1	.01005	31.133	.0014
X3	1	.00016	.495	.5079
X1X1	1	.00003	.102	.7606
X2X2	1	.00031	.963	.3644
X3X3	1	.00009	.280	.6156
X1X2	1	.00011	.348	.5766
X1X3	1	.00281	8.710	.0256
X2X3	1	.00151	4.684	.0736

* * * Inference on Coefficients * * *

Coef.	Estimate	Standard Error	t-statistic	Prob. of Larger |t|	Variance Inflation
INTCEP	1.790	.01271	140.9	.0000	8.000
X1	-.030	.00480	-6.2	.0008	1.000
X2	.027	.00480	5.6	.0014	1.000
X3	-.003	.00480	-.7	.5079	1.000
X1X1	-.001	.00570	-.2	.8207	1.382
X2X2	-.006	.00570	-1.1	.3077	1.382
X3X3	-.003	.00570	-.5	.6156	1.382
X1X2	-.004	.00635	-.6	.5766	1.000
X1X3	.019	.00635	3.0	.0256	1.000
X2X3	.014	.00635	2.2	.0736	1.000

TABLE A6 - NR50 TENSION PRESSURE IN ELASTOMER

RUN	PREDICTED	OBSERVED	DIFFERENCE
1	1.638	1.720	-.082
2	1.646	1.630	.016
3	1.629	1.450	.179
4	1.397	1.320	.077
5	1.825	1.760	.065
6	2.223	2.260	-.037
7	1.376	1.250	.126
8	1.535	1.310	.225
9	1.977	2.070	-.093
10	1.833	1.930	-.097
11	1.049	1.330	-.281
12	1.652	1.560	.092
13	1.861	2.010	-.149
14	1.580	1.620	-.040
15	2.030	2.030	.000
16	2.030	2.030	.000

R-squared (percent)	Adjusted R-squared	Est. Std. Dev. of Model Error	Mean	Coefficient of Var. (percent)
84.090	60.225	.2027	1.705	11.89

* * * Analysis of Variance * * *

Source	DF	Sum of Squares	Mean Square	Overall F	Prob. of Larger F
Regression	9	1.304	.1448	3.524	.0696
Residual	6	.247	.0411		
Corrected Total	15	1.550			

* * * Sequential Statistics * * *

Indep. Variable	Degrees of Freedom	Sum of Squares	F-statistic	Prob. of Larger F
X1	1	.0242	.590	.4717
X2	1	.4247	10.332	.0183
X3	1	.0921	2.240	.1851
X1X1	1	.0501	1.219	.3119
X2X2	1	.4047	9.846	.0201
X3X3	1	.1061	2.580	.1593
X1X2	1	.0288	.701	.4346
X1X3	1	.0761	1.850	.2227
X2X3	1	.0968	2.355	.1758

* * * Inference on Coefficients * * *

Coef.	Estimate	Standard Error	t-statistic	Prob. of Larger |t|	Variance Inflation
INTCEP	2.030	.1434	14.16	.0000	8.000
X1	.042	.0542	.77	.4717	1.000
X2	-.174	.0542	-3.21	.0183	1.000
X3	.081	.0542	1.50	.1851	1.000
X1X1	-.042	.0643	-.65	.5416	1.382
X2X2	-.227	.0643	-3.52	.0124	1.382
X3X3	-.103	.0643	-1.61	.1593	1.382
X1X2	-.060	.0717	-.84	.4346	1.000
X1X3	.098	.0717	1.36	.2227	1.000
X2X3	-.110	.0717	-1.53	.1758	1.000

TABLE A7 - NR50 MAXIMUM BOND STRESS STEEL-ELASTOMER

RUN	PREDICTED	OBSERVED	DIFFERENCE
1	1.025	1.023	.002
2	.980	1.005	-.025
3	1.021	1.005	.016
4	.989	.970	.019
5	1.017	1.014	.003
6	.984	.978	.006
7	.951	.904	.047
8	.932	.912	.020
9	.996	.996	.000
10	1.052	1.081	-.029
11	.905	.953	-.048
12	.954	.936	.018
13	.981	1.014	-.033
14	1.037	1.033	.004
15	1.052	1.052	.000
16	1.052	1.052	.000

R-squared (percent)	Adjusted R-squared	Est. Std. Dev. of Model Error	Mean	Coefficient of Var. (percent)
77.754	44.385	.03772	.9955	3.789

* * * Analysis of Variance * * *

Source	DF	Sum of Squares	Mean Square	Overall F	Prob. of Larger F
Regression	9	.02983	.003315	2.330	.1577
Residual	6	.00854	.001423		
Corrected Total	15	.03837			

* * * Sequential Statistics * * *

Indep. Variable	Degrees of Freedom	Sum of Squares	F-statistic	Prob. of Larger F
X1	1	.00372	2.615	.1570
X2	1	.00284	1.999	.2071
X3	1	.00371	2.608	.1575
X1X1	1	.00080	.564	.4812
X2X2	1	.01463	10.284	.0184
X3X3	1	.00207	1.453	.2735
X1X2	1	.00009	.064	.8086
X1X3	1	.00008	.055	.8225
X2X3	1	.00189	1.329	.2928

* * * Inference on Coefficients * * *

Coef.	Estimate	Standard Error	t-statistic	Prob. of Larger |t|	Variance Inflation
INTCEP	1.052	.02667	39.44	.0000	8.000
X1	-.016	.01008	-1.62	.1570	1.000
X2	-.014	.01008	-1.41	.2071	1.000
X3	-.016	.01008	-1.61	.1575	1.000
X1X1	-.009	.01196	-.79	.4612	1.382
X2X2	-.041	.01196	-3.41	.0144	1.382
X3X3	-.014	.01196	-1.21	.2735	1.382
X1X2	.003	.01334	.25	.8086	1.000
X1X3	.003	.01334	.23	.8225	1.000
X2X3	-.015	.01334	-1.15	.2928	1.000

TABLE A8 - NR50 MAXIMUM VON MISES STRESS IN SHIMS

RUN	PREDICTED	OBSERVED	DIFFERENCE
1	120.308	114.000	6.308
2	151.071	149.000	2.071
3	159.280	159.000	.280
4	199.043	206.000	-6.957
5	181.673	178.000	3.673
6	151.436	155.000	-3.564
7	182.645	188.000	-5.355
8	161.408	171.000	-9.592
9	165.814	157.000	8.814
10	157.565	162.000	-4.435
11	165.882	155.000	10.882
12	123.497	130.000	-6.503
13	193.964	187.000	6.964
14	173.414	176.000	-2.586
15	132.000	132.000	.000
16	132.000	132.000	.000

R-squared (percent)	Adjusted R-squared	Est. Std. Dev. of Model Error	Mean	Coefficient of Var. (percent)
93.922	84.806	9.598	159.4	6.02

* * * Analysis of Variance * * *

Source	DF	Sum of Squares	Mean Square	Overall F	Prob. of Larger F
Regression	9	8541.2	949.0	10.302	.0051
Residual	6	552.7	92.1		
Corrected Total	15	9093.9			

* * * Sequential Statistics * * *

Indep. Variable	Degrees of Freedom	Sum of Squares	F-statistic	Prob. of Larger F
X1	1	79.4	.862	.3890
X2	1	2096.0	22.754	.0031
X3	1	492.7	5.349	.0600
X1X1	1	146.5	1.590	.2541
X2X2	1	150.4	1.633	.2485
X3X3	1	2953.2	32.059	.0013
X1X2	1	40.5	.440	.5319
X1X3	1	1860.5	20.197	.0041
X2X3	1	722.0	7.838	.0312

* * * Inference on Coefficients * * *

Coef.	Estimate	Standard Error	t-statistic	Prob. of Larger |t|	Variance Inflation
INTCEP	132.0	6.787	19.45	.0000	8.000
X1	2.4	2.565	.93	.3890	1.000
X2	12.2	2.565	4.77	.0031	1.000
X3	5.9	2.565	2.31	.0600	1.000
X1X1	9.9	3.043	3.25	.0174	1.382
X2X2	4.2	3.043	1.39	.2139	1.382
X3X3	17.2	3.043	5.66	.0013	1.382
X1X2	2.3	3.393	.66	.5319	1.000
X1X3	-15.2	3.393	-4.49	.0041	1.000
X2X3	-9.5	3.393	-2.80	.0312	1.000

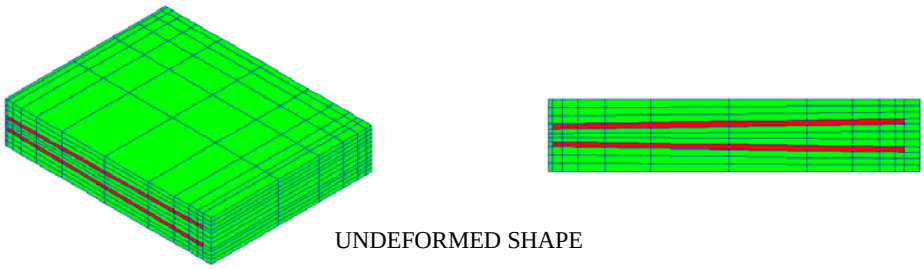

UNDEFORMED SHAPE

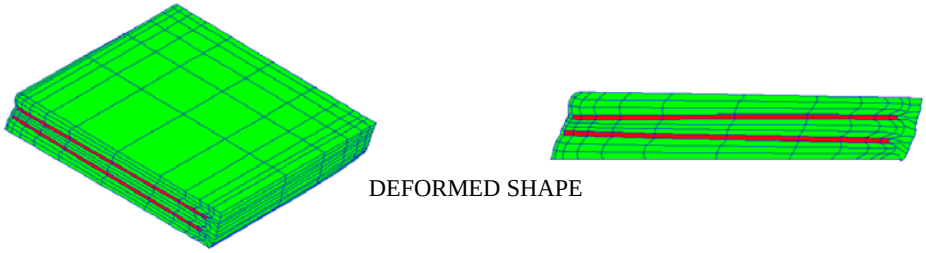

DEFORMED SHAPE

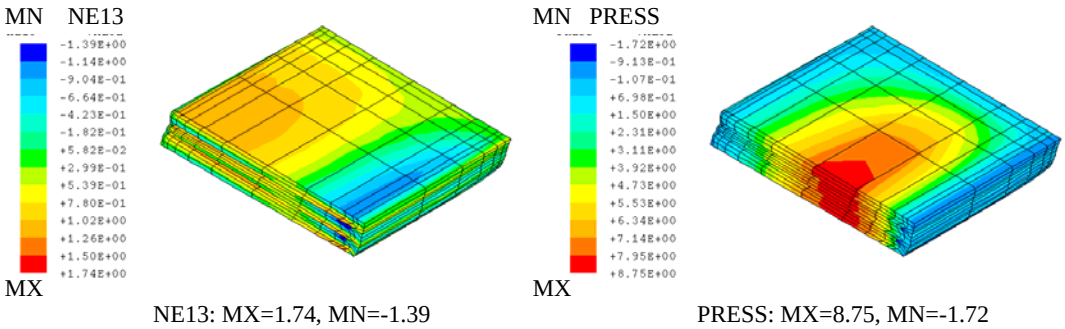

NE13: MX=1.74, MN=-1.39

PRESS: MX=8.75, MN=-1.72

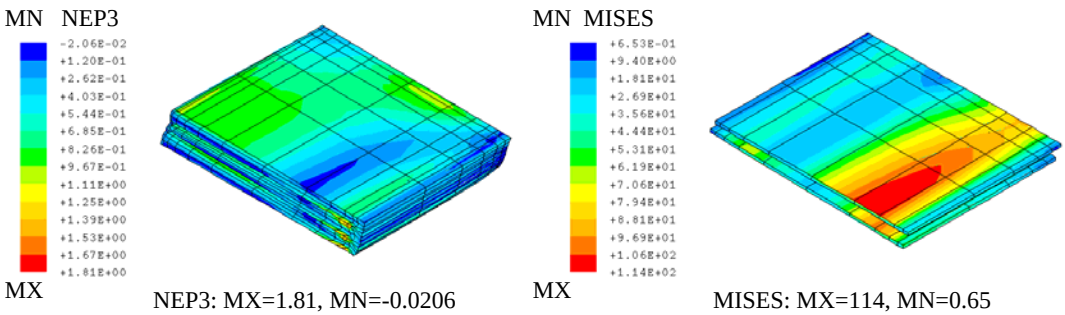

NEP3: MX=1.81, MN=-0.0206

MISES: MX=114, MN=0.65

Figure A-1: Finite Element Results for Run1 – NR50

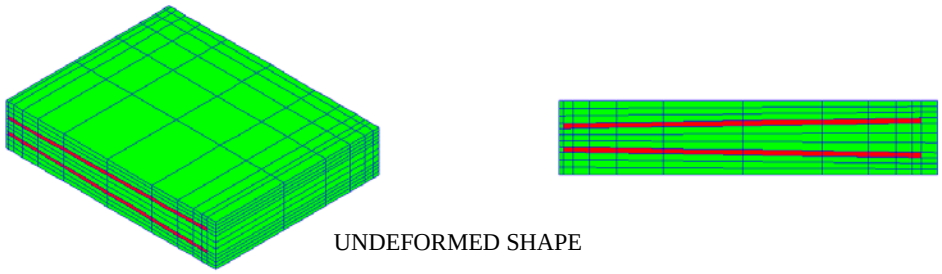

UNDEFORMED SHAPE

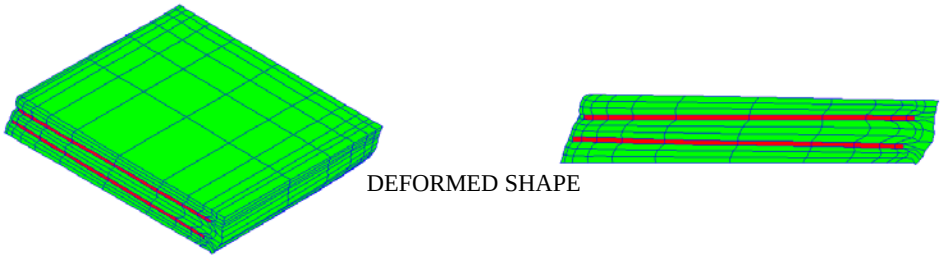

DEFORMED SHAPE

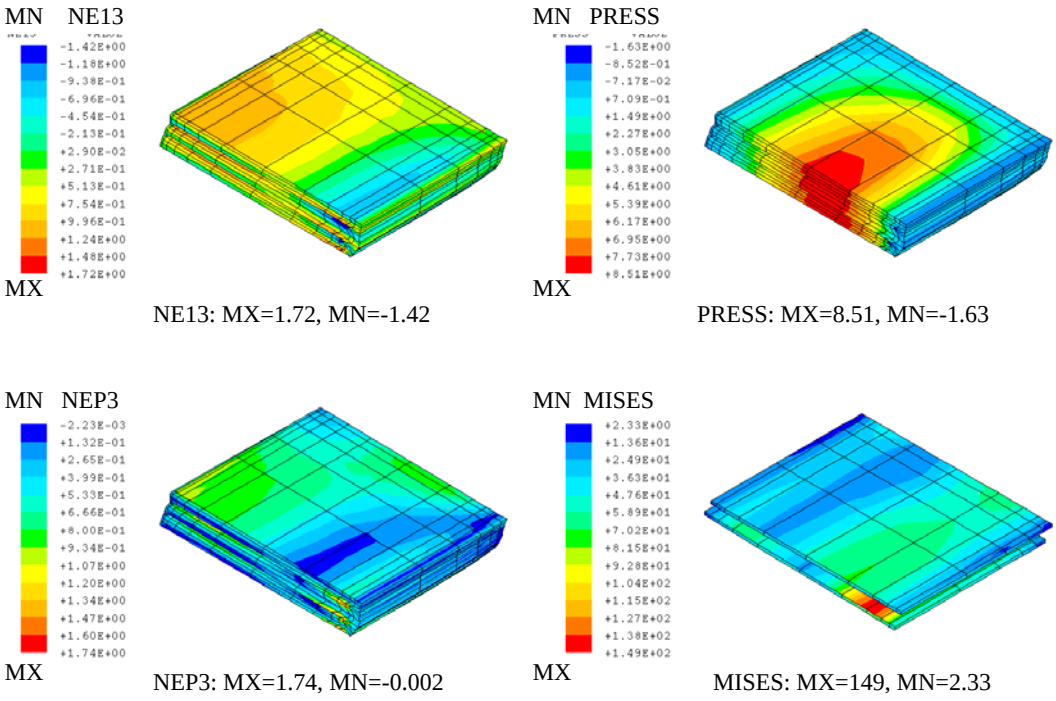

NE13: MX=1.72, MN=-1.42

PRESS: MX=8.51, MN=-1.63

NEP3: MX=1.74, MN=-0.002

MISES: MX=149, MN=2.33

Figure A-2: Finite Element Results for Run2 – NR50

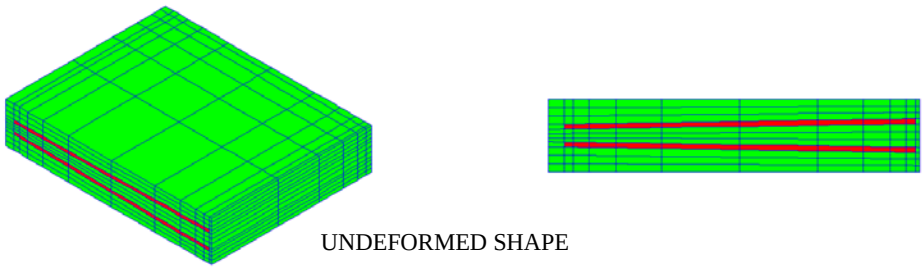

UNDEFORMED SHAPE

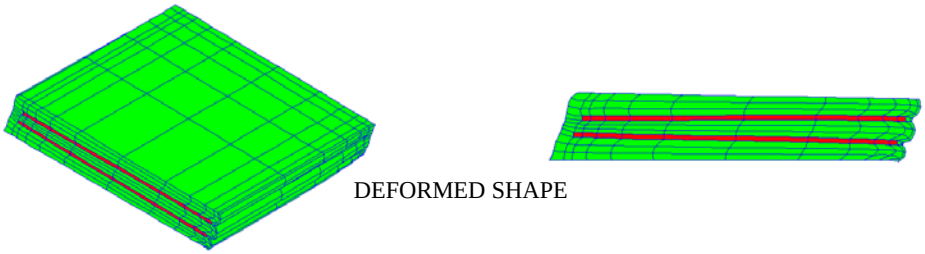

DEFORMED SHAPE

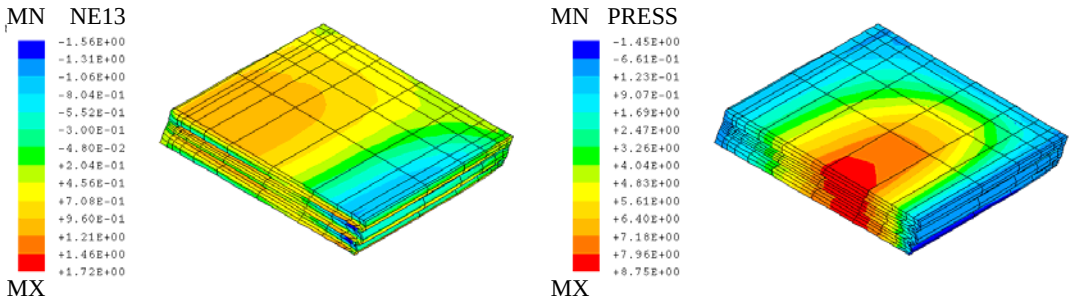

NE13: MX=1.72, MN=-1.56

PRESS: MX=8.75, MN=-1.45

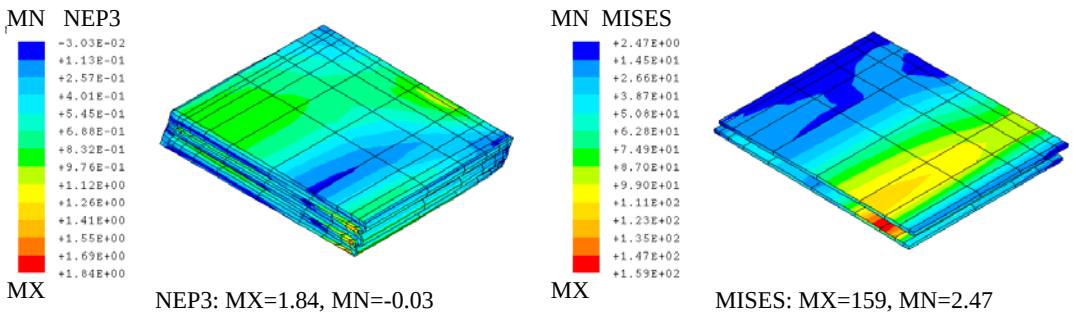

NEP3: MX=1.84, MN=-0.03

MISES: MX=159, MN=2.47

Figure A-3: Finite Element Results for Run3 – NR50

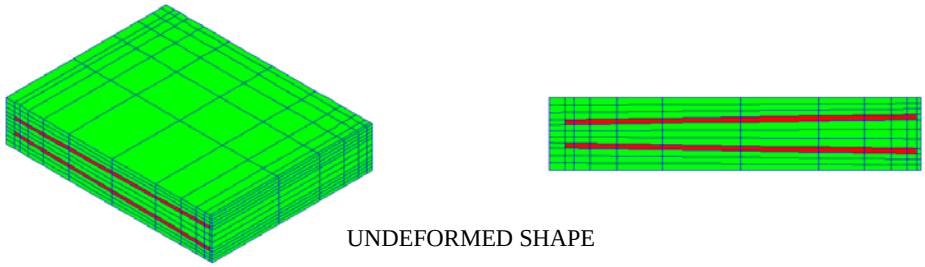

UNDEFORMED SHAPE

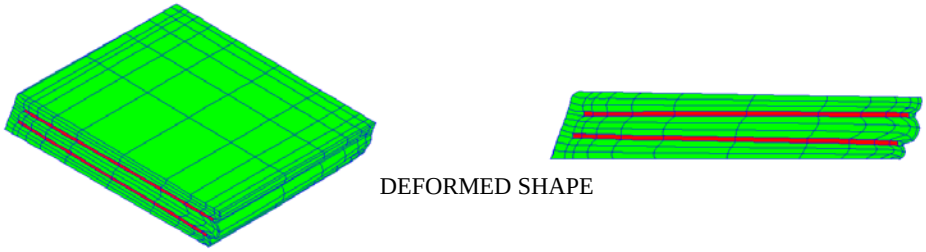

DEFORMED SHAPE

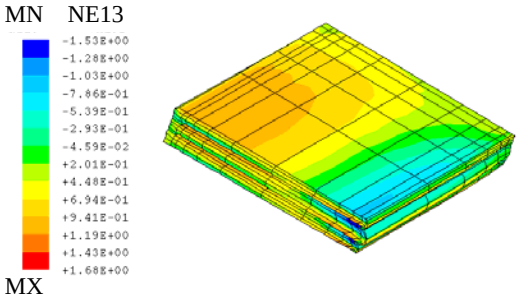

NE13: MX=1.68, MN=-1.53

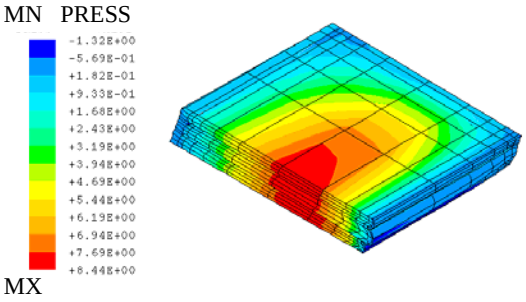

PRESS: MX=8.44, MN=-1.32

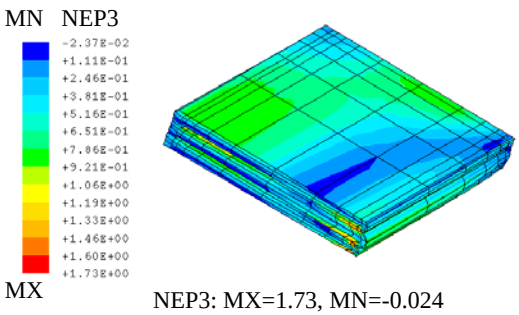

NEP3: MX=1.73, MN=-0.024

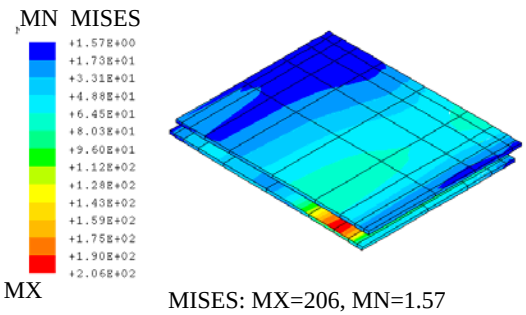

MISES: MX=206, MN=1.57

Figure A-4: Finite Element Results for Run4 – NR50

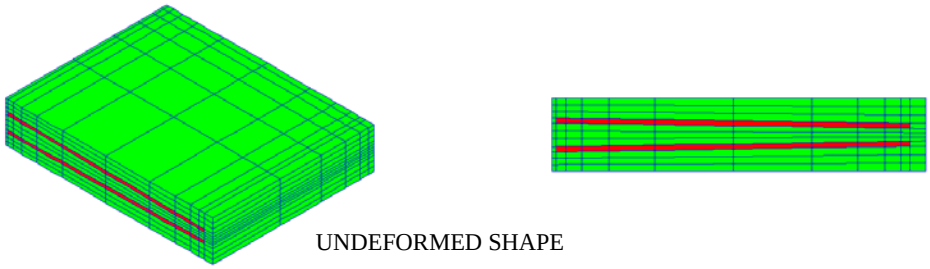

UNDEFORMED SHAPE

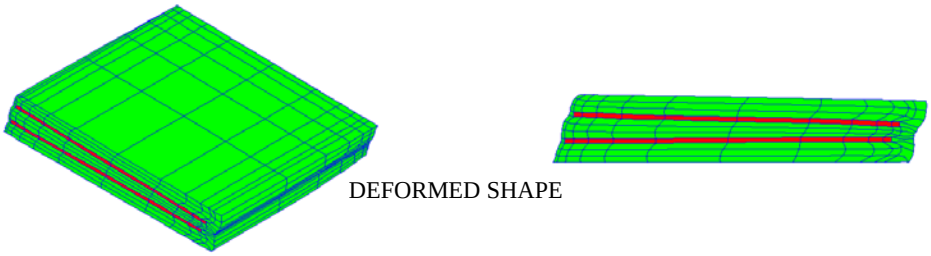

DEFORMED SHAPE

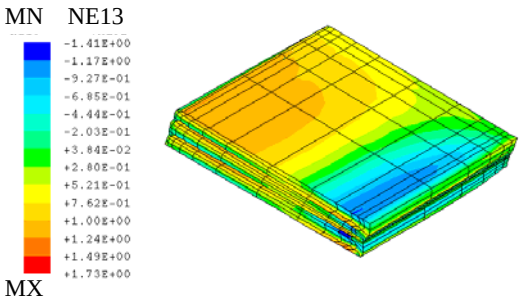

NE13: MX=1.73, MN=-1.41

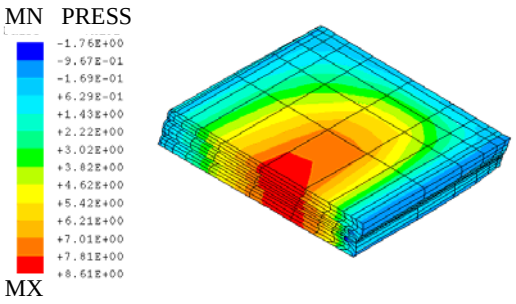

PRESS: MX=8.61, MN=-1.76

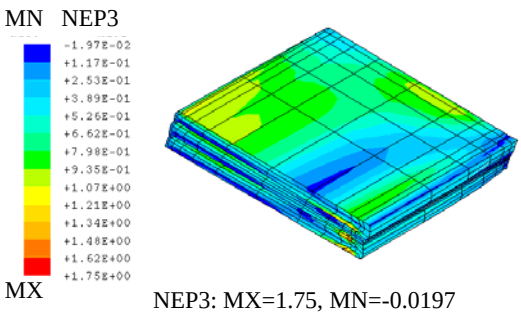

NEP3: MX=1.75, MN=-0.0197

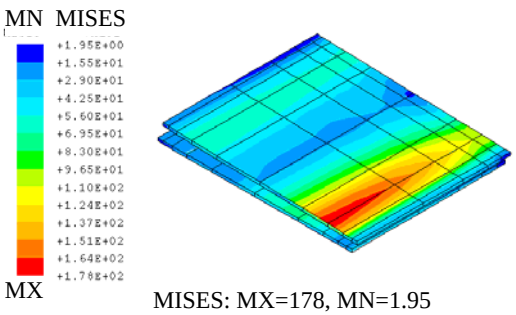

MISES: MX=178, MN=1.95

Figure A-5: Finite Element Results for Run5 – NR50

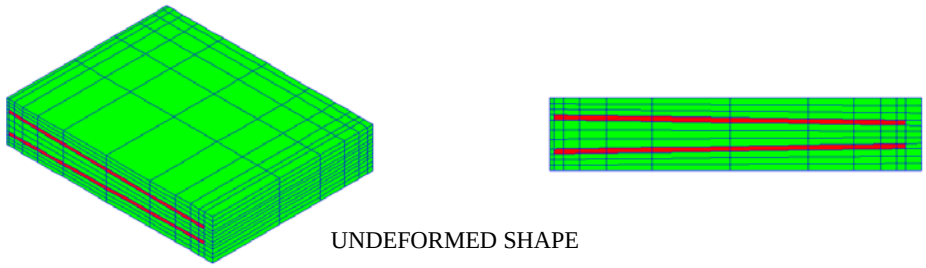

UNDEFORMED SHAPE

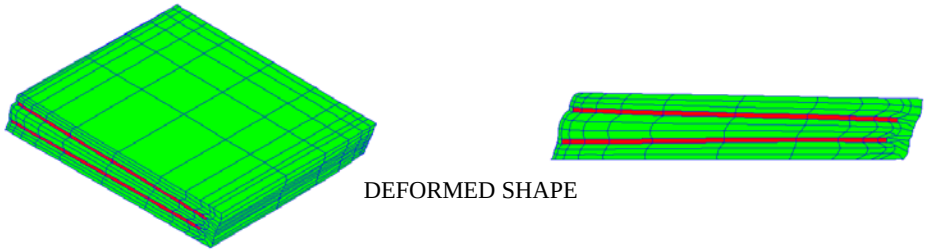

DEFORMED SHAPE

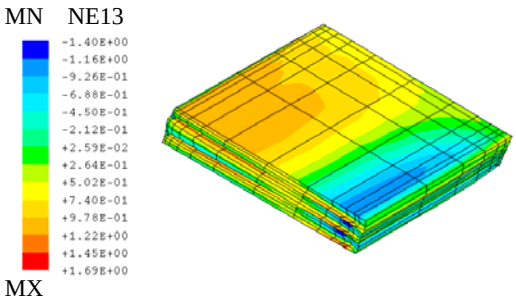

NE13: MX=1.69, MN=-1.40

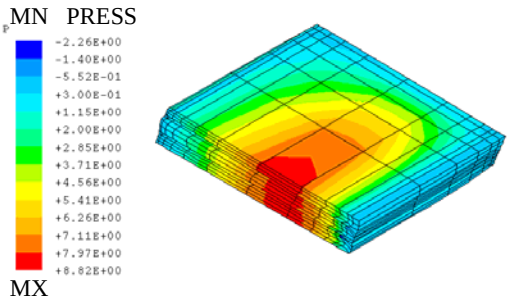

PRESS: MX=8.82, MN=-2.26

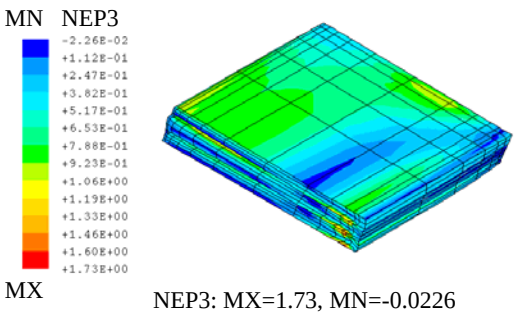

NEP3: MX=1.73, MN=-0.0226

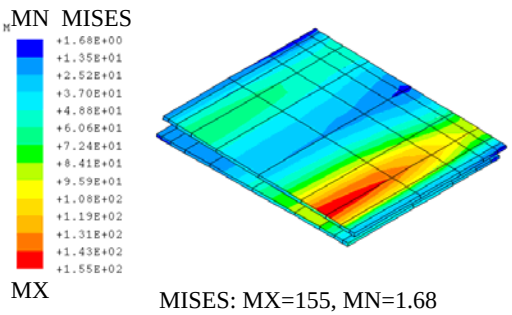

MISES: MX=155, MN=1.68

Figure A-6: Finite Element Results for Run6 – NR50

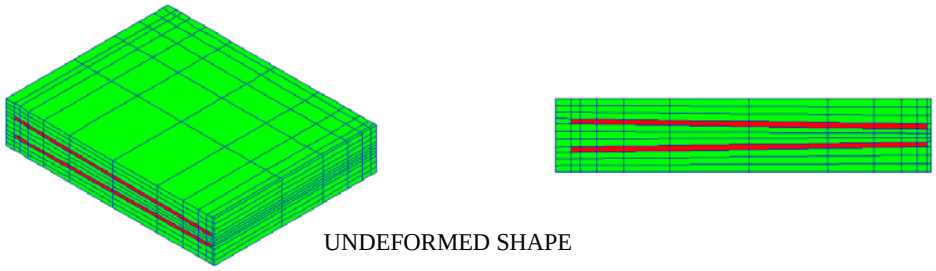

UNDEFORMED SHAPE

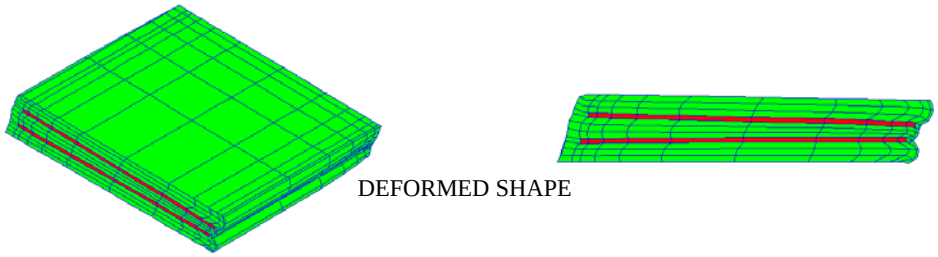

DEFORMED SHAPE

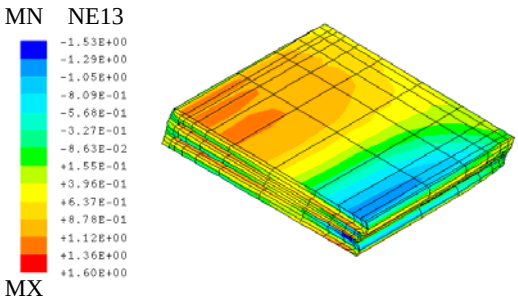

NE13: MX=1.60, MN=-1.53

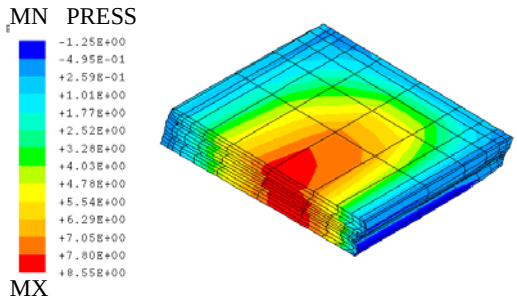

PRESS: MX=8.55, MN=-1.25

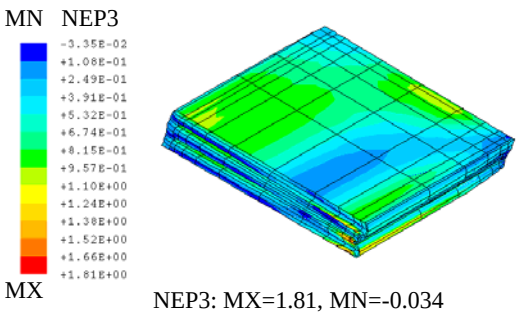

NEP3: MX=1.81, MN=-0.034

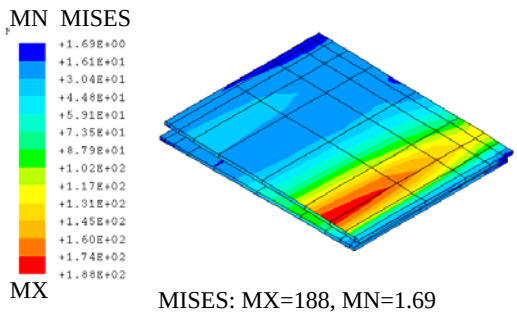

MISES: MX=188, MN=1.69

Figure A-7: Finite Element Results for Run7 – NR50

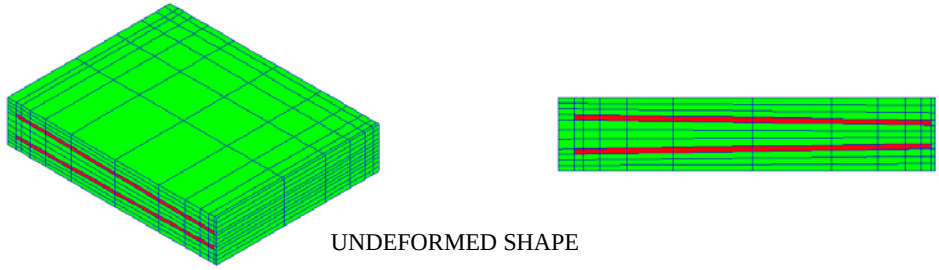

UNDEFORMED SHAPE

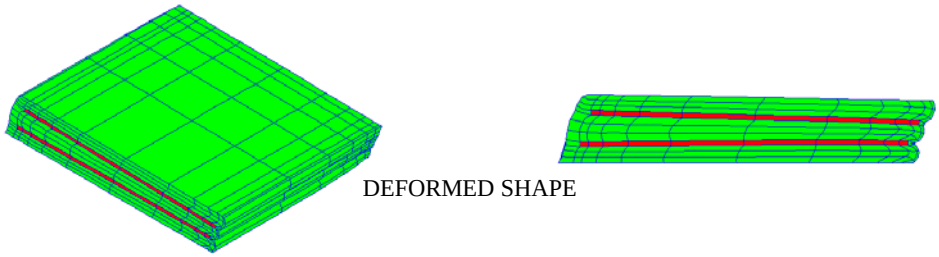

DEFORMED SHAPE

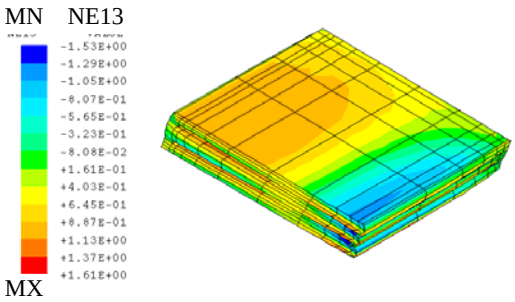

NE13: MX=1.61, MN=-1.53

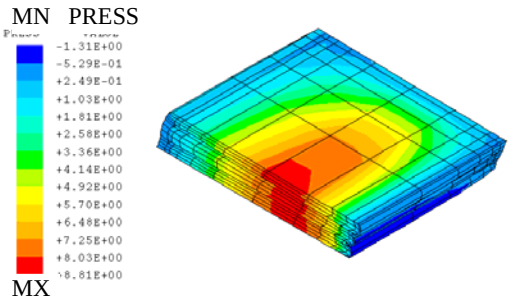

PRESS: MX=8.81, MN=-1.31

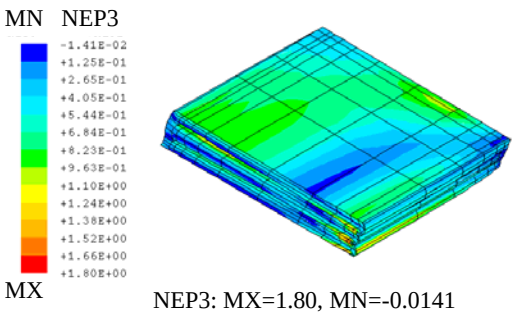

NEP3: MX=1.80, MN=-0.0141

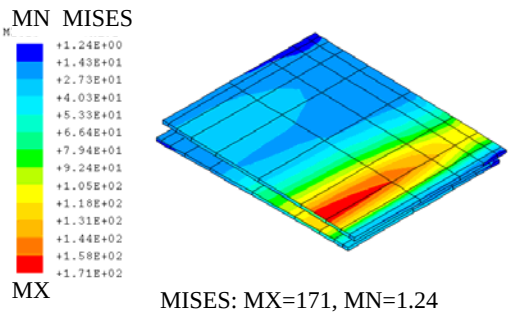

MISES: MX=171, MN=1.24

Figure A-8: Finite Element Results for Run8 – NR50

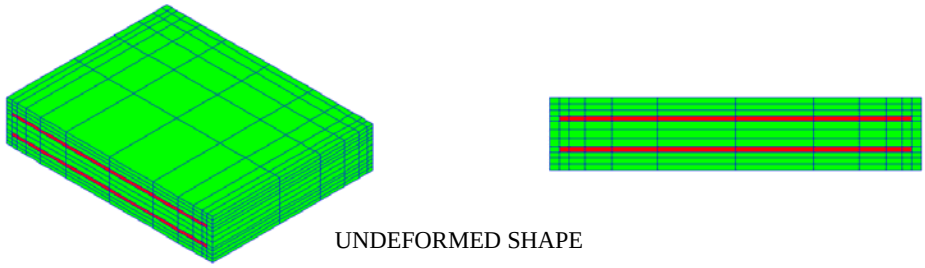

UNDEFORMED SHAPE

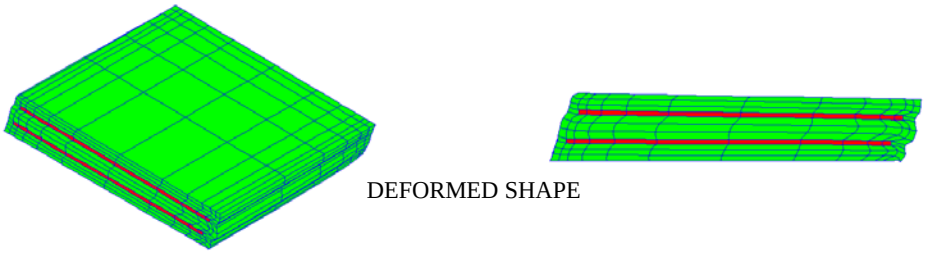

DEFORMED SHAPE

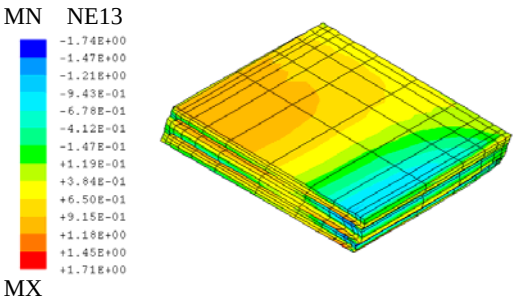

NE13: MX=1.71, MN=-1.74

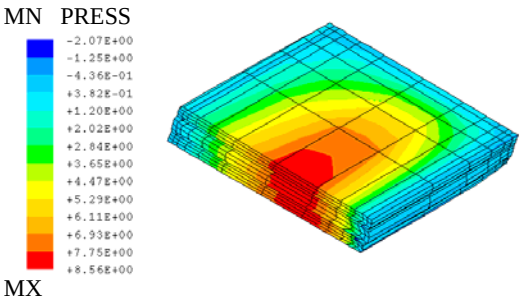

PRESS: MX=8.56, MN=-2.07

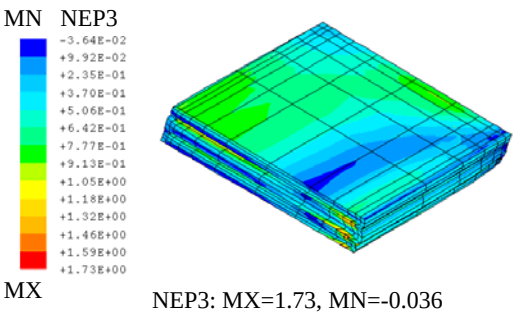

NEP3: MX=1.73, MN=-0.036

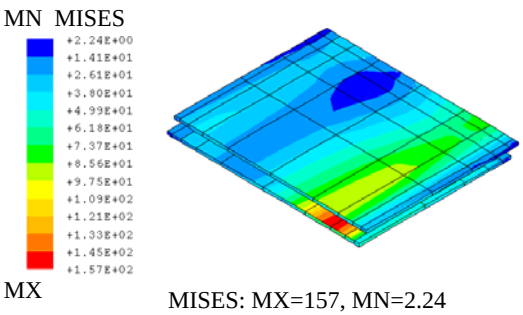

MISES: MX=157, MN=2.24

Figure A-9: Finite Element Results for Run9 – NR50

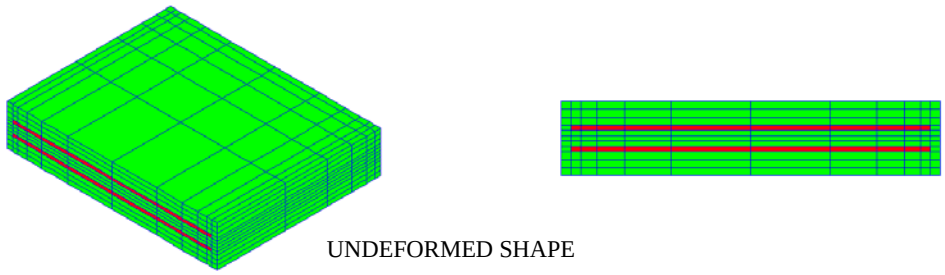

UNDEFORMED SHAPE

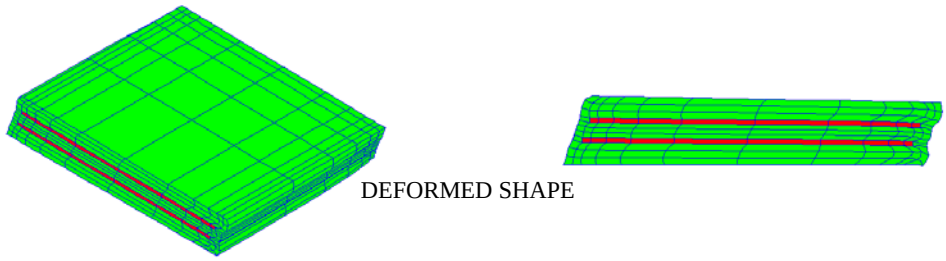

DEFORMED SHAPE

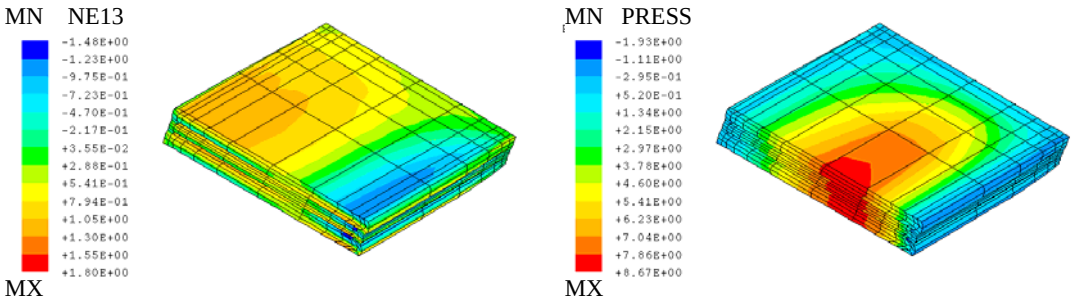

NE13: MX=1.80, MN=-1.48

PRESS: MX=8.67, MN=-1.93

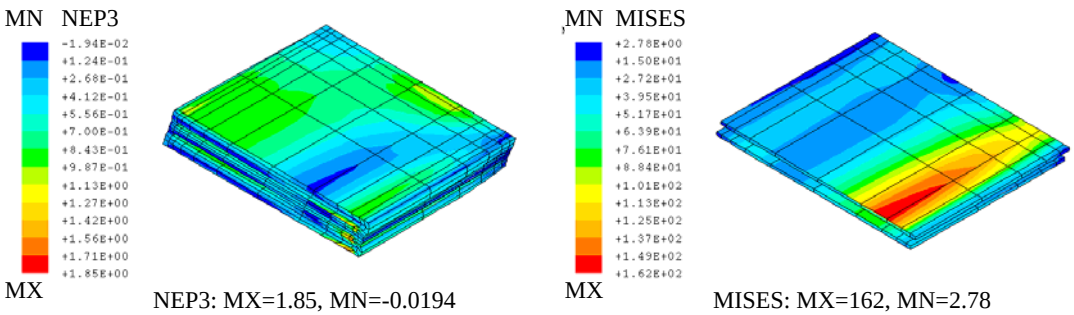

NEP3: MX=1.85, MN=-0.0194

MISES: MX=162, MN=2.78

Figure A-10: Finite Element Results for Run10 – NR50

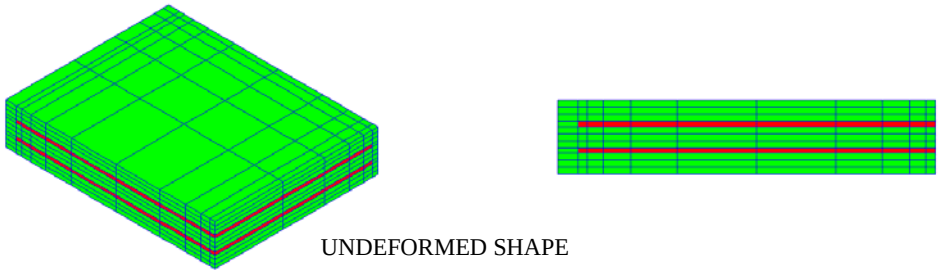

UNDEFORMED SHAPE

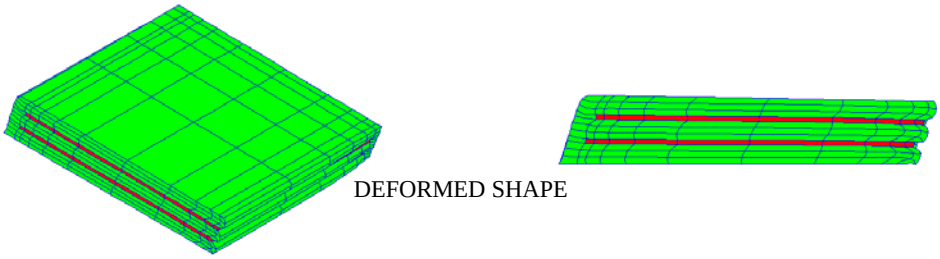

DEFORMED SHAPE

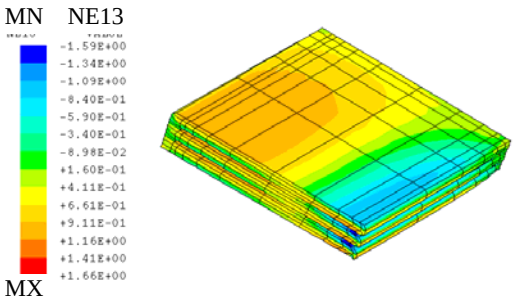

NE13: MX=1.66, MN=-1.59

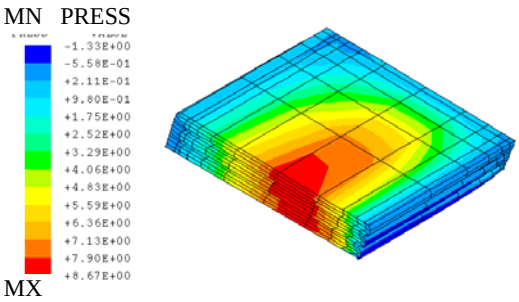

PRESS: MX=8.67, MN=-1.33

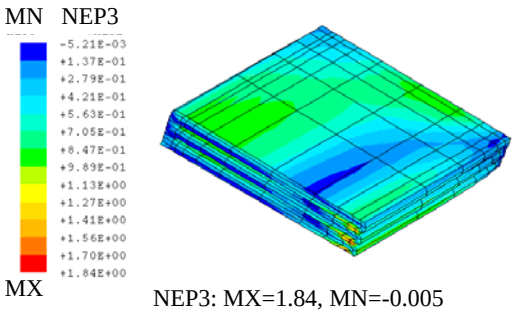

NEP3: MX=1.84, MN=-0.005

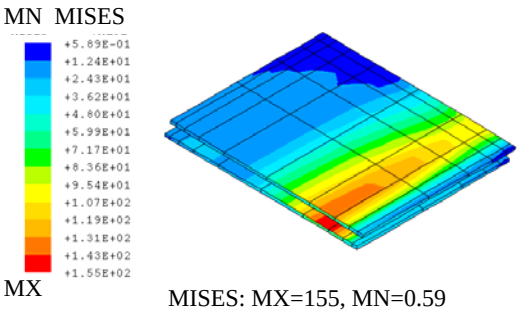

MISES: MX=155, MN=0.59

Figure A-11: Finite Element Results for Run11 – NR50

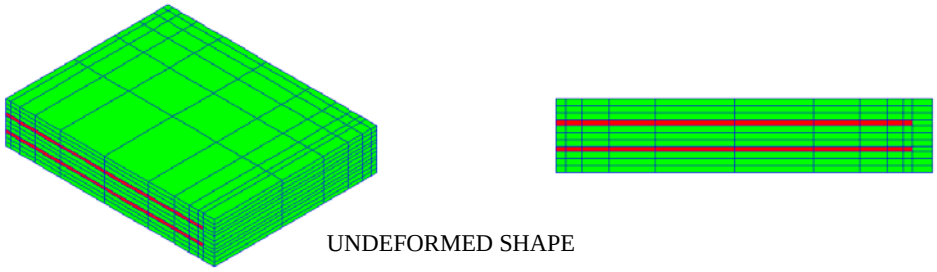

UNDEFORMED SHAPE

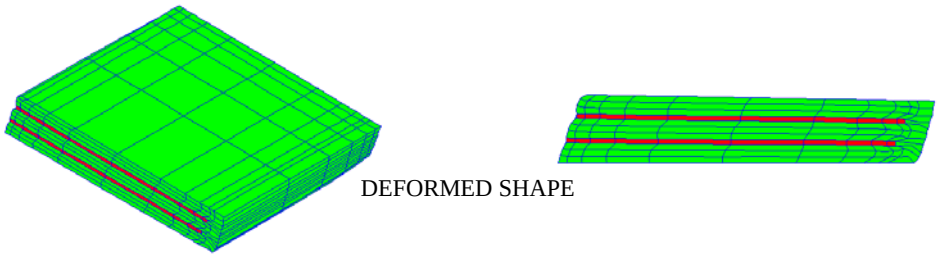

DEFORMED SHAPE

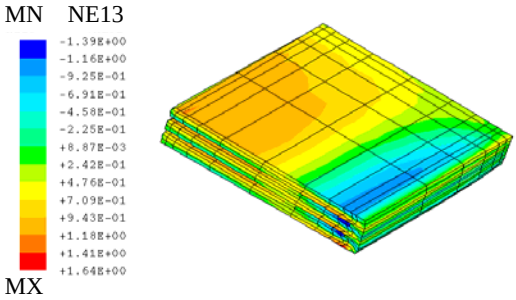

NE13: MX=1.64, MN=-1.39

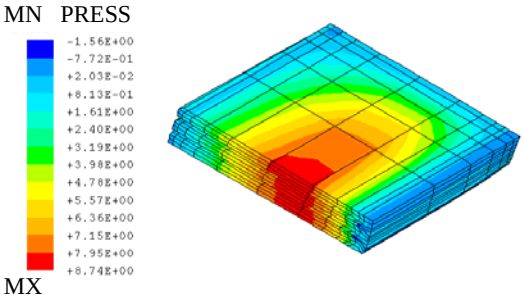

PRESS: MX=8.74, MN=-1.56

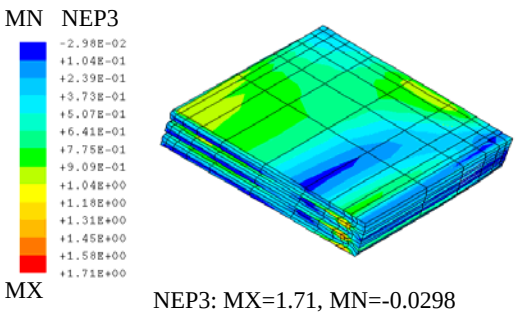

NEP3: MX=1.71, MN=-0.0298

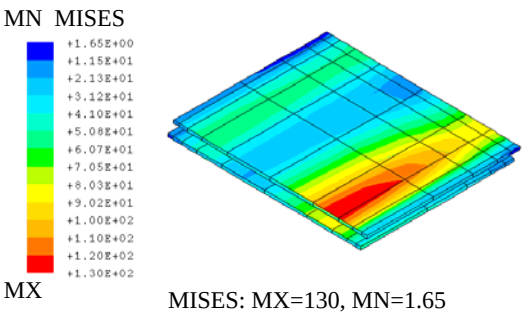

MISES: MX=130, MN=1.65

Figure A-12: Finite Element Results for Run12 – NR50

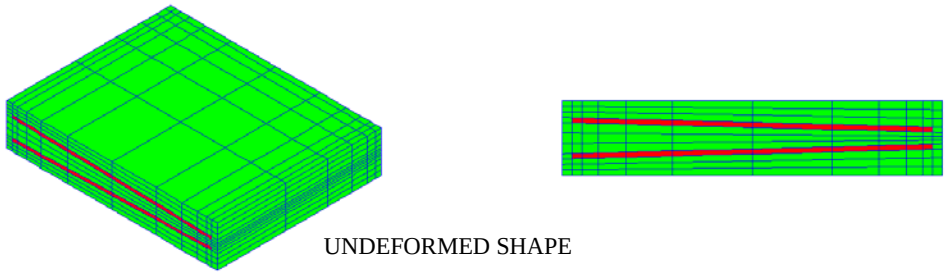

UNDEFORMED SHAPE

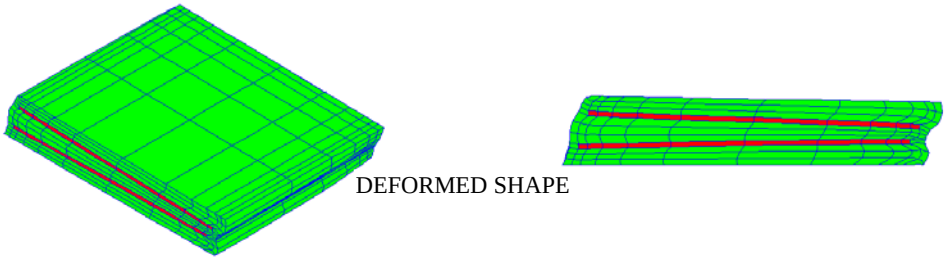

DEFORMED SHAPE

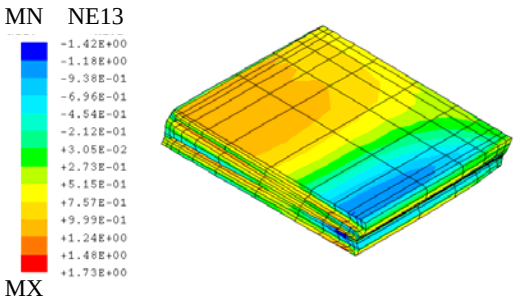

NE13: MX=1.73, MN=-1.42

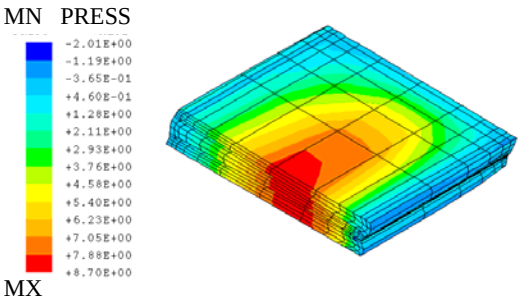

PRESS: MX=8.70, MN=-2.01

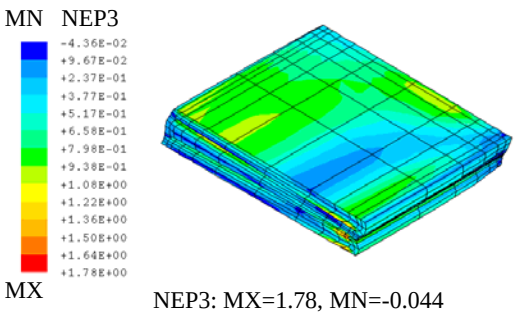

NEP3: MX=1.78, MN=-0.044

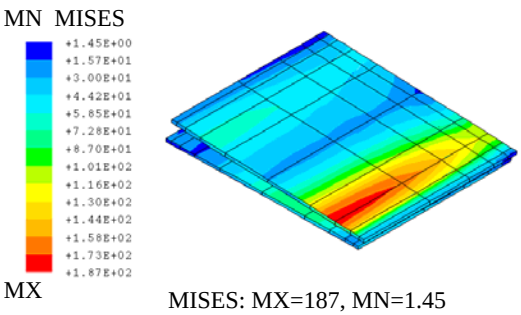

MISES: MX=187, MN=1.45

Figure A-13: Finite Element Results for Run13 – NR50

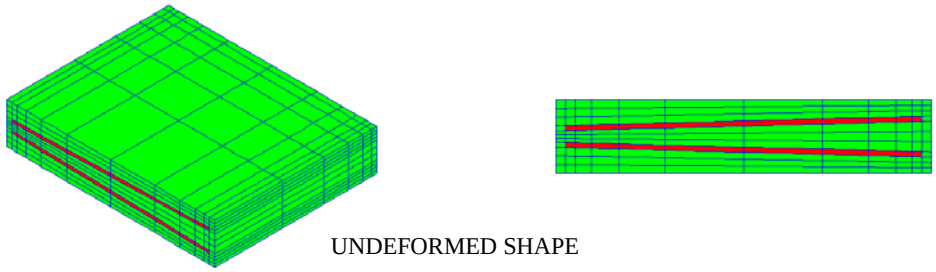

UNDEFORMED SHAPE

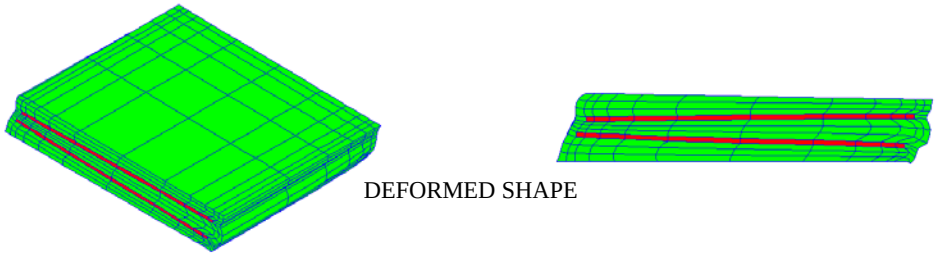

DEFORMED SHAPE

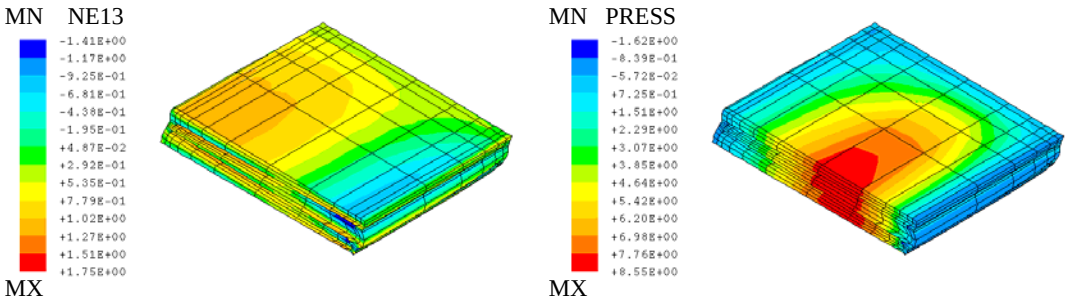

NE13: MX=1.75, MN=-1.41

PRESS: MX=8.55, MN=-1.62

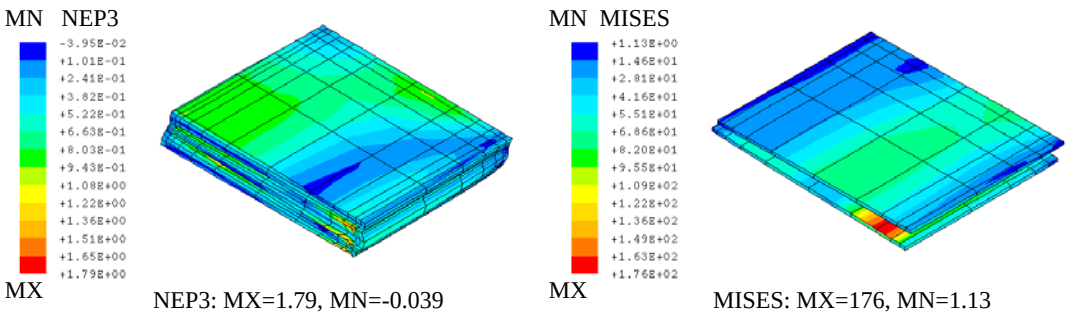

NEP3: MX=1.79, MN=-0.039

MISES: MX=176, MN=1.13

Figure A-14: Finite Element Results for Run14 – NR50

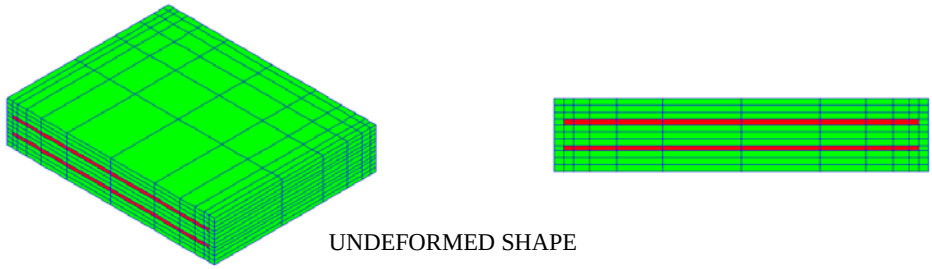

UNDEFORMED SHAPE

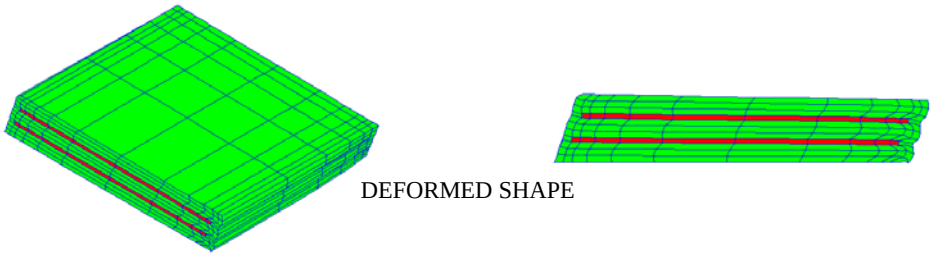

DEFORMED SHAPE

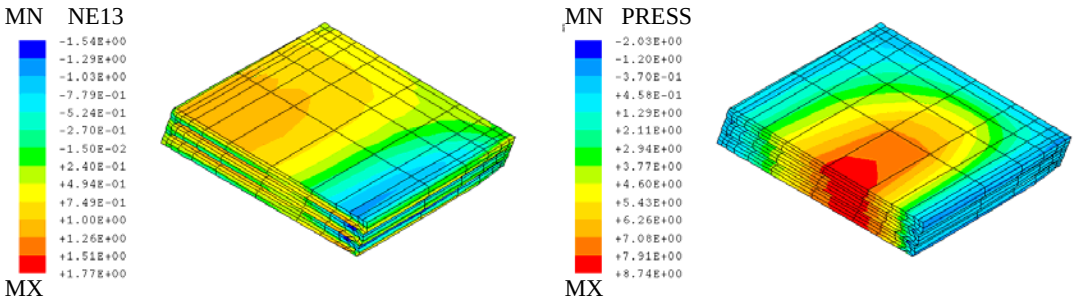

NE13: MX=1.77, MN=-1.54

PRESS: MX=8.74, MN=-2.03

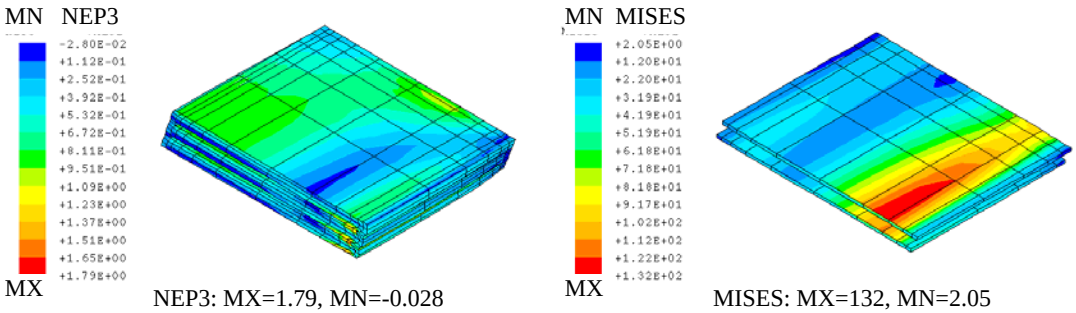

NEP3: MX=1.79, MN=-0.028

MISES: MX=132, MN=2.05

Figure A-15: Finite Element Results for Run15 and Run16 – NR50

Appendix B

This Appendix is a supplement of Chapter 3. The results of full-scale creep tests and small-scale stress relaxation tests are included in this Appendix.

Full-Scale Creep Tests

The results of full-scale creep tests for NR50, CR50, NR70 and CR70 are shown in Figures B1 through B8. These figures also show the results of a regression analysis and the regression equations that relate the total deflection to time and load variation in the region of the measurements.

Stress Relaxation Tests

Plots of shear modulus versus time at the three different strain levels are shown in Figure B9 through B20 based on 1x1 specimen testing. These figures also show the results of a regression analysis and regression equations that relate the shear modulus to time.

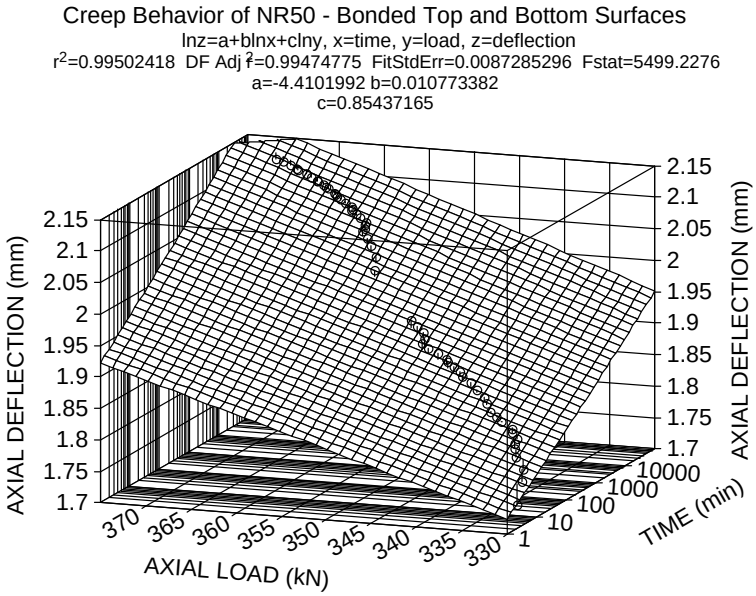

Figure B1 : NR50-Bonded End Plates, Creep Test Data and Regression Results

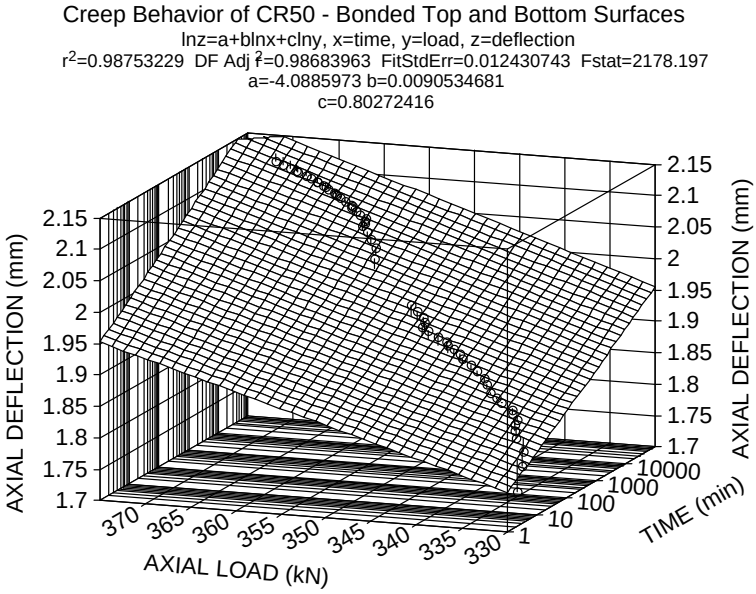

Figure B2 : CR50-Bonded End Plates, Creep Test Data and Regression Results

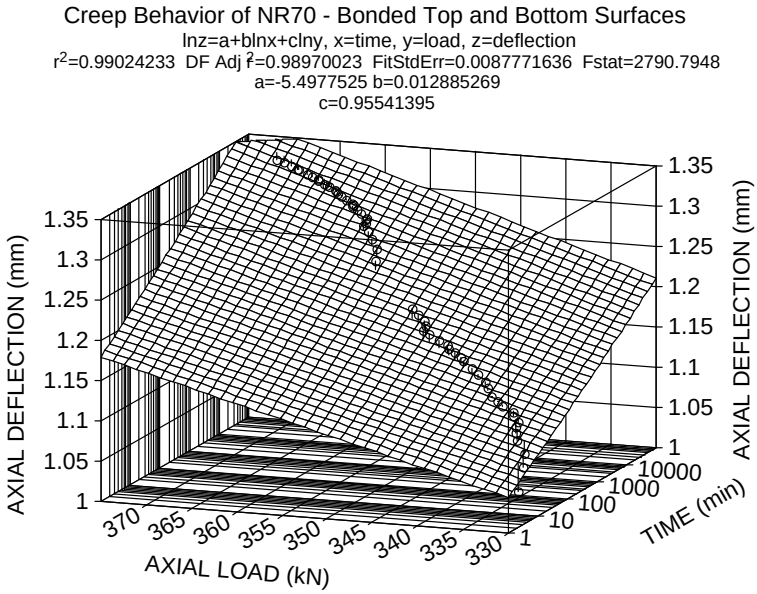

Figure B3 : NR70-Bonded End Plates, Creep Test Data and Regression Results

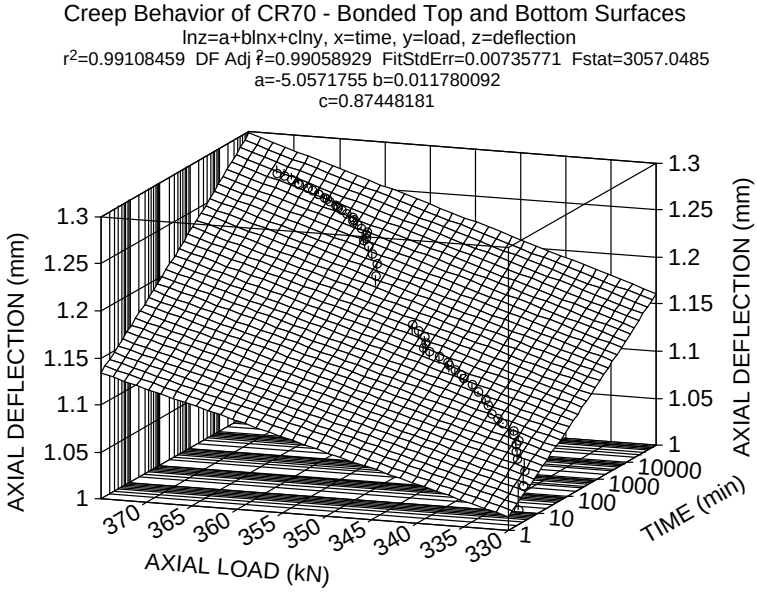

Figure B4 : CR70-Bonded End Plates, Creep Test Data and Regression Results

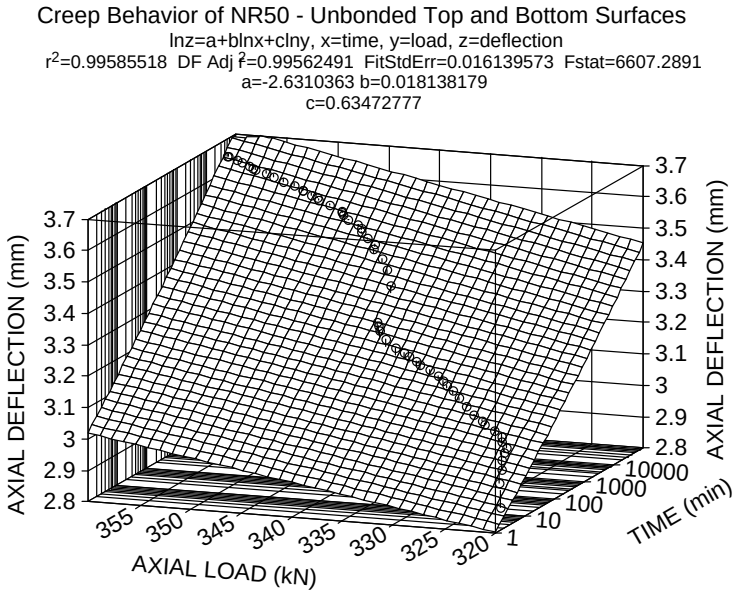

Figure B5 : NR50-UnBonded End Plates, Creep Test Data and Regression Results

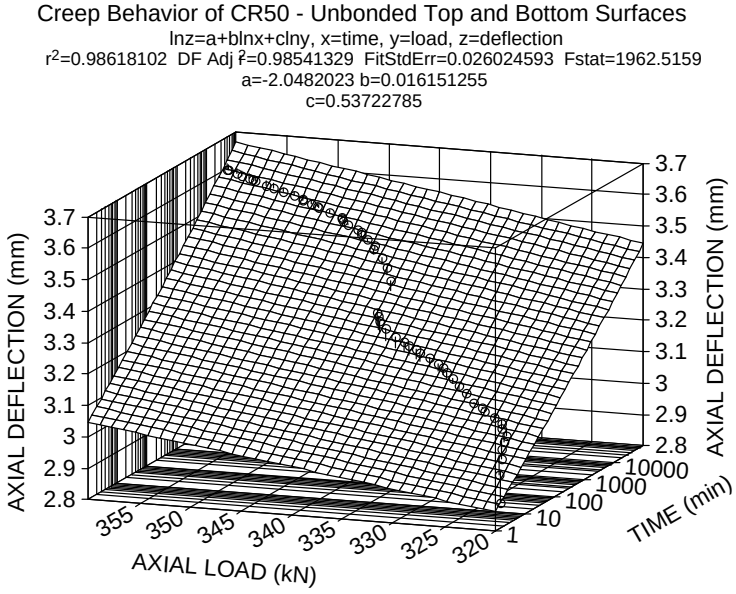

Figure B6 : CR50-Unbonded End Plates, Creep Test Data and Regression Results

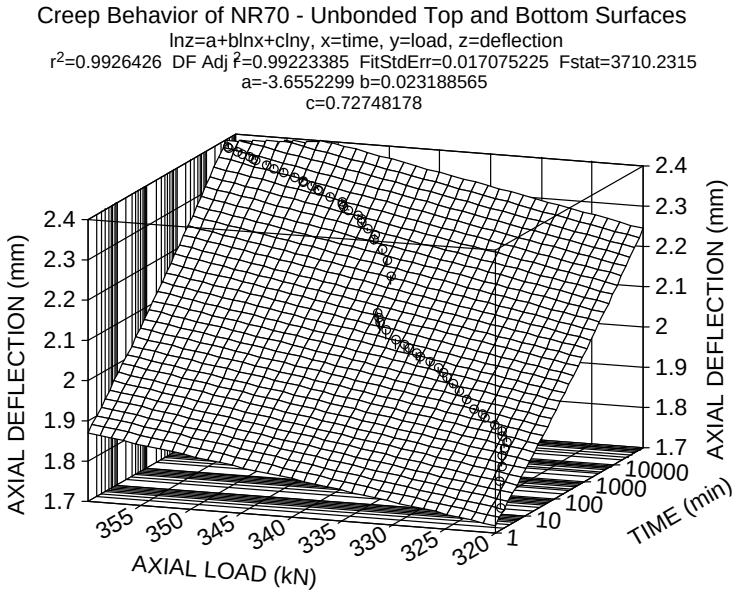

Figure B7 : NR70-Unbonded End Plates, Creep Test Data and Regression Results

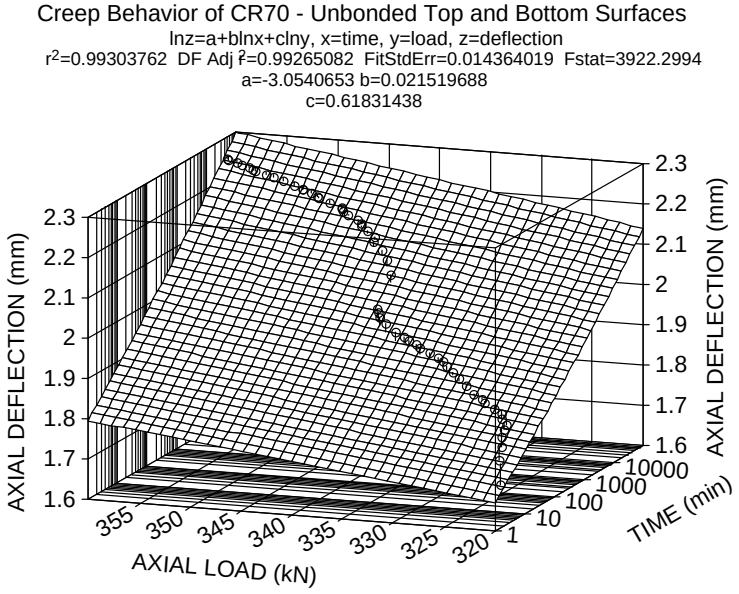

Figure B8 : CR70-Unbonded End Plates, Creep Test Data and Regression Results

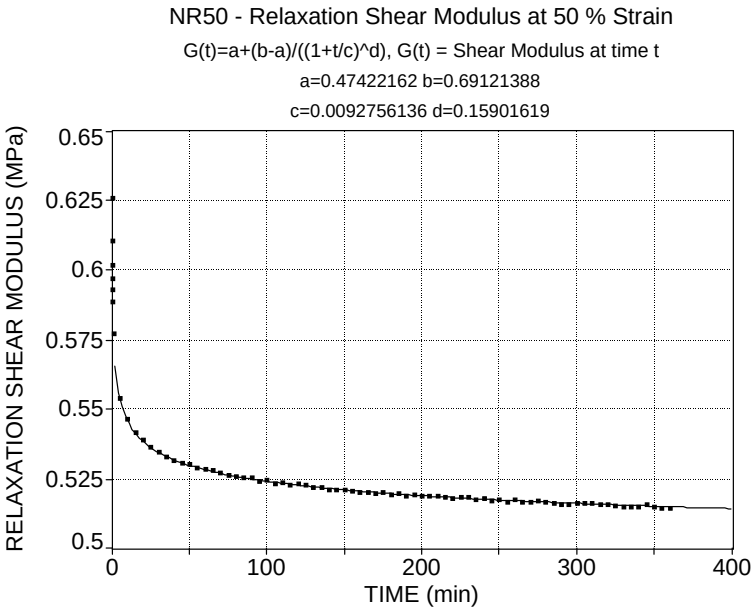

Figure B9: Relaxation Shear Modulus for NR50 Rubber at 50% Shear Strain and 32 C Temperature

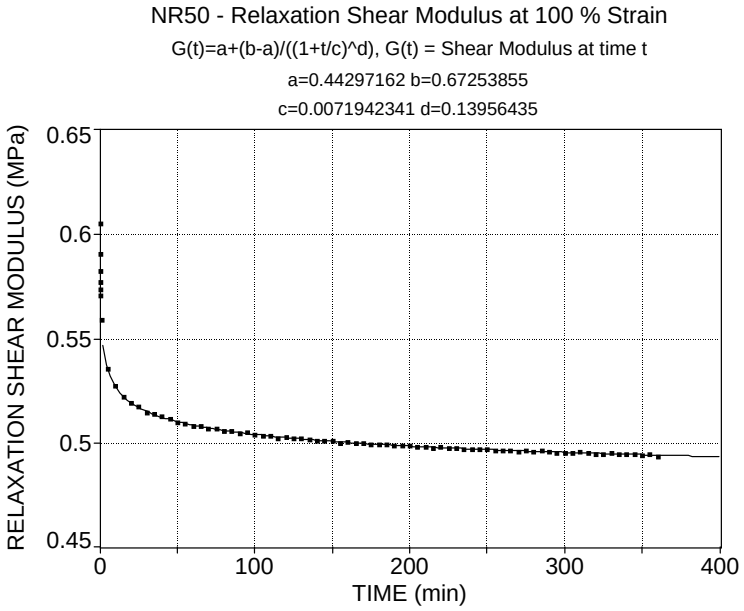

Figure B10: Relaxation Shear Modulus for NR50 Rubber at 100% Shear Strain and 32 C Temperature

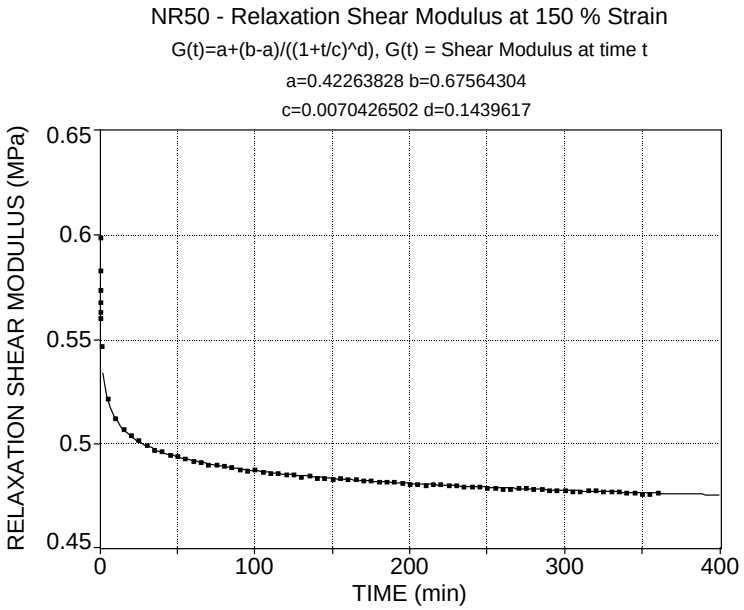

Figure B11: Relaxation Shear Modulus for NR50 Rubber at 150% Shear Strain and 32 C Temperature

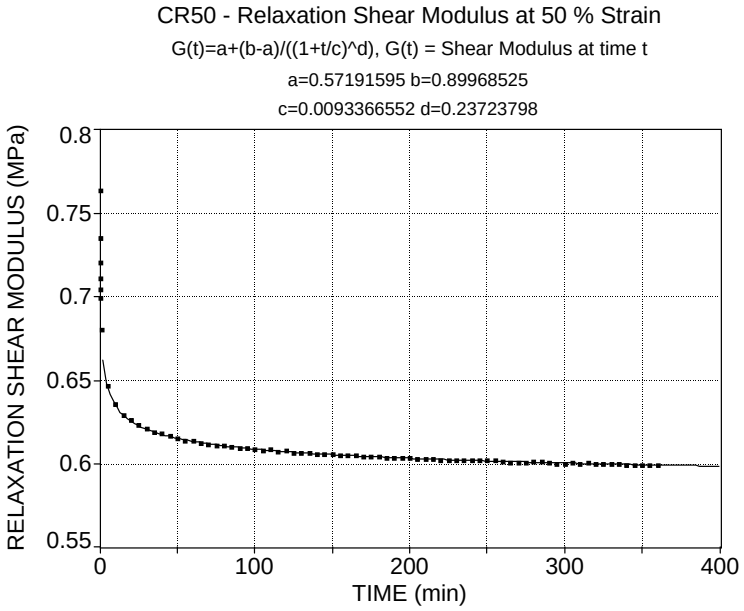

Figure B12: Relaxation Shear Modulus for CR50 Rubber at 50% Shear Strain and 32 C Temperature

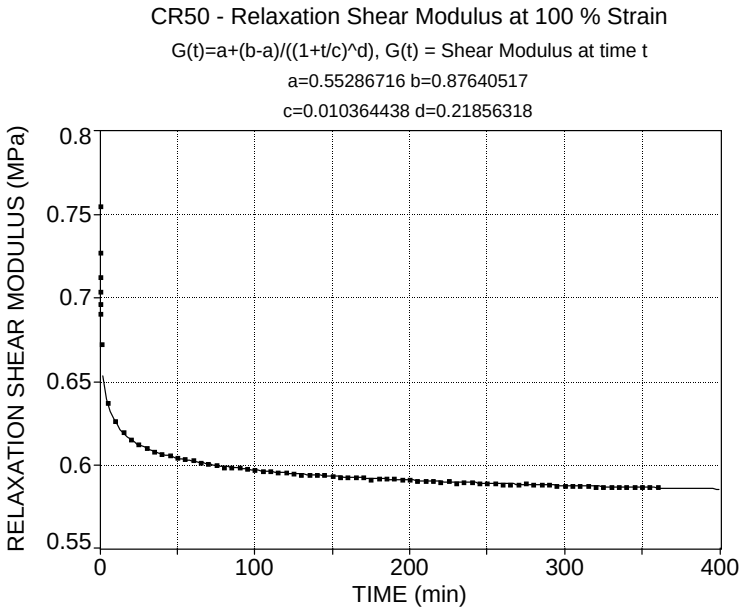

Figure B13: Relaxation Shear Modulus for CR50 Rubber at 100% Shear Strain and 32 C Temperature

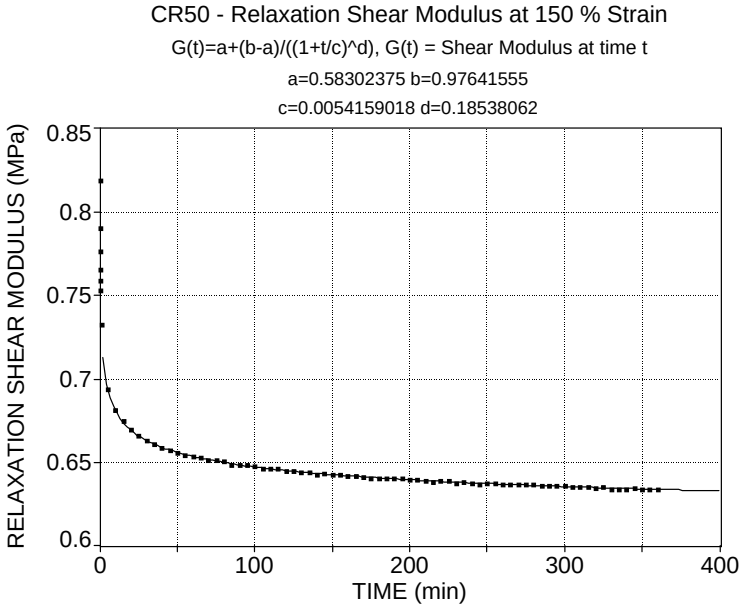

Figure B14: Relaxation Shear Modulus for CR50 Rubber at 150% Shear Strain and 32 C Temperature

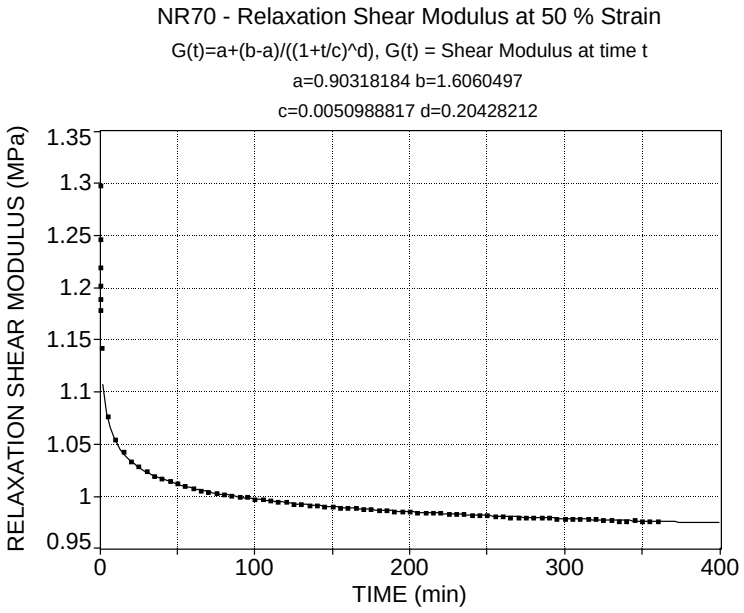

Figure B15: Relaxation Shear Modulus for NR70 Rubber at 50% Shear Strain and 32 C Temperature

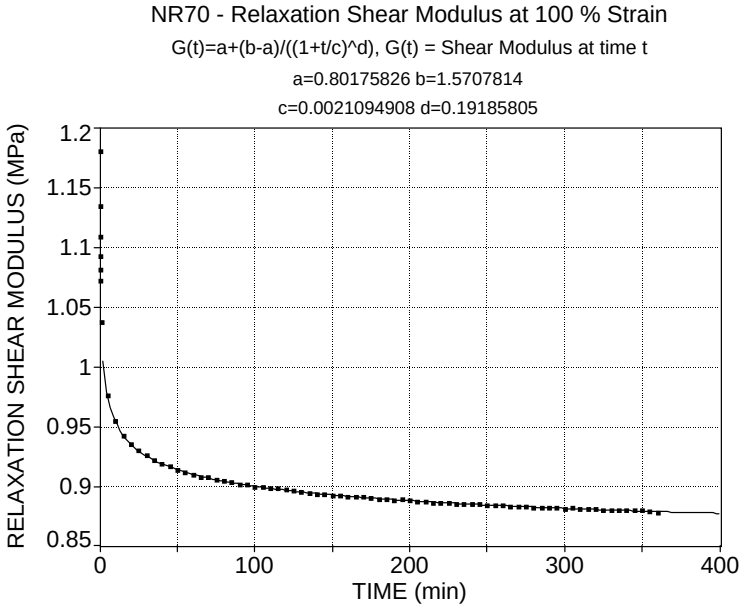

Figure B16: Relaxation Shear Modulus for NR70 Rubber at 100% Shear Strain and 32 C Temperature

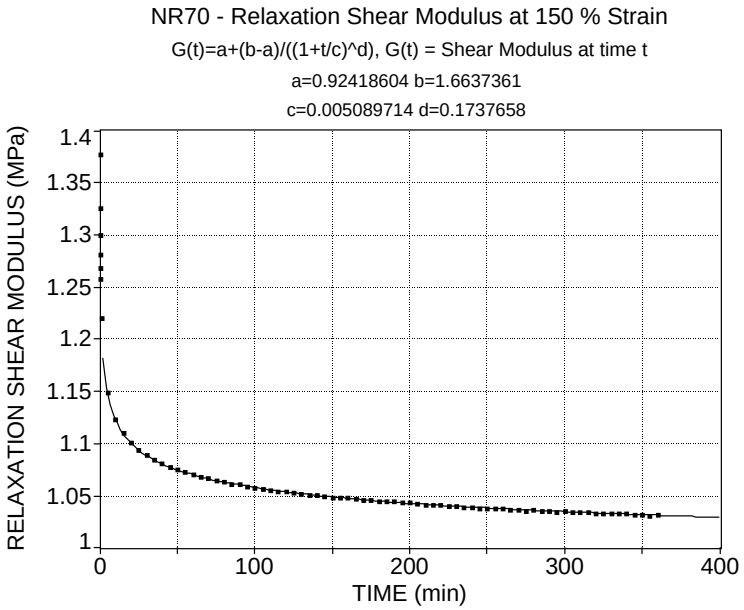

Figure B17: Relaxation Shear Modulus for NR70 Rubber at 150% Shear Strain and 32 C Temperature

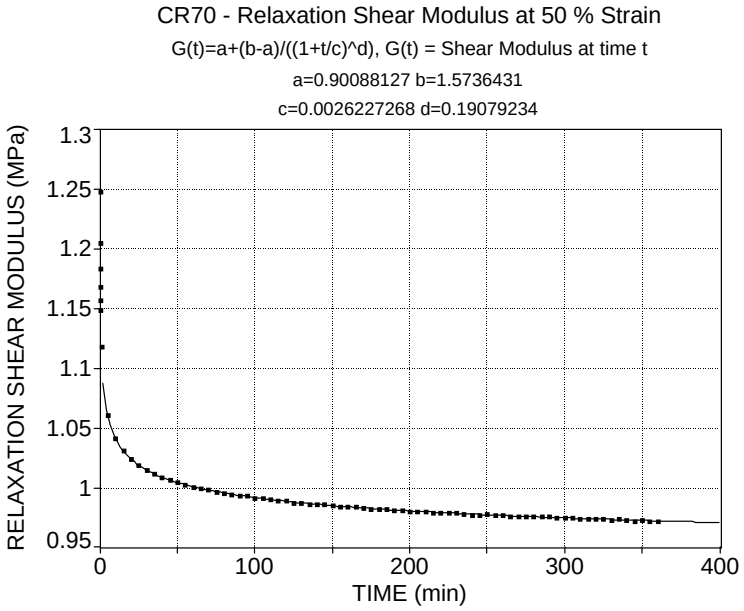

Figure B18: Relaxation Shear Modulus for CR70 Rubber at 50% Shear Strain and 32 C Temperature

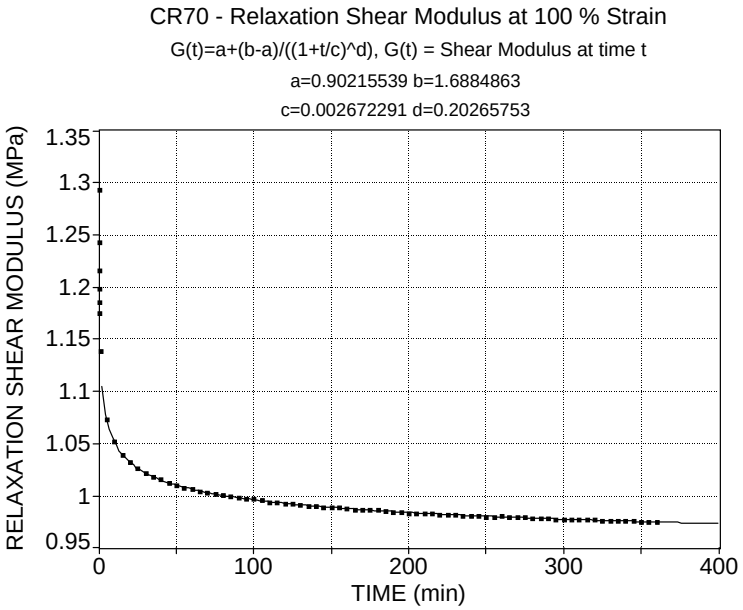

Figure B19: Relaxation Shear Modulus for CR70 Rubber at 100% Shear Strain and 32 C Temperature

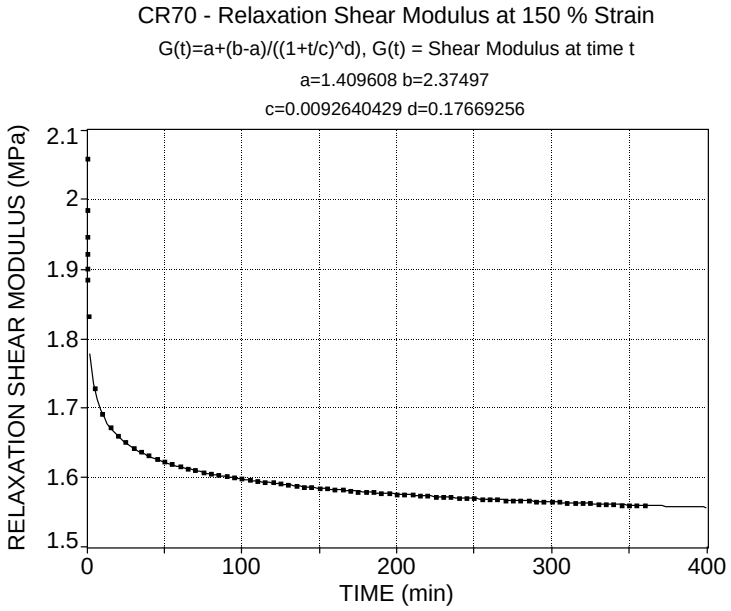

Figure B20: Relaxation Shear Modulus for CR70 Rubber at 150% Shear Strain and 32 C Temperature

Appendix C

This Appendix is a supplement of Chapter 5 and contains the results of finite element analysis of the small-scale specimen. As mentioned in Chapter 5 the small-scale specimen was designed with the aid of finite element analysis. The results of the final iteration are presented here to show the state of stresses and strains in the 8, 5 and 2.5 mm small-scale specimens when subjected to an instantaneous decompression of 21 MPa.

Finite Element Model and Boundary Conditions

The finite element (FE) model and boundary conditions for the 8 mm small-scale specimen is shown in Figure C1. The FE models of 5 mm and 2.5 mm specimens are same as 8 mm specimen except for rubber layer thickness. Since rubber is an almost incompressible material, the finite element model of the rubber portion was prepared using axisymmetric eight node quadratic hybrid finite elements. In these type of elements, pressure degrees of freedom are added to enforce a linear pressure variation inside the finite element such that the nearly incompressible material behavior is appropriately incorporated. The hybrid elements are mixed formulation elements, using a mixture of displacement and stress variables with an augmented variational principle to approximate the equilibrium equations and compatibility conditions (ABAQUS, Theory Manual). The steel parts were modeled using axisymmetric eight node quadratic elements.

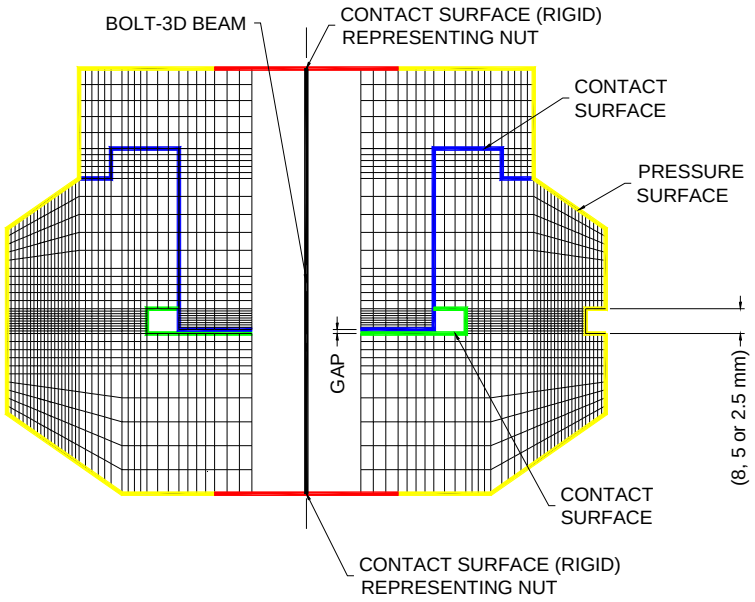

Figure C1: Small Scale Specimen – Finite Element Model and Boundary Conditions

Since axisymmetric elements were used to prepare the FE model of the small-scale specimen, two separate models were prepared to represent the quadrants "with cover rubber" and "without cover rubber" respectively. Both models are shown in Figure C1. The left side model is "with cover rubber" and the right side model is "without cover rubber". The bolt was modeled using a three-dimensional beam element while the nuts were modeled as two rigid contact surfaces connected to the beam element. Pre-tension or the make-up load in the bolt was simulated by means of thermal contraction. The hyper-elasticity of the rubber was modeled using Yeoh's approximation described in Chapter 2. The material constants are shown in Figure 5-3 (Chapter 5).

Analysis Procedure

ABAQUS, a general purpose finite element code was used for the finite element analysis. Structural analysis consisted of nonlinear quasi-static analysis with geometric and material nonlinearities to incorporate the effects of large deformation and large strains. Nonlinear static analysis required the solution of nonlinear equilibrium equations, for which Newton-Rapson numerical method was used. The solution was obtained as a series of increments, with iterations within each increment to obtain equilibrium. Since several nonlinearities were acting simultaneously, the loads were applied in small increments to assure correct modeling of history dependent effects and to increase the computational efficiency.

Load Cases

To simulate the effect of instantaneous decompression, the small-scale specimens were subjected to two load cases:

- Load Case-I: An external pressure of 21 MPa on the pressure surface shown in Figure C1 in conjunction with an axial displacement was applied
- Load Case-II: An axial displacement without external pressure was applied.

Load Case I represents the load corresponding to compressed state while Load Case II represents the load corresponding to decompressed state. The axial displacement for 8 mm specimen was calculated such that the resulting bulge shear strain and tri-axial stress ($PRESS = -\frac{1}{3}(\sigma_1 + \sigma_2 + \sigma_3)$) were nearly same as

that of a typical full-scale bearing in the bulge region. Note that $\sigma_1, \sigma_2, \sigma_3$ are the three principal stresses and PRESS represents the pore pressure in an elastomer layer fully saturated with fluid/gas. Since the objective of the present study was to evaluate the effect of thickness under same constraining load, the axial displacement for 5 mm and 2.5 mm specimens were calculated so that the resulting axial load was exactly same as that of the 8 mm specimen without external pressure. As mentioned in Chapter 5, the axial load on 8mm specimen was approximately 180 kN. The axial displacements for 8 mm, 5 mm and 2.5 mm specimens were 1.05 mm, 0.70 mm and 0.51 mm respectively. These displacements correlate fairly well with the displacements of actual test specimens tabulated in Table 5-1 (Chapter 5) as determined by their load-deflection tests. To apply these displacements to the finite element model, the "GAP" shown in Figure C1 was made equal to 1.05 mm, 0.70 mm and 0.51 mm for 8 mm, 5 mm and 2.5 mm models respectively. A negative ΔT was applied to the bolt element until the "GAP" was fully closed.

Results and Interpretation

Figures C2 and C3 show the FEA results for 2.5 mm specimen. The FEA results for 5 mm specimen are shown in Figures C4 and C5 while Figures C6 and C7 show the FEA results for 8 mm specimen. In these Figures, (a), (b) and (c) show deformed shape, pore pressures (PRESS) and shear strains (NE12) respectively in elatomer layer under Load Case I while (d), (e) and (f) show

deformed shape, pore pressures (PRESS) and shear strains (NE12) respectively in elastomer layer under Load Case II.

Figures C8 and C9 show DELTA-P in elastomer layers for models "without cover" and "with cover" respectively. DELTA-P is the difference in pore pressures between Load Case I and Load Case II and represents the change in pore pressure due to instantaneous depressurization. If the instantaneous depressurization is the main cause of damage then explosive decompression damage can be expected in the elastomer region where DELTA-P is greater than 9.1 MPa - the pressure that causes damage in voids of unconstrained elastomer described in Chapter 5. As shown in Figures C8 and C9, as the thickness of rubber layer decreases, the region with DELTA-P greater than 9.1 MPa also decreases. Therefore, less damage is expected in thinner rubber layers. This correlates fairly well with the experimental observations presented in Chapter-5. Note that the analysis based on the above concept predicts some damage in 2.5 mm specimen, however no significant damage was observed. This discrepancy can be attributed to the influence of other variables such as rate of decompression, visco-elastic effects at high temperature and compressibility, solubility and diffusion of methane in elastomer, that were difficult to include in the present finite element analysis. Further research is needed to account for these effects in the analytical model. However, the present method gives conservative results.

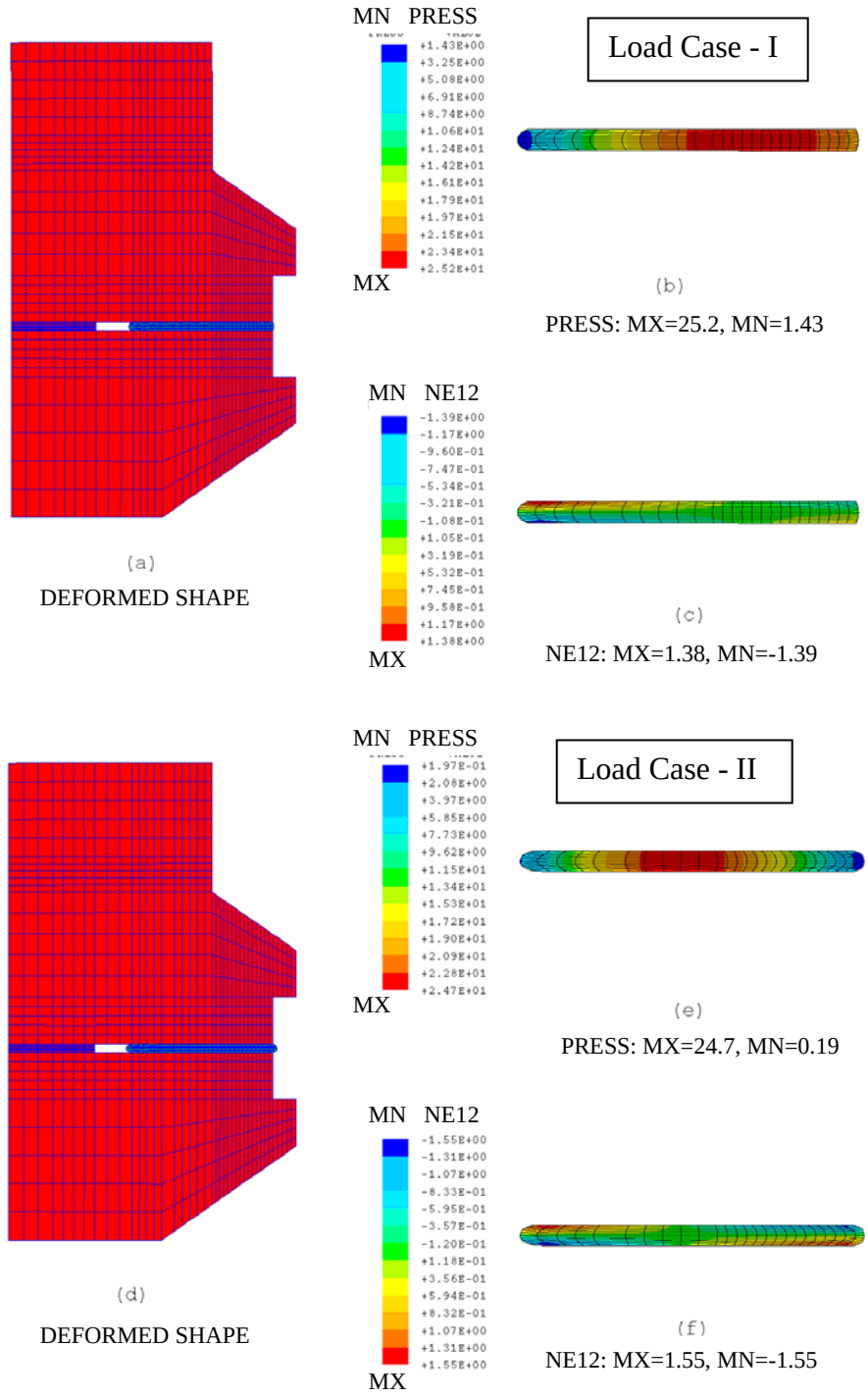

Figure C2: Finite Element Analysis Results for 2.5 mm Small Scale Specimen in No-Cover Quadrant

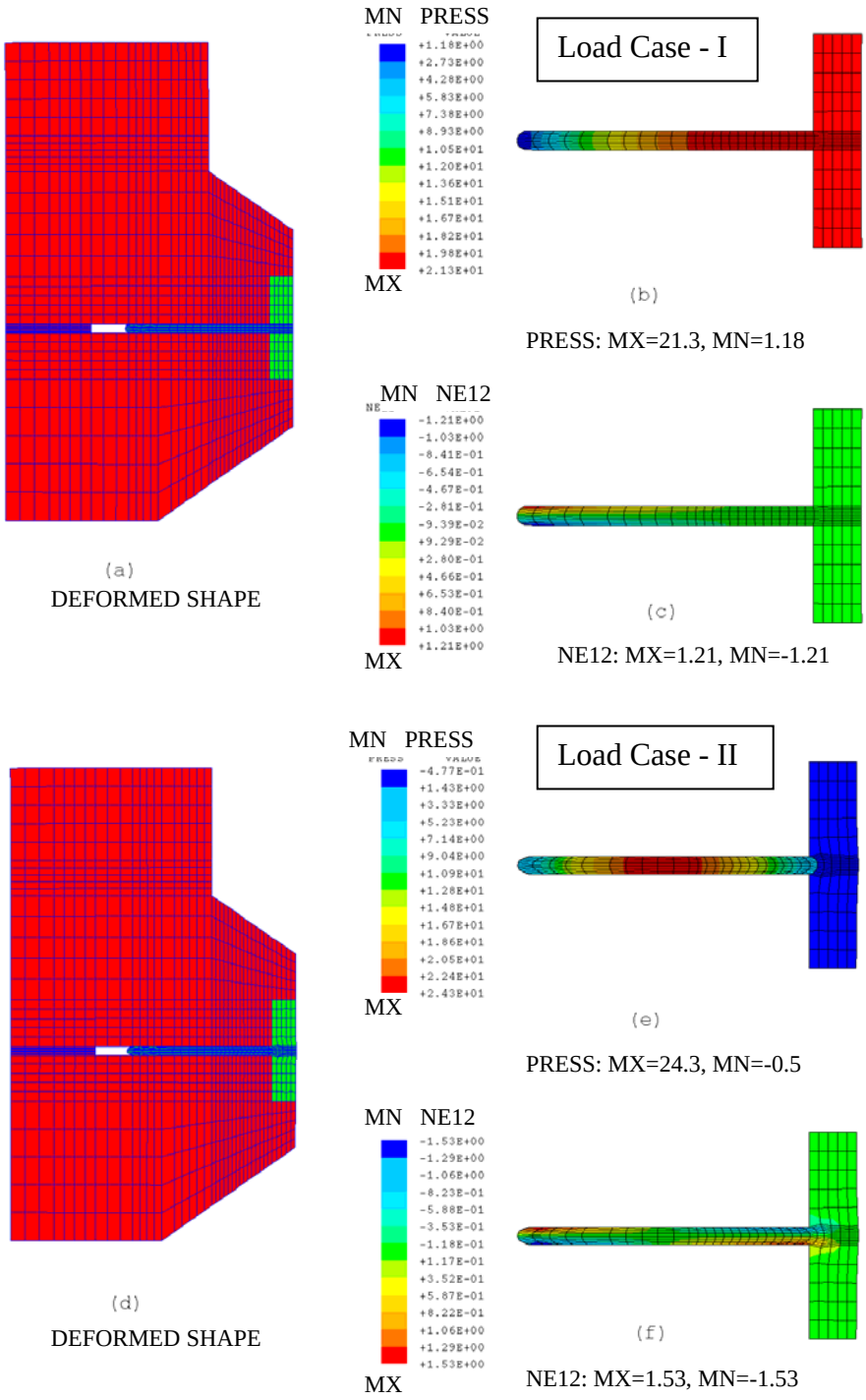

Figure C3: Finite Element Analysis Results for 2.5 mm Small Scale Specimen in Covered Quadrant

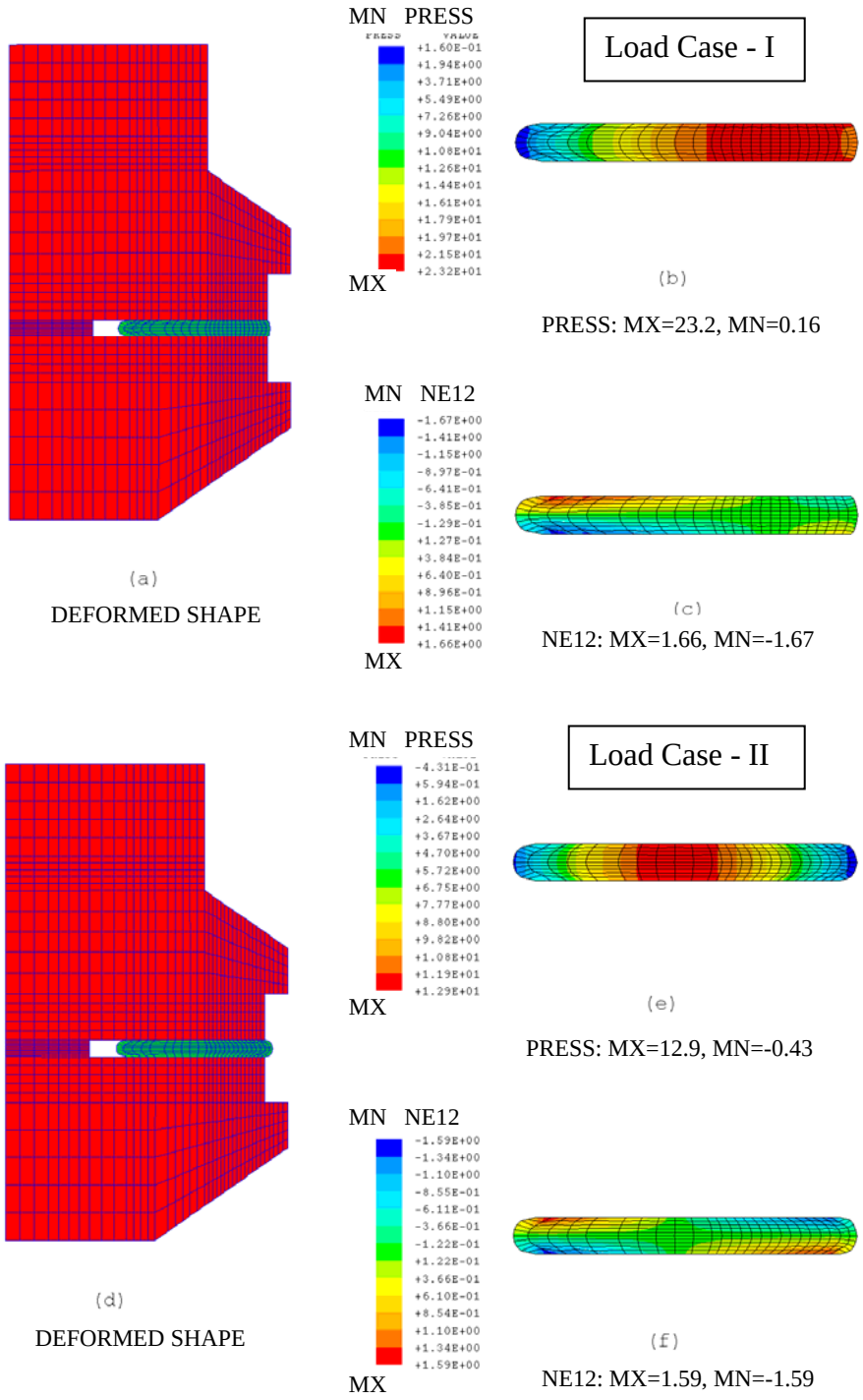

Figure C4: Finite Element Analysis Results for 5 mm Small Scale Specimen in No-Cover Quadrant

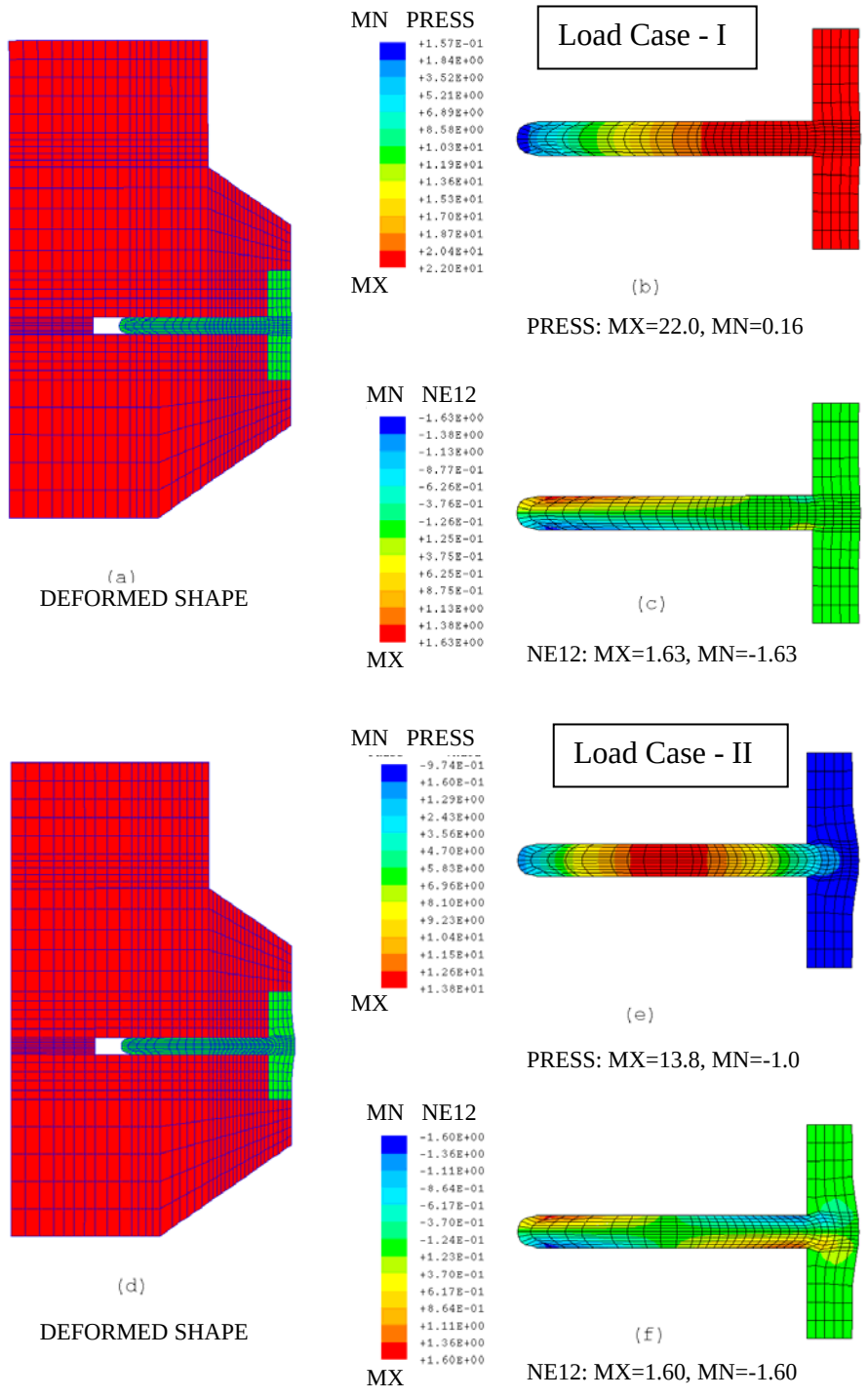

Figure C5: Finite Element Analysis Results for 5 mm Small Scale Specimen in Covered Quadrant

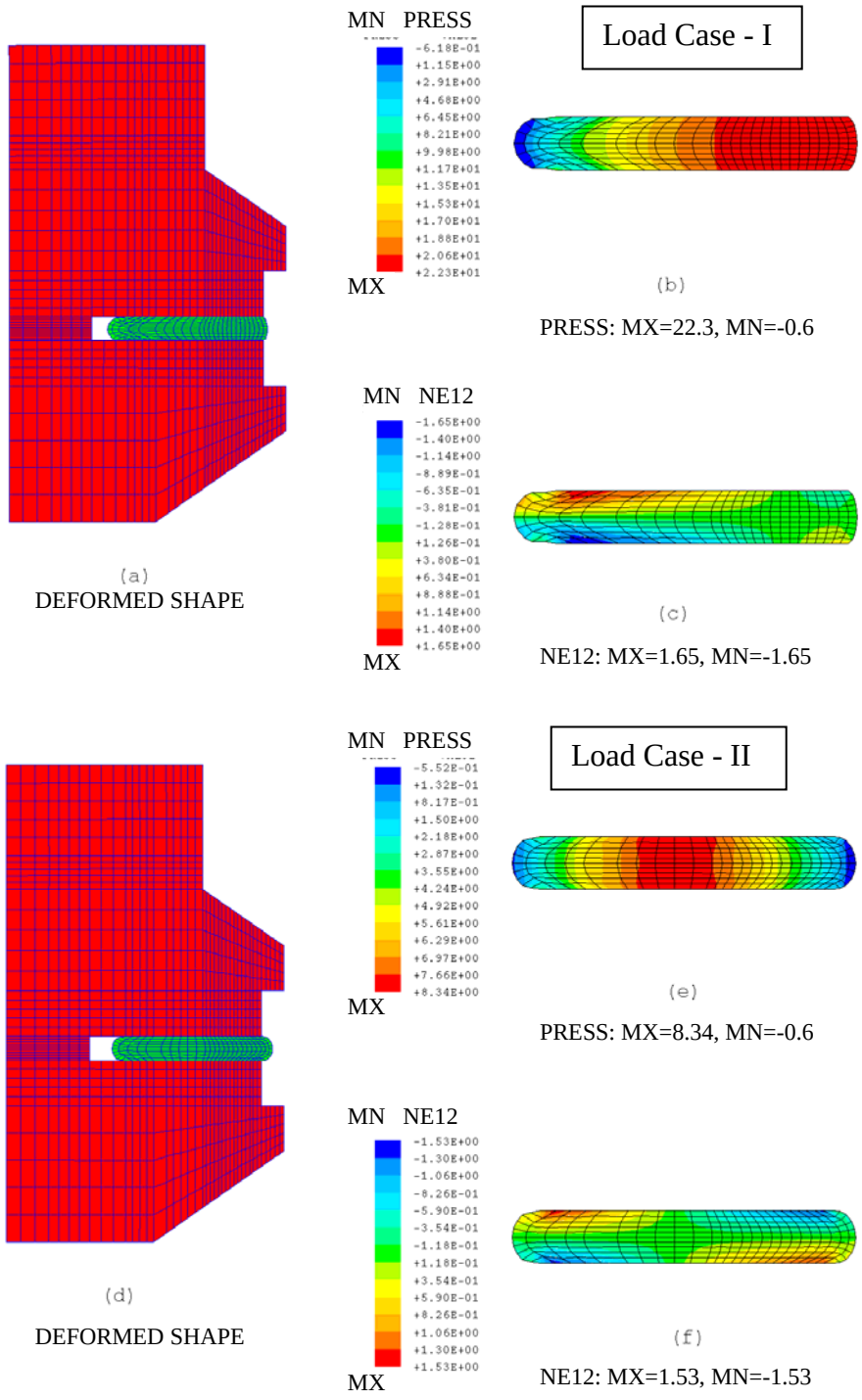

Figure C6: Finite Element Analysis Results for 8 mm Small Scale Specimen in No-Cover Quadrant

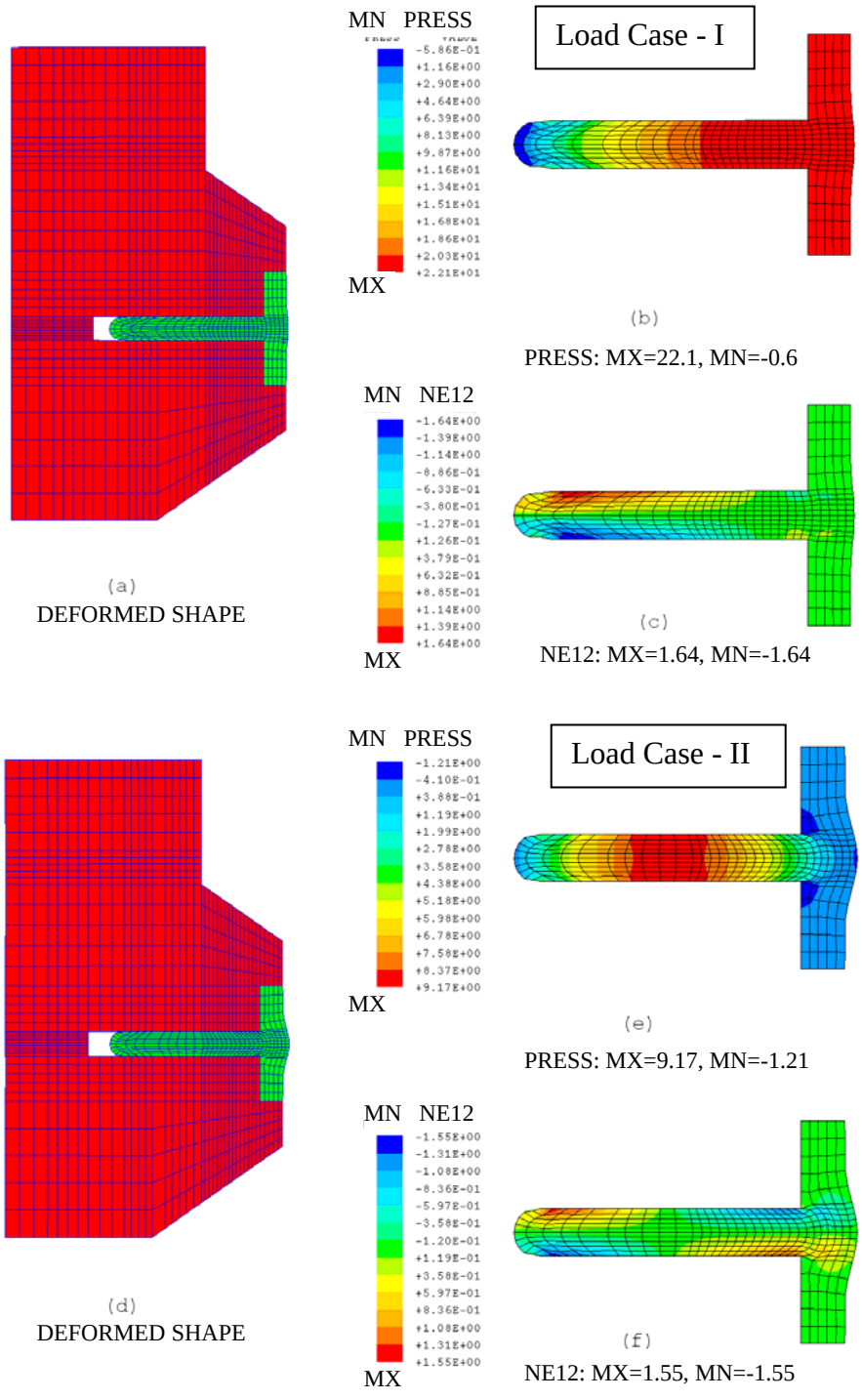

Figure C7: Finite Element Analysis Results for 8 mm Small Scale Specimen in Covered Quadrant

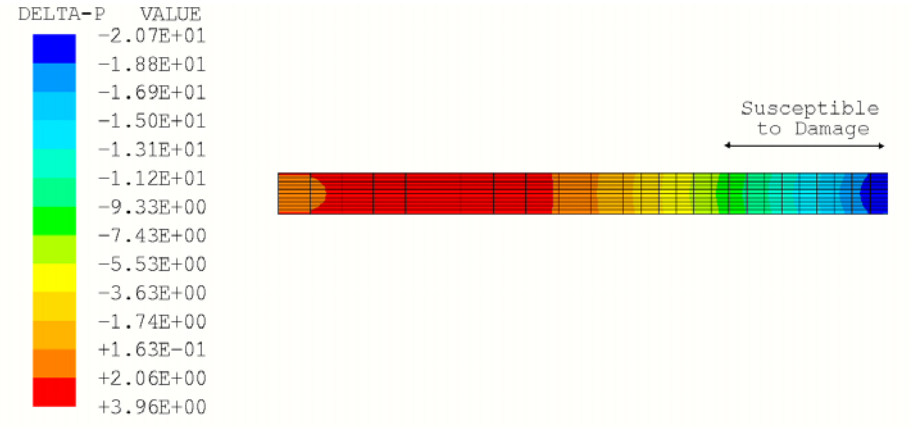

(a) 2.5 mm Elastomer Layer

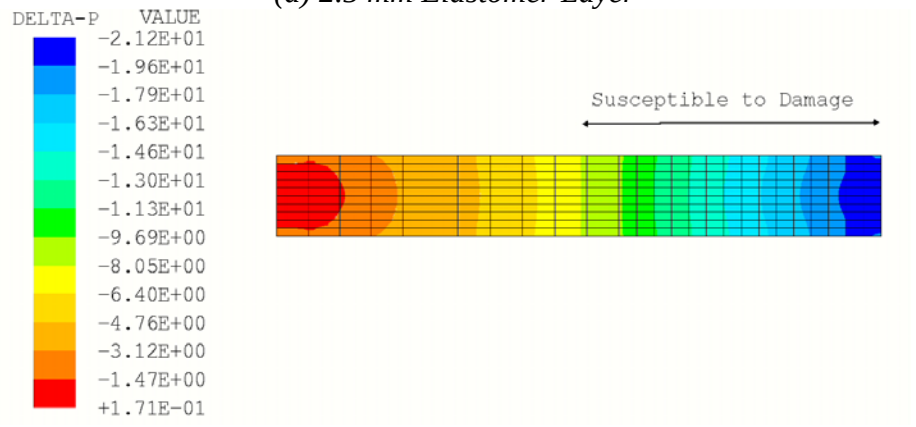

(b) 5 mm Elastomer Layer

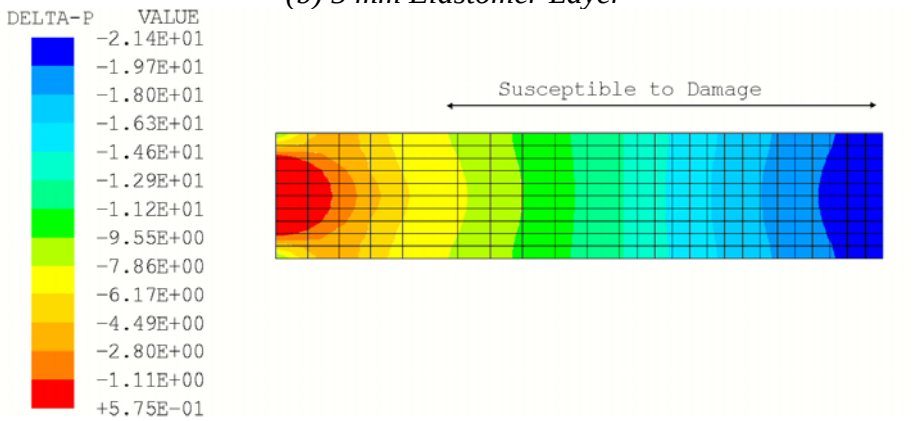

(c) 8 mm Elastomer Layer

Figure C8: DELTA-P (MPa) in Various Elastomer Layers without Cover
(Note: The width of all three layers is 38 mm)

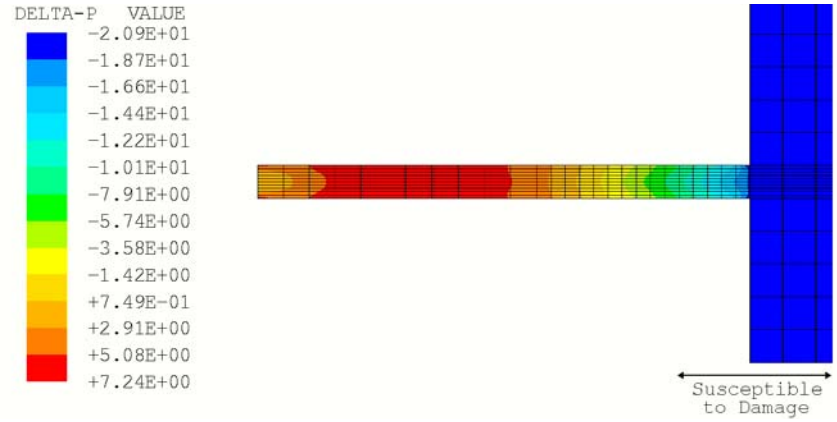

(a) 2.5 mm Elastomer Layer

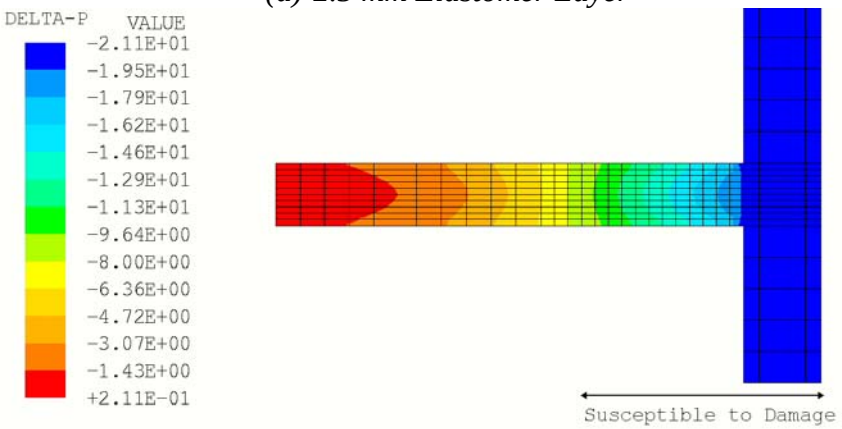

(b) 5 mm Elastomer Layer

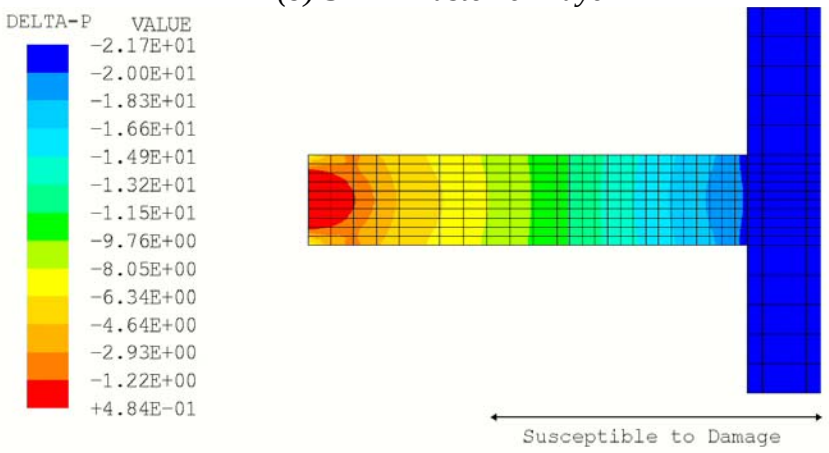

(c) 8 mm Elastomer Layer

Figure C9: DELTA-P (MPa) in Various Elastomer Layers with Cover
(Note: The width of all three layers is 38 mm and the cover thickness is 6 mm)

Bibliography

AASHTO, Standard Specification for Plain and Laminated Elastomeric Bridge Bearings, M251-97 (1997).

AASHTO, Standard Specification for Highway Bridges, Fifteenth Edition, (1992).

AASHTO, Standard Specification for Highway Bridges, Sixteenth Edition, (1996).

AASHTO LRFD , Bridge Design Specification, Interim Revisions, (1998).

AASHTO LRFD, Bridge Design Specifications, First Edition, (1998).

AASHTO LRFD, Bridge Construction Specifications, First Edition, (1998).

ASTM D 1566-97, Standard Terminology Relating to Rubber, (1997).

ASTM D395-89, Rubber Property – Compression Set, (1989).

ASTM D4014-89, Standard Specification for Plain and Laminated Elastomeric Bearings for Bridges, (1989).

ASTM D573-88, Standard Test Method for Rubber- Deterioration in an Air Oven, Reapproved, (1994).

ASTM D2240-86, Standard Test Method for Rubber Property: Durometer Hardness.

Barker, L.R., "Accelerated and Long-Term Ageing of Natural Rubber Vulcanizates", NR Technology, Vol. 19, No. 2 (1988).

Briscoe, B. J., Savvas, T., Kelly, C. T., "Explosive Decompression Failure of Rubbers : A Review of the Origins of Pneumatic Stress Induced Rupture in Elastomers", Rubber Chemistry and Technology v 67 n 3 (1994).

Briscoe, B. J., Zakaria, S., "Gas-induced Damage in Elastomeric Composites", Journal of Materials Science v 25 n 6 (1990).

Brown, R. P., "Physical Testing of Rubber", Chapman & Hall, London, UK, (1996).

Cain, D., Zollo, D., Chen, L. Y., Hong, I., "Elastomeric Seal Design, Analysis, and Material Selection for Severe Oil Field Service", Proceedings of the International Offshore Mechanics and Arctic Engineering Symposium (1990), Houston TX.

Clark, L. J, Manley, T. R, "Stress Relaxation Studies", Proceedings from the International Rubber Conference: IRC 86. v 1 (1986) Goteborg, , Swed, Swedish Inst of Rubber Technology Sweden.

Crozier, W., Stoker, J., Martin V. and Nordlin, E., "A Laboratory Evaluation of Full Size Elastomeric Bridge Bearing Pads", California Department of Transportation Report CA-DOT-TL-6574-1-74-26, June, (1994).

Curro, J. G., Salazar, E. A.," Physical And Chemical Stress Relaxation Of Elastomers", Rubber Chemistry and Technology v 50 n 5 (1977).

Derham, C. J.,"Creep and Stress Relaxation of Rubbers", Journal of Materials Science v 8 n 7 (1973).

Doody, M.E., Noonan, J. E., "Long-Term Performance of Elastomeric Bridge Bearings", Special Report FHWA/NY/SR-98/129, Transportation Research and Develoopment Bureau, New York State Board of Transportation (1998).

Ferry, J. D., Viscoelasitc Properties of Polymers, 3rd Ed., Wiley, New York, (1980).

Freakley, P. K., Payne, A. R., Theory and Practice of Engineering with Rubber, Applied Science Publishers, London (1978).

Gent A N, Tompkins DA ,"Nucleation and Growth of Gas Bubbles In Elastomers", Journal of Applied Physics, v 40 n 6 (1969).

Gillen, Kenneth T, "Effect Of Cross-Links Which Occur During Continuous Chemical Stress-Relaxation", Macromolecules v 21 n 2 (1988).

Griffiths, A. D., "Material Selection and Product Design for Resistance to Explosive Decompression", Discussion Forum and Exhibition on Offshore Engineering with Elastomers, (1985), London, England.

Hamed, G. R, " Materials and Compounds", Engineering with Rubber, Hanser Publishers, Munich (1992).

Hamzeh, O., Tassoulas, J. L. and Becker, E. B., “Analysis of Elastomeric Bridge Bearings”, Report No. 1304-5, Center for Transportation Research, University of Texas, Austin, August, (1995).

Herrick, R. C., “Development of Laminated Elastomeric Bearing”, No. ASD-TDR-63-769 Franklin Institute Report F-B1883, Wright-Patterson Air Force Base Ohio (1963).

Hibbitt, Karlsson and Sorenson, ABAQUS Standard Version 5.8, Theory Manual, (1998).

Ho, Emily, Flitney, R. K., Nau, B. S., “Prediction of Fluid Behavior in Elastomeric Seals”, Proceedings of the International Offshore Mechanics and Arctic Engineering Symposium (1993), Glasgow, Scotland.

Hogan, M., Gunderson, R. H., Stevenson, A., “Predicted Change in Shear Modulus of Semi-EV NBR and NR Elastomer Compounds Over Thirty Years”, Corrosion 97, Paper 79, NACE International Conference, Houston (1997).

ISO 188, Accelerated Ageing or Heat Resistance Tests, International Standards Organization, (1982).

ISO 8013, Determination of Creep in Compression or Shear, International Standards Organization, (1988).

ISO 815, Determination of Compression Set at Ambient, Elevated or Low Temperatures, International Standards Organization, (1991).

John, Peter William Meredith, Statistical Design and Analysis of Experiments, New York, Macmillan (1971).

Kawabata, E, Kawai, H, “Strain Energy Density Functions of Rubber Vulcanizates from Biaxial Extension”, Advances in Polymer Science, 24, 89 (1977).

Lindley, P.B., “Engineering Design with Natural Rubber”, Malaysian Rubber Technology Bulletin, Malaysian Rubber Producers Research Association, (1978).

Moakes, R. C., “Long Term Natural Ageing”, RAPRA Members Journal, Parts 1 and 2, pp. 53-63 (1975).

Mullins, L., “Engineering with Rubber”, CHEMTECH v 17 n12 (1987).

Mullins, L., Tobin, N. R., “Stress Softening of Rubber Vulcanizates”, Journal of Applied Polymer Science v 9, (1965).

Nakauchi, H., Tanaka, K., Yokoyama, C., Miyazaki, M., and Yamazaki, N., ”Characterization of a 100-Year-Old Rubber Bearing by Microanalytical Methods”, Journal of Applied Polymer Science; Applied Polymer Symposium 50, 369-375(1992).

OSI Document SP1K-23-017, Rev. D., “History and Usage of Flex Joint and Bearing Products Fabricated by Oils States Industries”, (1996).

Peters, L. A., Vicic, J. C., Pugh, T. L., “Optimizing Carbon Black Loading for Explosive Decompression Resistance of Fluoroelastomers for Oil Field Service”, Rubber World v 199 n2 (1988).

Potts, D. J., “Explosive Decompression Resistance of Elastomers in Gas Duties”, Discussion Forum and Exhibition on Offshore Engineering with Elastomers, (1985) London, England.

Reinhardt, C. M., Kovitch, F. J., “Elastomer Flexjoints for TLP Tethers/Systems”, Proceedings of the International Offshore Mechanics and Arctic Engineering Symposium (1985), Dallas, TX.

Rivilin, R. S., “In Rheology: Theory and Applications,” F.R. Eirich, Ed., Academic Press, New York (1956).

Rivilin, R. S., Saunders, D. W., “Large Elastic Deformatins of Isotropic Materials –VII. Experiments on the Deformation of Rubber,” Phil. Trans. Roy. Soc. A 243, 251 (1951).

Schmidt, W. E., “Design, Testing and Performance of Elastomeric Bearings”, IBM Technical Disclosure Bulletin, Proc, Prepr Pap, May 7-9 (1974) Washington DC, USA, Paper: 883.

Shade, W. N., Legg, D.W., “Explosive Decompression Resistance of Centrifugal Compressor O-Ring Seals: A comparative Test Summary and Procedure”, Journal of Engineering for Gas Turbines and Power, Transactions of ASME v 110 n 2 (1988).

Shelton, J. Reid, “Review of Basic Oxidation Processes in Elastomers,” Rubber Chemistry and Technology, 45, 359 (1972).

Stanton, J. F., Roeder, C. W., Elastomeric Bearing Design, Construction, and Materials, NCHRP Report 248, (1982).

Takayama, M., Morita, K., ”Creep Tests of Full-Scaled Laminated Rubber Bearings,” American Society of Mechanical Engineers, Pressure Vessels and Piping Division (Publication) PVP Seismic, Shock, and Vibration Isolation Proceedings of the 1998 ASME/JSME Joint Pressure Vessels and Piping Conference v 379 (1998) San Diego, CA, , USA, Sponsored by : ASME ASME Fairfield NJ USA.

Vitt, S. P., “Elastomeric Bearings for High Load Applications”, ASME Paper 74-PET-11, September 15, (1974).

Yeoh, O. H., “Characterizaton of Elastic Properties of Carbon-Black-Filled Rubber Vulcanizates,” Rubber Chemistry and Technology, 63, 792, (1990).

Yeoh, O. H., “Some Forms of The Strain Energy Function for Rubber.” Rubber Chemistry and Technology v 66 n 5 (1993).